A systems study of nutrient uptake in plants

Ishan Ajmera

School of Biosciences

University of Nottingham

This dissertation is submitted for the degree of

Doctor of Philosophy

2015

I would like to dedicate this thesis to my mom and my dad for their unconditional love, support and sacrifices which have strengthened me to pursue my dreams.

Declaration

I hereby declare that except where specific reference is made to the work of others, the contents of this dissertation are original and have not been submitted in whole or in part for consideration for any other degree or qualification in this, or any other University. This dissertation is the result of my original research and includes nothing which is the outcome of work done in collaboration, except where specifically indicated in the text. This dissertation contains fewer than 45000 words including appendices, bibliography, footnotes, tables and equations and has less than 60 figures.

Ishan Ajmera
2015

Acknowledgements

"Whoever travels without a guide needs 200 years for a two-day journey"

This insightful quote from the Sufi poet Rumi well relates with my PhD journey, which would have not timely reached its destination without the guidance and support of some amazing people, both in my academic and personal life. This all has happened with the grace of almighty god.

This thesis would have never come to fruition without the guidance and support of my humble supervisors, Prof. Charlie Hodgman and Dr. Chungui Lu. In particular, I am in-debt to Charlie for sharing his wide knowledge, experiences and most importantly, time, to nurture my research skills. Also, a big thanks go to him for directing, encouraging and keeping me motivated throughout my PhD. A special thank go to Chungui for all his encouragement and being more of a friend, than a mentor. I am thankful to Chungui for persuading and supporting me to conduct my own experiments in the laboratory. At this stage, I would like to remember (Late) Prof. Ping Wu, who had inspired this project along with my supervisors. I would like to thank him in my memories, for all his guidance and personal communications during my visit to his lab in Zhejiang.

Many thanks go to Dr. Dov Stekel for all his guidance and advice over the past four years, especially on the parametrisation of my models. I am very grateful to Dr. Leah Band for her support and expert assistance in developing the multi-cell models presented in this thesis. I would also like to thanks Dr. Scott Young and his technical team including Dr.Saul Vazquez-Reina and Lolita Wilson for all their assistance in generating ionomics data. A big thanks to Manuel Martinez for his help while conducting the experiments.

I am thankful to Dr. Liu Zhang, Dr. Zhefeng Lin, Dr. Daniele Dietrich, Dr. Anthony Bishopp, Dr. Kamal Swarup, Dr Rupert Fray, Dr. Erik Murchie, Dr. Susan Liddell, John Vaughan-Hirsch and Mark Meacham for their help in my wet lab experiments. I would like to acknowledge Dr. Jitender Giri (NIPGR, INDIA) for sharing his data and conducting experiments to test some initial hypotheses. Also, I would like to

thank Dr. John Fozard, Dr. Nathan Mellor and Dr. Micheal Pound for their support in the development of multi-cellular models. A special thank to Emma Hooley for all the administrative support during 4 years of my research.

Thanks to Mohammed Cherkaoui, Reuben Newsome, Mudassar Iqbal, Karan Bhatt, Sankalp Arya, Faraz Khan, Nitin and Pooja for being wonderful friends and supporting me during the tough times of my PhD. Special thanks go to my family and friends back home for all their love and support, especially during this fours years. I grateful to the International office, University of Nottingham for offering me a scholarship to carry out this PhD and The Gen foundation (London), for their financial support.

Publications

Manuscripts generated as the part of this thesis

Ajmera, I. , Wu, P., Hodgman, TC. , Lu, C. An integrative systems perspective on plant phosphate research. *New Physiologist* (under revision)

Hodgman, TC. and **Ajmera, I.** 2015. The successful application of systems approaches in plant biology. *Progress in Biophysics and Molecular Biology*, **117**(1), 59-68

Other manuscripts

Chelliah, V., Juty, N., **Ajmera, I.**, Ali, R.,...(15 co-authors).., Laibe, C. 2014. BioModels: ten-year anniversary. *Nucleic Acids Research*, **43**(D1), D542–D548.

Ajmera, I., Swat, M., Laibe, C., Novère, N. Le, and Chelliah, V. 2013. The impact of mathematical modeling on the understanding of diabetes and related complications. *CPT: Pharmacometrics & Systems Pharmacology*, **2**(7), e54.

Abstract

The case for improving Phosphorus-Use Efficiency in crops is widely recognised. Although much is known about the underlying molecular and regulatory mechanisms, improvements have been hampered by the extreme complexity of phosphorus (P) dynamics in soil and plants (across all physical scales), including its soil chemistry and uptake, distribution and deficiency responses in plants. The urgency and direction of phosphate research is also being driven by the limited availability of finite P stocks to farmers and the need to reduce environmental hazards. Thus, systems approaches become essential to identify the most potent (combinations of) target genes for improving phosphate uptake and utilisation in crops. This study has applied these approaches with the aim of increasing understanding of the regulation of phosphate uptake at three separate spatial scales, primarily in rice, but also in *Arabidopsis*.

The first and major part of this study has focused on the cell scale, wherein novel mathematical models for molecular regulation of phosphate acquisition have been developed. Owing to the sparsity of the data, advanced techniques for parameter fitting were employed, which resulted in an original model, which accurately reflected the profiles of all the genes apart from PHO2. It was clear that miR399-mediated degradation was insufficient to explain the apparent early reduction in PHO2 mRNA levels. Five hypotheses were explored mathematically, of which the most plausible is that there is a phosphate-sensitive transcriptional repressor (PsTR) of PHO2 mRNA synthesis. To support this hypothesis, mRNA was extracted from phosphate-starved and untreated roots over a short, 12-hour time course. Quantitative Polymerase Chain Reactions (qPCR) of PHO2 mRNA both confirmed the early decline predicted by the hypothesis and also revealed a temporary restoration of mRNA levels, which points to PHO2 (a type-2 ubiquitin ligase) regulating its own transcript levels. Sensitivity analysis of these models indicates that the utilisation rate of cytosolic phosphate is the biggest influence on this system.

Output from simulations with the original and PsTR models qualitatively reproduced the phenotypes of various published phosphate-research papers, with the exception of RNA-SEQ data in which phosphate-starved rice roots were resupplied with

phosphate. In this instance, the observed rapid drop in mRNA levels for PHO2 and IPS1 were incorrectly predicted, pointing to one or more other regulatory mechanisms not represented in these models. The IPS1 gene encodes a long non-coding RNA that has a poly-A tail. Its RNA also binds to miR399 and accumulates to extremely high levels in plant roots during phosphate stress. A sudden loss of IPS1 would release the bound miR399 causing the observed rapid loss of PHO2 mRNA. The observed IPS1 profile can be explained by either the gene having a "super-promoter" that is capable of extremely high RNA synthesis under low phosphate conditions, or the transcript being protected from degradation by phosphate-sensitive RNA-binding proteins. Informatics analyses favour the latter and a revised model incorporating RNA protection was found to have parameters for IPS1 synthesis that are similar to those normally used in modelling gene regulation. The analyses also point to PUMILIO proteins playing this role.

The second part of this work has explored the role of tissue geometry in determining root phosphate levels and flux. Multi-cellular vertex-based models of published *Arabidopsis* and rice root cross-sections were produced using CellSeT, into which equations for phosphate uptake, flux and utilisation were embedded using OpenAlea. Simulations suggest that *Arabidopsis* trichoblasts have lower cytosolic phosphate levels than neighbouring epidermal cells, because they have a larger area through which phosphate flows into the inner tissues. This implies that trichoblasts are more sensitive to phosphate stress and reduced phosphate levels could therefore be part of the trigger for initiating root-hair growth. Adding root hairs of varying lengths into this geometry shows that a hair does not have to grow much before the phosphate levels in this trichoblast exceeds those in the neighbouring cells and that phosphate flows to them. This potentially suppresses root-hair formation in nearby trichoblasts. The rice simulations show that aerenchyma dramatically reduce cytosolic phosphate in surrounding cells and point to a role for lacunae in rapid uptake of phosphate, without the need for large water fluxes. Alongside aerenchyma, a higher proportion of fluid-filled lacunae could be a desirable trait for improving nutrient-uptake efficiency.

At the whole-plant scale for the third part of this work, a time-course dataset has been generated to record the effect of phosphate starvation over 21 days on the uptake dynamics of eleven other macro- and micro-nutrients. This dataset will be of use in future systems studies of nutrient uptake and interactions.

Contents

List of Figures

List of Tables

Chapter 1

Introduction

Ensuring a secure and sustainable food supply for the growing human population is a global priority. With the increasing scarcity of fresh water, limited availability of land and fertiliser stocks, and global climate change, current agricultural production is unsustainable, particularly as phosphate fertiliser stocks are forecast to become prohibitively expensive as global supplies run out. As phosphorus (P) is an essential nutrient for crop growth and production, global P security has a direct implication for global food security. In addition, adverse environmental and socio-economic consequences of excessive application of phosphate fertilisers have further heightened the concern regarding sustainability of P in agricultural systems.

Various approaches have been proposed to address this global challenge, which either aim to improve fertiliser management strategies, develop efficient recycling processes or modify plant traits (Syers *et al.*, 2008). In longer run, the latter presents the ultimate solution, which involves exploitation of genetic variation and modification of target genes to breed crop varieties that can thrive in poorer soils with minimum phosphate input. Crop improvement programs to improve Phosphate-Use-Efficiency have received much attention for decades, but their success in terms of practical application has been limited to date (Gaxiola *et al.*, 2011). This is particularly due to the extreme complexity of phosphate dynamics in both soil and plants, which involves several physico-chemical and spatio-temporal factors/traits and interactions between them. Certainly, there is an increasing need for smarter approaches to untangle the coordination between the molecular and phenotypic responses to low phosphate availability, in order to inform the development of phosphate-efficient high-yielding crop varieties.

Nearly half of the global population consume rice as the major source of their diet. Thus, the development of rice varieties able to thrive in poorer soils with less input

can significantly contribute to achieving global food security. Also, from a research perspective, rice is the ideal model to study cereal crops/monocots due to its relatively simple genetic structure.

1.1 Aims and Objectives

The aim of this research project is to make a positive impact towards sustaining food security and reducing environmental pollution by increasing understanding of the regulation of phosphate uptake principally in rice. The scope of this study stretches across physical, temporal and biological scales and combines theoretical and experimental methodologies. The specific objectives of this thesis are to:

- Develop and study parameterised mathematical models of the molecular regulation of phosphate uptake in rice, with a view to gaining a quantitative understanding of the processes involved.
- Develop and study multi-cellular models for phosphate uptake and flux using realistic root cross-sections to identify potential mechanisms by which root anatomy is influenced by and contributes to nutrient uptake.
- Generate data to study the impact of phosphate stress on the uptake dynamics of other nutrients.

1.2 Thesis outline

In this thesis, three physical (i.e. cell, tissue and whole-plant) and two biological (i.e. elements/ions and molecular) scales have been explored, under typical and deficient external phosphate conditions. This was done mainly using theoretical (mathematical, statistical and bioinformatics) approaches, but laboratory experiments were also performed to generate the data and validate some model predictions. This thesis is structured in the following manner :

Chapter 2 is derived from a review currently under revision for New Physiologist (Ajmera I.,Wu P., Hodgman TC., Lu C. 2015, submitted). It presents a detailed literature survey illustrating the extreme complexity associated with phosphorus dynamics in soil and plants, outlines the current strategies for improving phosphate use and introduces integrative systems approaches. The latter includes their prior applications in the area of plant biology and their potential role to direct and enhance research informing the development of high-yielding phosphate-efficient crops.

In Chapter 3, the development of mathematical models for the molecular regulation of phosphate uptake are described. They have been parameterised by fitting to gene expression data for miR399, PHO2 and IPS1.This study has revealed that the well established miR399-mediated regulation of PHO2 mRNA is insufficient to explain its dynamics, especially, at early times following phosphate stress. Five hypotheses have been tested mathematically of which the most likely is that a drop in cytosolic phosphate activates a repressor of PHO2 transcription. A short time-course experiment confirmed the early decline in PHO2 mRNA levels and also indicated that PHO2 might negatively regulate its own transcription.

Chapter 4 extends the previous chapter. The models incorrectly predicted the RNA profiles of PHO2 and IPS1 in response to phosphate resupply. Following sequence, structural and expression analyses, an expanded regulatory model has lead to the credible hypothesis that IPS1 RNA is protected from degradation in phosphate starved plants. The protecting agents are most likely to be phosphate-sensitive RNA-binding proteins. Chapter 3 and 4 have been structured in the style of manuscript in which the results and discussion are presented before the methods.

In Chapter 5, multi-cellular models of phosphate uptake and flux through realistic root cross-sections for *Arabidopsis* and Rice are developed. Different geometries including root hairs of different lengths and root cortical aerenchyma, have been tested to explore their effects on cytosolic phosphate levels. Chapter 5 presents the data and methods first so that it is easier to understand how the simulation results were generated. Chapter 6 concludes this thesis by compiling the findings of this work in the form of experimentally testable hypotheses and proposing future directions for extending this study.

The main body of the thesis is supplemented with six appendices. Appendix A consists of the time-series ionomics data from normal and Pi-starved plants. Appendices B and C relate to Chapter 2. Appendix B describes current strategies implemented at global, national and field scales for improving efficiency of phosphorus management, recycling and reuse. Appendix C comprises a catalogue of systematically classified, published models for various plant systems. Appendix D and E includes various supplementary information for Chapters 3 and 4, respectively.

Chapter 2

Literature Review

Abstract

This review chapter illustrates the extreme complexity associated with phosphorus dynamics in soil and plants. This includes its soil chemistry and uptake, distribution and deficiency responses in plants. After outlining the current strategies for improving phosphate use and stressing the need for translational research, integrative systems approaches are introduced. This includes their prior applications in the area of plant biology and their potential role to direct and enhance research informing the development of high-yielding phosphate-efficient crop varieties.

2.1 Introduction

On current trends, global agricultural production needs to double by 2050 to feed the projected increase in the human population (Ray *et al.*, 2013). With the advent of green revolution, crop production in past four decades kept pace with the food demand (Godfray *et al.*, 2010), but this has been through unsustainable farming practices, including deforestation, increasing use of chemical fertilisers, biocides, and modernised irrigation techniques. This has led to a loss of biodiversity, degradation of land quality, scarcity of fresh water and environmental pollution (Gregory & George, 2011). Consequently, in recent years there has been stagnation or slowing of crop-yield growth (Ray *et al.*, 2012). Indeed, the challenge now is to revive the rate of agricultural production with minimal environmental impacts, limited resources and socio-economic constraints.

Currently, agriculture practice has become highly dependent on the use of fertilisers, without which global food production would reduce to half (FAO, 2002). Particularly, the dependency on phosphate fertilisers has become unsustainable, as the stocks of phosphate ore are finite and are forecasted either to run out or become prohibitively expensive in the next 5-10 decades (Gilbert, 2009). Given the fact that phosphorus is a non-replaceable limiting resource essential for food production, global phosphorus security has a direct implication for global food security. In addition, the concern over sustainability of phosphorus also arises from environment issues such as eutrophication caused by the runoffs from the fertilised fields (Elser, 2012).

Various possible approaches have been suggested and being assessed to address this global challenge (Johnston & Steen, 2000). Most of these either aim to improve fertiliser management strategies, develop efficient recycling processes or modify plant traits (Syers *et al.*, 2008). The latter has received greater attention for several decades, but the success in terms of practical application has been limited to date (Gaxiola *et al.*, 2011).

2.2 Fate of phosphorus in soil

Phosphorus is an essential element in nucleic acids, phospholipids, phospho-proteins and metabolites. These encompass all physiological aspects of plant growth and development (Maathuis, 2009). In nature, elemental phosphorus (P) always exists in combination as “phosphate” anions. Depending on the source, phosphate in soil can be broadly characterised as organic (Po) and inorganic (Pi). Unlike other macronutri-

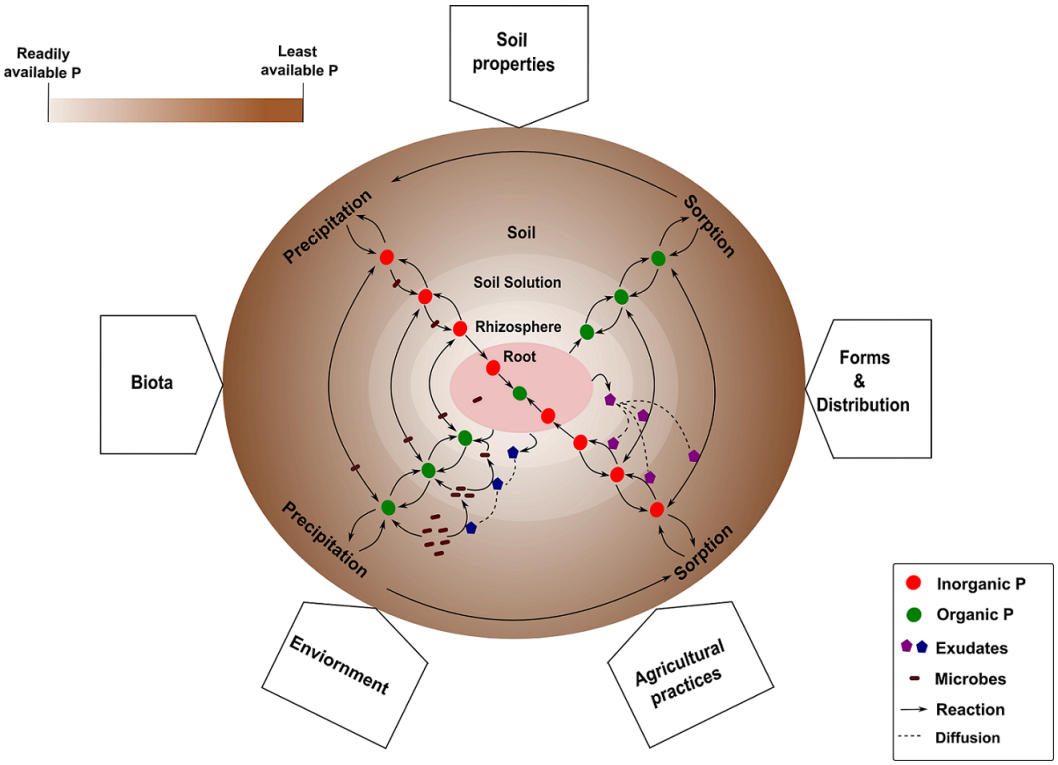

Figure 2.1: Phosphorus dynamics in soil.
The availability of P is shown as a series of concentric ellipses (in shades of brown) around a root (coloured in pink). The box on the lower right defines the entities and their reactions, while the flanking pentagons denote the factors affecting P availability.

ents, the concentration of soluble phosphate, mostly Pi, in the soil is often low, owing to its complex physico-chemistry, making it a major limiting factor for plant growth (Schachtman *et al.*, 1998) . The dynamics of phosphorus in soil is depicted in Figure 2.1 and described as follows.

2.2.1 Phosphate dynamics in soil

The dynamics of soil phosphate and its availability to plants, broadly depend upon: its forms and soil distribution, soil properties (physical, chemical and biological), environmental conditions, biotic content and agricultural practices (Ziadi *et al.*, 2013) .

Forms and distribution

Phosphorus is most abundant in the upper layers of soil, particularly in the top 15 cm and greatest in the top 5cm of soil (Jobbagy & Jackson, 2001). Distribution to any further depth in soil is either through addition of fertilisers or lysis of crop-root residues (Larsen, 1967). To some extent, its mobility and bioavailability depend upon its form. Soil phosphate can be broadly characterised as organic (Po) and inorganic (Pi), depending on their source. They differ in their behaviour and fate in soil (Shen *et al.*, 2011), but are equally adept at supplying phosphate ions. Plants prefer Pi, but Po accounts for >50% of the total soil phosphate (Schachtman *et al.*, 1998), acts as an important reservoir, and certain forms can be directly taken up by plants.

Being trivalent, phosphate is able to react with mono-, di- and trivalent cations. As a result, particles having a high anion exchange capacity (for example Al/Fe oxides and clays) will form strong bonds with phosphate producing stable compounds that are often insoluble and immobile. In contrast, anions, such as silicates, sulphates, and carbonates, compete with phosphate for sorption sites, increasing phosphate availability in the soil solution. This is known as mineralization. The presence of phosphate binding and competing particles varies with the soil type and its reaction with phosphate also depends on various other factors (Shen *et al.*, 2011).

In agronomic terms, soil phosphorus is conceptually characterised to exist in four different pools on the basis of its accessibility to plants (Johnston & Steen, 2000; Syers *et al.*, 2008). The first phosphorus pool is the soil solution from where it is immediately taken up by the roots. In the second pool, phosphorus is weakly bound to soil particles and can be readily transferred into soil solution during phosphorus limitation. Third pool consists of more strongly absorbed and less readily extractable phosphorus that can eventually become available to the plant, while the phosphorus in fourth pool has extremely low extractability, probably spanning over a period of many years. The inter-exchangeability of phosphorus between different pools mainly relates to the differences in the bonding energy for the phosphate across the various sites within the soil matrix. Often, the bound phosphorus eventually tends to form less readily soluble compounds with strong bonding energies. This lost or trapped phosphate poses environmental risk in the form of eutrophication (Johnston & Steen, 2000).

Soil properties

Mineralization and immobilisation of phosphorus occurs simultaneously in the soil and the net process is determined by soil carbon: phosphate ratio (Marschner, 2008). Besides these, the release of Pi from Po is also affected by organic matter content, soil mineralogy, soil moisture, temperature and pH (Shen *et al.*, 2011). Additionally, Pi loss is also influenced by the competition from Po for the sorption sites (Berg & Joern, 2006).

Compared to coarse-textured podzolized soils, fine-textured gleyed soil tends to release more phosphate through water extraction and allow a higher rate of diffusion. Soil aeration and compaction have opposite effects on phosphate diffusion. Compact soil has diminished pore spaces and a decreased thickness of water films on soil particles through which phosphate diffuses. This also limits oxygen in the soil, which restricts Pi absorption by roots. In contrast, well aerated soil enables roots to respire and produce the energy needed to exude metabolites that promote phosphate mineralisation. Soil pH is an important factor affecting phosphate speciation and availability. The maximum solubility and corresponding availability of Pi in most soil occur in pH range 6 – 7 (Schachtman *et al.*, 1998; Ziadi *et al.*, 2013).

Environmental effects

Soil phosphate exists as primary and secondary minerals. Primary phosphate minerals are very stable and release phosphate in the available form by a quite slow weathering process in order to meet with the crop demand. In contrast, secondary phosphate minerals have variable dissolution rates depending on the particle size and soil pH. Weathering of the parent material contributes to the pool of available soil phosphate (Cross & Schlesinger, 1995).

Low temperature and moisture reduces the availability of soil phosphorus and its uptake by plants. Seasonally snow-covered temperate soils are subjected to freezing and thawing cycles (FTCs), which stimulate soil mineralisation and lysis of residual plant cells thereby elevating available Pi and Po during early spring. With the given projection of increase in air temperature in coming decades, cold and temperate regions may encounter an increase in number of FTCs due to reduced snow coverage. This could result in either an increase in or loss by runoff of available phosphate in early spring (Ziadi *et al.*, 2013).

Drying and re-wetting cycles in soil follow rainfall of particularly high intensity and short duration. This rapidly alters soil water-content and in turn concentration

of available phosphate. During re-wetting, the levels rise as a result of disintegration of occluded soil organic matter and increased microbial activity. The latter is thought to utilise soluble organic phosphate compounds which then get released during the drying phase. Unfortunately, there is little information in the literature on the long-term impacts of climate change on this process (Ziadi *et al.*, 2013).

Biotic effects

Phosphate availability is increased by mycorrhizal symbiosis, microflora, plant root architecture and exudation. Mycorrhizal hyphae can be very long and carry Pi from large distances to the plant, in exchange for photosynthate. Soil biota slowly convert Po into Pi by mineralisation, thereby increasing phosphate levels, and it has been observed that the Po fraction drops during crop growth. The release of exudates from root and biota reduce the pH with the effect of solubilising Pi, and the root structure provides a network for rain water to get to where it will most benefit phosphate solubilisation. Altogether, these biological controls significantly alter soil physico-chemical properties and phosphate availability (Hinsinger *et al.*, 2015; Richardson *et al.*, 2011).

Effect of agricultural practices

The first and second pools of soil phosphorus contribute most toward available phosphate. It is, therefore, important to determine soil phosphate levels so that the optimum level of fertiliser can be applied to the soil. The level achieving 90-95% of maximum crop yield is referred to as "critical soil-P level", and several tests have been developed for this purpose (Kruse *et al.*, 2015; Wolf & Baker, 1985). The interpretations of different tests might vary and do not always correlate. In long-term field experiments on four different soil types, the critical soil-P ranged from 10 to 28 mg/kg for the optimal yields of wheat, maize and rice (Bai *et al.*, 2013).

The type of mineral phosphate fertiliser significantly affects the soil physico-chemical properties (Shen *et al.*, 2011), thus, it is essential to identify an appropriate sort for the soil properties in the field. In acidic soil, the application of powdered phosphate rock showed relatively efficient crop growth, though, even after applying bulk quantities of mineral fertilisers, crops barely capture 15-20% of the total phosphate applied (Schachtman *et al.*, 1998). Other ions are also applied in fertilisers. These might not only affect the soil chemistry, as noted above, but also the ability of crops themselves to take up phosphate. Thus, sufficient nitrate is needed for efficient phosphate acquisition (Panigrahy *et al.*, 2009).

Agricultural practices such as crop rotation, tillage and fertilisation also have an impact on phosphate availability. Crop species and varieties vary in their root systems and soil organic-matter deposition, which affect both their uptake efficiency and the available-phosphate level. To avoid stratification in the topsoil, ploughing and harrowing (i.e. tillage) allow the mixing of phosphate throughout the ploughing layer (10-20 cm)

2.2.2 Phosphate dynamics in rhizosphere

The volume of soil around living roots that is directly influenced by various root activities, including growth, uptake, respiration and rhizo-deposition, is referred to as the rhizosphere (Hinsinger *et al.*, 2005, 2015; McNear Jr., 2013). Depending on the considered activity, this root-soil interface ranges from the sub-µm to supra-cm scale (Hinsinger *et al.*, 2009). It forms the primary site for nutrient availability (Syers *et al.*, 2008). To meet with plant demand, soluble phosphate in the soil solution should be replaced 20 to 50 times per day by delivering more from bulk soil into the rhizosphere. Owing to its low availability and slow diffusion (10^{-12} to 10^{-15} $m^2 s^{-1}$) in soil, high phosphate uptake rates create a depletion zone (~ 0.2 - 1 mm) and concentration gradient away from the root surface in the rhizosphere. The above mentioned biotic effects particularly come into play here.

2.3 Fate of phosphate in plants

2.3.1 Phosphate dynamics in tissues, cells and organelles

The primary sites for phosphate uptake from the soil solution are the root tips, epidermal cells (especially those with root hairs) and cortical cells via apoplastic diffusion (Raghothama & Karthikeyan, 2005). As the concentration of phosphate ions in soil solution and apoplasm ($<10\,\mu M$) is far less than that in cytosol ($5-17\,mM$), epidermal and cortical cells acquire phosphate against an electrochemical potential gradient using an active co-transport process (Schachtman *et al.*, 1998). Inside the cell, Pi participates in various processes with destinations being dependent on the tissue type and metabolic requirement. It will also move towards the stele via plasmodesmata to supply phosphate to the rest of the plant (Smith, 2002; Smith *et al.*, 2003). However, it is used to produce nucleic acids, phospholipids, metabolites such as P-esters and phosphorylated proteins (Veneklaas *et al.*, 2012).

For proper functioning of plant processes, it is essential to maintain Pi homeostasis. Within cells, this is achieved by tightly regulating the phosphate concentration in each organelle. On entering a cell, Pi traverses the membrane of different organelles in exchange for other solutes or protons. In Pi sufficient conditions, vacuoles serve as the storehouse, accounting for 85-95% of total cellular phosphorus (Pratt *et al.*, 2009). They act as a source or sink to maintain cytoplasmic phosphate levels. Vacuolar Pi uptake occurs via both ATP- and pyrophosphate-responsive proton pumps that exhibit saturation kinetics with a Km of $\sim 5\,mM$ (Rausch & Bucher, 2002). Translocation by chloroplastic and Golgi phosphate transporters can affect Pi allocation across the plant (Shen et al., 2011). Though mitochondria are a major site for metabolism, little is known about Pi transport across the mitochondrial inner membrane (Poirier & Jung, 2015; Zhu *et al.*, 2012).

2.3.2 Phosphate dynamics across whole plant

The concentration of Pi in xylem ranges from 1 to $7\,mM$ in phosphate deficient and sufficient plants, respectively (Mimura *et al.*, 1996). The gradient of hydrostatic pressure and water potential in the xylem drives the transport of Pi across the plant in response to physiological demand (Smith *et al.*, 2003). Phosphate can be transferred between phloem and xylem via the few intermediary cambial cells separating them, so that it can reach the tissues where it is most needed. In Pi sufficient conditions, root-acquired Pi is transported to the younger leaves through the xylem, while phosphorus from older leaves is returned to the phloem as a mixture of Pi and Po. When shoot-to-root translocation exceeds demand in the root, a considerable transfer of Pi back to the shoot via the xylem is suspected to occur in roots (Schachtman *et al.*, 1998).

In the life cycle of a plant, most phosphate is absorbed during the vegetative phase of growth. During the reproductive stages, approximately 65-85% of this phosphate is remobilised as salts of K, Mg, Fe and Zn to the developing seed in the form of phytic acid (Raboy, 2009). The enzyme phytase releases the phosphate from the grain during germination. Hence, seed phytate is the major source of phosphorus to support seedling establishment, especially in P-deficient soil (Marschner, 1995).

2.4 Response to phosphate starvation

Since the concentration of phosphate in soil solution is quite low (Pierre & Parker, 1927), plants are often prone to phosphate stress. Being essential for growth and development, phosphate uptake and utilisation need to be tightly regulated. The concentration of cytosolic phosphate is generally thought to remain constant under normal circumstances (Raghothama, 1999) though on short time scales fluctuations have been observed (Pratt *et al.*, 2009). This involves transport of phosphate between various inter- and intra- cellular phosphate pools (Mimura, 1999, 2001) .The membrane-bound phosphate transporters are regulated by various genes, discussed below.

When phosphate is abundant, its rate of absorption exceeds demand. Under such conditions, plants prevent phosphate toxicity by reducing uptake from the soil, increasing phosphate efflux and storage in the vacuoles (Schachtman *et al.*, 1998). Conversely, under limiting conditions, plants maintain cytosolic phosphate levels in several ways: eliciting processes to facilitate the availability of external phosphate and increasing its uptake, recycling and consumption of nonessential molecules containing phosphorus (Sánchez-Calderón & et Al., 2011). These processes principally take place at three sites, which will be considered in turn.

2.4.1 Shoot

With the depletion of vacuolar phosphate reserves, a lack of cytoplasmic phosphate reduces photosynthesis (Foyer & Spencer, 1986), eventually inhibiting plant growth and development. Typical phenotypic symptoms of phosphate deficiency include stunted shoot growth and branching, dark to blue green colouration of leaves, weaker and thin stems, reduced tillering, imperfect pollination, fewer flowers, delayed maturity, poor grain quality and low yield (Kennelly *et al.*, 2012). Phosphorus deficiency in leaves may interfere with the normal opening of the stomata and compartmentation of Pi leading it to be in cytosol and chloroplasts, presumably for metabolic processes (Hernandez & Munne-Bosch, 2015; Pratt *et al.*, 2009). It triggers senescence of older leaves, mobilising phosphate from older to younger leaves, meristems, flowers and seeds (Smith, 2002). Moreover, starved plants translocate roughly half of the phloem-derived Pi back to the xylem (Jeschke *et al.*, 1997) .

At the cellular level, various physiological changes are triggered, such as reduced photosynthesis, increased sugar concentration, accumulation of anthocyanin, transfer of di-galactosyl-diacyl-glycerol (DGDG) galactolipid from chloroplasts to mitochondria and release of vacuolar phosphate that may be insufficient to compensate for

the decreasing cytosolic Pi levels (Jouhet *et al.*, 2004; Zhang *et al.*, 2014). Besides these, alteration in the expression of development and shoot-specific genes has been observed (Hammond *et al.*, 2003). Currently, the molecular mechanism underlying local phosphate sensing and signalling in the shoot remains unknown.

2.4.2 Root

Persisting phosphate deficiency alters the Root System Architecture (RSA) by stimulating lateral-root development, expanding the absorptive root-surface area by increasing both root-hair length and density, and in some species, attenuating primary root elongation and development of cluster roots (Lambers *et al.*, 2011; Niu *et al.*, 2012; Péret *et al.*, 2011).

Generally, RSA is under the regulation of developmental and hormone related genes Svistoonoff *et al.* (2007) . In addition, cell division is perceived to govern phosphate demand in growing organs and determines the magnitude of expression of Phosphate Starvation Induced (PSI) genes (Lai *et al.*, 2007) . On sensing low phosphate, a reduced rate of root cell elongation and progressive exhaustion of root meristematic cells causes attenuation of primary root growth (Ticconi *et al.*, 2009) . Along with the proliferation of lateral roots, this leads to shallow root systems allowing better exploration for phosphate in the top soil (Williamson *et al.*, 2001). Moreover, lateral roots promote phosphate solubilisation by secretion of exudates (Niu *et al.*, 2012). In general, this includes organic anions (malate, citrate and oxalates), enzymes (phosphatase, phytases), phenolic acids and protons (Richardson *et al.*, 2011). Owing to the exhaustion of primary root meristem, mitotic activity is shifted to the site of lateral root formation, thereby increasing their number (Sánchez-Calderón *et al.*, 2005). Each lateral root then behaves like a primary root, eventually growing more lateral roots of its own (Lopez-Bucio *et al.*, 2002).

Root-hair proliferation is arguably the most characteristic local response to phosphate deficiency and is regulated by an array of cellular and genetic processes (Foreman & Dolan, 2001; Schiefelbein & Somerville, 1990) . Under phosphorus stress, the emergence of root hairs closer to root tips increases the root surface area, elevating the potential for phosphate uptake (Ma *et al.*, 2001). The final length of root hairs is related to the level of metabolic activity in these cells, which is elevated under phosphate stress. These cells may eventually die off, providing anchorage to the roots and their nutrients used elsewhere in the plant. Along with root hairs, cluster or secondary roots are a feature of some plant species that play a key role in phosphate uptake. Internal phosphate is known to regulate cluster/secondary root formation (Niu *et al.*,

2012). Enhanced phosphate uptake inhibits the formation of cluster/ secondary roots thereby removing the need to invest energy and material in their growth.

All the above changes are the results of various cellular and sub-cellular modifications. Thus, it is important to understand the fate of individual tissues in response to phosphate stress, especially the epidermis and pericycle, see Figure2.2, and cortex (see below). Cell division and rate of elongation are reduced significantly modifying the root anatomy, as observed in longitudinal and transverse sections (Ma *et al.*, 2001). In *Arabidopsis*, these modifications result in more cortical cell files and smaller epidermal cells, thereby increasing root-hair density (Ma *et al.*, 2003).

Under mild phosphate stress, lateral root formation is stimulated prior to the attenuation of primary root growth in *Arabidopsis* (Lopez-Bucio *et al.*, 2002). Moreover, in response to various stresses, cortical cells undergo programmed cell death forming aerenchyma in many species (He *et al.*, 1992). Certainly, these architectural and anatomical adaptations have underlying molecular mechanisms which still remain ambiguous (Zhang *et al.*, 2014).

2.4.3 Rhizosphere

Plants also respond to phosphate deficiency by altering the biochemical environment of the rhizosphere (Javot *et al.*, 2007). This involves exudation of organic anions, principally malate or citrate, and enzymes such as phosphatases, which competitively bind with the cationic phosphate partners and liberate the phosphate from organic compounds, respectively(Dakora & Phillips, 2002; Tomscha *et al.*, 2004). Some exudates promote recruitment of soil microbes by providing a carbon source and chemoattractants (McNear Jr., 2013), for example, strigolactones (Czarnecki *et al.*, 2013). These microbes in turn release exudates, which solubilise inorganic and organic phosphate substrates (Richardson *et al.*, 2011).

Commonly, plants use fungal symbionts, Arbuscular Mycorrhizal Fungi (AMF), to enhance phosphate and other nutrient forage and acquisition. AMF grow within root cortical cells and subtends hyphae far into the soil (Smith *et al.*, 2011). Influx of P in roots colonized by mycorrhizal fungi is 3-5 times higher than in non-mycorrhizal roots. In response to low phosphate, exuded strigolactones stimulate hyphal AMF branching thereby attracting them to the plants (Brewer *et al.*, 2013). The consequent interplant root-hyphal network offers increased exploration for soil phosphate (Paszkowski & Gutjahr, 2013).

Upon AMF colonisation, some phosphate transporters are repressed, particularly

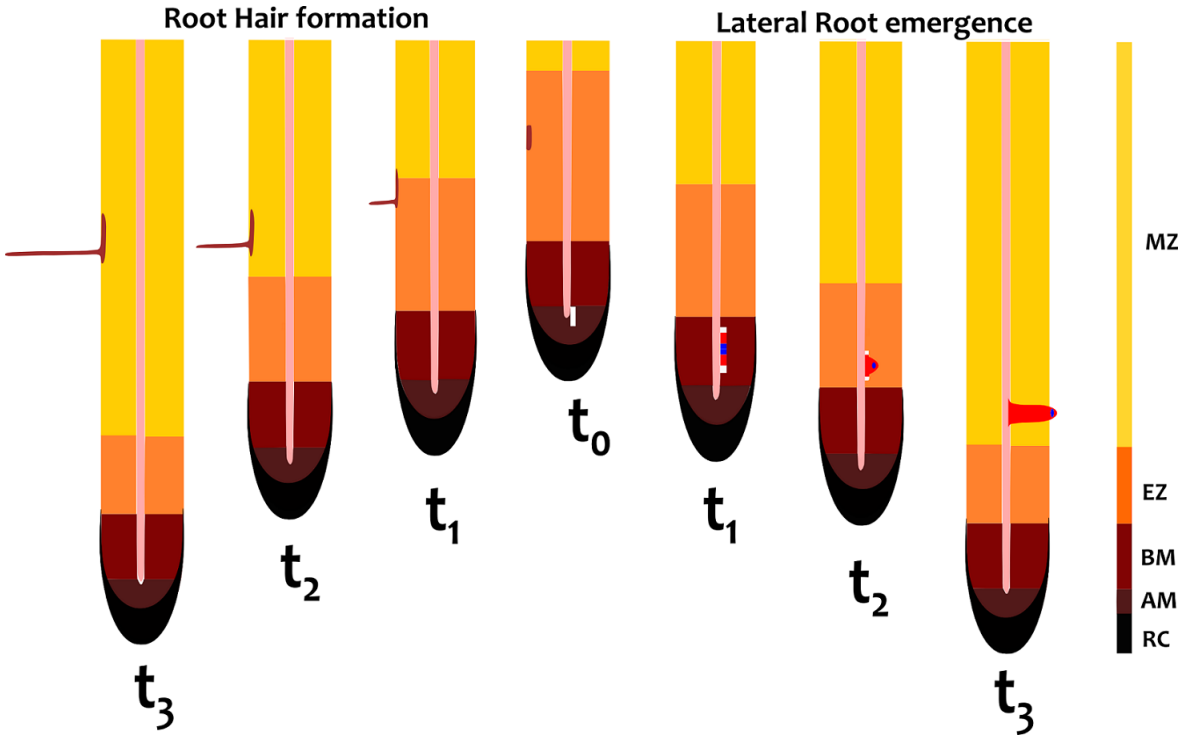

Figure 2.2: Root hair and lateral development under phosphate stress.
The stages of root hair and lateral root development are depicted at four times (t0 – t3) from the onset of phosphate depletion. The Root Cap, Apical Meristem, Basal Meristem (sometimes referred to as the Transition Zone), Elongation Zone, Mature Zone and vasculature are respectively coloured in black, dark red, orange yellow and pink. As time progresses, the lengths of the meristem and elongation zone get shorter. A root hair starts to grow at the end of the elongation zone and under normal conditions would reach the length seen at t2, though under phosphate starvation grows to almost twice the length as seen at time t3. In the case of a new lateral root, the founder cell is shown in white, the developing quiescent centre in blue and the rest in red. It is initiated at an early stage of phosphate stress, but does not emerge until considerably later and at a place where exudates have had time to solubilise some of the soil phosphate.

in the epidermis, while several phosphate-starvation-induced genes are activated, including P-type H+ ATPase, mycorrhizal-induced phosphate transporters and phosphatases (Zhang *et al.*, 2014). Furthermore, with the high availability of phosphate in the soil, the rate of AMF colonization decreases perhaps due to decrease in root exudation (Smith *et al.*, 2011). Besides phosphate uptake, the AMF also influences root system architecture, most prominently, by enhancing lateral root formation. The mechanism of AMF colonisation and its associated effects on phosphate uptake and RSA has been extensively reviewed by (George *et al.*, 1995; Paszkowski & Gutjahr, 2013)

2.4.4 Integrated response

All the above PSRs act at different scales (Figure2.3). Plants integrate intrinsic and extrinsic factors eliciting such responses to counter phosphate stress. This relies on both local and systemic sensing/signalling mechanisms that monitor external and internal phosphate status. External phosphate is sensed by a local system, mainly in the root-tip, and independently modulates primary growth and root hair development in *Arabidopsis* (Chiou & Lin, 2011). Along with genetic regulation, hormone dynamics play an important role in such local responses, see Figure2.4.

Internal phosphate status is governed by systemic signalling, to increase phosphate availability, recycling, uptake and transport (Lin *et al.*, 2013). This involves metabolic reprogramming, degradation of expendable nucleic acids and de-repression of high-affinity phosphate transporters (Panigrahy *et al.*, 2009), see Figure2.4. Moreover, lateral and cluster root growth are also partially regulated at a systemic level (Zhang *et al.*, 2014).

Systemic signalling (Figure2.3b) integrates the local responses across the plant by trafficking various signals through the vasculature. This encompasses phloem-mediated shoot-to-root signals (miRNAs, sugars and CAX - Ca^{2+}/H^{+} transporters) and xylem-mediated root-to-shoot signals (phosphate, cytokinins and strigolactones). A large body of work has been done on systemic signalling and has been reviewed elsewhere (Lin & Chiou, 2008; Lin *et al.*, 2013).

Phosphate deprivation triggers various metabolic modifications, especially in shoot, to increase mobilisation and reduce utilisation of internal plant phosphate (Jones *et al.*, 2015; Plaxton & Tran, 2011). Primarily, photosynthesis, glycolysis and respiration are affected. These result in lower requirement for orthophosphate or adenylates, remobi-

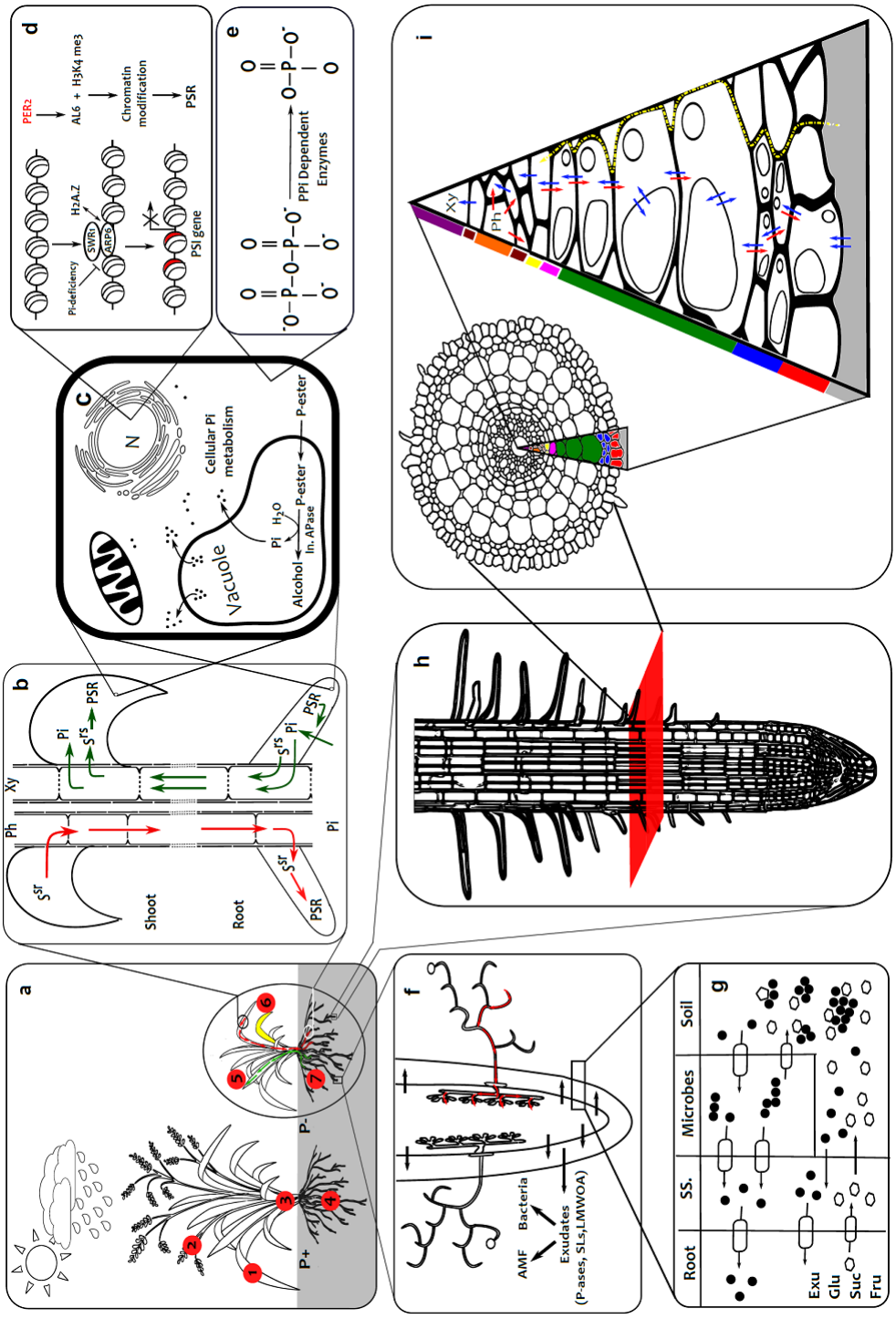

Figure 2.3: Integrated overview of phosphate starvation responses.

Figure2.3 Integrated overview of in phosphate starvation responses.The responses and signalling mechanisms operate at a range of scales and different locations which are depicted in nine connected panels: (a) denotes the whole plant and field scale; the numbers in red circles represent under normal and low-phosphate conditions (1) phosphorus playing a major role in various plant growth and developmental process including photosynthesis; (2) the highest level of phosphate being found in the vegetative parts of the young plant, which on maturation move into (3) fruit and seeds; (4) root development correlating with phosphate levels; (5) phosphate helping to increase water use efficiency and contribute to disease resistance; (6) abnormal leaf discolouration under low phosphate conditions; and (7) shallow root system with more root hairs and lateral roots. (b) denotes the whole plant scale with systemic signals SSR from shoot through the phloem to the root and SRS from the root to the shoot through the xylem, inorganic phosphate (Pi), and of course water and other nutrients also go up to the shoot by this route. (c) denotes cells from any part of the plant which respond to phosphate deprivation altering lipid content, releasing phosphate stores from the vacuole where phosphate is liberated from esters by Acid phosphatases (APase). (d) denotes the epigenetic effects (principally chromatin modification) that influence transcription of PSR genes. (e) denotes the pyrophosphate-dependent glycolytic bypass enzymes and metabolic inorganic phosphate recycling system. (f) denotes rhizosphere activities, specifically the exudation of acid phosphatases (P-ases), Strigalactones (SLs) and Low Molecular Weight Organic Acids (LMWOA) which stimulate bacterial activity and attract Arbuscular Mycorrhizal Fungi (AMF) that form arbuscular structures within the root – mycorrhizal delivery of phosphate is depicted in red. (g) denotes a close-up view of the rhizosphere boundaries between the root, soil sheath (SS), microbes and soil where exudates and sugars (Glu – glucose, Suc – sucrose and Fru – fructose) are secreted through efflux transporters respectively to solubilise phosphate compounds and stimulate bacteria to do the same and phosphate is imported through transporters of varying affinity; the exudates/sugars, transporters and phosphate are respectively depicted by hollow ellipses, lozenzes with directional arrows and black circles. (h) denotes the alteration in meristem and elongation zone length and the formation of root hairs. (i) denotes a cross section through a root and the paths taken during phosphate uptake: the positions of different tissues within a root, namely epidermis, exodermis, schlerenchyma+ cortex, endodermis, pericycle, phloem, cambium and xylem are marked respectively by red, blue, green, pink, yellow, orange, pale brown and purple; and transport of shoot-to-root signal molecules, symplastic/interorganellar phosphate and apoplastic phosphate are depicted respectively by red, blue and dashed yellow arrows.

lization of phosphate, conversion of phosphorylated glycolytic intermediates to sugars and organic acids and modulation of various primary and secondary metabolite concentrations (Morcuende *et al.*, 2007; Plaxton & Carswell, 1999). The primary metabolites includes polyols, organic acids, amino acids, polyhydroxy-acids, fatty acids, nitrogenous compounds and phosphates, while secondary metabolites includes glucosinolates, benzoides, phenylpropanoids and flavonoids (Pant *et al.*, 2015).

Interestingly, the concentration of sugars, particularly sucrose, increases in the shoot in response to low phosphate (Hammond & White, 2008) and has implications for the transcriptional reduction of photosynthesis (Hermans *et al.*, 2006)and transcriptional elevation of sulfolipids, galactolipids, phosphatase, RNase, phosphoenolpyruvate carboxylase (PEPcase), anthocyanins and inorganic phosphate transporters (Karthikeyan *et al.*, 2007; Solfanelli *et al.*, 2006). Such alterations recycle substantial amount of phosphate by compensating for phosphate precursors, protect nucleic acids and chloroplast against photo-inhibition and facilitate phosphate availability in and uptake from the rhizosphere (Hammond *et al.*, 2004; Hernandez & Munne-Bosch, 2015). Furthermore, the export of triose-phosphates from the chloroplast is reduced, producing starch and releasing phosphate (Natr, 1992). Although hexokinase activity is down-regulated under phosphate stress (Rychter & Randall, 1994), its role in sugar mediated phosphate starvation signalling is unclear (Hammond & White, 2008).

Increased shoot sucrose up-regulates the expression SUC2 transporters proteins, which transfer sucrose to the phloem (Lloyd & Zakhleniuk, 2004) serving as a systemic signal (Muller *et al.*, 2007). This correlates with the expression of various PSI genes, giving several of the root and rhizosphere responses described above (Hammond *et al.*, 2003; Obata & Fernie, 2012; Ticconi & Abel, 2004). Sucrose has been postulated to be a phosphate sensor. However, its effect is downstream of the initial phosphate sensing (Muller *et al.*, 2007), negating this notion.

Phosphate deficiency triggers a cascade of responses involving a large number of genes (Rojas-Triana *et al.*, 2013), summarised in Figure2.4, while there are tissue-specific difference in the expression levels of PSR genes under normal conditions, presented in Table2.1, revealing a greater level of complexity in the system. PSR genes are classified as early or late in expression (i.e. within few hours or over one day of phosphate depletion) and whether they are shoot-, root- or non-specific. In *Arabidopsis*, the early genes encode protein kinases, Transcription Factors of the MYB, ERF, WRKY and bHLH families, phosphate transporters, exudates, membrane remodelling and the initiation of lateral root formation (whose emergence is not until

later times). The late responsive genes mainly encode the downstream regulators for phosphate transport, recycling and metabolic bypass processes (Chiou & Lin, 2011; Lin *et al.*, 2009). Recently, OsCSLF6, a cellulose-synthase like protein, has been identified in rice, which was found to affect Pi accumulation and root development, by modulating carbon metabolism (Jin *et al.*, 2015). This novel understanding has opened a new avenue for research.

On locally sensing low phosphate around the root tip, the activities of PDR2, LPR1/2, SCR and SHR attenuate primary root growth in *Arabidopsis* (Chiou & Lin, 2011; Scheible & Rojas-Triana, 2015). In roots, persisting low phosphate elicits expression of genes involved in phosphate uptake, exudation and, importantly, hormone regulation leading to altered RSA. In addition to PSR genes, chromatin remodelling, post-transcriptional and post-translational modifications also play an important in regulating PSRs (Lan *et al.*, 2015; Plaxton & Shane, 2015).

The core pathway underlying phosphate acquisition involves dissociation and sequential sumoylated activation of a Phosphate-Responsive transcription factor (named PHR1 in *Arabidopsis* and PHR2 in rice) (Rubio *et al.*, 2001). This triggers a network of responses that include gene activation, microRNA-mediated repression, a reduction in directed ubiquitination and active trafficking of phosphate transporters to the plasma membrane (Liu *et al.*, 2014). Furthermore, recent study on *Arabidopsis* indicates PHR1 as a prominent factor for metabolic reprogramming under phosphate stress (Pant *et al.*, 2015). However, the molecular mechanism underlying this interplay is yet to be deciphered.

Gene	MSU id (LOC_Os)	EES	Cortex	EPS
ARP6	01g16414			
At4**	03g05334			
bHLH32	03g15440			
CAX1	11g05070			
CAX3**	02g21009			
IPK1	04g56580			
IPS1**	03g05334			
LPR1	01g03530			
MYB62**	01g03720			
PHF1	07g09000			
PHO1	02g56510			
PHO2	05g48390			
PHR1	03g21240			
PHR2	07g25710			
PHT1;1**	04g10800			
PHT1;2	03g05620			
PHT1;4	04g10750			
PHT1;6	08g45000			
PHT1;8	10g30790			
PHT2;1**	02g38020			
PLD1	05g29050			
PTF1	06g09370			
SIZ1	05g03430			
SPX1	06g40120			
SPX3	10g25310			
SQD1	07g01030			
ZAT6**	03g32230			

Very high | High | Medium | Low | Very low | Nil

Table 2.1: Expression of PSI genes in rice root tissues under normal conditions. EES: Epidermis, Exodermis, Sclerenchyma ; EPS: Endodermis, Pericycle, Stele **Overall expression is very low, relative differential expression in shown Note: The table is generated using the dataset available on RiceXPro database (ricexpro.dna.affrc.go.jp). This gene expression dataset represents different tissue types from root tip and elongation zone, under normal conditions

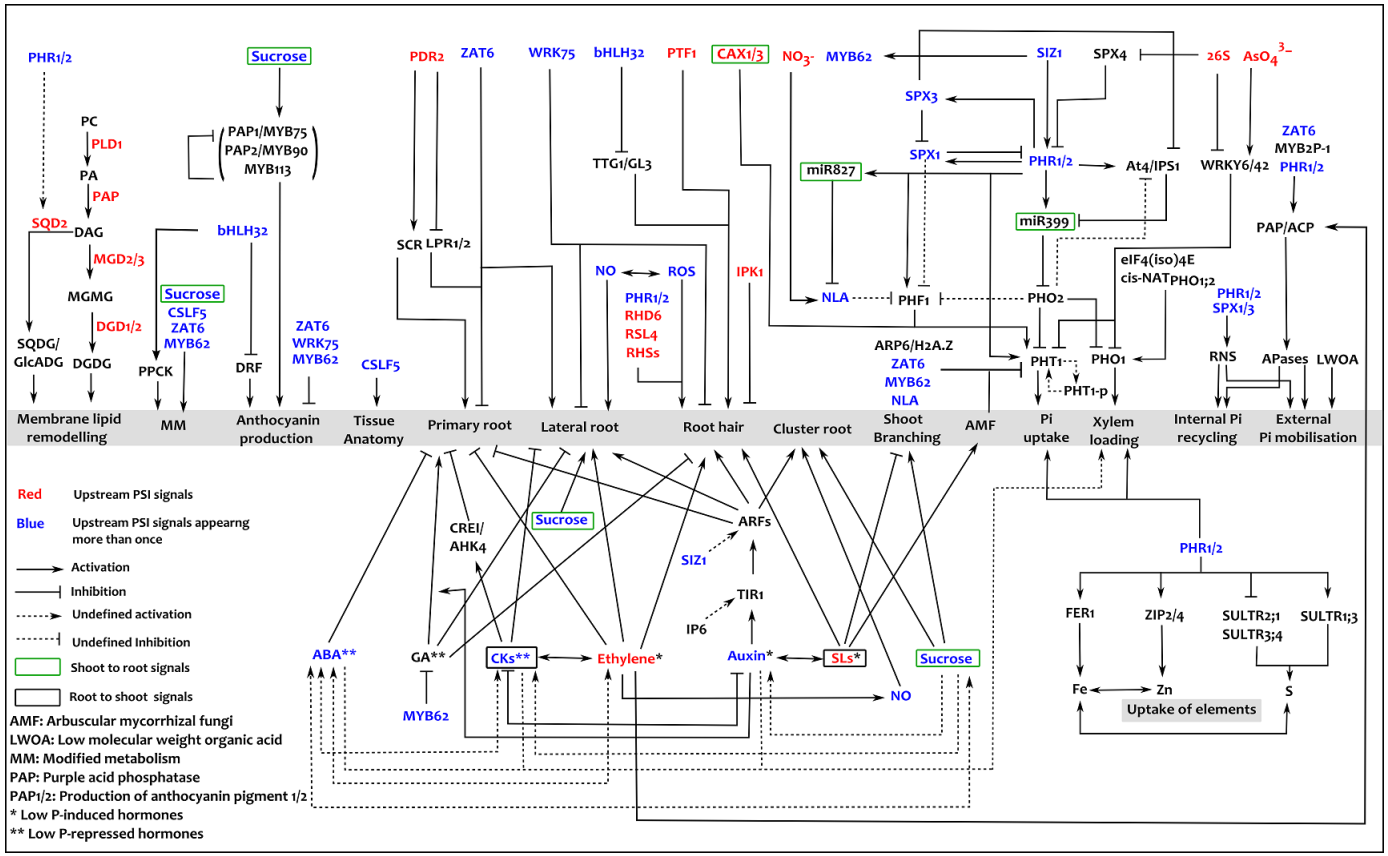

Figure 2.4: Molecular signalling in phosphate starvation responses.
The different responses are specified in the grey bands, with hormonal regulation and transcription factor/signal/enzyme regulation delineated respectively below and above; the upstream signal and regulators are denoted in red and blue depending on whether or not they feature one or more than once in the network, with some in green and purple boxes respectively to denote shoot-to-root and root-to-shoot systemic signals; the types of edges (interactions) and meaning of the acronyms are shown in the key on the lower left.

2.4.5 Core regulators of Pi-starvation responses

Various regulators (genes, transcripts, miRNA, proteins, hormones and ions) relevant to Pi-stravation responses are depicted in Figure2.4. Each of these regulators are briefly described as follows:

PHR1/2 Phosphate starvation Response-1 (PHR1) gene encoding a MYB transcription factor is the key regulator component that binds to P1BS DNA motif of PSR genes, prompting series of adaptive responses against Pi stress in plants. Based on amino acid sequence homology, two PHR genes, OsPHR1 and OsPHR2 were identified in Rice, of which OsPHR2 is the orthologue of AtPHR1. Both AtPHR1 and OsPHR2 genes encoding MYB protein are involved in Pi signalling pathways and regulates other PSR genes. Overexpression of only OsPHR2 results in increased Pi accumulation in the shoot while mimicking Pi starvation responses under sufficient Pi conditions. PHR1 is a key transcriptional activator regulating Pi uptake, mobilisation, anthocyanin accumulation and carbon metabolism (Bari *et al.*, 2006; Rubio *et al.*, 2001; Zhou *et al.*, 2008).

SIZ1 As the expression of AtPHR1 is independent of Pi status, post-translational modification is suggested to be the regulatory factor for PHR1 activity. Supporting this hypothesis, the SIZ1 gene, encoding a SUMO E3 ligase, was identified as the post-translational regulator for PHR1 protein. Proteomic identification of *in-vitro* sumoylated Arabidopsis proteins found modifications to AtPHR1 as predicted by sequence motif analysis (Miura *et al.*, 2005). SIZ1-mediated sumoylation is involved in PSRs both dependent and independent PHR1. Besides Pi deficiency, SIZ1 is also involved in other oxidative stress responses such as salt, drought and cold (Miura & Ohta, 2010; Miura *et al.*, 2007, 2011a, 2013). Under Pi stress, SIZ1 negatively regulates root architecture remodelling, by preventing auxin patterning, and anthocyanin accumulation. This suggests that SIZ1 acts as both negative and positive regulator for different Pi stress responses by activating or repressing PSR genes (Miura *et al.*, 2011b). Furthermore, increased expression of certain PSR genes in Atsiz1 mutants represents SIZ1 as a downstream regulator of Pi starvation sensing mechanism, while the expression of genes that are not specifically involved in Pi starvation responses indicates that SIZ1 may be a critical upstream regulator for such determinants (Castro *et al.*, 2012).

miR399 In plants, different stress conditions up-regulate the expression of specific miRNAs that contributes to stress-adaptation responses, by reducing the availability of its target mRNAs. These short, non-coding regulatory RNAs recognize specific mRNA through target mimicry, leading to translational repression or site-specific cleavage. The microRNAs are one of the key regulators involved in Pi-deficiency signalling and regulation of Pi homeostasis. Under Pi stress, miR399 is specifically up-regulated by MYB transcription factor PHR1. Although miR399 is expressed in both roots and shoot tissues, its expression levels remain relative high in shoot. Mature miR399 is translocated via the phloem to the root system, where they elicit appropriate action. This movement of miR399 serves as the systemic signal for increasing Pi uptake by roots while communicating between shoots and roots, and maintaining Pi homeostasis. Six members of miR399 family are found in Arabidopsis while there are eleven members in rice(Aung *et al.*, 2006; Bari *et al.*, 2006; Franco-Zorrilla *et al.*, 2007; Kuo & Chiou, 2011; Lin *et al.*, 2008; Pant *et al.*, 2008).

PHO2 PHO2 mRNA has five miR399 binding sites in it 5' untranslated region. Both PHO2 and miR399 are co-localized, mainly in vascular tissues but are expressed in opposite fashion. PHO2 encodes an ubiquitin-conjugating E2 enzyme (UBC24) that causes degra- dation of Pi transporters and other gene products involved in translocating Pi from root to shoot. In roots, miR399 binds to PHO2 transcript resulting in the formation of silencing complexes (double stranded RNAs) that are eventually cleaved. The absence of UBC24 proteins promotes expression of transporter proteins, facilitating increased Pi uptake (Aung *et al.*, 2006; Bari *et al.*, 2006; Hu *et al.*, 2011).

At4/IPS1 At4/IPS1 expression is activated by SUMOylated PHR1 and its transcript negatively regulates miR399 activity in order to maintain optimum Pi levels. At4/IPS1 transcript being partially complementary to miR399 is unable to cleave miRNA but rather sequester it. At4/IPS1 thus functions as a riboregulator, interrupting miR399-PHO2 binding. This concomitantly reduces Pi uptake and shoot Pi content. In Pi deficient conditions, At4/IPS1 is upregulated in order to prevent Pi toxicity by lowering the availability and activity of miR399 (Franco-Zorrilla *et al.*, 2007; Hou *et al.*, 2005; Shin *et al.*, 2006).

PHT In higher plants, Pi absorption is mediated by two types of Pi and H+ symporters: low affinity and high affinity Pi transporters, acting constitutively and under low Pi conditions, respectively. Among all Pi transporters families in plants (PHT1-PHT4), members of the PHT1 family form integral membrane proteins involved in

Pi uptake and translocation across the plant. Arabidopsis and rice respectively have 9 and 13 members in their PHT1 families. Of the rice transporters, OsPHT1;2 and OsPHT1;6 are highly induced by Pi starvation. OsPHT1; 6 is involved in Pi uptake and translocation across the plant whereas OsPHT1; 2 is a low-affinity Pi transporter involved in translocation of stored Pi in plant. OsPHT1; 8 is distinctly expressed in various tissues and organs in order to regulate Pi homeostasis while OsPHT1; 11 and OsPHT1; 13 are AMF-induced. More details pertaining to PHT1 transporters can be found in review by (Nussaume *et al.*, 2011; Poirier & Jung, 2015).

In PHT2 family, only PHT2; 1 has been functionally characterised. PHT2; 1 is a low-affinity Pi transporter, preferentially expressed in chloroplast (Versaw & Harrison, 2002). PHT3 proteins belong to mitochondrial phosphate transporter family, mediating the mobilisation of Pi across inner mitochondrial membranes (Poirier & Bucher, 2002). A fourth family, PHT4, has been characterised in Arabidopsis and play a role in Pi transport between the cytosol and chloroplasts, plastids and Golgi complex (Guo *et al.*, 2008). Additionally, Phosphate Transporter Traffic Facilitator (PHF1) has been identified to play a role in transfer of PHT1 transporters proteins from ER to the plasma membrane, enabling Pi uptake (Bayle *et al.*, 2011; Gonzalez *et al.*, 2005)

PTF1 OsPTF1, a rice bHLH transcription factor, is Pi-starvation induced in roots and shoots. Overexpression of OsPTF1 enhances plant tolerance to Pi stress by elevating tillering ability, root-to-shoot ratio and phosphate content in plants. Under low Pi conditions, this mutant showed a significant increase in root surface area, leading to high Pi uptake, but no high-affinity Pi transporter genes were up-regulated. Moreover, OsPTF1 also regulates the expression of genes involved in the efficient utilization of absorbed Pi in plant (Li *et al.*, 2011; Yi *et al.*, 2005).

MYB62, WRKY75, bHLH32 and ZAT6 In addition to PHR1/2, other transcription factors from MYB, WRKY, bHLH and C2H2 ZFPs families also acts as the key components in PSRs. In Arabidopsis, overexpression of MYB62, a phosphate-starvation-induced (PSI) transcription factor, negatively regulates the expression of several PSR genes and suppresses GA biosynthesis. MYB62 is, thus, presumed to link GA signalling and PSR (Devaiah *et al.*, 2009). Plant-specific WRKY transcription factor family are involved in various stress responses. WRKY75 is involved in modulation of Pi acquisition by positively regulating several Pi starvation responses. In contrast, WRKY75 negatively controls lateral-root and root-hair growth independently of Pi

status. WRKY6 and WRKY42, are involved in PSR by regulating the expression of PHO1. In normal conditions, WRKY6 inhibits PHO1 transcript by binding to its promoter to maintain Pi homeostasis. During Pi stress, PHO1 inhibition is relieved by 26S mediated proteolysis of WRKY6 proteins, enabling xylem loading and translocation of Pi from root to shoot (Chen *et al.*, 2009; Devaiah & Raghothama, 2007; Devaiah *et al.*, 2007b).

Of the two Pi deficiency induced bHLH transcription factors, bHLH32 serves as the negative regulator while OsPTF1 is the positive regulator. In Arabidopsis, bHLH32 represses a wide range of biochemical and morphological Pi-starvation-induced processes. It down-regulates the expression genes encoding phosphoenolpyruvate carboxylase kinase (PPCK) that modifies the metabolism to secure optimal Pi levels. PPCK genes are upregulated by TTG1 and GL3 which interact with bHLH32. Besides this, FXB2 also interacts with bHLH32 and negatively regulates PSRs. Altogether, it is suggested that FBX2 can potentially recruit bHLH32 triggering degradation of other bHLH32 interacting protein, i.e. TTG1 and GL3, thereby modulating PSR (Chen *et al.*, 2007, 2008).

ZAT6, a C2H2 zinc-finger transcription factor, is upregulated at low Pi concentrations and function as the transcriptional repressor. ZAT6 overexpressed Arabidopsis seedlings exhibits attenuated expression of several PSR genes, reduced Pi content, short primary roots and retarded growth. Also, the root architecture is altered in older ZAT6 over- expressed plant lines, with increased lateral root growth resulting in increased root to shoot ratio and Pi content. ZAT6 thus regulates root development independent of plant Pi status, influencing Pi acquisition and homeostasis (Devaiah *et al.*, 2007a; Liu *et al.*, 2013).

SPX proteins Several proteins of the yeast PHO regulon possess SPX domains and are involved in Pi sensing and signalling (Secco *et al.*, 2012a). Although equivalent thePHO regulon does not exist in plants, proteins containing SPX domain in plants play an essential role in maintaining Pi homeostasis. It is directly involved in fine-tuning of Pi transport and signalling through physical interaction with other proteins. In plants, they are classified into four families, based on the presence of additional domains, namely SPX, SPX-EXS, SPX-MFS and SPX-RINGs. In Arabidopsis and rice, the family with single SPX domain, consists of four and six members respectively. Expression of these single SPX domain genes is differentially regulated under Pi stress and occurs downstream to SIZ1-PHR1. These proteins have a broad range of subcellular localization, ranging from roots, stems, leaves, cotyledons and pollens and are

specifically involved in regulating Pi uptake and mobilisation (Secco *et al.*, 2012b).

Phosphate starvation strongly induces the expression of AtSPX1 and AtSPX3 while AtSPX2 is weakly induced and AtSPX4 is suppressed. AtSPX1 positively regulates several PSR genes by inhibiting AtSPX3. In rice, the orthologue of AtSPX3, OsSPX1 is positively regulated by OsPHR2 but provides a negative feedback, counteracting the activity of OsPHR2(Liu *et al.*, 2010; Wang *et al.*, 2009a,b). The constitutive transcription factor OsPHR2 remains bound to OsSPX4 in presence of Pi. Under Pi stress, proteasome-mediated degradation of SPX4 leads to the release of PHR2, in turn triggering the signalling for PSRs (Lv *et al.*, 2014). SPX proteins with additional EXS domains play a critical role in xylem loading of Pi (Secco *et al.*, 2010) while understanding of other two SPX families with MFS and RING domain is very limited, with the exception of NLA protein from SPX-RING family (Lin *et al.*, 2010) .

Acid Phosphatases (APases) and Ribonucleases (RNases) In response to Pi starvation, plant enhances the expression of genes encoding APases and RNases. Intracellular APases play a role in recycling of Pi from expendable intracellular organophosphate pools while secretion of APases mobilise Pi from organophosphates prevalent in soil. The regulation of APase gene expression is known to be complex under Pi deprivation, where certain temporal and tissue-specific APase isoforms are induced with associated down regulation of other APases. The upregulated intracellular and secreted APases have been characterised as Purple APases (PAPs) (Zhang *et al.*, 2011). In Arabidopsis, PHR1, WRKY75 and ZAT6 TFs regulate PSI APases whereas PAP26 is up-regulated by post-transcriptional mechanisms (Hurley *et al.*, 2010; Robinson *et al.*, 2012; Tran *et al.*, 2010; Veljanovski *et al.*, 2006). Nucleic acids in organic matter decaying in soil are also used as the Pi source by the plant. In low Pi conditions, plants induce the expression of RNases, namely RNS1 (released into the rhizosphere) and RNS2, to cleave nucleic acids releasing Pi (Bariola *et al.*, 1994; Green, 1994).

Calcium and Inositol Polyphosphates (IPs) Calcium ions (Ca2+) and Inositol Polyphosphates (IPs) are the vital secondary messengers mediating signals involved in plant responses to abiotic stresses. Cytoplasmic Ca ion concentrations are regulated by sequestration of Ca into endomembranes. A tonoplast Ca2+/H + antiporter, CAX1 and its homologue CAX3 sequester Ca into vacuoles and have implication in Pi-starvation responses. CAX1 and CAX3 are preferentially expressed in leaves and roots, respectively. Analyses on cax1, cax3 and cax1/cax3 double mutants have indicated the role of CAX1 and CAX3 in plant growth, hormone responses and ion

homeostasis. Moreover, only the cax1/cax3 double mutant showed higher shoot Pi than wild type plants, suggesting the involvement of Ca2+ in Pi homeostasis (Cheng *et al.*, 2005; Mei *et al.*, 2009).

An inositol polyphosphate kinase-1-1 (IPK1-1) gene encodes inositol tetrakisphosphate (IP4) and inositol pentakisphosphate 2-kinase (IP5-2K) involved in the biosynthesis of phytate (i.e. inositol hexakisphosphate kinase (IP6)), which may function as a co-factor of TIR1 auxin receptor (Tan *et al.*, 2007). The ipk1-1 mutant showed over-accumulation of Pi in leaves similar to pho2 mutants(Stevenson-Paulik *et al.*, 2005). In low Pi conditions, ipk1 mutants produce long root hairs and show less sensitivity to high external Pi, suggesting the possible role of IP signals in PSR. As IP4, IP5 and IP6 act downstream of IP3, calcium can possibly link with Pi homeostasis through IP3 modulation (Chiou & Lin, 2011).

Reactive Oxygen Species (ROS) The concentration of ROS drastically increases in roots soon after the deprivation of Pi or other nutrient. This eventually triggers the expression of several nutrient-starvation-induced gene thereby eliciting different adaptive responses. Moreover, nutrient-specific differential localisation of ROS in root tissues is presumed to have implications in RSA modulation. Specifically, during Pi stress, ROS are produced in the cortex and may act as a signal for the initiation and development of lateral roots(Shin *et al.*, 2005; Tyburski *et al.*, 2009).

Hormones Phytohormones play a pivotal role at various stages of growth and develop- ment. Modulations in Pi availability alter synthesis, sensitivity and transport of hormones to elicit PSRs. Hormones, including Auxin, Cytokinins, Ethylene, Gibberellin, Abscisic acid and Strigolactones, have implications in almost all Pi-induced RSA alterations, and has been reviewed in (Rubio *et al.*, 2009).

In particular, Auxin and the associated polar auxin transport mechanism simulate lateral formation in response to Pi stress but arrest primary root growth. However, attenuation of primary root growth and stimulation of root hairs may be independent of auxin. Thus, there are suggestions for the coexistence of both auxin dependent and independent pathways for PSI-RSA modulation. A recent finding has shown that SIZ1 negatively regulates PSI- RSA remodelling through the control of auxin patterning (Miura *et al.*, 2011b). Notably, the role of auxin in Pi homeostasis is more complex and needs further investigation(Chiou & Lin, 2011; Lopez-Bucio *et al.*, 2002; Mayzlish-Gati *et al.*, 2012; Overvoorde *et al.*, 2010; Perez-Torres *et al.*, 2009; Zhang *et al.*, 2014).

Like auxin, the hormone ethylene inhibits primary root growth and promotes lateral-root and root-hair elongation, but not initiation. There are also some suggestions for ethylene-independent pathways for root-hair development in low Pi conditions. Additionally, there are indications of crosstalk between ethylene signalling, programmed senescence and Pi homeostasis. The role of ethylene in Pi starvation has been broadly reviewed by (Nagarajan & Smith, 2012).

Cytokinins promote shoot growth but inhibit lateral root formation. On the other hand, Pi starvation decreases the sensitivity and levels of cytokinins, thereby suggesting a bidirectional interaction between cytokinins and Pi signalling. However, there are also arguments regarding the role of cytokinins as a systemic repressor of PSI genes. Additionally, they inhibit galactolipid synthesis in response to Pi stress (Martin *et al.*, 2000; Yuan & Liu, 2008).

Gibberellin (GA) also plays a negative role in response to Pi stress. Under low Pi conditions, the level of bioactive GA decreases, and in turn causing accumulation of DELLA proteins, which negatively regulate GA responses and modulate several significant adaptive PSRs. GA – DELLA mediated signalling contributes to PS-specific RA modulation and anthocyanin accumulation but not in Pi uptake and the regulation of PSR genes (Devaiah *et al.*, 2009; Jiang *et al.*, 2007).

In response to Pi deficiency, a novel class of phytohormones, named strigolactones, are synthesised in roots that act as a rhizosphere signal ,inducing hyphal branching in AMF (Czarnecki *et al.*, 2013). In species like Arabidopsis, that are not the host of AMF, strigolactones are also transported to the shoot in order to modulate shoot architecture (Cheng *et al.*, 2013; Marzec *et al.*, 2013; Mayzlish-Gati *et al.*, 2012). Thus, strigolactones serve to improve both Pi acquisition and utilisation (Umehara *et al.*, 2010). There are also some speculations regarding the involvement of Abscisic acid (ABA) in PSRs (Jaschke *et al.*, 1997; Trull *et al.*, 1997). Though no direct relationship between has been established, it has been proposed that ABA could suppress the expression of PSI genes by regulating ABA-INSENSITIVE1 (ABI1) protein phosphatase 2C (Ribot *et al.*, 2008).

Ions In recent times, the elemental composition, the Ionome, of a plant tissue has been identified as a multivariable signature, defining the specific physiological state of the plant, including phosphate stress (Baxter, 2009, 2010; Lahner *et al.*, 2003; Salt, 2004; Salt *et al.*, 2008)). The corre- lated accumulation of different elements is largely driven to maintain vacuolar, cytoplasmic osmolarity and charge balance, and also serves as a detoxification mechanism (Conn & Gilliham, 2010). In Arabidopsis leaf,

phosphate limitation has been observed to increase the concentrations of B, Zn and As and decrease the concentration of P, Cu and Co Baxter *et al.* (2008) while in maize leaf, it significantly increases the concentration of K, Mn, Zn, V, Ni and Rb and deceases the concentration of S, Mg, Ca, Mo, Sr, Li and As (Schlüter *et al.*, 2013). Different cell types accumulate certain elements in varying amounts in their vacuoles. The role and mechanisms underlying the cell-specific distribution of different elements in plants is poorly understood. Although the location of element accumulation is fairly robust, alterations in expression of certain solute transporters, through genetic modification or by growth under stress, result in perturbations to these patterns (Conn & Gilliham, 2010). For example, it has been shown that P limitation increases As uptake via high-affinity Pi transporters while N deficiency increases Pi uptake via a miRNA/NLA signalling pathway. More such examples can be found in (Baxter & Dilkes, 2012; Ohkama-Ohtsu & Wasaki, 2010).

2.5 Current strategies for improving phosphate use

Of the total phosphorus used for global food production annually, only 20% actually becomes part of the food consumed, while the majority is lost permanently or temporarily at various stages from mine to fork (Cordell & White, 2013). Such considerable losses offer substantial opportunities for improving efficiency of phosphorus management systems, recycling and reuse and enhancing uptake and use efficiency by plant. These opportunities operate at different scales; global, national, local, field and plant scales. Major initiatives at the field and higher scales could help in ensuring adequate phosphate supply for many decades to come. The existing global, national and field scale strategies and practices are described in Appendix B and (Withers *et al.*, 2015). However, there is still a need in the long term to improve plant genotypes.

Plant phosphorus use efficiency (PUE) can be referred to as the ability of plant species to produce optimal yield under P limiting conditions. Improving plant PUE requires enhanced phosphate acquisition from the soil (Phosphate Acquisition Efficiency; PAE) and increased utilisation of phosphorus in the processes leading to high productivity (Phosphate Utilisation Efficiency; PUtE) (Reynolds *et al.*, 2012). For many years, modifying root systems and function have been the target to improve phosphate efficiency in plants either by breeding or developing transgenics (Syers *et al.*, 2008). Using either strategy, the potential routes to improve PAE include modification of RSA, root anatomy, rhizodeposition, rhizosphere-microbial interaction and phosphate acquisition; and to enhance PUtE includes optimisation of harvest index while re-

ducing plant phosphorus demand and/or enhancing its internal utilisation/recycling. Far more progress has been achieved toward understanding the mechanisms underlying PAE than PUtE, perhaps because of the complexity of the processes involved. Various targets (genes or traits) for improving PAE and PUtE (Ha & Tran, 2014; Lopez-Arredondo *et al.*, 2014; Rose *et al.*, 2013; Zhang *et al.*, 2014) and the costs and benefits of different P-uptake mechanisms (Brown *et al.*, 2013) have already been reviewed.

Compared to conventional and marker-assisted breeding, transgenic approaches have been successful in introducing single genes to improve, mostly, PAE, at least, offering a proof-of-concept for their activity (Scheible & Rojas-Triana, 2015). At various occasions, the result are not reproducible or have negatively affected other traits, and it is currently unclear how to predict the trade-offs. Altogether, the low success rate for developing phosphate efficient crop varieties (Clemente *et al.*, 2013; Mittler & Blumwald, 2010; Ramaekers *et al.*, 2010; Richardson, 2009; Tian *et al.*, 2012), emphasises the need for smarter approaches.

2.6 Translational studies

Model organisms serve as a platform for the comparatively easy study of fundamental processes and to establish new technologies (Committee PSRS - 2011). *Arabidopsis* has been the principal model, with rice increasingly becoming the model monocot (Flavell, 2009). Having uncovered mechanisms in model species, it is logical to find out if these same mechanisms are present in crops, and hence have potential commercial applications. This is known as *translation* of knowledge or techniques, and has some notable successes (Chew & Halliday, 2011; Oono *et al.*, 2013a). Comparative genomics has been instrumental in recommending homologous genes for further investigation in crop species (Monaco *et al.*, 2014).

With respect to the PSR, much of the core regulatory network has been identified in model species and this appears to be conserved across most plant species (Fang *et al.*, 2009). Table2.2 lists the putative homologues of the core PSR genes in the major crop species, which should be the first choice for study in the organism concerned. It has been reported that there are many similarities between *Arabidopsis* and wheat in the network regulating flowering, though one position is not held by the homologue but a different gene (Amasino & Michaels, 2010). Moreover, genome annotation is incomplete, especially with regard to non-protein coding RNA, like IPS1. This is because they are not detected by conventional gene-finding algorithms, might rarely

be expressed and/or have little sequence conservation. However, orthologues may exist across multiple crop species and currently can only be found using bespoke computational tools (Li *et al.*, 2003).

Genetic variation for phosphate starvation responses, both in shoot and root, has been demonstrated across wide range of plant species. Often, variations for complex phenotypic traits are controlled by many genetic loci and might be uncovered by genome-wide association studies (GWAS) and determination of Quantitative Trait Loci (QTLs). The latter, linking root traits with PAE, have been identified in rice, wheat, common bean, *Arabidopsis*, soybean, barely and maize (Vance, 2010). The loci and underlying genes can become the focus of breeding programmes (Chin *et al.*, 2011; Lynch, 2011).

In view of the above, selecting natural variants in landraces or wild-relative crops performing well in resource deficient conditions forms an excellent material for breeding programmes. This can combine yield traits from elite varieties with resource traits from landraces. For example, a low Pi tolerance QTL known as Pup1, was identified by crossing (Pi tolerant *indica* landrace) Kasalath with (Pi sensitive *japonica* cultivar) Nipponbare (Wissuwa *et al.*, 2002). The resultant introgressed Pup1 rice varieties respectively showed 170% and 250% increase in Pi uptake and grain yield in P limiting soil. The gene responsible for the Pup1 trait was identified as PSTOL1, encoding a protein kinase. Incorporation of this gene into Pi-sensitive varieties enhanced early root growth, thereby enabling more Pi uptake. However, the mechanism by which PSTOL1 results in this phenotype is yet to be characterised (Gamuyao *et al.*, 2012).

Results from laboratory experiments can potentially apply to plants growing under field conditions; this form of translation is possible. However, the external environment is highly dynamic and variable, especially soil. Hence, extensive field evaluation is needed to determine whether a desirable trait found in laboratory-grown plants is still seen under agricultural conditions (Tonelli & Inze, 2009). In some cases, laboratory experiments become difficult, e.g. in establishing mycorrhizal systems, making field studies inevitable.

On the other hand, experiments are carried out in laboratories to reduce the number of variables, leading to substantially lower research costs and make discoveries easier to achieve. But, in natural conditions, plants are confronted with a combination of stresses (Giehl *et al.*, 2014), eliciting non-additive responses. Such responses are often unpredictable and could not be extrapolated by studying individual stress in the laboratory (Mittler & Blumwald, 2010). Though difficult, mimicking field environment in the laboratory can provide a more realistic view of plant responses. Indeed,

such lab experiments required interpretation of huge multi-dimensional datasets, for which high performance and advanced computational techniques could be helpful. Altogether, bidirectional translation from field to lab and vice versa is required.

2.7 Integrative systems approaches

A systems approach considers both the components (nodes) and their interactions (edges) within the system. Where these interactions result in feedback circuits, the system becomes complex in the mathematical (and often the common) meaning of the term and can lead to counter-intuitive behaviour, for example (Péret *et al.*, 2012). For biology, a node can represent a type of molecule, pathway, cell, tissue, organism and population, depending on the physical scale of the system of interest. From this, it is clear that a node at one scale may form a system when considered at a lower scale. Likewise, above the biological (plant) population, there are local (field), national and global scales.

The word 'Integrative' means serving or tending to integrate. In biology, this is often considered to mean integrating systems at the same scale, for example, biochemical with signal-transduction and gene-regulatory networks. However, the mechanistic linkage between genotype and phenotype is likely to cross scales. Furthermore, a quantitative understanding of the system processes requires activities that include mathematics and statistics; and biological systems are so complex that informatics and computer science should also be involved. Integrative systems approaches consist of activities that address an issue by considering it as a (potentially multi-scale) system whose study employs a multi-disciplinary network of people. Experience has shown that these approaches can lead to novel discoveries and solutions (Hodgman & Ajmera, 2015).

The development and analysis of models are characteristic features of systems approaches. In this context, a 'model' is a simplified representation of a dataset or a system, which provide a quantitative understanding of the data or system. A data model reveals structure and relationships within a dataset. Biological examples include QTL analysis and GWAS, but also inferred networks derived from *omics* data (Lee *et al.*, 2015; Marbach *et al.*, 2012; Pan *et al.*, 2013). A system model represents the mechanism of the system, and can either be static or dynamic. The latter represents the combined rates of change of its components as a result of their interactions and system inputs, and can explain unexpected behaviour. These models can also be extended to include the physical structure of the system in two or more dimensions,

allowing even organ and whole plant growth to be modeled. All these modelling approaches have already been extensively reviewed (Hill *et al.*, 2013; Lavenus *et al.*, 2012; Lucas *et al.*, 2011).

There are three main reasons for developing these models (Hodgman & Ajmera, 2015). The first is to test current understanding to see if it stands up to quantitative scrutiny. Often this shows that there is a gap in current knowledge, suggesting areas for further laboratory study. The second is that they provide a platform to carry out *in-silico* experiments to predict behaviour under many more circumstances than would be financially viable *in-vivo*. Hence, there third reason is to find out what are the most incisive experiments to carry out to make useful discoveries.

2.7.1 Need for these approaches in plant P research

From its global scarcity down to its incorporation into food, phosphorus is a supremely complex and multi-dimensional issue (Cordell & Neset, 2013), for which there is unlikely to be a single solution. Undoubtedly, integrated strategies at the higher scales outlined above will produce short and medium term benefits, but ultimately P supply is finite. Improving PUE is therefore essential in the long run to reduce environmental impacts, increase the nutritional value of grains and improve farm economies. However, current breeding strategies have had little success, owing to a poor understanding of the molecular mechanisms underpinning traits and their interactions (Veneklaas *et al.*, 2012). Integrative systems approaches can obviously assist in this area by helping to identify the components of (and their relative contributions to) traits of interest. Figure 2.3 and 2.4, depict the phosphate-related systems from molecular to field scales, and provide a starting point for integrative research into improving PUE.

Gene	Arabidopsis	Rice	Maize	Sorghum	Brachy	Wheat	Barely	Soybean	Tomato	Potato	Brassica	Grape	Medicago	Populus
Prefix	**At**	**LOC_Os**	**GRMZ2G**	**Sb**	**Bradi**	**Traes_**	**MLOC_**	**GLYMA**	**Solyc**	**PGSC0003 DMG4000**	**Bra0**	**VIT_**	**MTR_**	**POPTR_0**
ARP6	3g33520	01g16414	088487	08g21780	2g10130	2BL_221EC0BB1 1BL_51C489EEB 2AL_4DCD06BE9 2DL_E17A1BB12	64804	04G07540 06G26590	05g018600	14966	30818	11s0016g05490	ND	018s12840 002s03430
At4, IPS1	5g03545 3g09922	03g05334 01g0838350**	086179 843352	ND	ND	4AL_D7C83DB52 4BL_00AAC9279	ND	ND	ND	ND	ND	ND	ND	ND
bHLH32	3g25710	03g15440 01g06640	043854 088443	01g040450 03g005250	1g67500 2g03830	4DL_7BD3165FB 4AS_DD16F89E7 4BL_A2B32FCEE	66385	12G14400	07g053290	23577	26510 25158	10s0003g01160	5g066080	004s05480
CAX1	1g08960	11g05070	004414	08g002860	4g42870 4g42880	5BL_6A7BE3F0C 5AL_97C4C3E20 5DL_B669983C4 5AL_B925FC757	21103 16013	03G39920	01g098800	28607	31650	14s0128g00240	7g113730	013s02590
CAX3	3g51860	01g37690 02g21009	011592	03g024820 04g010130	2g41090	2AL_26065F906 2BL_445F5B3B7 2DL_2A2F4F62B 3AL_3CA77B366	17450 13658	01G30610 01G30643 03G07910 03G07950 18G43000	09g005260	11787	12833	08s0007g02240	7g068380 4g016720	006s10080 016s12290
IPK1	5g42810	04g56580	150496	06g31650	5g24890	2AL_55460AE54 2BL_A465A5769 2DL_EFEF40224	38910	14G07880	04g080670	03698 15950	27458	18s0001g12910	ND	005s25180
LPR1	1g23010	01g03530 01g03549 01g03620	086727 054050	03g007480 03g007470 03g007440	2g01850	4DS_DE0D4FCF6 4BS_ECDA94252 1BS_5144C54E4 4BS_06EE678FF	79739	20G26270 10G41010	05g008290	30551	24558	01s0011g04720	ND	010s12440
miR399	2g34208 1g63005 5g62162 2g34202 2g34204 2g34208	*osa MIR399-a-k	*zma MIR399-a-j	*sbi MIR399-a-k	*bdi-MIR399 a-b	*tae-MIR399	*hvu-MIR399	*gma-MIR399 a-h	*sly-MIR399	*stu-MIR399 a-o	*bna-MiR399 a-c	*vvi-MIR399 a-i	*mtr-MIR399 a-t	*ptc-MI399 a-e
MYB62	1g68320	01g03720	096358 162709	03g007360	2g01960	3AS_0A8F6B069 3AS_5E49D447AF 3B_5033C9A8	65555	10G41930 20G25110	05g009230	14550	04041 04297	01s0011g03730	1g110460	008s12130 010s13290
PHF1	3g52190	07g09000	158489	02g005080	1g55000	7BL_48A3E8A28 5DL_42842D4B4	22417	10G34380 20G33180	11g007780	*G404027324 *G402027324	06909	13s0074g00010	ND	008s02920 010s23870
PHO1	3g23430	02g56510	466545	04g036730	3g54920	6DL_C4D2B23A 6BL_6D7561359 6BL_0325BEAA4 6BL_CB0A10DC9	12153 56639	10G00720 10G32670 20G34390 02G00640	09g090360	17163	14948 23727	05s0049g01410	2g077690 1g075640	008s16930 010s07970 008s18760
PHO2	2g33770	05g48390 05g48400	381709	09g028110	2g16960	1DL_F122253A3 1AL_E5224B6EA 5BL_196F297B6 1BL_241A3B9EF	53410	07G31360 13G24810 13G31290 15G08040	02g078210	29724	21874	00s1927g00020 00s0265g00070	2g013650 4g020620	004s04350 011s05240

Table 2.2: PSI genes in *Arabidopsis* and their respective orthologs in different crop varieties

PHR1	4g28610	03g21240 07g25710	006477 162409	01g036440 02g010520	1g63530 1g28920	3DS_0240F189D 4AS_7220D33B3 3AS_6EEB8D2B2 3B_6780F56DD	5585 60198	19G35080 10G04540 03G32350	06g008200 09g072830	23467	10355 11042 24188	07s0005g04120	7g098250	002s25960
PHT1;1	5g43350	04g10800	170208	06g002560	5g02750	4AL_81AC819EF		02G008401 0G00950 10g33030 20G34616	03g00530 03g00560	13403	27491 35977 33675	05s0049g00920 05s0049g00930	1g043200 1g043290 1g043220	0010s08270
PHT1;4	2g38940	08g45000 04g10690 03g05610 10g30790	045473 154090	06g002800 01g046900 01g020570	5g02730 3g27680	4AL_C56125840		03G31950 10G04230 13G18421 19G34710	06g034200 09g066410 09g073010	03798 03839 10288 10289 17503	0107 5069 5070 5071 17093 17275	07s0005g03290 07s0005g03300	5g068140	005s24500 005s24510
PHT2;1	3g26570	02g38020	092780	04g024630	3g47550	6AL_294A98532 6BL_6BC705098 6BL_5C168B1DD 7DL_53DB0C6B3	6818	08G38840 18G20870	05g013510	18604	25212 34242	00s0291g00060	8g069390	008s19070
PLD1	3g16785	05g29050 01g20860	066485	01g017850 03g012720	2g27950	1AL_11AB1B224 1BL_884FA4347 1DL_AA198212F	70374	09G04620 15G16270	01g065720	09598	22178	05s0077g01830	1g083620	008s23240 010s00850
PTF1	5g58010	06g09370	024530	10g006250	1g46700	7AS_D56F0F9E5 7BS_13A10F94A 7DS_68E3ACF8E	59503	06G38935	12g100140	22058	20398 06788	11s0016g00380	3g027650	006s13790
SIZ1	5g60410	05g03430 03g50980	155123 002999	09g002225 08g000380	2g38030 4g45080	1AS_92E04BC2B 1DS_F0BE8ABFA 1DS_F292A52F1 4BS_F74B411CB	38182 53617 60545	13G40325 11G15880 12G07590 12G21070 12G29270	06g010000 11g069160	08114	02681 20249	06s0004g03180	2g093730 4g060510	004s21990 008s04190 009s02040
SPX1	5g20150	06g40120	171423	04g006990 10g023590	1g36610 3g07470	7AL_2DSB863A7 7BL_DD88849AE 7DL_B994066FA	54859	06G07260	12g009480	02890	06543 20088	11s0016g05330	1g012440	006s06880 018s13140
SPX3	2g45130	10g25310 03g29250	370780	01g032880 01g023270	1g60250	2BS_E9B276FE4 7AL_40678A3B5 2AS_96D993EDD 7DL_AC271F4EE	62152	01G33170 03G03820	01g090890	2601	00373 40324	05s0077g00270	ND	002s14470 014s06020 017s00240
SQD2	5g01220	07g01030 01g04920 03g15840	100652 049190	02g000240 03g006480 01g040150	1g59860 2g02800 1g67200	2BL_4CF076AAB 2AL_218CD1AAD 3B_4DEB64E2E 3DS_CBE46365A	63045 12521	07G17680 01G27840 03G14200	09g014300 10g085100	11091 20317	05694 09633	08s0007g01940	4g015260 7g067340	006s09880 016s12010
ZAT6	5g04340	03g32230	106026	01g031900	1g16010 2g49250 4g03340	4BS_FE945DFC 4DS_98E9655C8 4DS_676CACEAC	54674 51405 70662	17G35430	01g107170	34322	09464	03s0091g00690	1g106730	002s12010

The table is mainly produced using Arabidopsis gene ids as the reference and compiling their orthologs from Plant ensemble database (http://plants.ensembl.org/). Some gene ids are adopted from table 1 of (Calderón-Vázquez *et al.*, 2011), ND: No data, (*) miR399 orthologs are taken from miRBase database (http://www.mirbase.org/), (**) is the RAP id and does not include prefix like MSU id of other rice genes.

2.7.2 Current systems activities

Following the pioneering work by (de Wit, 1959), there has been a constant effort to develop and improve crop models that predict the performance of the genotype and assess the design of the adaptive strategies for the given environmental condition (Tardieu, 2010). A large number of mathematical and computational models have been developed over the last 10-15 years, improving the understanding on various aspects of plant processes across scales of biological organisation. As part of this literature survey, over 165 models for different plant process were systematically classified based their physical scales, modelling method and gains from the models. The catalogue of these models is presented Appendix Cand have been published (Hodgman & Ajmera, 2015).

With regard to resource acquisition by plants, a range of models at various physical (generally, supra-tissue) scales has been developed. These represent aspects of uptake of nutrient, water or contaminants (Heppell *et al.*, 2015b; Keyes *et al.*, 2013; Leitner *et al.*, 2010; Payvandi *et al.*, 2014; Ptashnyk *et al.*, 2011; Roose & Fowler, 2004; Thornley, 1976; Zygalakis & Roose, 2012; Zygalakis *et al.*, 2011), and the effect of microbial (Schnepf & Roose, 2006; Schnepf *et al.*, 2008, 2011), and exudate dynamics on soil nutrient availability (Kirk, 2002). Pertaining to phosphorus, most models have focused on its dynamics in soil, to identify ways of optimising phosphate availability (Amijee *et al.*, 1991; Barrow, 1983; Grant & Robertson, 1997; Silberbush & Barber, 1983; Tinker & Nye, 2000). Such models highlight the fact that when soil factors determine the availability of Pi at the root surface, the effect of having more transporters becomes negligible. The number and type of transporter is crucial, but primarily for avoiding Pi toxicity. Furthermore, modelling has shown that a small optimisation of RSA can lead to a large increase in Pi acquisition (Heppell *et al.*, 2015a; Wissuwa, 2003), PAE can be enhanced by increased root hair length and longevity rather than their density (Brown *et al.*, 2013) and root cortical aerenchyma is beneficial for PUE by reducing metabolic and exploration cost (Postma & Lynch, 2011b).

Traditionally, forward genetics was used to identify genes by cross-breeding and phenotypic screening, which is very time consuming. Omics technologies are a form of integrative approach, as they bring together data notionally for all genes, transcripts etc. Computational techniques have allowed these datasets to be brought together (in databases) for comparison and advanced data modelling (to produce interaction and inferred regulatory networks). Some of the inferred gene regulatory networks underlying different processes in roots are listed in Table 2.3. Such activities allow prioritisation of large gene lists so that trait-related genes can be found in much shorter timescales (Hickman *et al.*, 2013; Pan *et al.*, 2013).

Biological phenomenon	Species	Data type	Inference method	Reference
Lateral root formation	*Arabidopsis*	time-series RNA seq	Time-Delay Correlation algorithm	(Lavenus *et al.*, 2015)
Root epidermis cell differentiation	*Arabidopsis*	cell type-specific temporal microarray dataset (from genetic and hormonal perturbation)	Bayesian inference approach	(Bruex *et al.*, 2012)
Stele-specific transcriptional regulation	*Arabidopsis*	cell type-specific temporal microarray dataset along with Y1H and Y2H data	Bayesian inference approach	(Brady *et al.*, 2011)
Nitrate-driven transcriptional regulation	*Arabidopsis*	time-series microarray data (from control and treatment)	Machine learning approach	(Krouk *et al.*, 2010)
Secondary cell wall synthesis in root xylem under abiotic stress	*Arabidopsis*	tissue-specific microarray dataset (from abiotic stress condition) and Y1H data	Statistical packages (SIRENE,GENIE3 Inferelator, TIGRESS and ANOVerence)	(Taylor-Teeples *et al.*, 2014)
Root transcriptional regulation	*Arabidopsis*	curated microarray data	ARACNe algorithm	(ChavezMontes *et al.*, 2014)
Lateral root initiation	*Arabidopsis*	time-series microarray data	Probablistic boolean and dynamic bayesian approaches	(Muraro *et al.*, 2013)
Nitrate responsive downstream regulation of auxin receptor AFB3 in roots	*Arabidopsis*	microarray data(from control and mutants)	Virtualplant platform	(Vidal *et al.*, 2013)
Gene-metabolite response to sulphur stress	*Arabidopsis*	microarray and metabolite dataset(from control and treatment)	Pearson correlation algorithm and MetaGeneAlyse web tool	(Nikiforova *et al.*, 2005)
Early phosphate deficiency signaling in roots	*Arabidopsis*	time-series microarray dataset with short time-interval (from control and treatment)	Coexpression-based gene clustering	(Lin *et al.*, 2011)
Carbon/Nitrogen-responsive molecular regulation	*Arabidopsis*	time-series microarray dataset (from control and treatment)	Coexpression-based gene clustering	(Gutierrez *et al.*, 2007)

Table 2.3: Inferred network models concerning various processes in plant roots.

2.7.3 Next steps

The current crop models include the concept of PUE, but only in terms of movement of phosphorus from one compartment to another and ultimately into seed. There is no connection made to the genotype of the plant. Certainly, there is an increasing need to

explore, in greater detail, the interactions between genotype, phenotype, environment and agricultural practices. More specifically, improving crop PAE should take into account both root and soil characteristics, but this should not be at the expense of the above-ground PUtE processes. Both aspects of PUE are vital and need equal consideration.

Prior work has modeled the aspects of P acquisition. In the context of Figure 2.3, this includes models representative only of panels a, f and g. The other panels relate to different aspects of PUtE, including phosphate metabolism, remobilisation and transport across plants, and have received little attention by modellers. Given the past record, the application of systems approaches can certainly improve the understanding of these processes, thereby offering both a genetic and quantitative insight into all the components of PUE. Plant biologists and modellers should also pay attention to the connections between the different aspects of PUE, because changes in one aspect/scale will probably impact on and feedback from others.

A set of candidate genes for crop improvement are represented in Figure 2.4 and Table 2.2, but there are too many to work upon. Moreover, altering one gene may very well impact upon other parts of the regulatory/signalling network. Thus, prioritisation of genes is needed so that effort can be focused on the most likely candidates. An essential step in this direction is to integrate the datasets for the genotype, phenotype, soil conditions, management practices and other environmental factors, thereby bridging the gaps between genes and complex phenotypes and in turn, aiding gene prioritisation. Models allow implicit integration of molecules to whole plant physiology and environment enabling rapid evaluation of different traits on PUE and their connection with different genotypes. Potentially, multi-scale models could be used to assess the long-term impacts of a genotype on soil nutrient dynamics, crop productivity and sustainability of the cropping system for a wide range of environmental conditions.

Finally, from an integrative systems perspective, a complete understanding of the molecular basis of PUE would be insufficient. This is because the mechanisms for phosphate uptake and utilisation affects other plant subsystems and vice versa. For example, its links to salt tolerance and the uptake of other nutrients are well established (Chapin III, 1991; Miura *et al.*, 2011a; Raven, 2015; Selim, 2015). In view of this, identifying genotypes appropriate for a different soil and environmental conditions are also needed. Therefore, it will also become necessary to study the effects of improving PUE on other traits, and finding optima among these competing effects to achieve adequate crop yield in a given environment is a daunting challenge. Systems

approaches seem to be the best way to find such optima.

Adoption of systems approaches might require some changes to research practice. Apart from closer interaction between biologists of various skill sets and (mathematical and computational) modellers, new types of experiment need to be designed. Multiscale models require multiscale dataset for both model development and testing of predictions (Band et al., 2012). Particularly, dynamic studies necessitate time-course data to discover how quickly different processes are affected. Furthermore, laboratory experiments should closely mimic field conditions and one example is to grow plants at different levels of phosphate input. This would show the order in which the different plant subsystems respond to phosphate depletion.

2.8 Conclusion

The research to develop Pi-efficient crop varieties is hampered by extreme complexity on many fronts. The latter ranges from molecular interactions in both soil and plants, through agricultural practice, to national and geopolitical issues surrounding the cost of P supply. In addition, plant responses to low phosphate can trigger other stresses and vice versa. It is no surprise, therefore, that attempts to improve PUE have met with little success, because various factors/traits and their interactions need to be taken into consideration. Models (mathematical or computational) are able to represent and explain complex behaviour, meaning that systems approaches have a good track record of making important novel discoveries in comparatively short timescales. In the case of the crop models, they continue to have practical benefit to farmers. Clearly, integrative systems approaches should be brought to bear in phosphate research, so that the open questions remaining in this area can be addressed. Furthermore, modelling can help in ranking potential target genes (and combinations thereof) on how likely they are to elicit the desired phenotype or trait. Essentially, multidisciplinary groups working on the different aspects of phosphate research (particularly at the different scales) must come together and share a platform, so that models linking genotypes to desirable traits can emerge. Furthermore, practical benefits are likely to accrue faster if the systems projects turn away from purely scientific endeavours to include application or translation of results to crop species under field conditions. The most appropriate projects can be identified through increased engagement with industrial companies, farmers and governmental licensing agencies.

Chapter 3

miR399-independent regulation of PHO2 in phosphate starved plants

Abstract

This chapter describes the development of mathematical models for the molecular regulation of phosphate uptake in rice. These models were parameterised by fitting to gene expression data for miR399, PHO2 and IPS1. The model simulations revealed that the well established miR399-mediated regulation of PHO2 mRNA is insufficient to explain its dynamics, especially, at early times following P stress. Thus, five potential hypotheses have been proposed and were tested *in-silico*. Among these, the hypothesis that a drop in cytosolic phosphate activates a repressor of PHO2 transcription was found to be most likely. A short time-course experiment confirmed the early decline in PHO2 mRNA levels and also indicated that PHO2 might negatively regulate its own transcription.

3.1 Introduction

The regulatory network of phosphate (Pi) uptake includes seven key members, abbreviated to SIZ1, PHR2, IPS1, miR399, PHO2/LTN1, PHO1 and PHTs (see Chapter 2 for more details). SIZ1 alters the activity of proteins by covalently attaching SUMO peptides. PHR2 (equivalent to PHR1 in *Arabidopsis*) is a transcription factor that is activated by SIZ1 under Pi-deficient conditions and directly binds to the promoters of IPS1 - a long non-coding RNA and miR399 (Chiou & Lin, 2011; Lin *et al.*, 2009). Next, miR399 causes mutual degradation of expression of PHO2 mRNA, which encodes a ubiquitin-conjugating enzyme E24 (UBC24) that causes the degradation of PHTs (high-affinity phosphate uptake transporters) and PHO1 proteins, which move Pi into the xylem (Bari *et al.*, 2006; Hu *et al.*, 2011). In addition, IPS1 reversibly sequesters miR399 to tightly regulate PHO2 level when the Pi supply is limited (Franco-Zorrilla *et al.*, 2007). However, the reasons for the bulk increase in IPS1 levels in response to phosphate stress are unclear.

This study focuses on the regulation of phosphate uptake as this is often a limiting factor for plant growth and development (Shen *et al.*, 2011). A novel mathematical model for molecular regulation of phosphate acquisition under its deficiency in rice has been developed, with a broad aim to inform the development of phosphorus-efficient crop varieties. This study has identified an area of phosphate regulation where current knowledge was insufficient, that is the regulation of PHO2 mRNA levels, especially, at early times following Pi stress. Credible hypotheses for these are presented along with preliminary laboratory evidence for two extra levels of regulation of PHO2 mRNA synthesis. In the long term, the models developed here could be integrated with other models that concern different nutrients, growth conditions, productivity and environment responses of a plant. For that reason, two extra species (variable) SIZ1 and PHR2 have been explicitly included in these models, as they are respectively linked to stress and other aspects of root anatomy and physiology (see Figure 2.4).

3.2 Results

3.2.1 A new mathematical model for molecular regulation of phosphate acquisition in plants

Uni-compartmental mathematical models describing the regulation of phosphate

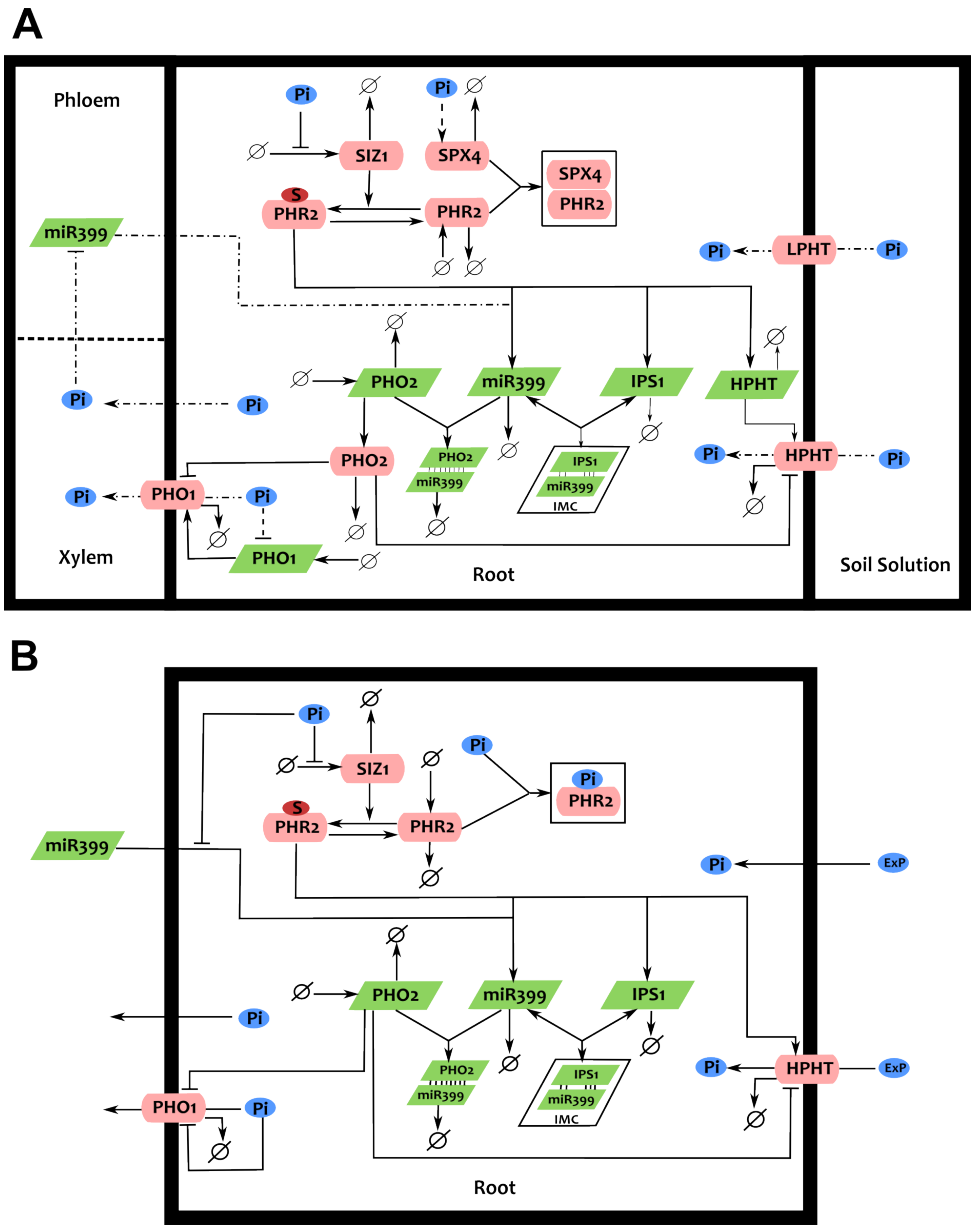

Figure 3.1: Molecular regulation of Pi uptake in plants.
Panel A represents the detailed molecular network regulating Pi acquisition. Thick black boxes represent different compartments i.e. soil-solution, cell and vasculature (including phloem and xylem). The simplified version of the network is depicted in Panel B. Protein, ligand, mRNA, complexes and Pi ions are denoted by rectangles (pink), red ellipse, parallelogram (green), squares (transparent) and blue ellipse, respectively. Label acronyms are defined in Table 3.1. Pointed solid arrow denotes direct interactions and fluxes, barred arrow denotes inhibition or repression and dashed lines represent indirect interactions. ø denotes indigenous production and degradation of the molecules.

Species acronym	Species name	Species type	Initial value
SIZ1	SUMO E3 ligase 1	Protein	0
PHR2	Phosphate starvation Response 2	Protein	0
PHR2S	SUMO-bound PHR2	Protein-ligand complex	0
miR399	miRNA-399	micro-RNA	0
PHO2	Phosphate 2	mRNA	1 (fold)
PHO1	Phosphate 1	Membrane protein	0
PHT	(High-affinity) Phosphate transporter	Membrane protein	0
IPS1	Induced by Phosphate Starvation 1	long non-coding RNA	0
IMC	IPS1-miR399 complex	RNA complex	0
CytoPi	Cytosolic phosphate	Ion	5000 (μM)
E	External Pi	Ion	200 (μM)

Table 3.1: List of model variables and their initial values.

uptake in plants have been developed, using the simplest plausible molecular network presented as Figure 3.1B. The acronyms for variable names are defined in Table 3.1.

3.2.1.1 Model assumptions

The model represents phosphate regulation in a hydroponic growth chamber. The root is represented as a single cell with constant volume flanked by external solution and vasculature because that is the resolution of most of the data generated. This cellular compartment acts as a sink for external phosphate and a source for the internal plant phosphate. The decline in Cytosolic phosphate (CytoPi) levels (in seconds and minutes) and the induced genetic/molecular response (hours and days) occur at different time-scales.

In the model, both low-affinity and high-affinity phosphate transporters are assumed to be embedded in the cell membrane, corresponding to all families of Pi transporters.The constitutively expressed low-affinity transporters account for some basal Pi uptake under all conditions. The rate of phosphate utilisation is assumed to be constant and is solely dependent upon availability of Pi in cytoplasm. External Pi concentration in the model is considered to remain constant under normal and deficient conditions at $200\,\mu M$ and $0.0001\,\mu M$, respectively. Given the upper limit for the concentration of cytoplasmic phosphate (i.e. $25\,mM$) (Schachtman *et al.*, 1998) and the proportion of it stored in the vacuoles (~80%) (Bieleski, 1973; Poirier & Bucher, 2002), the CytoPi level is assumed to be at a steady state of $5\,mM$ under typical

hydroponic external P condition i.e 200 µM.

The abundance of an mRNA species is used as a proxy for protein concentration, assuming that protein concentration is at quasi steady state. The molecular regulation of Pi uptake is found to be conserved across various plant species (Chiou & Lin, 2011). Thus, the half-lives for all the transcripts in the model correspond to those of *Arabidopsis* (Narsai *et al.*, 2007). Published evidence (Secco *et al.*, 2013) and qRT-PCR results in the Appendix Figure D.2 shows that PHR2 mRNA levels (and hence total protein) remain roughly constant. PHR2 is defined as the level of unbound PHR2 available for sumoylation by SIZ1. SUMOylation of PHR2 is countered by de-SUMOylating enzymes, potentially SUMO proteases (Conti *et al.*, 2008; Kurepa *et al.*, 2003), whose activity is assumed to be constant . In the first instance, it is assumed that PHO2 mRNA synthesis is also constant because there is no evidence to the contrary. The binding of IPS1-mR399 is relatively weaker than PHO2-miR399 binding because of the 3bp insertion in the middle of miR399 binding site in IPS1, while the dissociation rate of IPS1-IMC complex (k_8) is assumed to be lower than their association rate (k_7). Finally, for simplicity, the system is assumed to be well mixed and homogenous because roots consist of various cells and long time scales (hours) are represented.

3.2.1.2 Equations

The model is represented by a system of ten coupled non-linear ordinary differential equations (ODEs). The model applies the law of mass action, Michaelis–Menten and Hill kinetics, for the appropriate reactions depicted in Figure3.1B. Henceforth, the rates of endogenous production and degradation are denoted by "m" and "d" respectively along with relevant subscripts, and square brackets denote concentrations. Most molecular species in the model are assumed to undergo some basal endogenous degradation, corresponding to their half-lives. The equations are:

$$\frac{d\,[SIZ1]}{dt} = m_1 \left(\frac{k_1^n}{k_1^n + [CytoPi]^n} \right) - d_1[SIZ1] \tag{3.1}$$

$$\frac{d\,[PHR2]}{dt} = m_2 - k_2[PHR2][CytoPi] - \frac{m_3[PHR2][SIZ1]}{k_3 + [PHR2]} + k_4[PHR2S] - d_2[PHR2] \tag{3.2}$$

$$\frac{d\,[PHR2S]}{dt} = \frac{m_3[PHR2][SIZ1]}{k_3 + [PHR2]} - k_4[PHR2S] \tag{3.3}$$

$$\frac{d\,[miR399]}{dt} = \frac{\beta}{\left(1 + [CytoPi]\right)} + \frac{m_4[PHR2S]^n}{k_5^n + [PHR2S]^n} - k_6[miR399][PHO2] - k_7[miR399][IPS1] + k_8[IMC] - d_3[miR399] \tag{3.4}$$

$$\frac{d\,[PHO2]}{dt} = m_5 - k_6\,[miR399][PHO2] - d_4[PHO2] \tag{3.5}$$

$$\frac{d\,[PHO1]}{dt} = \frac{m_6}{(1 + [CytoPi])\,(1 + [PHO2])} - d_5[PHO1] \tag{3.6}$$

$$\frac{d\,[PHT]}{dt} = \left(\frac{m_7[PHR2S]^n}{k_9^n + [PHR2S]^n} \right) \frac{1}{(1 + [PHO2])} - d_6[PHT] \tag{3.7}$$

$$\frac{d\,[IPS1]}{dt} = \frac{m_8[PHR2S]^r}{k_{10}^r + [PHR2S]^r} - k_7[miR399][IPS1] + k_8[IMC] - d_7[IPS1] \tag{3.8}$$

$$\frac{d\,[IMC]}{dt} = k_7[miR399][IPS1] - k_8[IMC] - d_7[IMC] \tag{3.9}$$

$$\frac{d\,[CytoPi]}{dt} = \frac{k_{11}[PHT][E]}{k_{12} + [E]} + \frac{k_{13}[E]}{k_{14} + [E]} - \frac{k_{15}[PHO1][CytoPi]}{k_{16} + [CytoPi]} - U[CytoPi] \tag{3.10}$$

The activity of SIZ1 protein is inhibited by cytosolic phosphate (CytoPi). The constitutive transcription factor PHR2 remains bound to Pi-stabilised SPX4. For simplicity, CytoPi is assumed to interact directly with PHR2 in equation3.2. Unbound PHR2 is sumoylated by SIZ1 forming PHR2S, and is de-sumoylated by deSUMO enzymes. The active PHR2S triggers the production of miR399 both in root and relatively higher in shoot. Acting as a systemic signal, the bulk amount of miR399 from shoot translocates via phloem into the root system. miR399 binds with PHO2 transcripts causing mutual degradation. PHR2S also activates the production of the long non-coding RNA, IPS1, that sequesters with miR399, forming a reversible complex (IMC). The production of xylem loading protein PHO1 is inhibited by CytoPi and PHO2. The production of high-affinity Pi transporters (PHTs) is activated by PHR2S but degraded by PHO2. PHTs along with constitutive low-affinity transporters take up external phosphate (E) , adding to the pool of CytoPi. The acquired Pi is loaded into the xylem via PHO1 proteins and internally stored or utilised within the cellular compartment.

3.2.2 Data generation and model parameterisation

The model consists on 35 parameters, namely m_i, k_j, d_l, β, U,n, and r, where $i = 1, ..., 8$, $j = 1, ...16$, and $l = 1, .., 7$ (Table 3.2 and 3.3). The magnitude of these parameters were either adopted from the literature, assumed, calculated or estimated.

3.2.2.1 Known, assumed and calculated parameters

Values of 9 parameters, mainly the degradation rates, were obtained directly from the literature (Narsai *et al.*, 2007). The binding constant for miR399 and PHO2 (k_6) is assumed to equal 0.009, on the basis of the published data (Zinovyev *et al.*, 2013). The Hill co-efficient (n) was set to 2 in keeping with many models of gene regulation while Hill co-efficient for IPS1 (r) was set to 4 to achieve the observed delayed and steep increase in IPS1 levels. The inhibition co-efficients for SIZ1 (k_1), PHO1 and PHT were set to unity, in order to optimize the number of parameters for estimation. Even if these values were estimated, their accuracy would be questionable due to the lack of relevant data. The value of m_5, k_{13} and U were calculated by using the steady state levels of the respective variables (see Note 1 in AppendixD). Altogether, the values of 16 parameters have been deduced, Table 3.2

Parameter name	Description	Value	Units	Ref.
m_5	Maximal production rate of PHO2	0.3742	h^{-1}	C
k_1	Inhibition co-efficient for SIZ1	1	h^{-1}	A
k_6	Binding constant for miR399 and PHO2	0.009	h^{-1}	R**
k_{12}	$k_m$for phosphate uptake by HPHT	23	μM	R*
k_{13}	V_{max} for phosphate uptake by LPHT	47125	h^{-1}	C
k_{14}	$k_m$for phosphate uptake by LPHT	177	μM	R*
d_1	Rate of SIZ1 degradation	0.0289	h^{-1}	R
d_2	Rate of PHR2 degradation	0.0289	h^{-1}	R
d_3	Rate of miR399 degradation	0.0578	h^{-1}	R
d_4	Rate of PHO2 degradation	0.3741	h^{-1}	R
d_5	Rate of PHO1 degradation	0.0866	h^{-1}	R
d_6	Rate of PHT degradation	0.0866	h^{-1}	R
d_7	Rate of IPS1 degradation	0.1386	h^{-1}	R
U	Rate constant for internal utilisation of Pi	5	h^{-1}	C
n	Hill coefficient	2	dl	A
r	Hill coefficient for IPS1	4	dl	A

Table 3.2: List of known, assumed and calculated parameters.
Abbreviations used have the following meaning. A : assumed value, C : calculated value (see Note1 in Appendix D), dl : dimensionless, h : hours, HPHT : High-affinity Phosphate Transporters, LPHT : Low-affinity Phosphate Transporters, R : degradation rates from (Narsai *et al.*, 2007), R*: kinetic value of transporters from (Nussaume *et al.*, 2011) and R** : miRNA binding affinity from (Zinovyev *et al.*, 2013)

3.2.2.2 Parameter estimation

The remaining 20 parameters were estimated by fitting the model to the dataset, which largely includes qRT-PCR data generated as the part of this study and RNA-SEQ data available in literature (Secco *et al.*, 2013).

Data generation Certain parameters would be very difficult to determine. For example, the maximal production of PHT at the cell membrane would be difficult to be obtain directly and cannot be linked to mRNA concentration as PHO2 causes degradation of its protein.The case is similar for PHO1. Measuring SIZ1 activity and PHR2 protein levels and degree of SUMOylation would fall beyond the time-frame of this work. On the other hand, their mRNA levels remain relatively stable regardless of external Pi concentration and thus cannot be proxied for the dynamics of their protein

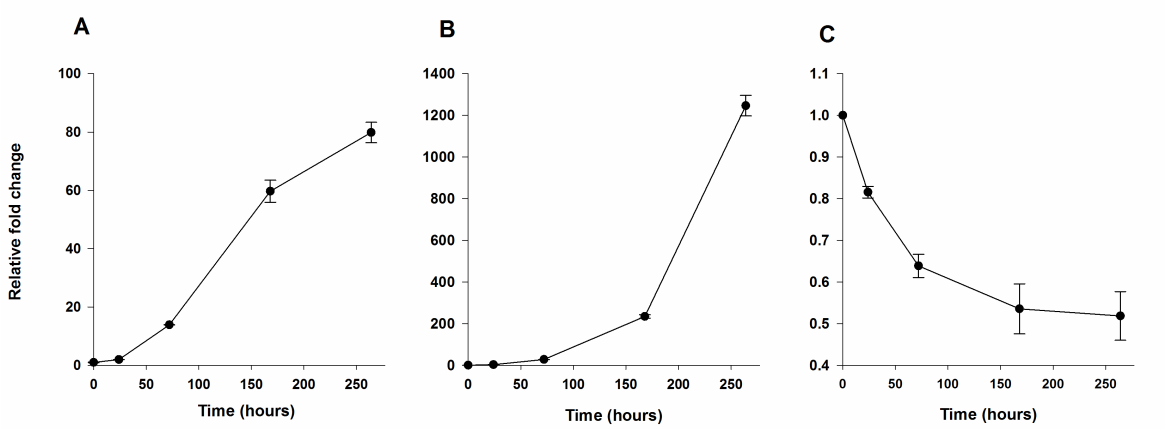

Figure 3.2: Expression profiles of miR399, IPS1 and PHO2 under Pi-deficient conditions.
A, B and C respectively depicts relative fold change in the levels of mature miR399s, IPS1 and PHO2 in root of rice (cv. Nippobare) seedling grown under P deficient condition.The expression levels are relative to the +P condition at time point zero. Errors bars are SE and n = 3. Relative expression levels were normalized to that of an internal control, Os-ACTIN.

products. Whole-root data for phosphate concentrations cannot be used for parameter estimation alongside transcriptomics data, because they change in different time scales and include vacuolar as well as cytosolic Pi. In view of the above, only the expression of miR399, IPS1 and PHO2 can easily be measured for parameter estimation.

Time-course experiment was carried out, where germinated seedlings were grown hydroponically for 15 days in Pi-sufficient medium before transferring half of the plants to Pi-deficient solution for 11 days. Quantitative RT-PCR (qRT-PCR) was performed to determine the fold change in their mRNA levels (Figure 3.2). IPS1 showed the strongest induction (more than 1000-fold). Experimental details are described in the Methods section below. For model fitting, the published fold change RNA-SEQ profile for PHO2 (Secco *et al.*, 2013) was also included along with the generated dataset.

Model fitting to data This work faces the challenge that the data available are comparatively sparse for a model of this size. The values of 20 parameters were estimated by fitting the model to the 50 data points corresponding to the the fold changes in the miR399, PHO2 and IPS1 level in response to P stress. Thus, no units were assigned to the parameters, except for the time in hours (h). The dataset includes both generated and published data points. Model fitting was conducted

using a software named MONOLIX that incorporates the suite of parameter inference techniques, detailed in the Methods section. At the start of parameter estimation, the initial values of the variable were set to zero, with the exception of PHO2 and CytoPi, which were initially set to 1 and 5000, respectively.

All the estimated parameters are listed in Table 3.2 and 3.3, including the mean of the estimated parameter along with their standard deviation. Most estimated values are within the biologically relevant range, except for the parameters concerning IPS1 synthesis, m_8 and r, whose magnitude were relatively higher than other parameters. Given the known short half-life (i.e ~5 hours) of IPS1, a high maximal expression level of the promoter (i.e. $m_8 = 693.33$) is essential to achieve the observed IPS1 level under P deficient conditions. The values for the rate of PHO1 production (m_6), uptake velocity for high affinity transporters (k_{11}) and kinetic parameters for CytoPi efflux by PHO1 (k_{15} and k_{16}), are relatively very small. This is due to lack of data for their respective variables. Perhaps, for the similar reason, the values for k_2 and k_4 were poorly estimated with higher standard deviation than their mean, but due to their small magnitudes they do not hinder further investigation at this stage. However, these estimates are explored further in later sections.

3.2.3 Sensitivity and robustness analysis

Global sensitivity analysis was performed (Figure 3.3A and C) to investigate non-linear effects of the model parameters on the model output by simultaneously varying all of them (See Methods for details). The integrated response (i.e. total sensitivity of the model output across the time-course with respect to the variation of parameters) shows that most system (state) variables are sensitive to the parameter (m_2) - the rate of PHR2 synthesis, Figure 3.3A. As PHR2 is central to the regulation of P uptake, its rate of synthesis is bound to affect various downstream variables, ranging from PHR2S to IPS1. The concentration of CytoPi is most sensitive to the rate of its internal utilisation (U). Though time-dependent response (i.e.sensitivity of the model output with respect to the change of parameters at different time points) suggests that the sensitivity of CytoPi to U remains high for initial 72 hours upon P stress after which it decreases by 1.6 fold, Figure 3.3C. This is indicative of the stress response going into action. Notably, U is also the most sensitive model parameter followed by m_2.

Robustness is the property of a system that maintains its function(s) under perturbations. Robustness analysis was performed to investigate the robustness of the model

Parameter name	Description	Value	s.d.	Units
m_1	Maximal production rate of SIZ1	0.422	0.004	h^{-1}
m_2	Maximal production rate of PHR2	0.2	0.001	h^{-1}
m_3	V_{max} for PHR2 sumoylation	3.532	0.005	h^{-1}
m_4	Maximal production rate of miR399	6.639	0.021	h^{-1}
m_6	Maximal production rate of PHO1	0.003	0.0004	h^{-1}
m_7	Maximal production rate of PHT	2.6083	0.0171	h^{-1}
m_8	Maximal production rate of IPS1	693.33	0.0032	h^{-1}
k_2	Rate constant for PHR2-CytoPi interaction	0.002	0.013	h^{-1}
k_3	Michaelis constant for PHR2 sumoylation	1.147	0.003	h^{-1}
k_4	Rate constant for PHR2S deSUMOylation	0.008	0.065	h^{-1}
k_5	Activation coefficient for miR399 production	28.89	0.0006	h^{-1}
k_7	Binding constant for IPS1 and miR399	2.49e-7	0.01e-7	h^{-1}
k_8	Dissociation constant for IMC	1.19e-7	0.02e-07	h^{-1}
k_9	Activation coefficient for PHT production	0.769	0.017	h^{-1}
k_{10}	Activation coefficient for IPS1 production	64.69	0.0074	h^{-1}
k_{11}	Partial V_{max} for HPHT	0.1251	0.024	h^{-1}
k_{15}	Partial V_{max} for phosphate efflux by PHO1	0.0546	0.025	h^{-1}
k_{16}	$k_m$for phosphate efflux by PHO1	0.1174	0.024	dl
β	Flux of miR399 from shoot to root	0.1682	0.02	h^{-1}

Table 3.3: Parameter estimates and with their respective standard deviation.

variables against the total parameter variation. This analysis identifies CytoPi as the most robust variable underlining the fact that the system always tries to keep its concentration constant (Figure 3.3B). The high-affinity phosphate transporters (PHTs) are the next most robust variable, reflecting system's need to use these transporters only when necessary. On the other hand, IPS1 is the least robust variable, reflecting its very large change in concentration. It also worth noting that IPS1 shows a large variation in its level between different rice varieties upon P stress (Oono *et al.*, 2013b).

3.2.4 The model fits miR399 and IPS1 data under phosphate stress conditions

The model fit to the generated (fold change) data for miR399 and IPS1 transcripts is good, Figure 3.4. In accordance with the experimental data, the model predicts the induction of miR399 and IPS1 upon Pi starvation and their minimal steady state expression under the Pi-sufficient condition. Furthermore, all the data points for miR399 and IPS1 lie within the range of certainty of the model fits and the model description and parameters for miR399 and IPS1 are consistent with the experimental data. This cannot be said for PHO2, which is discussed in the next section

3.2.5 Poor model fit to PHO2 time-course data

Upon Pi stress, the observed level of PHO2 mRNA starts to decrease within 6 hours but does not disappear completely. Figure 3.5 shows that the model reflects the latter, presumably because IPS1 is binding some of the miR399 that has been produced. However, the model is not showing the early decrease in PHO2 mRNA. This can be explained by the fact that model has only miR399 as the phosphate-responsive degrader of the mRNA and its levels begin to rise only after a 1-3 day delay. This suggests that something else is affecting PHO2 levels.

The potential phosphate-responsive candidates could be an RNA (mRNA, micro-RNA or lnc-RNA) or protein (enzyme or RNA-binding protein). Two candidate RNAs could be IPS1 and PHO2;2 - a splice variant of PHO2 expressed from an upstream P-responsive promoter (Secco *et al.*, 2013). Both are capable of forming stable ds-RNA structure with PHO2 mRNA, Figure 3.6, but whether these structures would be

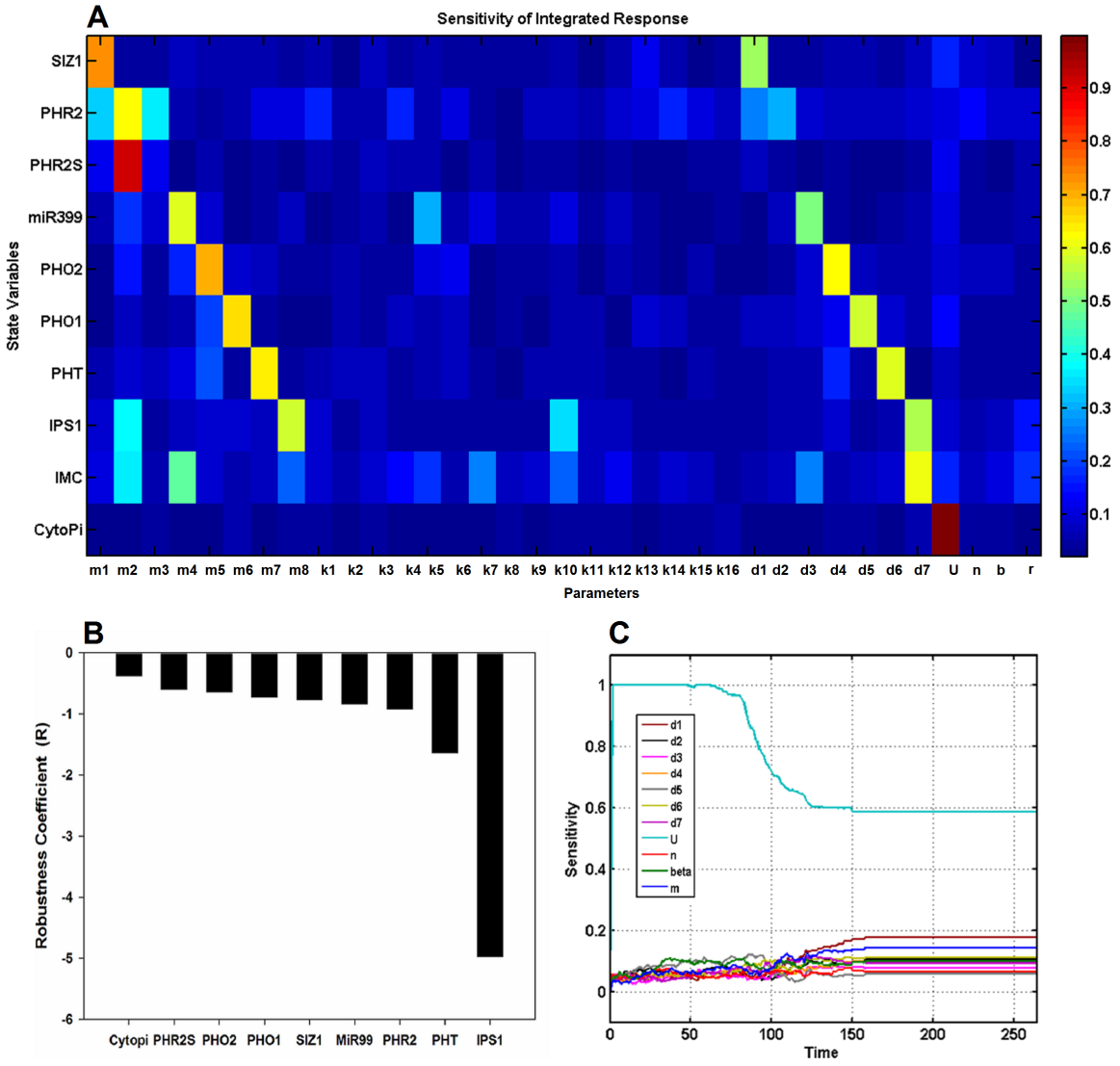

Figure 3.3: Global sensitivity and robustness analysis of the parameterised model. Panels A depict the heat-map for multi-parametric global sensitivities for the integrated response of different parameters on the system variables.The sensitivities are between 0 and 1, where a value closer to 1 reflects the higher sensitivity of the model output to the respective parameter. Panel B presents the robustness of the individual variables in the model. The robustness co-efficient (R) is usually calculated as a negative value. The closer the R to zero, the more robust the variable to perturbation (parameter variation). Panel C depicts the sensitivity of CytoPi to different parameters at different time points.

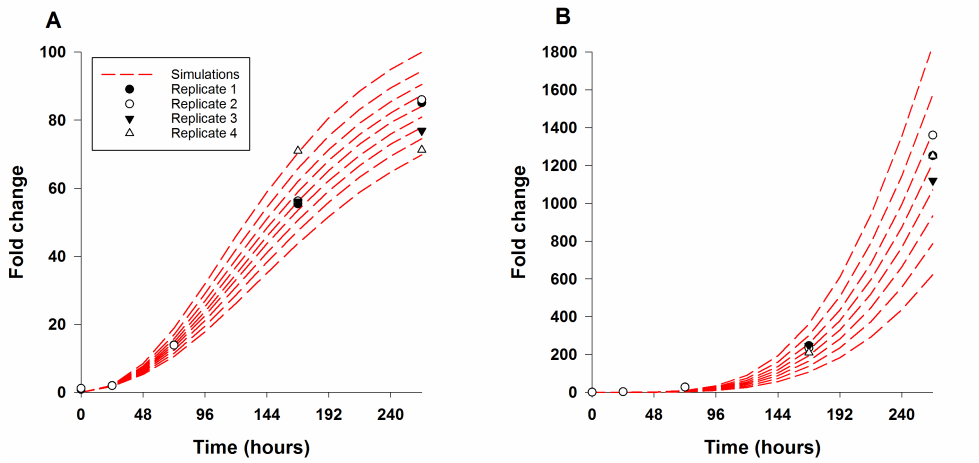

Figure 3.4: Model fits to IPS1 and miR399.
All experimental data points for (A) miR399 and (B) IPS1 (presented in Figure 3.2) lie within the 80% prediction interval of the model (red dashed lines). Simulation have been carried out by sampling parameter values from normal (Gaussian) distributions with means and standard deviations given from the parameter fitting in Monolix. The box on the top left give the details of the data points.

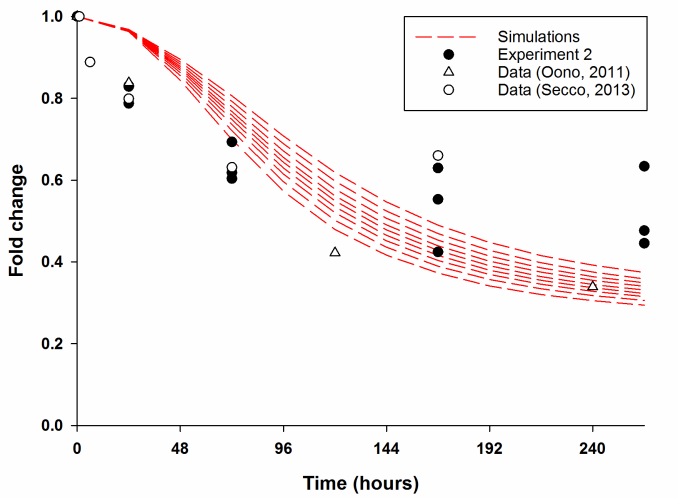

Figure 3.5: Model fit to PHO2 data
The dataset corresponds to the one presented in Figure 3.2 supplemented with the fold change mRNA-seq data published in (Oono *et al.*, 2011; Secco *et al.*, 2013).The fit to the data is very poor. Almost none of the data points fall within the certainty limits of prediction interval of the model (dashed red lines). This simulation have been carried out by sampling parameter values from normal (Gaussian) distributions with means and standard deviations given from the parameter fitting in Monolix. The box on the top right give the details of the data points.

Figure 3.6: Interaction prediction for PHO2 with IPS1 and PHO2;2.
PHO2 sequence are aligned with the interacting regions of (A) IPS1 and (B) PHO2;2. The sequences are shown close together where base-pairing can occur. The 13bp stretch with IPS1 is particularly striking.

cleaved is unclear. However, IPS1 is expressed too late to play this early role. The published mRNA-seq dataset (Secco *et al.*, 2013) was used to carry out a BLAST search with a sub-sequence that spans the PHO2;2-PHO2 splice junction, Figure 3.7. This indicates that PHO2;2 did not appear until 3 days of Pi starvation, which again is too late to explain the early decrease in PHO2 mRNA levels.

3.2.5.1 Hypotheses and mechanistic models for early PHO2 inhibition

Five hypotheses are considered as potential mechanistic explanations for the observed PHO2 dynamics. The first four hypotheses assume some unknown regulator Z acting as (i) a Pi-dependent transcriptional activator of PHO2 (PdTA) - eqs. 3.11 and 3.12, (ii) a Pi-dependent protector of PHO2 mRNA (PdRP) - eqs. 3.11 and 3.13, (iii) a Pi-sensitive binder of PHO2 mRNA causing mutual degradation (PsMD) - eqs. 3.14 and 3.15, or (iv) a Pi-sensitive transcriptional repressor of PHO2 (PsTR) - eqs. 3.14 and 3.16. The fifth hypothesis assumes a Pi-sensitive RNase promoting degradation of PHO2 mRNA in absence of CytoPi (PsRA) - eq. 3.17. All these hypotheses are diagrammatically presented in Figure 3.8. Each hypothesis was tested as an individual model with an attempt to fit the complete data set. In this round of parameter estimation, k_6 and d_4 are also included for estimation while previously estimated parameters in Table 3.2 - 3.3, were used as the initial values.

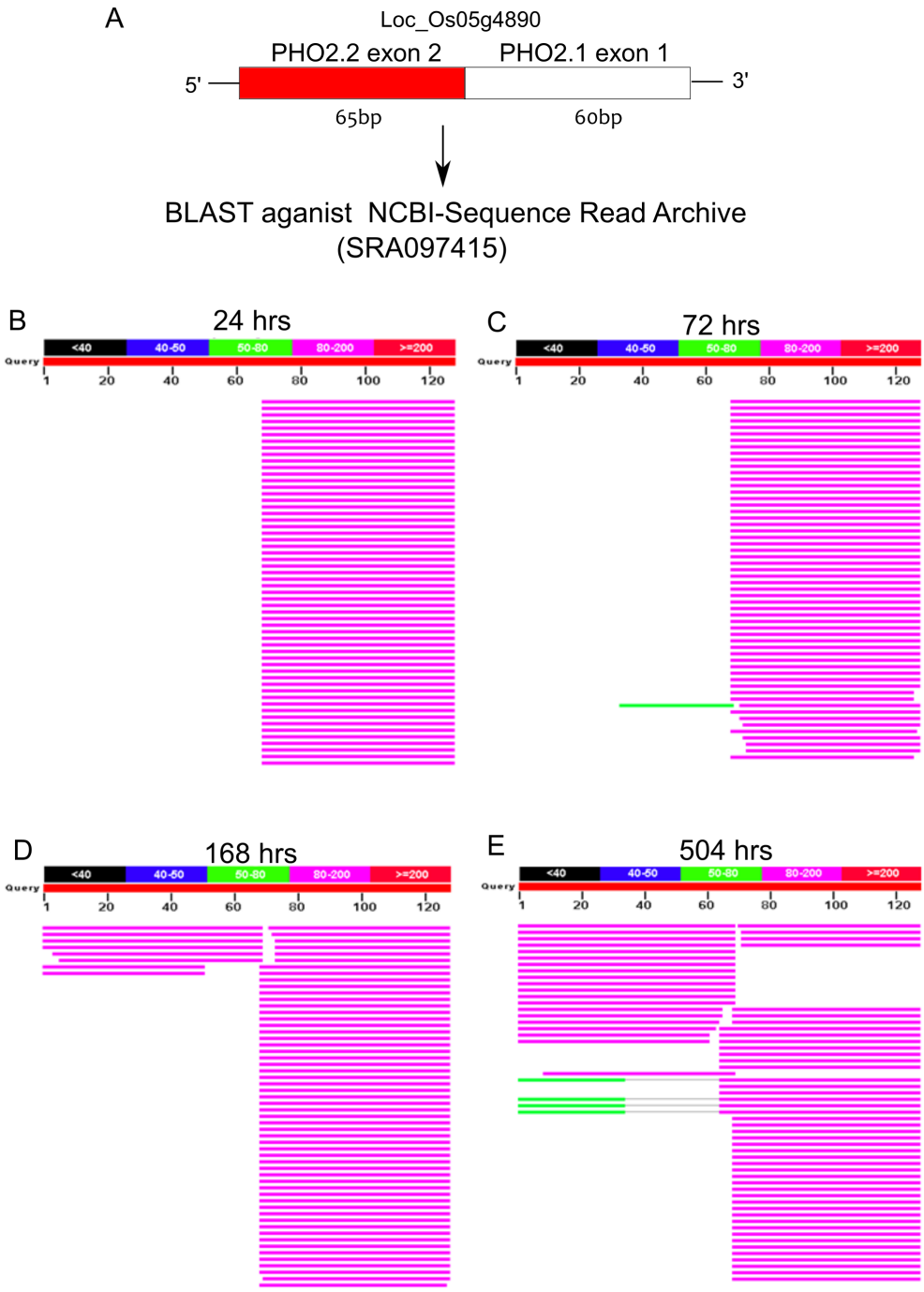

Figure 3.7: Qualitative view for the expression of PHO2.2 at different time-points under phosphate stress.
(A) A sub-sequence (125 bp) that spans the OsPHO2;2-OsPHO2 splice junction (B-E) BLAST output summary image from querying sequence datasets from plants starved respectively for 24,72, 168 and 504 hours. Each bar corresponds to an individual RNA-SEQ read, which is colour coded on the basis of its sequence similarity

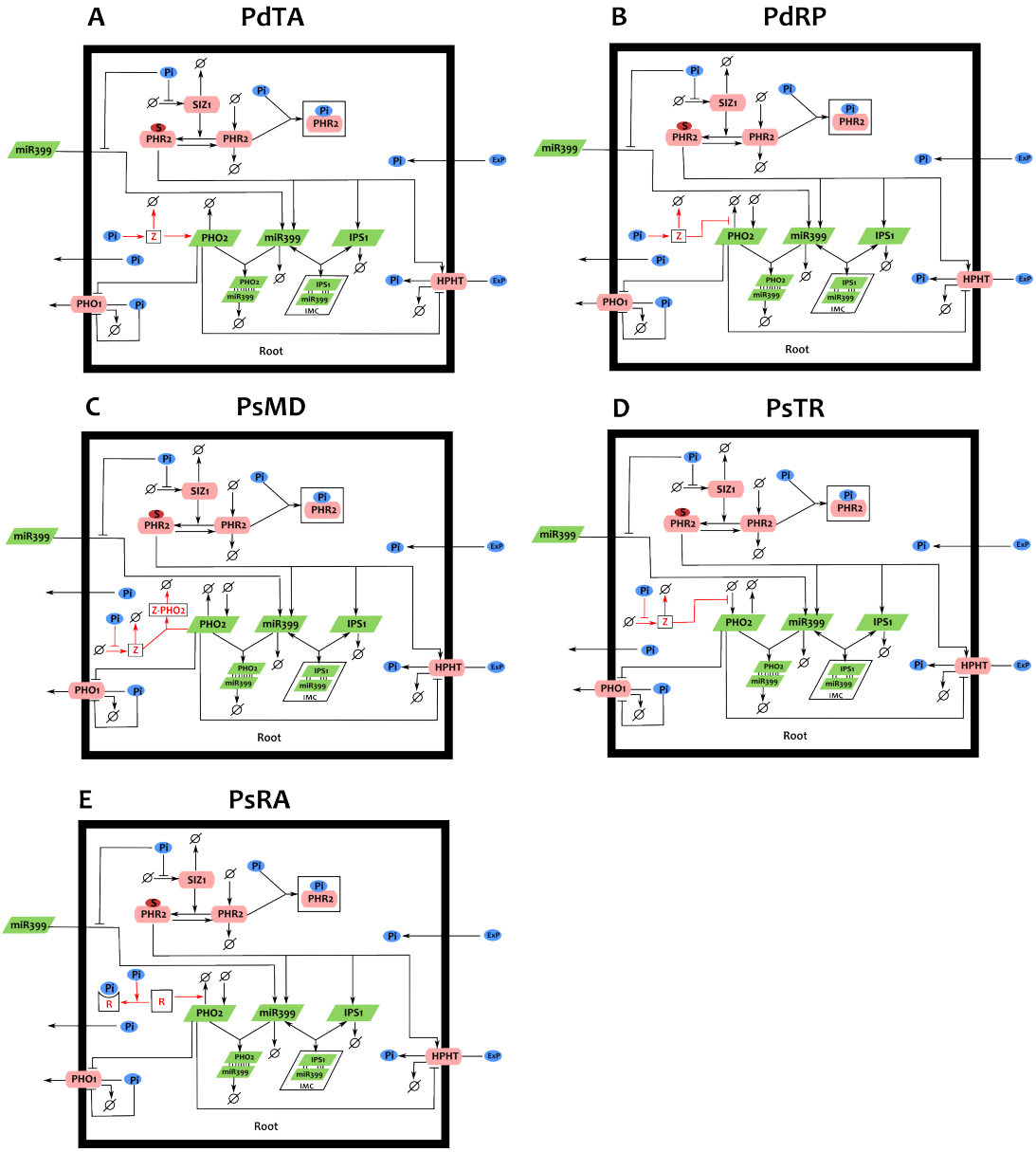

Figure 3.8: Schematic representation of the five hypotheses to explain the observed PHO2 dynamics under P deficient conditions.
Panel (A-E) depicts individual hypotheses (model) in a single root cell (thick black box). Red lines and letters denote the assumed reactions and species, respectively. Each hypothesis assumed the presence of an unknown regulator Z (A-D) or R (E) acting in different manners. Protein, ligand, mRNA, complexes and Pi ions are denoted by rectangles (pink), red ellipse, parallelogram (green), squares (transparent) and blue ellipse, respectively. Pointed solid arrows denote direct interactions and fluxes, barred arrows denote inhibition or repression, and dashed lines represent indirect interactions. ø denotes endogenous production and degradation of the molecules.

$$\frac{d\,[Z]}{dt} = m_9\,[CytoPi] - d_8[Z] \tag{3.11}$$

$$\frac{d\,[PHO2]}{dt} = m_5[Z] - k_6\,[miR399][PHO2] - d_4[PHO2] \tag{3.12}$$

$$\frac{d\,[PHO2]}{dt} = m_5 - k_6\,[miR399][PHO2] - \frac{d_4[PHO2]\,k_{17}}{(k_{17} + [Z])} \tag{3.13}$$

$$\frac{d\,[Z]}{dt} = \frac{m_9\,k_{18}}{(k_{18} + [CytoPi])} - d_8[Z] \tag{3.14}$$

$$\frac{d\,[PHO2]}{dt} = m_5 - k_6\,[miR399][PHO2] - d_4[PHO2][Z] \tag{3.15}$$

$$\frac{d\,[PHO2]}{dt} = \frac{m_5\,k_{19}}{(k_{19} + [Z])} - k_6\,[miR399][PHO2] - d_4[PHO2] \tag{3.16}$$

$$\frac{d\,[PHO2]}{dt} = m_5 - k_6\,[miR399][PHO2] - d_4[PHO2] - \frac{k_{20}[PHO2]}{(1 + [CytoPi])} \tag{3.17}$$

All five models show a good fit to the PHO2 (Figure3.9), miR399 and IPS1 dataset (see Appendix Figure D.3 and D.4), with -2 log-likelihood values lower than the original model. Using the inferred Akaike Information Criterion (AIC), statistical analysis values indicate that the hypothesis models offer significantly better fits to the data compared the the original model, Table3.4. This also implies the hypotheses better represent the observed PHO2 dynamics under low P conditions. Though the estimated half-life of PHO2 (i.e d_4) for PdRP and PdTA and the binding constant for miR399 and PHO2 (i..e.k_6) for PsMD and PdTA were in appropriate ranges, their respective SDs are high, see Appendix Table D.3. Among the five hypotheses, PdRP gives the lowest AIC value and, statistically, it is the best hypothesis for PHO2 dynamics. However, there is a qualitative difference between the models in predicting the 6-hour time point, for which only PsMD and PsTR are able to capture the early

drop in PHO2 level upon P stress. The time at which PHO2 mRNA levels drop can be used to differentiate between these pairs of models.

Model	AIC	-2LL	T	$\triangle AIC$	k	P-value
PiOM	238.70	142.70	48	-	-	-
PdRP	192.2	88.2	52	46.5	4	4.14E-11
PdTA	206.58	106.58	50	32.12	2	1.43E-08
PsRA	211.51	111.5	50	27.19	2	1.69E-07
PsMD	218.86	106.86	56	19.84	8	1.88E-05
PsTR	234.31	122.31	56	4.39	8	8.96E-03

Table 3.4: List of AIC, -2 log-likelihood and P-value for the hypothesis models. The AIC and log-likelihood values were generated for each model while estimating parameters using MONOLIX. The relationship between between the P-value and $\triangle$AIC is following: $P\,value{=}Probability\,(\chi^2_k > \triangle AIC + 2k)$ (Murtaugh, 2014). Here, k is the degree of freedom (i.e. the difference in T - the total number model parameters, including both structural and statistical model). Using this relationship, P-value was calculated using Chi-squared distribution (CHIDIST) function in Microsoft Excel, while comparing the AIC value and number of parameters for each hypothesis model with the original model (PiOM).

3.2.5.2 PsTR is the best model

mRNA was purified from rice roots after 0, 3, 6 and 12 hours of Pi starvation and fold changes in PHO2 levels were determined by qRT-PCR (Figure 3.10). Almost 80% of PHO2 mRNA was lost by 3 hours of P stress but recovered slightly at 6 and 12 hours. In contrast, its level in P sufficient conditions, if anything, increased slightly. This profile favours the PsMD and PsTR models. Of these, phosphate binding sites are more likely in proteins than RNAs. Thus, PsTR is the most probably model explaining PHO2 dynamics. However, experimental validation is needed to confirm this further.

Notably, the maximal repression co-efficient for Z (k_{17}) in the PsTR model is a critical parameter attributing to the internal P sensing mechanism and tightly regulating early PHO2 kinetics under P deficient condition. The partial recovery also implies some feedback mechanism that attempts to maintain PHO2 transcript levels. For example, PHO2 might ubiquitinate and hence degrade it own activator, such a

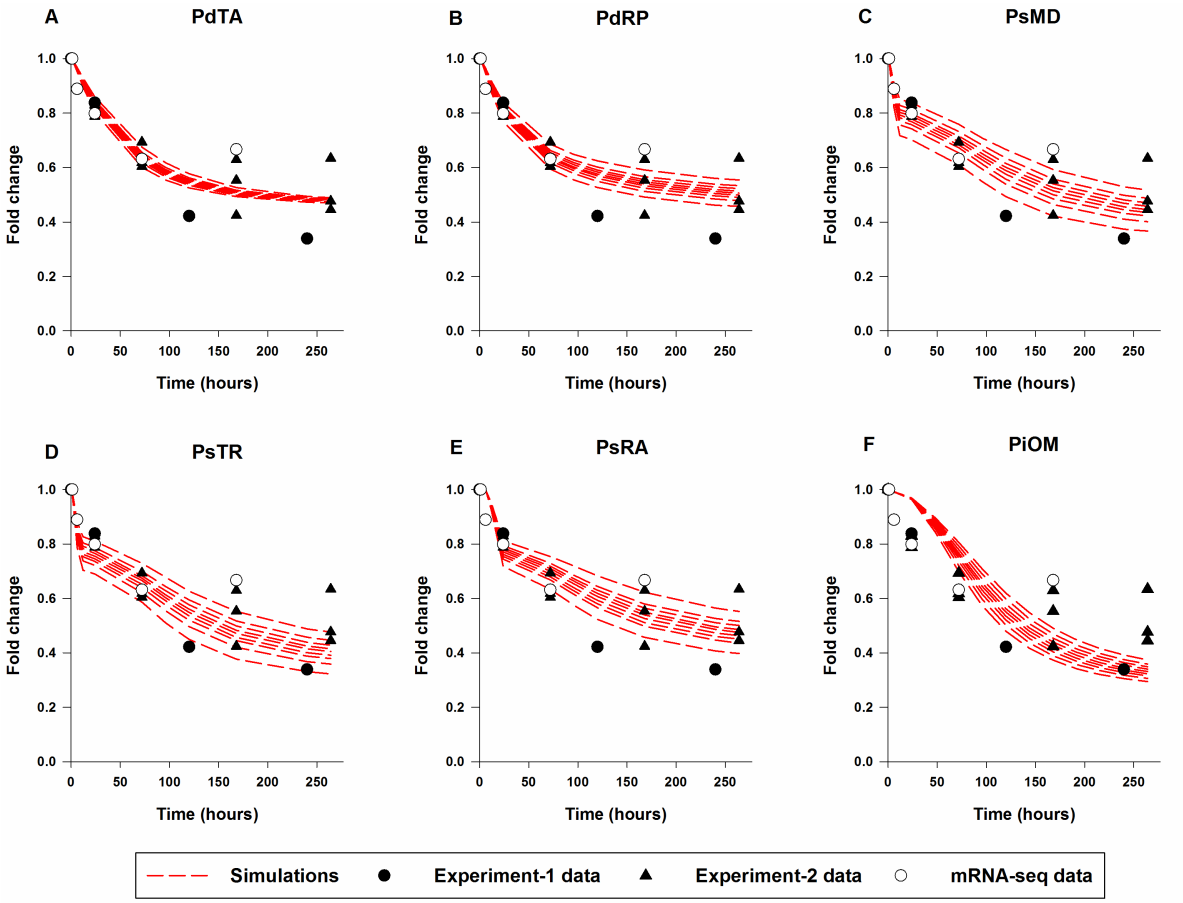

Figure 3.9: Fitting of different hypothesis models to PHO2 data.
Panel A-E depicts the fit offered by each hypothesis, while Panel F represent the fits of the original model, now named PiOM. Red dashed lines represent the 80% prediction interval of the respective models. These simulations have been carried out by sampling parameter values from normal (Gaussian) distributions with means and standard deviations given from the parameter fitting in Monolix. The box on bottom center give the details of the data points. Fold change mRNA-seq data is adopted from (Oono *et al.*, 2011; Secco *et al.*, 2013)

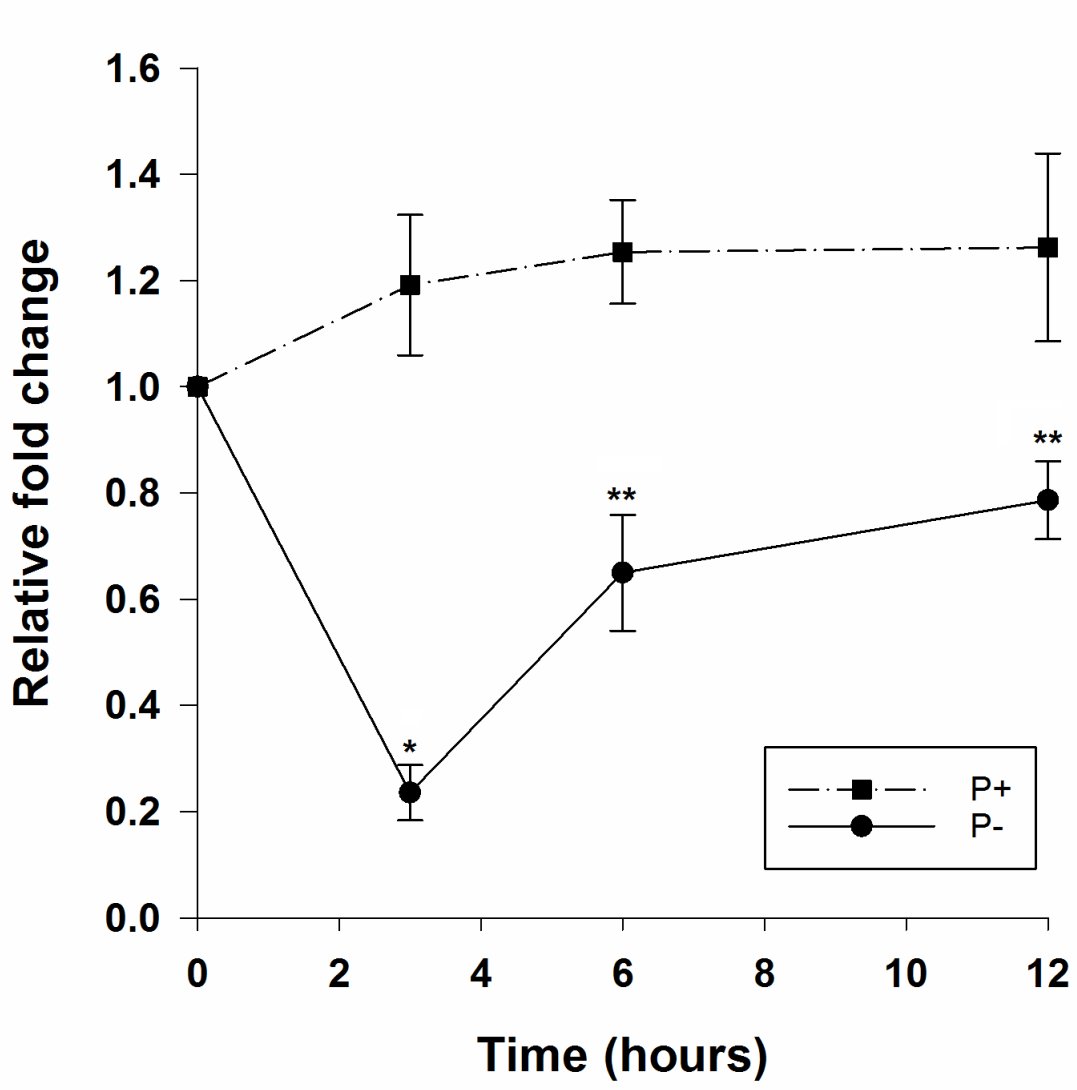

Figure 3.10: Relative fold change in the levels of PHO2 transcript following 12 hours of Pi-stress.
The expression levels are relative to the +P condition at initial time point zero. Errors bars are SE and n = 3. Data significantly different from the corresponding controls are indicated (*P $<$ 0.01; **P$<$0.05 Student's t test in Microsoft Excel). Relative expression levels were normalized to that of an internal control, Os-ACTIN. Very similar results have been independently determined by Jitender Giri's group (personal communication, NIPGR, India)

mechanism could also explain why the mRNA does not completely disappear, but uncovering the details of this mechanism falls beyond the scope of this work.

3.2.6 Model predictions

Thus far the models have been parameterised and refined using data from Pi-starved roots. Its completeness in representing the system for Pi starvation responses depends on it ability to correctly predict system behaviour under various genetic and environmental scenarios. The PsTR model was used to perform perturbation analysis. As mentioned earlier, there is a lack of data for PHO1, PHTs and phosphate flux. The values for the uptake velocity for high affinity transporters (k_{11}), rate of PHO1 production (m_6) and kinetic parameters for CytoPi efflux by PHO1 (k_{15} and k_{16}) were estimated to be lower than might be expected. Since the published perturbations involves modification of high-affinity phosphate transporters expression, these parameters were altered to bring them closer to expected values (see Table 3.5). In addition, a constant corresponding to the basal expression of high affinity transporter, the maximal inhibition of both PHT and PHO1 by PHO2 and maximal inhibition of PHO1 by CytoPi, were respectively introduced and set to 0.009, 0.01 and 100. These alteration and addition of parameters were done such that maintaining CytoPi at the steady state. Hence, these alterations do not affect the quality of the model fit to the dynamics of miR399, PHO2 and IPS1 (see Appendix Figure D.5).

Parameter	Previous estimates value	New value
m_6	0.0028	2.7
k_{15}	0.054	555.3
k_{16}	0.1174	11.831
k_{11}	0.1251	17250

Table 3.5: Altered parameters values for perturbation analysis

Figure 3.11 compares the output from simulation (in which the model has been modified to correspond to various scenarios either by introducing a constant or stunting the production rate of the variable to zero, to represent overexpression or knockdown conditions, respectively) with the published figures. They show a good qualitative agreement with observations from mutant studies and contribute to validation of the model. Though this could simply because these observations were used in defining the original network topology.

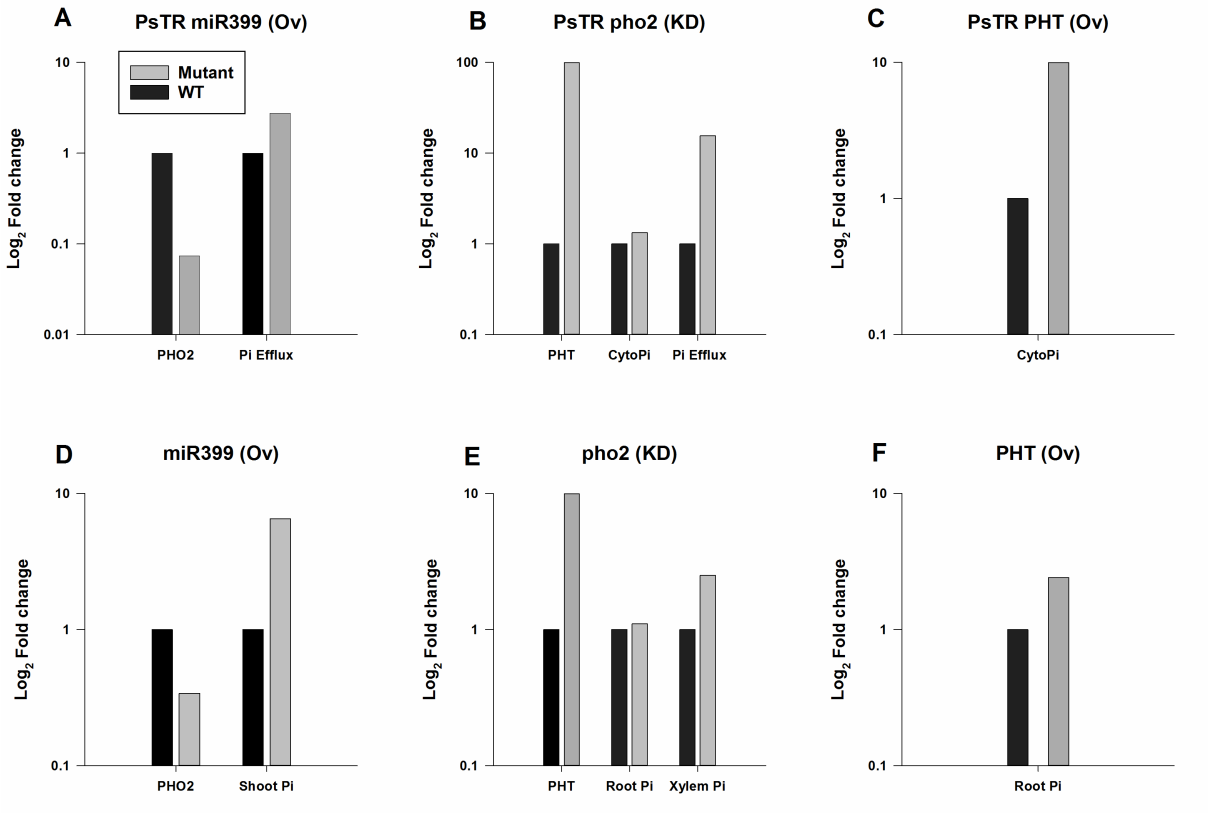

Figure 3.11: Perturbation analysis on PsTR model.
The overexpression condition for (A) miR399 and (C) PHT were simulated by adding a constant respectively set to 100 and 1 in the corresponding equation of the variables. (B) PHO2 knock-down condition was simulated by setting its initial condition and production rate to zero. (D-F) Replotted published data for different mutant studies as titled in the respective panels. D-E from (Cao *et al.*, 2014; Hu *et al.*, 2011); F from (Jia *et al.*, 2011)

3.3 Discussion and Conclusion

The aim of this work has been to gain a quantitative understanding of the molecular mechanism regulating phosphate acquisition in plants, with a view ultimately to inform the development of phosphate-efficient crop varieties. As a part of this study, mechanistic mathematical models for the key molecular network regulating phosphate uptake have been developed. Time course qRT-PCR data for the key regulators of the P signaling network under phosphate-deficient conditions were generated. Parameters for the model were estimated by fitting to these and other published data (Oono *et al.*, 2011; Secco *et al.*, 2013), using a non-linear mixed-effect modeling approach (Laveille, 2014). The temporal expression level from this original model (PiOM) well

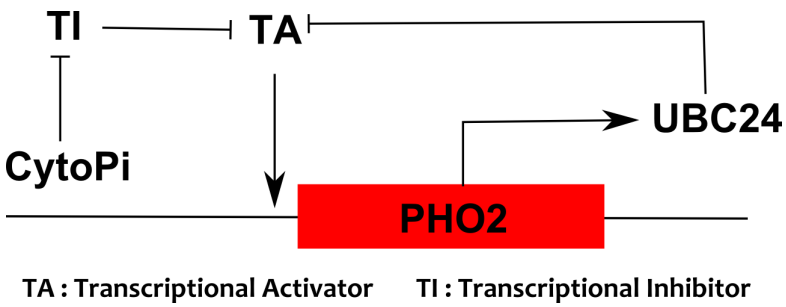

Figure 3.12: Potential model for PHO2 regulation under phosphate deficient condition.

fitted the observed values for miR399 and IPS1, but not PHO2 mRNA, which showed a 24 hours delay before levels started to drop. The latter can be attributed to the slow appearance of miR399.

This result suggests that there is an extra Pi-stress mechanism causing an early reduction in PHO2 mRNA levels. Five hypothetical mechanisms were modeled, of which a phosphate-sensitive transcriptional repressor (PsTR) was the most credible on the basis of improved overall fit to the data, fitting to the observed 6 hour time point value and, prior knowledge of allosteric regulation in general. To aid resolution of the hypothetical mechanisms, qRT-PCR data were generated for four points over 12 hours of P starvation. Independent testing confirmed the result that 80% of PHO2 mRNA is lost by 3 hours, at a rate close to the normal for RNA. This level is partially restored by 6 hours, indicative of PHO2 regulating its own level of transcription, as this is the time scale in which DELLA regulates its own expression (Band *et al.*, 2012a).

This lead to a hypothesis for regulation of PHO2 expression as shown in Figure 3.12. PHO2 is expressed courtesy of a Transcriptional Activator (TA), whose degradation it mediates to maintain constant PHO2 levels. However, TA binding efficiency (and hence rate of transcription) is impaired by the binding of a Transcriptional Inhibitor (TI) or Transcriptional repressor (Z) (see Figure 3.8), which can only act when Pi is low.

Mostly likely TA is a transcription factor that could undergo ubiquitination by PHO2 (UBC24) protein. While the early drop and partial recovery of PHO2 transcript following Pi stress indicate the instantaneous interaction between TA and TI. Sequence analysis of the upstream region 500bp of OsPHO2 gene (presented in Appendix D) have predicted various transcription factor binding sites, see Appendix table D.8. This largely includes signatures for MYB, WRKY, bHLH, bZIP, MAD-box and

DOF transcription factor families. The expression profiles of corresponding family members under deficient Pi conditions are presented in Appendix figure D.6. In response to Pi stress, the contrasting expression pattern within the members of same family is observed. Interestingly, some members across all the presented families follow the pattern similar to that of PHO2 mRNA upon Pi starvation. However, experimental analyses are required to investigate the precise identity of TA and its potential ubiquitination by PHO2 protein. The understanding of TA would subsequently allow the identification of TI.

Indeed, PsTR hypothesis can be tested by conducting two sets of experiments. The first set aims to identify the transcriptional activator (TA) of PHO2 from the predicted list, its interacting proteins (TI or Z) and potential forms of post-translational modification. The second set of experiments tests the hypothesis of PHO2 auto-regulation. Introducing a point mutation, say by CRISPR technique (Jeffry & Keith, 2014), to inactivate the enzyme's catalytic activity should block the negative feedback. If the hypothesis is correct, under normal Pi condition the mRNA level should be higher and constant and the plant might show symptoms of Pi toxicity. Loss of external Pi should result in an early drop in mRNA levels that do not increase in the 6-12 hour time frame. The same phenotype should be seen by removing the ubiquitination sites of TA.

The models developed in this study are relative simple. However, there are various avenues by which they could be improved or expanded. These include refinement of internal Pi utilisation, root-to-shoot and shoot-to-root signaling kinetics, tissue specificity and, importantly, external Pi in soil, which would deplete over time. In the current models, utilisation U is assumed to be solely dependent upon the CytoPi concentration. However, in reality internal Pi utilisation is an attribute of several processes. Thus, U could become a function of Pi storage and release from the vacuoles, nucleic acid synthesis and especially its degradation, the metabolic shift toward sulfolipids and symplastic diffusion between cells. All these are rather difficult to study experimentally, making parametrisation a challenge.

The effect of systemic signaling can be better represented by time-dependent variables (of which plant growth could be one) and delay-differential functions. Most laboratory data only consider the root as a whole, but open questions remain regarding any tissue specialisation in the regulation of P uptake and transport by roots, and the kinetic and paths through different root anatomies. These issue can begin to be addressed through multi-cellular models.

To conclude, this work has revealed four features. The first is that miR399-

mediated degradation is an insufficient explanation for the drop in PHO2 mRNA levels. The second is that its early decline is best attributed to some form of phosphate-sensitive transcriptional repression. Third feature appears from a short time-course dataset revealing the presence of a mechanism to maintain constant PHO2 mRNA level, perhaps through auto-regulation by PHO2 protein. Lastly, the model is validated by its simulations giving some qualitative responses consistent with the published experimental data, though there is one glaring exception which is the subject of the next chapter.

3.4 Materials and Methods

3.4.1 Plant Materials and Growth Conditions

3.4.1.1 Experiment 1, 2 and 3

Note: Experiment 1 was performed by Dr. Jing Shi at the College of Life Science, Zhejiang University (China) as a part of Collaboration with Nottingham and the produced data still remains unpublished while Experiment 2 and 3 were performed at School Biosciences, University of Nottingham (UK), as the part of this PhD thesis. However, similar protocols have been used to maintain the consistency of the data.

Rice (*Oryza sativa* cv Nipponbare) was used across all the experiments. Hydroponic experiments were performed under controlled conditions (day/night temperature of $24°C$ and a 12^{-h} photoperiod, 200 µmol photons $m^{-2}s^{-1}$), allowing 0.5 liters of hydroponic solution per plant. The hydroponic solution consisted of solution as described by Yoshida *et al.* (1976),containing $1.425\,mM\ NH_4NO_3$, $0.513\,mM\ K_2SO_4$, $0.998\,mM\ CaCl_2$, $1.643\,mM MgSO_4$, $0.075\,\mu M\ (NH_4)_6Mo_7O_{24}$, $0.25\,mM\ NaSiO_3$, $0.009\,mM\ MnCl_2$, $0.019\,\mu M\ H_3BO_3$, $0.155\,\mu M\ CuSO_4$, $0.152\,\mu M\ ZnSO_4$, and $0.125\,mM\ Na-EDTA-Fe$, with $320\,\mu M$ or NaH_2PO_4 replaced by$320\,\mu M$ $NaCl$, resulting in the +Pi and −Pi conditions. The pH of the solution was adjusted to 5.5, and the solution was renewed every 3 d. Rice seeds were first pre-germinated in tap water for 5 d before being transferred into the hydroponic solution, containing $320\,\mu M\ NaH_2PO_4$ (+Pi) for 15 days. In experiment 1 and 2, the 15 days old plants are transferred into the hydroponic solution, containing no NaH_2PO_4 (-Pi) for 11 days. In experiment 3, the 15 day old plants were transferred into the hydroponic solution, containing no NaH_2PO_4 (-Pi) for 24 hours. All experiment procedures such as media replacement, at interval of 3 days, and sample collection were performed at a similar time of the day to minimize possible circadian effects.

3.4.2 RNA Isolation and qRT-PCR Analysis

3.4.2.1 Experiment 1

Total RNA from frozen root samples was isolated using TRIzol reagent (Invitrogen) followed by treatment with DNase I (Qiagen) to eliminate genomic DNA contamination. cDNA was synthesized from 20 ug total RNA using Rever Tra Ace (TOYOBO) with oligo(dT) primer. qRT-PCR was performed using the FastStart Universal SYBR Green Master (Roche) on a LightCycler 480 Real-Time PCR system (Roche) according to the manufacturer's instructions. Relative expression levels were normalized to that of an internal control, Os-ACTIN. qRT-PCR for quantification of mature miR399 were performed following a published protocol (Varkonyi-Gasic *et al.*, 2007) and the corresponding primers are published in (Lv *et al.*, 2014). IPS1 primers used for qRT-PCR are listed in Appendix Table D.4.

3.4.2.2 Experiment 2 and 3

For total RNA isolation from frozen root using TRIzol reagent (Life Technologies) followed by treatment with DNase I (Qiagen) and column clean-up using RNeasy minikit (QIAGEN) to eliminate genomic DNA contamination. cDNA was synthesied using 5 µl of total RNA (500 ng) using SuperScript III First-Strand Synthesis kit (Invitrogen, Catalog No. 18080-400). The synthesized cDNA is cleaned from remaining RNA from an enzyme mix included in the kit (E.coli RNase H). qRT-PCR was performed using PerfeCTa qPCR SuperMix on a LightCycler 480 Real-Time PCR system (Roche). The detailed procedure is described in Appendix D. Relative expression levels were normalized to that of an internal control, Os-ACTIN as used in experiment 1. The primers for PHO2 and ACTIN are listed in Appendix Table D.4

3.4.3 Parameter estimation

3.4.3.1 Theory

The qRT-PCR data correspond to overall values for a population of multiple root cell types for 3 plants per biological replicate. With biological replication, observations are collection of n functions $f_i(t), i = 1...n$, one for each replicate. Often, the mean population function $\mu(t)$ characterises the overall temporal behaviour of the population. Furthermore, the observations are always subject to some level of measurement errors, inter-individual variability and some unexplainable variation. Integrating the variability of these is important to understand the population behavior and can be

captured using mixed-effect models. These statistical models or inference methods simultaneously account for both fixed and random effects on the observation from small sample sizes and sparse datasets. The fixed effects are population parameters (characteristic measures of the entire population) assumed to be the same at each time the data are collected, and random effects are random variables associated with each individual sample from a population. In contrast to linear models, non-linear mixed effect models consider the mathematical model (statistically referred to as a structural model) as the non-linear function of both fixed and random effects and involves approximation during the estimation.

With this notion, the unknown (population) parameters of the mathematical model were inferred by non-linear mixed-effects models implemented in the software named MONOLIX (MOdèles NOn LInéaires à effets miXtes), version 4.33s (Laveille, 2014), freely available at (http://www.lixoft.eu/). This software consist of algorithm that combine the Stochastic Approximation of Expectation Maximization (SAEM) algorithm with a Markov chain Monte Carlo (MCMC) procedure to estimate the maximum likelihood of the model parameters without any linearisation techniques. In MONOLIX, the statistical models are evaluated by using analytical model-selection tools, which includes information criteria such as Akaike information criterion (AIC) and Bayesian information criterion (BIC) and statistical tests such as Likelihood Ratio test and Wald Test. Such evaluation tools allow the building of improved statistical (and sometime structural) models, enhancing the precision of the estimates for the population parameters.

3.4.3.2 Algorithm

Initially, the individual parameters are simulated using an MCMC approach in the expectation step of SAEM algorithm. These individual parameters are then used to compute a stochastic approximation of the conditional expectation of the log-likelihood of the complete data. Subsequently, the complete log-likelihood is maximised to obtain the updated estimates of the population parameters. In practice, SAEM generates 1 to 5 random samples per individual per iteration to allow for an efficient and rapid convergence toward the solution. This burn-in period typically requires 200 iterations. Thereafter, the program accumulates random sample results for the next 300 iterations, to estimate the population means and inter-individual variances.

3.4.3.3 Execution

Model settings: Given that IPS1 RNA is partially complementary to miR399 (with 3 base mismatch), the binding affinity of miR399 toward IPS1 would be relatively weaker than that to PHO2. However, the release of IPS1 from the IPS1-miR399 complex would be slower than its binding. Assuming such a relationship, values of the parameter k_7(the binding constant for IPS1 and miR399) and k_8 (Dissociation constant for IPS1-miR399 complex) were indirectly deduced by estimating additional parameters (Y_1 and Y_2). These parameter were used purely for estimation purposes and is related to the known parameter k_6 (Binding constant for miR399 and PHO2), in following manner:

$$k_7 = \frac{k_6}{(1 + Y_1)} \text{ and } k_8 = Y_2 * k_7$$

MONOLIX settings The structural model (i.e. the Pi-regulation model) encoded in MLXTRAN format in a text file (Laveille, 2014), see Note 2 in Appendix D. This model and and the datasets were loaded onto the MONOLIX platform. Screen shot of the MONOLIX GUI platform is presented in Figure 3.13. The GUI platform is divided into four frames: the data and model, the initialization, the algorithms and the results. Each of these frames requires some input for the precise estimation of parameters. In this parameter estimation, the exercise following settings were used. In the data and model frame, the 'Combine1' observation model was selected for the model variable to which data are fitted. In the initialization frame, the initial value and standard deviation for the random effect for each parameter were entered. In the algorithm frame, the default Simulated Annealing option was unselected, the number of iteration (K1 and K2) and chains were respectively set to 800, 200 and 50. A new seed was generated for every run, and for other options the default settings were used. In the result frame, linearization was selected for standard errors and log-likelihood, while the conditional mode was selected for individual parameter options. Finally, estimation can be started using the run button given in the top centre. Details underlying all these options are well defined and explained in the tutorial available on the MONOLIX webpage (lixoft.eu/products/monolix/documentation).

Estimation settings: Due to the sparsity of dataset for parameters to be estimated, the inference was done by multiple sequential runs as follows. In the first run, the initial values of the parameters and their corresponding standard deviations were set

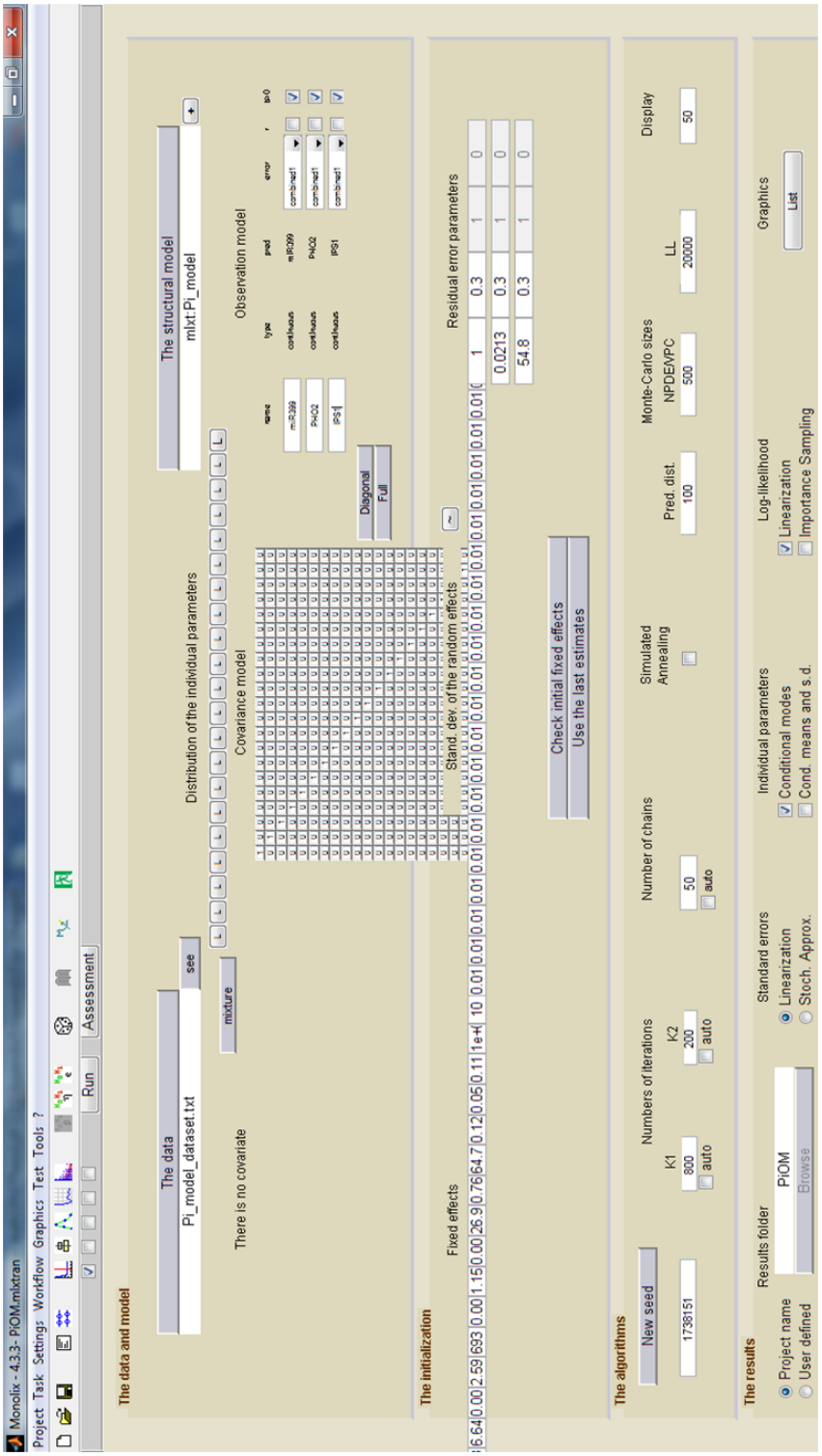

Figure 3.13: Screen capture of MONOLIX platform

to unity, and the program was executed. The resulting estimates were than assigned as the initial values for the second run. This cycle was repeated until the best fits were achieved. The algorithm initially struggled to find the range for certain parameters that would result in an acceptable fit to the extremely high IPS1 levels. Using the observation while manually exploring the parameter space, the initial values for m_8 andk_{10} were manually set to 1000 and 70 with standard deviation of unity. These adjustments gave appropriate estimates with acceptable fits to the observed data. The list for the initial values and estimates for the parameters and corresponding standard deviation from each run is given in Appendix D.

3.4.4 Model simulation and analysis

The model was defined and simulated in MATLAB using the solver ode45. This model was encoded in SBML format (Hucka *et al.*, 2003) using COPASI (Hoops *et al.*, 2006) and uploaded into the software named, Systems Biology Markup Language based Sensitivity Analysis Tool (SBML-SAT) to perform sensitivity and robustness analysis. Of the available options, multi-parametric algorithm was used to perform global-sensitivity analysis under default settings (Zi *et al.*, 2008). This algorithm randomly generates parameter values from a pre-defined uniform probability distribution thereby mapping the uncertainty of the parameters into the model output. Two output types were generated from this analysis: integrated and time-dependent response. The sensitivities from the integrated response corresponds to perturbation in each model variable (i.e. the area under the curve) with respect to the variation in the parameter during the time-course (Figure 3.3A) , while the latter reflect the perturbation at a time (Figure 3.3C). For robustness analysis, the Robustness-coefficient was recorded for all the variables from respective output plots and were replotted together as the bar-chart, Figure 3.3B.

3.4.5 Sequence analysis

3.4.5.1 PHO2.1 interaction prediction with IPS1 and PHO2.2

Sequences from PHO2.1, PHO2.2 (LOC_Os05g4890) and IPS1 (LOC_Os03g05334) were extracted from Plant Ensembl database (plants.ensembl.org). The interaction prediction was done using IntaRNA web tool (rna.informatik.uni-freiburg.de).

3.4.5.2 PHO2.2 dynamics under Pi stress

The sub-sequence spanning PHO2.1 and PHO2.2 was extracted from Plant Ensembl. The sequence was queried in BLASTN against NCBI-Sequence Read Archive (SRA097415), which contains sequence reads of all the samples (rice roots and shoots) collected in time-course Pi-starvation experiment (Secco *et al.*, 2013).

Chapter 4

IPS1 protection in phosphate starved plants

Abstract

The models developed in the previous chapter incorrectly predict the RNA profiles of PHO2 and IPS1 in response to phosphate resupply. Following sequence, structural and expression analyses, an expanded regulatory model has lead to the credible hypothesis that IPS1 RNA is protected from degradation in phosphate starved plants, which in turn leads to its very high level of accumulation. The protective agents are most likely to be phosphate-sensitive RNA-binding proteins.

4.1 Introduction

The previous chapter described validated models of the molecular regulation of phosphate uptake. These models were tested further to predict the dynamics of PHO2 and IPS1 when Pi is added backed to the external solution after the period of stress. However, the simulations incorrectly predicts the drastic drop in the IPS1 and PHO2 level in response to Pi repletion, see Figure4.1. This suggests that there must be some extra level of regulation concerning IPS1 and PHO2, which is not correctly represented in the current models. As much of the PHO2 regulations have been already explored in previous chapter, further attention was paid to IPS1.

There are two strike features concerning the dynamics of IPS1. The first is its extreme and unremitting elevation following 21 days of Pi stress and the second is its sudden drop within 24 hours of Pi repletion. The exact reason underlying these features of IPS1 dynamics is vaguely understood. Thus, this chapter explores IPS1 dynamics and its effect on PHO2 in both stress and repletion conditions. Various sequence and RNA-structure analyses and simulations from the refined models indicate that IPS1 RNA is probably protected from degradation during Pi stress.

4.2 Results and Discussion

4.2.1 Exploring IPS1 dynamics

The observed degradation rate of IPS1 during P repletion is very similar to the published value (Narsai *et al.*, 2007) for unstressed conditions that is currently in the models. This goes against the idea of a mechanism causing enhanced degradation upon P repletion and points to mechanism acting during P starvation. The IPS1 level is observed to rise more than 1000 fold within 21 days of P stress in roots. At present, the models account for this by having an extremely high rate of maximal synthesis ($m_8 = 669$) and a larger Hill co-efficient ($r = 4$) than is normally used to model transcriptional regulation, though the latter could represent an amplification mechanism. Elevated levels of IPS1 could therefore arise from either a Pi-sensitive "super-transcriptional complex" causing very high rates of synthesis or a Pi-sensitive protector that impedes IPS1 degradation. It is worth exploring published data to find evidence for these two hypotheses.

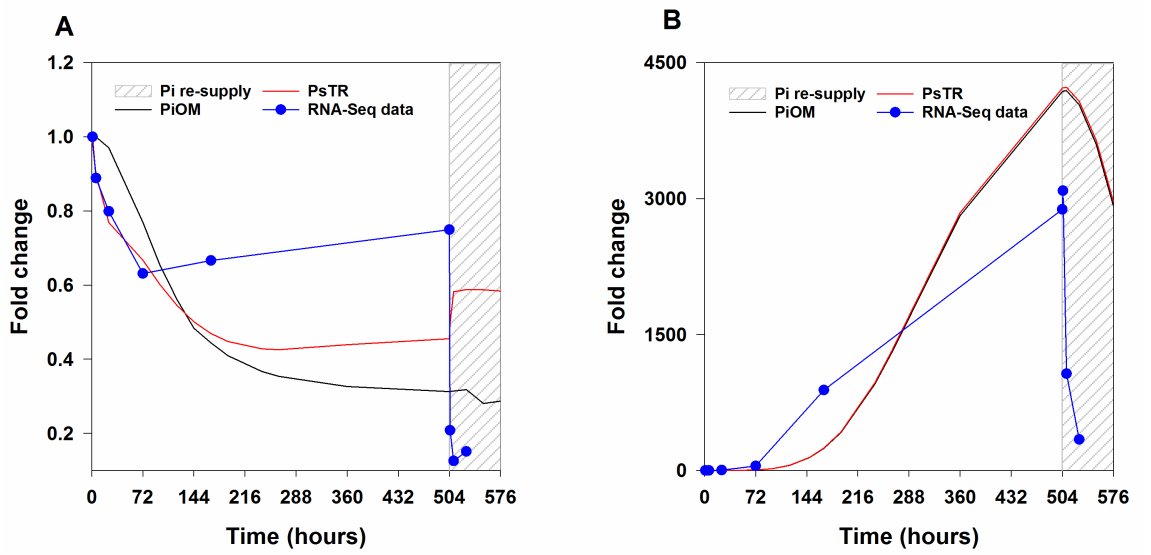

Figure 4.1: Observed and predicted profiles of PHO2 and IPS1 under Pi-stress and repletion condition.
A and B corresponds to PHO2 and IPS1 profiles, respectively. The blue-dashed lines shows the fold change in RNA-SEQ values from (Secco *et al.*, 2013), while the red and black line correspond to the output of the PsTR and PiOM models, respectively. The grey zones denote the period of P-resupply where the models significantly depart from the observed behaviour.

4.2.2 Evidence for a super promoter

Recent work on auxin-response elements (Mironova *et al.*, 2013) show how multiple Transcription Factor Binding Sites appear to act cooperatively rather than additively to cause higher levels of induction, with 7 binding sites causing the maximum stimulation of almost 30 fold over constitutive expression levels. In the case of IPS1, transcription is ~1000 times higher than constitutive levels. Around the IPS1 promoter (Figure 4.2), there are three copies of the P1BS motif to which PHR2S could bind (Rubio *et al.*, 2001). One of the P1BS sites is in the transcribed region, where RNA polymerase would at least temporarily separate the DNA strands, resulting in loss of PHR2S binding at that position. Furthermore, BLASTN searches with this upstream sequence revealed the presence of an un-annotated tRNA-gly gene on the anti-sense strand. This makes the potential regulatory region of IPS1 shorter, but data from (Secco *et al.*, 2013) indicate that the tRNA gene is also expressed in response to Pi stress, Figure 4.4. Hence, this sequence analysis does not rule out the possibility of an initiator complex that allows extremely high rates of synthesis but it seems most unlikely.

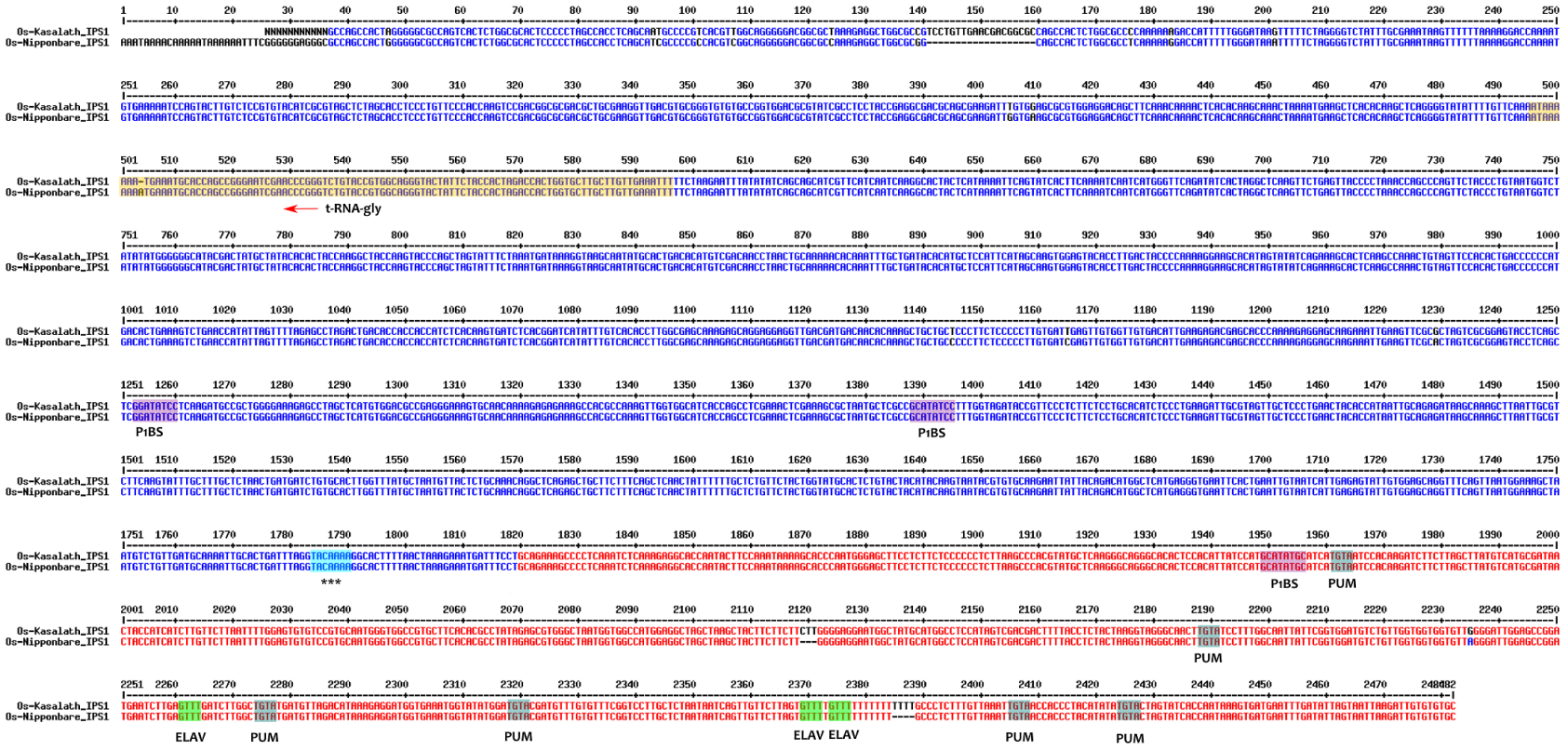

Figure 4.2: Multiple sequence alignment of IPS1 gene and its upstream regulatory region.
Red, blue and black text respectively corresponds to IPS1 gene, its upstream regulatory region and insertions in the Kasalath IPS1 sequence. Putative PHR2, Pumilio and ELAV-1 binding sites have been labeled P1BS, PUM and ELAV, and respectively shaded purple, blue-grey and green. The t-RNA-gly sequence and orientation has been labeled and shaded orange. The region shaped in sky blue with stars corresponds to predicted core promoter element.

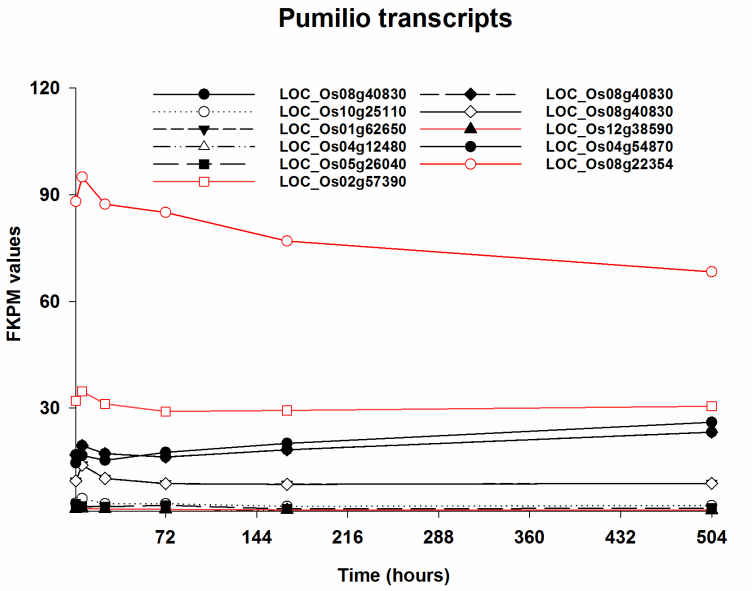

Figure 4.3: Expression profiles of different Pumilio genes under Pi-deficient condition.

4.2.3 Evidence for RNA protection

Two lines of evidence support this idea. First, RNA stability is known to be altered by protein binding. IPS1 is predicted to have two Pumilio binding sites near its 3´ end (Figure4.2), see Methods section. Role of Pumilio-RNA-binding proteins are well understood in animal systems(Spassov & Jurecic, 2003; Zamore *et al.*, 1997).Published transcriptome data (Secco *et al.*, 2013) show that the genes in this family are expressed at substantial levels and some may be elevated by Pi stress (Figure 4.3). Another predicted protein binding site near 3' end is for ELAV-like protein 1 (HuR). The nearest similar gene in plants are annotated as RNA-recognition and Poly-adenylate-binding proteins, making these candidate IPS1 protectors as well, see Methods section.

The second line of evidence is from RNA structure prediction. Querying 3' end sub-sequence of IPS1 RNA with different sizes of poly-A tract in BLASTN searches against NCBI-Sequence Read Archive (SRA097415) showed that the IPS1 poly A tail was usually ~18 bases. Centroid structures of IPS1, with and without, a poly A tail are shown in Figure4.5. These indicate that its poly-A tail considerably stabilises its

Figure 4.4: Expression regions around the IPS1 locus under normal, deficient and repleted Pi-conditions

A screen capture from the AnnoJ genome browser, representing the expression tracks of IPS1 locus and nearby genes (upstream and downstream) at different time-points under Pi sufficient, deficient and repletion conditions (plantenergy.uwa.edu.au/annoj/Secco_2013.html). The genes corresponding to respective tracks are denote on the top the image along with red arrow depict the direction of transcription.

structure through greatly increasing double stranded (ds) RNA formation, making it more resistant to attack by ribonucleases. One can envisage a protein which binds to the poly A tail (or to the polyA - polyU dsRNA region) in the absence of Pi. Upon repletion, this protein would no longer bind and IPS1 would revert to its original sensitivity to RNase degradation.

Figure4.6, also shows that 3' end of IPS1 has several stretches of complementary sequences which could potentially form a pseudo-knot. Bearing in mind that an 11 base-paired RNA sequence forms a complete cycle of a double helix, the 3' end of IPS1 can form a stem-loop consisting of two hydrogen bonding regions, 6 and 11 base pairs long. The terminal loop contains AATAAAG, which could form the pseudo-knot, and this structure could be stablised by the poly A tail hydrogen bonding to the 5' sequence to from a 12 and potentially 4 base paired region. Much smaller pseudo-knots are known to inhibit degradation by 3'exonucleases in plant RNA viruses (Gallie & Walbot, 1990; van Belkum *et al.*, 1985) , and could potentially play a role here. Taking everything into consideration, RNA protection is the more credible hypothesis and is worth investigating further.

4.2.4 Model incorporating IPS1 protection under phosphate stress

Using the PiOM and PsTR models, the IPS1 protection hypothesis can be tested by modulating the degradation rate of IPS1 and IMC as the function of CytoPi and examining Pi repletion conditions after a period of phosphate stress. The magnitude of the IPS1 degradation rate (d_{7*}) in the RNA Protection (RP) version of the models is defined as the product of original degradation rate of IPS1 (d_7) and the steady-state initial CytoPi concentration under normal Pi condition ($CytoPi$, $at\,time = 0$), see equations (4.1 - 4.4). In these new models, the degradation rates of IPS1 and IMC will decrease in response to low Pi, allowing IPS1 to accumulate and its reversible interaction with miR399 to form more IMC complexes. However, the degradation rates of IPS1 and IMC rapidly return back to normal upon Pi-resupply. The sudden degradation of IMC will thereby cause a rapid increase in the pool of miR399 and consequent short-term decline in PHO2. PiOM-RP and PsTR-RP model were fitted to the Pi-stress data set and parameters were re-estimated, see Appendix Table E.2.

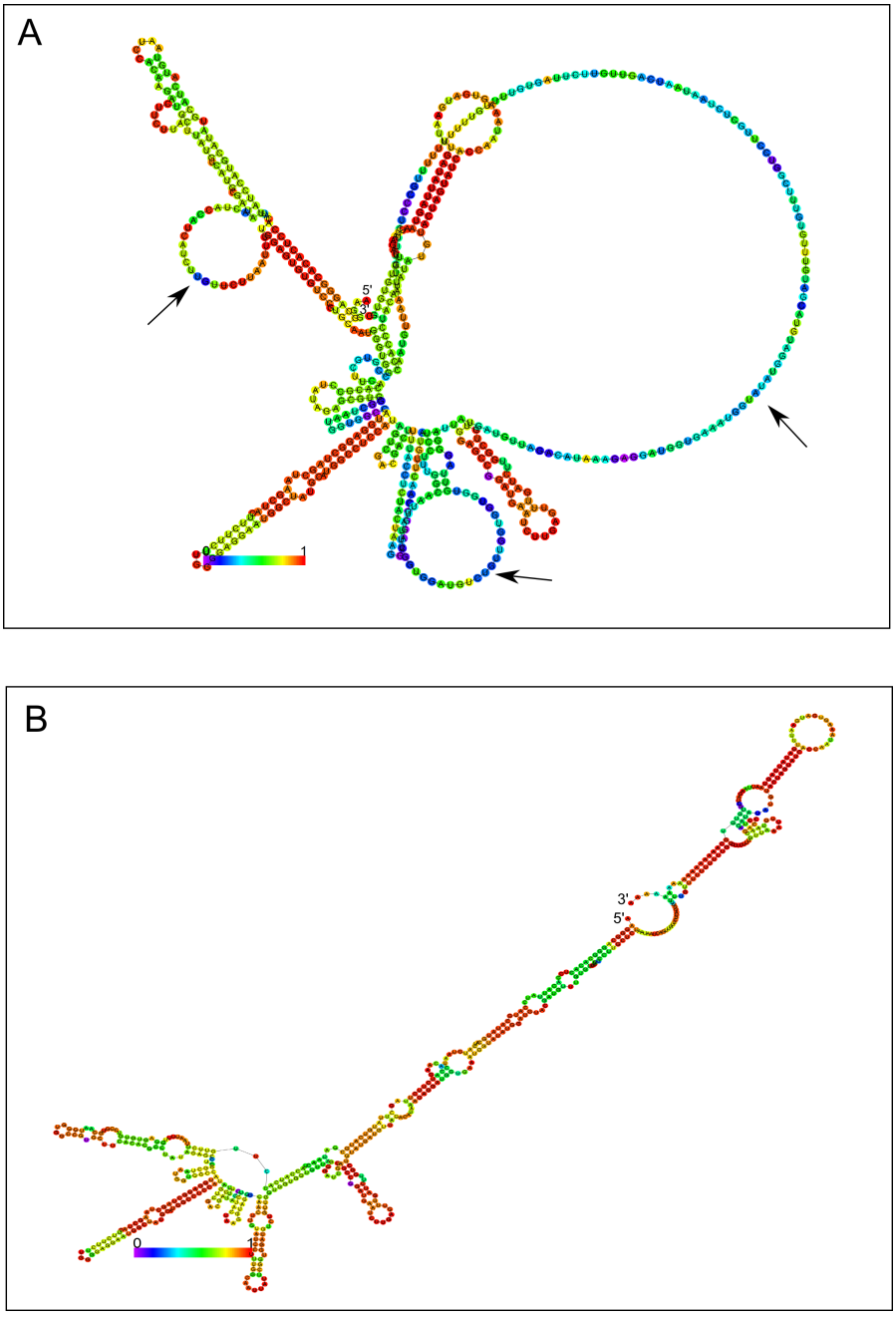

Figure 4.5: Centroid secondary structure prediction of IPS1 mRNA.
(A) IPS1 RNA without and (B) with a Poly A tail of 18 bases. The colour scale represents the probability among the ensemble of structures above the minimum free-energy structure that the base adopts to form the shown secondary structure. From red to violet denotes most to least probability. Arrows denote RNase sensitive sites.

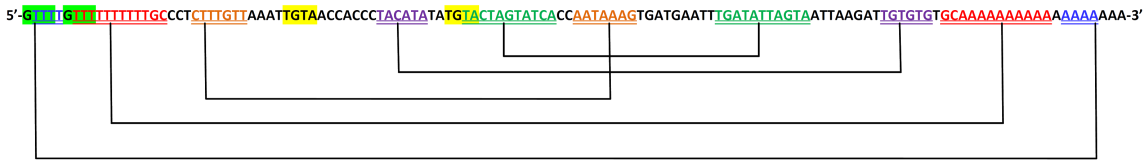

Figure 4.6: Potential pseudo-knot near 3' end of IPS1
The black lines show potential base-pairing structures near 3' end of IPS1. The predicted Pumilio protein binding sites are highlighted in yellow.

$$\frac{d\,[miR399]}{dt} = \frac{\beta.}{\Big(1 + [CytoPi]\Big)} + \frac{m_4[PHR2S]^n}{k_5^n + [PHR2S]^n} - k_6[miR399][PHO2] \qquad (4.1)$$
$$- k_7[miR399][IPS1] + k_8[IMC] - d_3[miR399]$$
$$+ d_{7*}[IMC][CytoPi]$$

$$\frac{d\,[IPS1]}{dt} = \frac{m_8[PHR2S]^r}{k_{10}^r + [PHR2S]^r} - k_7[miR399][IPS1] + k_8[IMC] \qquad (4.2)$$
$$- d_{7*}[CytoPi]\Big([IPS1] - [IMC]\Big)$$

$$\frac{d\,[IMC]}{dt} = k_7[miR399][IPS1] - k_8[IMC] - d_{7*}[IMC][CytoPi] \qquad (4.3)$$

$$d_{7*} = \frac{d_7}{CytoPi_{time=0}} = \frac{0.1386}{5000} = 2.7E-05 \qquad (4.4)$$

PiOM-RP and PsTR-RP models fit the observed PHO2 and IPS1 profiles under P depletion and repletion condition, see Figure 4.7. While exploring the parameter space for the binding constant for IPS1-miR399 (k_7), to gain appropriate fit to the observed repletion kinetic of PHO2 and IPS1, the value in the range of 10^{-5} gave the best fit and thus was manually adjusted accordingly to 1.9e-05. Though a relatively higher value than the previous estimates, the new value of k_7 is within the range of weak binding constants (i.e. 10^{-5}) for a RNA-microRNA interaction (Zinovyev *et al.*, 2013). However, these RP models are currently unable to explain the levels of IPS1 at 1 hour of P re-supply. This is perhaps because they assume CytoPi interacts directly

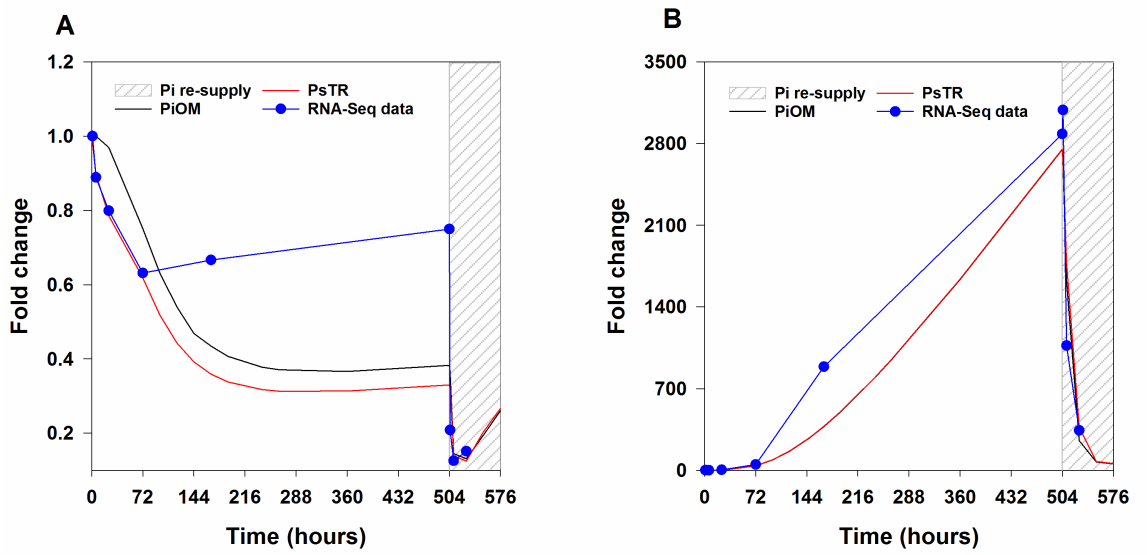

Figure 4.7: Simulation profiles of RNA-protection models under Pi-stress and repletion condition.
The observed and simulation profiles are respectively shown for (A) PHO2 and (B) IPS1. The grey zone denotes the period when external Pi was restored. The point with blue dashed line refer to the observed RNA-SEQ data (Secco *et al.*, 2013),while the red and black lines show the time profiles of the PiOM-RP and PsTR-RP models respectively.

with IPS1 while in reality it probably involves intermediary proteins.

It is also worth noting that the re-estimated parameters for IPS1 synthesis are significantly lower ($m_8 = 11.5$, $k_{10} = 33.6$ for PiOM and $m_8 = 10.5$, $k_{10} = 30.02$ for PsTR and (r close to 2) but are in keeping with values often seen in models of gene regulation. Though these results endorse the idea of IPS1 RNA protection under low P conditions, laboratory validation is the essential next step. The models can be completely fitted to the RNA-SEQ PHO2 profile by increasing the value of IPS1-miR399 binding constant (k_7) to 10^{-4}or setting IPS1 production rate (m_8) to 200. However, the biological relevance of these values is uncertain.

4.3 Conclusion

This work has revealed that the astonishingly high levels of IPS1 are best explained by the protection of phosphate-sensitive RNA binding proteins, for which PUMILIOs and other proteins are potential candidates. RNA protection is a known mechanism

in mammalian systems (Ford & Wilusz, 1999). This hypothesis could be tested by pulling down RNA-binding proteins using a synthetic IPS1 RNA, with and without poly A tail, from the freshly-made cell extracts of phosphate starved and repleted roots. The difference in the extracted proteins from different samples would point to potential Pi-sensitive RNA-binding proteins. These could be studied further by *in-vitro* experiments, perhaps involving Electrophoretic mobility shift assay (EMSA) (Hellman & Fried, 2007) or Liquid chromatography-tandem mass spectrometry (LC-MS/MS) (Gstaiger & Aebersold, 2009). In addition, various high-throughput methods for characterising RNA-protein interactions, reviewed in (Cook *et al.*, 2015), could be potentially used for further validation.

The three-dimensional structure of RNA is fundamental to various cellular processes, including RNA stability, processing, regulation, localization and turnover (Wan *et al.*, 2011). Such a 3D architecture of IPS1 RNA, perhaps along with the protein/s binding, could confers stability and increase the half-life in Pi starved roots. Thus, determining its structure is crucial to gain further insights into IPS1 dynamics. The most advance approach to determine secondary structure of RNA integrates the classic nuclease and chemical probing of RNA with next-generation sequencing technologies, thereby making it an high-throughput process (Foley *et al.*, 2015; Mortimer *et al.*, 2014) and can be used for IPS1. However, for tertiary structure, methods like X-crystallography and NMR spectroscopy could also be used (Mortimer *et al.*, 2014), providing sufficient quantities could be produced.

4.4 Methods

4.4.1 Multiple sequence alignment

The IPS1 sequence was extracted from the Rice Genome Browser (rice.plantbiology.msu.edu). Its Kasalath orthologue was found by performing a BLASTN search against the downloaded genome from the RAP-database (rapdb.dna.affrc.go.jp). The multiple sequence alignment was made using Multalin (multalin.toulouse.inra.fr).

4.4.2 RNA-binding protein prediction

Candidate proteins binding to IPS1 RNA were found using the RNA-Binding Protein Database (RBPD) (Cook *et al.*, 2015) . This curated database includes experimentally observed (both *in-vivo* and *in-vitro*) RNA-binding proteins (RBPs) with known RNA-binding domains for four metazoan species (human, mouse, fly and worm). The IPS1

sequence was queried across the database for RBP-binding sites with a threshold of 0.9. This lead to 13 potential RNA binding proteins and 37 binding sites across the IPS1 sequence, see Appendix E. As the predicted proteins were from animal systems, potential orthologues were found by performing BLASTP searches in Plant Ensembl. Credible results were found for only two plant orthologues, i.e. PUMILIO and ELAV-1 like proteins.

4.4.3 Centroid secondary structure prediction of IPS1 mRNA

RNA structures were generated using RNAfold (rna.tbi.univie.ac.at) with default settings. Centroid, rather than minimum free-energy, structures were generated as these show the most probable base-pairing regions in the ensemble of structure likely to be found above the most thermodynamically stable conformation.

Chapter 5

Multi-cell models for phosphate uptake and flux within root cross-sections

Abstract

In this chapter, multi-cellular models of phosphate uptake and flux through realistic root cross-sections for *Arabidopsis* and Rice are studied. Different geometries including root hairs of different lengths and root cortical aerenchyma have been tested to explore their effects on phosphate uptake and cytosolic phosphate levels. These suggest that cytosolic phosphate levels in trichoblasts may be a trigger for root-hair initiation and that fluid-filled lacunae may be a desirable trait for improving nutrient acquisition, without increasing costs in carbon and water.

5.1 Introduction

The structure of a single root is quite complex and consists of layers of different cell-types with specific functions. The number of cell layers and in some cases cell types, varies within a root (i.e. along the vertical length of the root) and between plant species. Most experimental studies on plant phosphate (Pi) acquisition consider the root as a whole or explicitly focus on a particular cell-type, but open questions remain regarding any tissue specialisation in the regulation of Pi uptake, transport, and it dynamics through different root anatomies. This highlights even further the need to develop multi-cellular models to study the interaction between different cell-types and explore the effect of different root anatomies on Pi uptake and transport.

Two approaches have been widely used to develop cell-based models of plant roots, namely includes Cellular Potts models (Glazier & Graner, 1993; Graner & Glazier, 1992) and vertex-based models (Nagai & Honda, 2001; Weliky & Oster, 1990). The main differences between them lie in the geometrical representation of individual cells and the manner in which physical and chemical interaction between the cells are handled. Cellular Potts (or Glazier-Graner-Hogeweg) models represent cells as collections of voxels (volumetric elements, typically cuboids) that undergo growth through stochastic relabeling rules. On other hand, vertex-based models describe cells as polygons (in two dimensions) or polyhedra (in three dimensions) (Fozard *et al.*, 2013). For plant tissues, this is particularly appealing as the relatively regular shape of cells can be well approximated, and symplastic growth can be naturally enforced by the sharing of vertices between neighboring cells. In view of this, various vertex-based models have been developed for different plant tissues (Dupuy *et al.*, 2008; Hamant *et al.*, 2008; Jonsson *et al.*, 2006; Merks *et al.*, 2011; Rudge & Haseloff, 2005; Stoma *et al.*, 2008)

As vertex-based modelling approaches have become more established, simulation platforms such as CellModeller (Rudge *et al.*, 2012, 2013), CHASTE (Pitt-Francis *et al.*, 2008), OpenAlea (Pradal *et al.*, 2008), and VirtualLeaf (Merks *et al.*, 2011) have been developed. These softwares allow efficient multicellular simulations by building on the existing collections of codes. However, the OpenAlea framework has been adopted in this study for a number of reasons: (a) it is an open-source freely distributed platform, particularly, intended for modeling multi-scale plant systems, (b) it is user-friendly and has a simple-to-read syntax, which allows even non computer scientists to prototype rapidly new scripts or to adapt existing ones, (c) it provides data structures for representing vertex-based tissues and routines to manipulate them, and above all, (d) it has an excellent track record in modeling fluxes through plant tissues (Band

et al., 2012b, 2014; Muraro *et al.*, 2014)

This study aims to establish multi-cellular vertex-based models of Pi uptake and flux through realistic root cross-sections. The *Arabidopsis* root has been used in various multi-scale modeling studies, because of its relatively fewer numbers of cells and simple anatomical structure. For this reason, multi-cell models for *Arabidopsis* and rice root have been developed. Different geometries were also considered to explore the effect of root-hairs and root cortical aerenchyma (RCA) on Pi uptake and transport. The model predictions were found to be consistent with the published findings, particularly for the role of root-hairs and aerenchyma on Pi uptake.

5.2 Data and Methods

5.2.1 Input data

The traced images for the horizontal cross section of *Arabidopsis* and Rice root were taken from (Péret *et al.*, 2009) and the aerenchymatous rice root was adopted from (Coudert *et al.*, 2010).

5.2.2 Overview of the methods

Figure 5.1 provides a general overview for the development of vertex-based models using the OpenAlea framework. It includes the set of python script and libraries, which have been extracted from the mainstream GUI-based OpenAlea software by the staff at the Centre for Plant Integrative Biology (CPIB) in collaboration with the OpenAlea team. This script-level OpenAlea framework has been refined for studies of hormone fluxes in multi-cell root models (Band *et al.*, 2014). There are four inputs in this framework; tissue geometry, process equations, model parameter, simulation parameters (time, intervals and cell-specific rules, if any) and finally, the parameters for plotting the output, often as the heat-map on the tissue geometry.

5.2.3 Tissue geometries

***Arabidopsis* and rice roots** All these images were colour inverted using a photo editing and processing software application named Picasa (picasa.google.com). The inverted images were segmented using CellSeT with default parameter settings (Pound

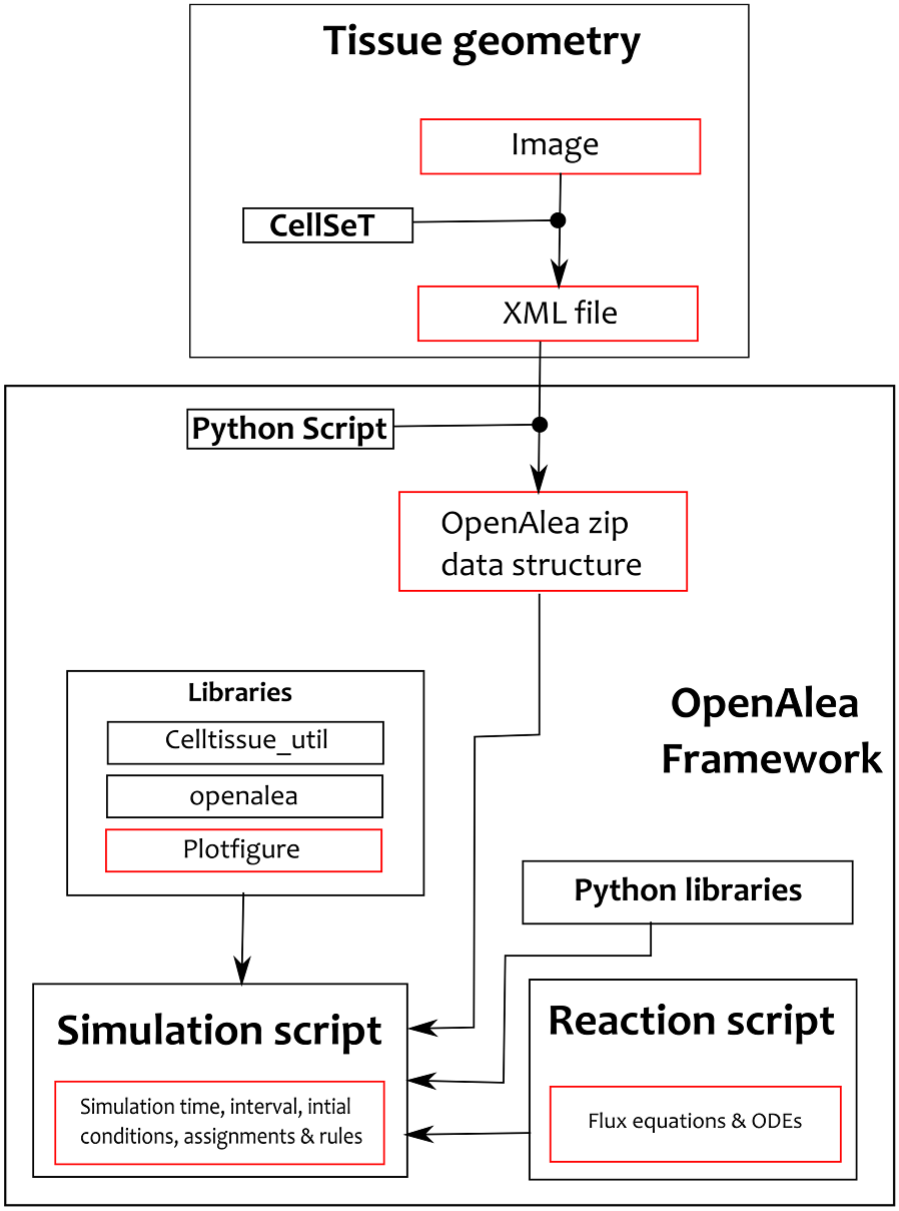

Figure 5.1: Flowchart for multi-cell model development and simulation. Red boxes denote the input data or user defined information, including the model equations and rules, provided by the author

et al., 2012). Automatic segmentation detected most of the larger cells but the geometries of smaller cells and less distinct regions, particularly stele in rice, were corrected manually.

Having detected the cell geometries, the different cell types were manually identified, labeled and recorded, Figure 5.2 E,J,O. The labeled cell types were denoted by a number. This assigned number was used in the later stages to define initial conditions, equations and establish rules for particular cell-types in the model. The geometrical data including a list of the walls bounding each cell and a cell-type annotation were exported to a file in XML format. The latter file was converted to the data structure (zip file) for input into OpenAlea using a separate python script.

Aerenchymatous rice roots In response to various stresses, including phosphate deficiency, root cortical cells undergo programmed cell death forming aerenchyma in many species (He *et al.*, 1992). Though the molecular mechanism underlying these anatomical adaptations still remains ambiguous, it is understood that root cortical aerenchyma have positive impacts on Phosphorus-Use Efficiency by reducing metabolic and root-exploration costs (Postma & Lynch, 2011b). In the view of this, a published image of an aerenchymatous rice root cross section (Coudert *et al.*, 2010) was adopted Figure 5.2K , to construct a vertex-based model. The central stele in this image was unclear, so it was modified by superimposing the stele from another rice-root image, Figure 5.2F . This altered image was segmented using CellSeT (see, Figure 5.2L-O). To study the explicit effect of aerenchyma without any impacts from cell numbers, size and area, the model was simulated on an additional rice root geometry in which aerenchyma with bypassing lacunae were manually incorporated into the original rice root image, Figure 5.3A-B.

Modified *Arabidopsis* co-ordinates to include root hairs Root hairs are known to be induced in response to low phosphate conditions (Niu *et al.*, 2012). Previous modelling studies have shown that phosphate acquisition efficiency can be enhanced by increased root-hair length and longevity rather than their density (Brown *et al.*, 2013). To test such observations, root hairs were manually introduced while segmenting the root cross section image for *Arabidopsis* in CellSeT. Four root hair cases were constructed : one each with no hairs, four short hairs, a single hair ($\sim 100\,\mu m$) and a single fully grown root hair ($\sim$ 1 mm), Figure 5.3. These respectively correspond to trichoblasts at the start of Rapid Elongation Zone (REZ), the elongation phase

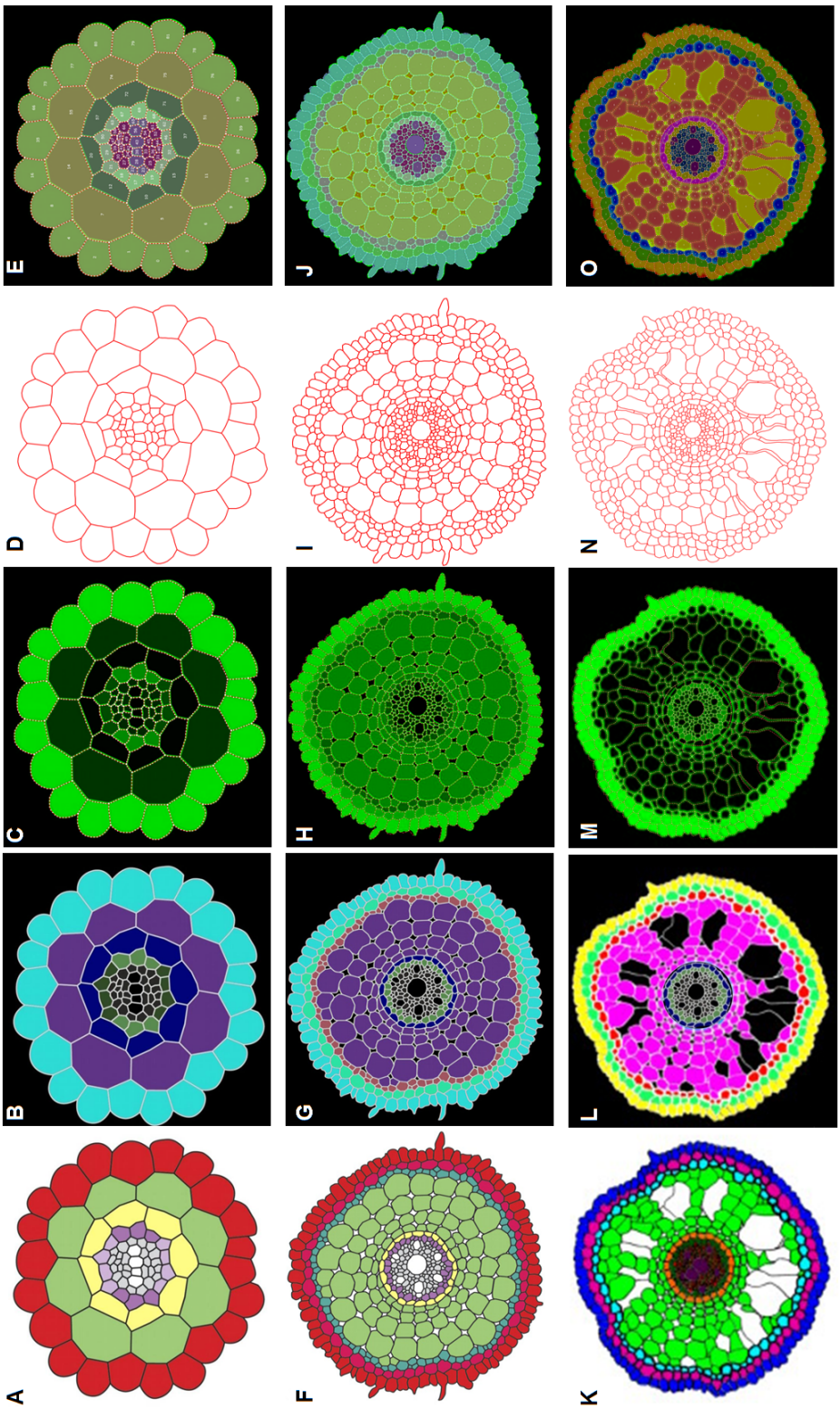

Figure 5.2: Manipulation of root cross-section images.
Original (A, F,K) and inverted (B,G,L) root sections of two model species *Arabidopsis thaliana* and *Oryza sativa* (rice). *Arabidopsis* root diameter is 100 μm (A-E) and rice root diameter is 300 μm (F-J). Aerenchymatous root diameter is 50 μm (K-O). The second and third column corresponds to segmented images while fourth column includes their annotations.Images A and F were adopted from (Péret *et al.*, 2009) and K was adopted from (Coudert *et al.*, 2010).

of a root hair just above the REZ and a position in the mature root. The diameter of root hair was scaled approximately to $10\,\mu m$. These measurement were obtained from (Grierson *et al.*, 2014). Normally, root hairs grow out straight but these have been folded with multiple turns purely for visual convenience. This does not affect the model simulations.

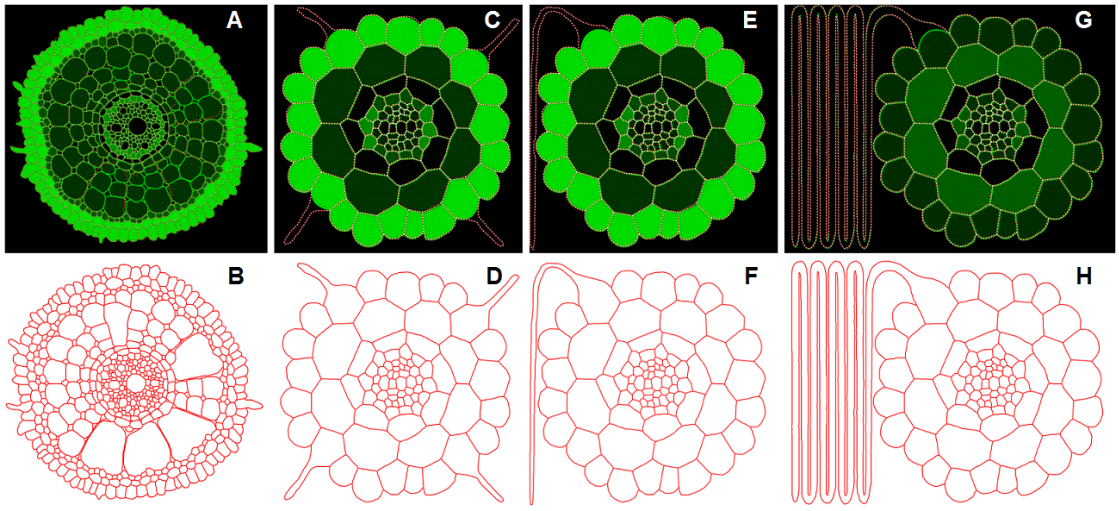

Figure 5.3: Manipulated segmentation of the root cross-section inverted images. A and B represents addition of aerenchyma in rice root cross-section while (C-H) represents the addition of root-hairs with different number and length.

5.2.4 Model development and simulations

5.2.4.1 Model assumptions

The models represent the roots of the plants grown in a hydroponic growth chamber. External phosphate concentration is considered to remain constant under deficient, normal and excess conditions at 0 µM, 200 µM and 2000 µM, respectively. It is assumed that the concentration of cytosolic phosphate (CytoPi) is homogeneous within each cell. For each cell (i), it is denoted by $[CytoPi]_i$. Generally, nutrients are loaded into the xylem to be transported across the plant while sugars and other molecules are transported from the shoot via phloem for the root growth (White, 2012). For simplicity, the xylem phosphate is fixed as constant at $7\,mM$ and phloem and cambium cells are fixed at $2\,mM$ with no flux outward to other cells. As a result, phosphate effluxed from the pericycle disappears on entering the xylem in the model. In addition, only symplastic transport and cellular compartments were considered for computing

CytoPi concentrations. Apoplastic routes (i.e. cell walls) between adjacent compartments have been neglected because these are likely to be substantially slower. The intercellular gaps are treated in the same way as an external source of phosphate, with constant concentration at 200 μM, allowing uni-directional phosphate flux into the surrounding cells. Furthermore, it was assumed that there is no phosphate flux into/out of aerenchyma while the lacunae are filled with fluid allowing phosphate to passage through them.

Following Chapter 3, the steady state CytoPi concentration was set at $5\,mM$ under normal external Pi condition (i.e $200\,\mu M$), for both *Arabidopsis* and Rice. The active transport of phosphate into the epidermal cells from external environment is represented by the Michaelis-Menten kinetics for low-affinity phosphate transporters (with $Km = 177\,\mu M$). For simplicity, the activation of high-affinity phosphate transporters under low phosphate conditions is neglected. From epidermal cells, phosphate radially moves towards the stele via plasmodesmata. This is assumed to occur in a concentration-dependent manner. Of the total phosphate in each cellular compartment, a constant amount of phosphate is regarded as stored in the vacuole or utilised in making nucleic acid and membranes, such that the CytoPi concentration remains constant at $5mM$ under normal external phosphate conditions. Due to the sparsity of data and the knowledge on the inter-cellular/tissue dynamics of phosphate, the time scale units for the simulation are not defined, while most parameter values are assumed and adjusted to obtain qualitative steady states for CytoPi concentration in the cells across the root cross section.

Given the 2D vertex structure, the volume of the cells were proxied by the respective cell area in the vertex-based model. The length of all the cells (vertical height) is assumed to be constant across the root section, Figure 5.6. This is unrealistic for root hairs, Figure 5.6B, whose diameter is 20 times smaller than that the length of an epidermal cell (Figure 5.6C).In the first instance, this is ignored.

5.2.4.2 Equations

The dynamics of phosphate in each cell are represented by an ordinary differential equation composed of three terms, each characterising different aspects of phosphate dynamics, see equations 5.1-5.3. These include phosphate uptake, its utilisation and storage in the cell and its flux between the cells. This equation is embedded in each cell of the model. The term for phosphate uptake is assigned only to the epidermal cells and the cells surrounding the intercellular gaps in the rice root geometries.

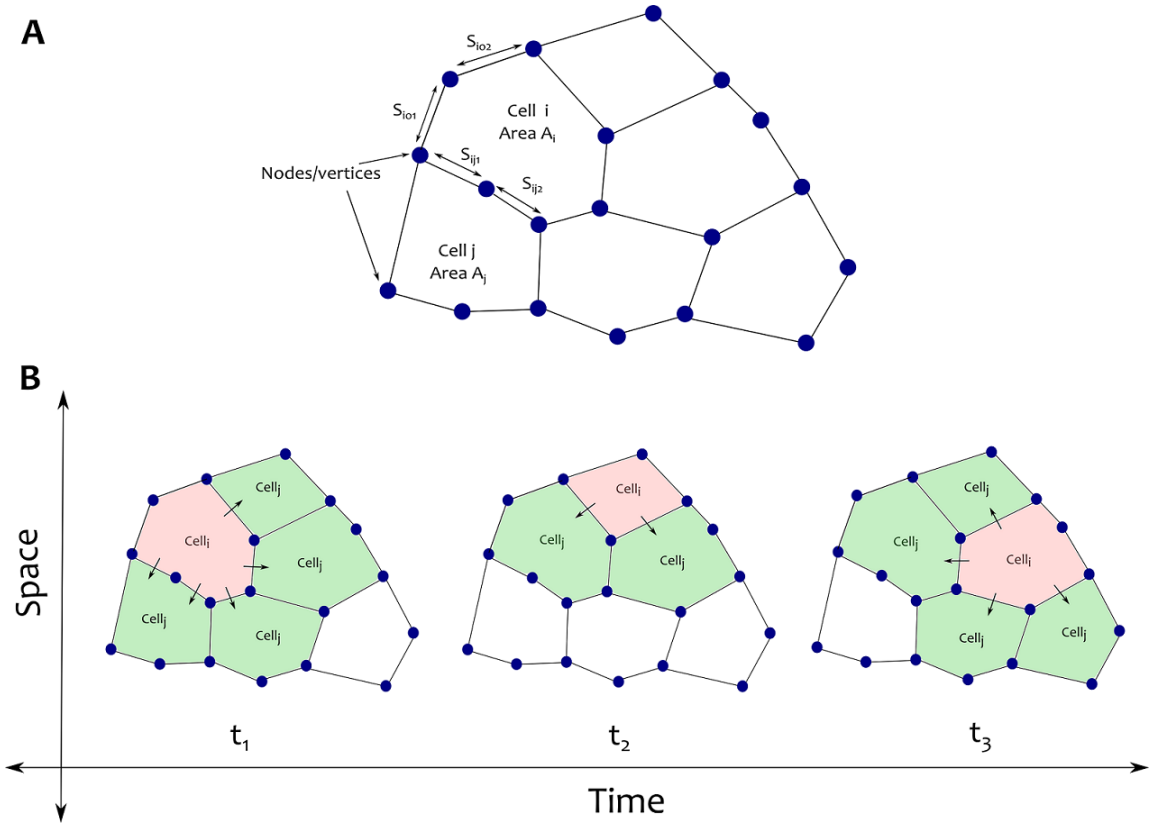

Figure 5.4: Schematic illustration of the vertex-based multicellular plant tissue. (A) The polygonal shaped compartments constituted by edges connecting different vertices (nodes). (B) the logic used to encode the CytoPi flux between the compartments within a vertex-structure across time and space.

In this vertex-based representation of root tissue, cells have a polygonal geometry, bounded by a set of walls (i.e. line segments), each of which connects a pair of vertices. Each wall consists of one or more straight wall segments. The cell-connectivity graph, cell areas and wall lengths are precomputed, as a data structure file, to make more efficient simulations with the real static geometry. Supposing the root (geometry) consists of N cells, the area of the cells were denoted by A_i for $i = 1, 2....N$ and C_i denotes the set of cells neighbouring cell i. If i and j are two neighbouring cells, S_{ij}, denotes the length of the exchange surface, which is equivalent to the distance between two vertices or nodes, Figure5.4A

Pi uptake The external (outer) surface of an epidermal cell wall is not shared with neighbouring cells. Therefore, such cell walls were identified from the data structure and their respective cells were treated as epidermal cells able to take up phospahte

from the constant external source (E), via an active transport process against the concentration gradient and by a small diffusion.

For cell (i) in the epidermis, the transport of Pi into the cell with respect to (t) is given by:

$$\frac{d\left[CytoPi\right]_i}{dt} = \frac{1}{A_i} \sum_{z \in D_i} S_{i,z} \left(\frac{PPHT\, E}{k + E} + Ppass\, E \right) \tag{5.1}$$

Here A_i is the area of the epidermal cell, D_i labels the set of n walls of cell i that are exposed to the external environment and $S_{i,z}$ denotes the length of these walls for $z = 1, 2, ...n$. Parameters $PPHT$ and k are the $Vmax$ and km for low-affinity phosphate transporters, E is the constant external phosphate concentration and $Ppass$ is background permeability of phosphate into the epidermal cell. In the case of rice roots, a similar mathematical equation is also applied for the uptake of P from the intracellular gaps between its surrounding cells.

Pi transport between the cells The diffusive flux of phosphate from a cell, labeled i, to an adjacent cell, j, (Figure 5.4B), is given by

For cell (i), except those corresponding to phloem, inter-cellular gaps and aerenchyma,

$$\frac{d\left[CytoPi\right]_i}{dt} = -\frac{1}{A_i} \sum_{j \in C_i} S_{i,j}\, Ppass_m \left(\left[CytoPi\right]_i - \left[CytoPi\right]_j \right) \tag{5.2}$$

where A_i is the area of the cell i, $S_{i,j}$ is the area of exchange surface between cell i and j, $Ppass_m$ is the phosphate permeability across the boundary between the two cells.

Pi utilisation

$$\frac{d\left[CytoPi\right]_i}{dt} = -U \left[CytoPi\right]_i \tag{5.3}$$

where U is the constant rate of internal Pi utilisation and vacuolar storage. In the case of lacunae (i.e. the spokes in aerenchymatous rice root), U was set to zero because they are considered to be metabolically inactive.

The equation combining these three term has five parameters, values of which were

either sourced from literature or assumed, see Table 5.1. These parameter values were used in all the respective *Arabidopsis* and Rice root geometries.

Parameter	Values for *Arabidopsis*	Values for Rice	Reference
$PPHT$	47125	47125	C
k	177	177	R
$Ppass$	0.0001	0.0001	A
$Ppass_m$	50	100	A
U	0.1	0.2	A

Table 5.1: List of parameters used in the multicellular models. Abbrevations are as following - A: assumed/adjusted, C: calculated and similar to k_{13} from Chapter 3 and R: adopted from (Nussaume *et al.*, 2011)

5.2.4.3 Simulations and plotting

Simulations were performed in Python (python.org) using the ODE solver lsoda from the odepack suite (Hindmarsh, 1983) to approximate numerically solutions of the differential equations for every cell. This solver exploits the sparsity of the Jacobian of the system of equations; and the sparsity pattern of the Jacobian is supplied to the numerical solver to improve the speed of the simulations. Simulations were run until the distributions and fluxes for the variable of interest reached their steady state and are visualised using the Python library (matplotlib) (Hunter, 2007)). Depicting the distribution of the steady-state phosphate concentration in a multi-cellular tissue geometry required choosing a range for the heat-map. This was defined automatically by the script to minimize subjectivity.

5.3 Results

5.3.1 Phosphate flux model for Arabidopsis root

The models for *Arabidopsis* roots, both with and with root hairs, achieved steady states of P flux under deficient, normal and high external Pi conditions (Figure 5.5). Trichoblasts were observed to have lower CytoPi concentrations compared to the other epidermal cells, more distinctly under high phosphate conditions. This is probably because these have two adjacent cortical cells rather than one and this presents a larger sink surface through which more Pi can be passed on. This opens the possibility that

reduced CytoPi could be part of the trigger for root-hair initiation. On the other hand, the xylem pole pericycle cells appear to have high Pi levels than their neighbouring pericycle cells, but this is probably an artifact arising from fixing the Pi concentration in the xylem.

Cases 2 and 3 under normal and high external Pi conditions in Figure 5.5 , show that even short hairs can elevate the CytoPi levels of surrounding cells. However, a full-length root hair has a large effect even at normal external Pi concentrations. As the emerging hair quickly brings in more Pi, this would raise Pi levels in the other trichoblasts and discourage further root hair formation nearby. The higher Pi levels in root-hair cells could also possibly limit root-hair length. All these simulations are based on the assumption that mature root-hair cells have an cubiodal protrusion whose volume is 1mm x $10\mu m$ x the length of the cell, Figure 5.6. This is obviously not the case, so further refinement is required.

5.3.1.1 Volume and surface area adjustment for root-hair cells

Given the above, the model should be modified to take account the difference in volume and surface area of root hair cells to see if there is any noticeable difference in the CytoPi levels and distribution (see Figure 5.6). As a first approximation, it is assumed that epidermal cell and root hairs are cylinders.

The average length and diameter of a mature root epidermal cell in *Arabidopsis* is $\sim 200\,\mu m$ (Beemster & Baskin, 1998; Duckett *et al.*, 1994) and $\sim 20\,\mu m$, respectively.

$$\therefore \text{Epidermal cell volume} = \pi r^2 l = \pi 10^2 * 200 = 20000\pi\ \mu m^3$$

The average length and diameter of mature root-hair is $\sim 1000\,\mu m$ and $\sim 10\,\mu m$, respectively (Grierson *et al.*, 2014).

$$\therefore \text{Root-hair volume} = \pi r^2 l = \pi 5^2 * 1000 = 25000\pi\ \mu m^3$$

$$\therefore \text{the volume of a root-hair cell is } 45000\pi\ \mu m^3$$

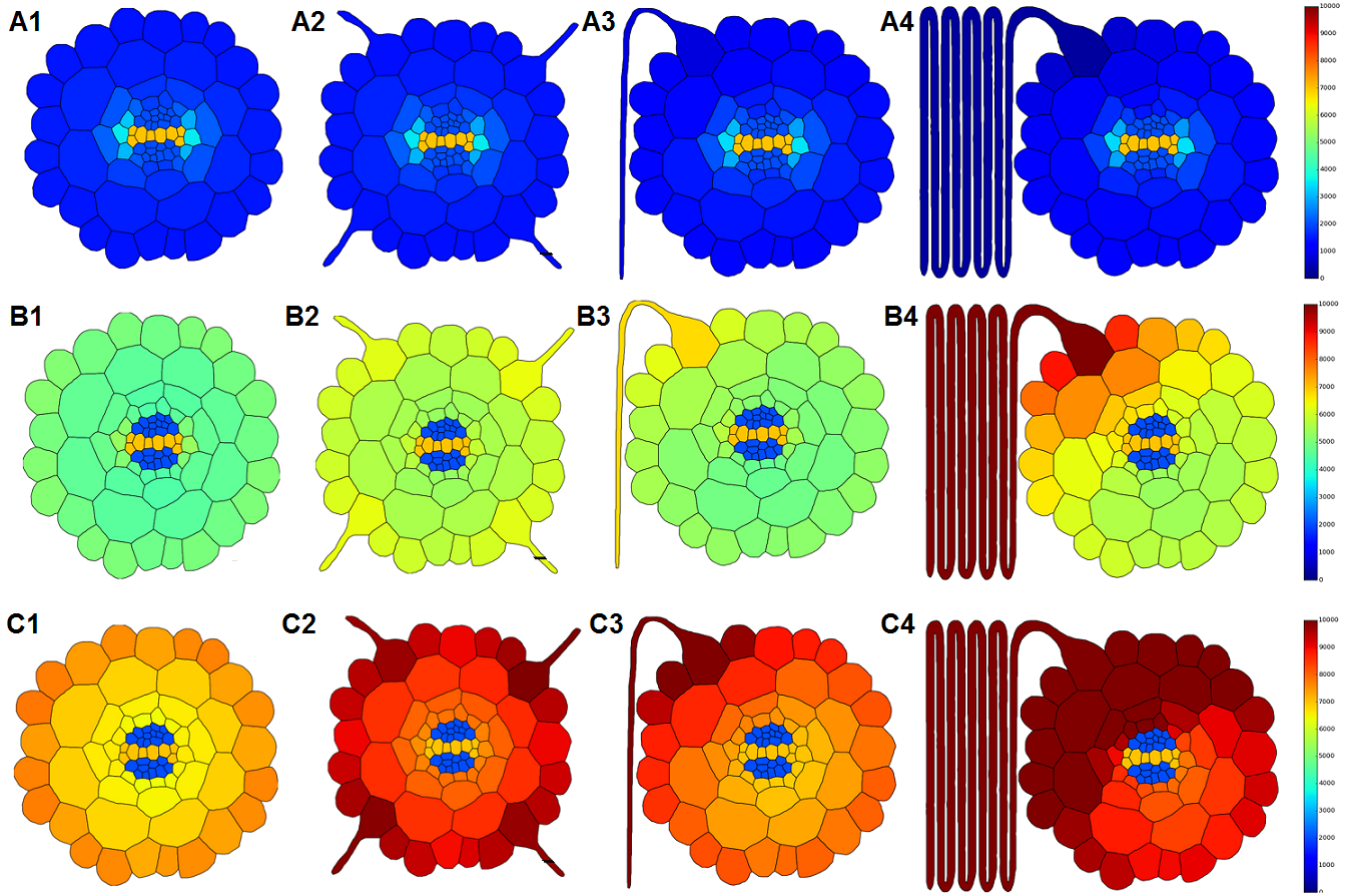

Figure 5.5: Steady state distribution of cytosolic Pi in *Arabidopsis*.
A,B and C corresponds to deficient, normal and high external Pi condition while number 1-4 denotes cases of *Arabidopsis* root with no hairs, four short hairs, a single hair ($\sim 100\,\mu m$) and a single fully grown root hair ($\sim 1mm$), respectively. The root diameter is$100\,\mu m$.

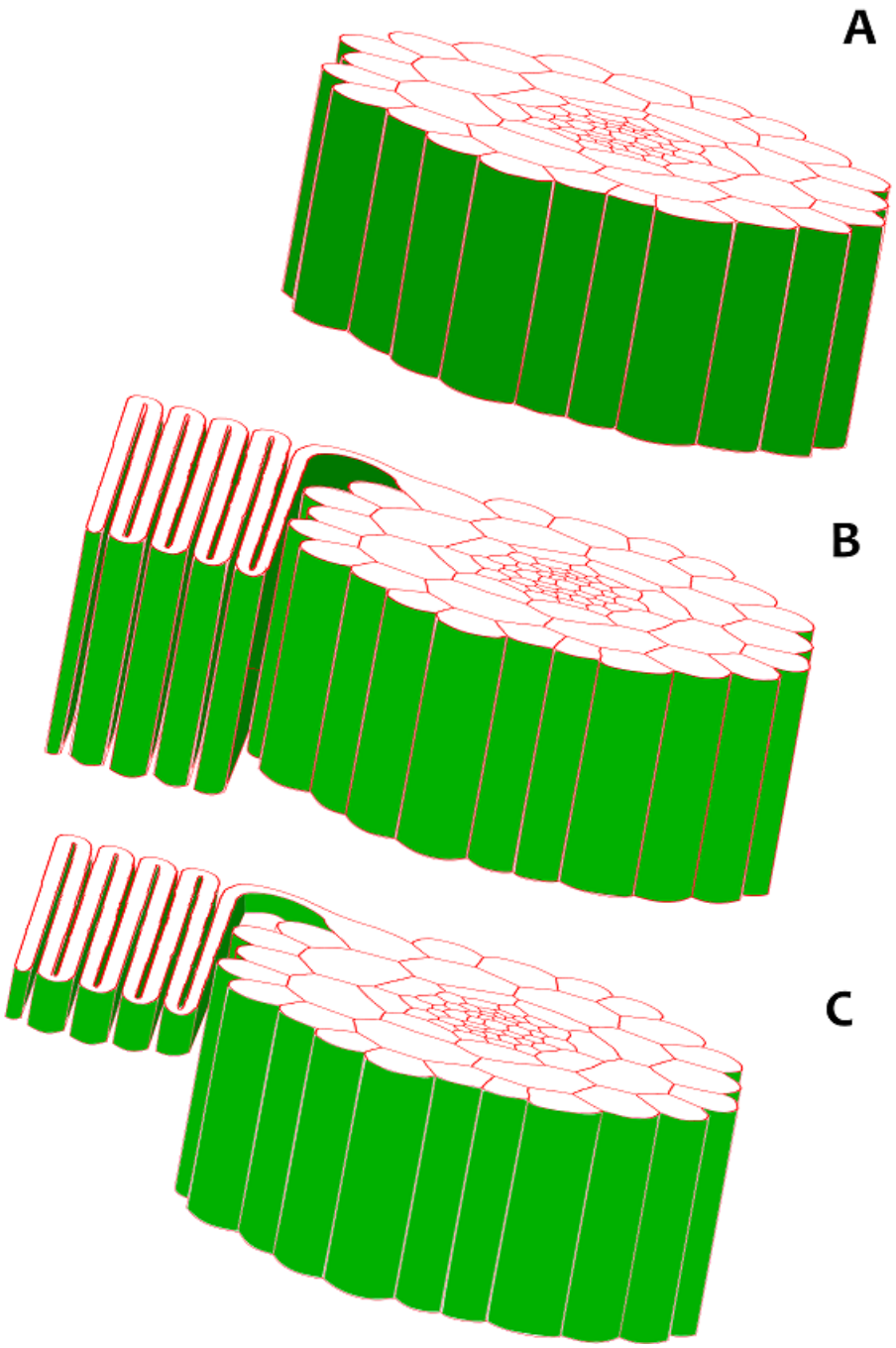

Figure 5.6: 3D geometry of root cross sections.
The length/height of all root cells, including root-hair are assumed to uniform (A and B), while under natural conditions, height/diameter of root hair cell is relative small (C).

$$\text{Volume increase upon adding root hair} = \frac{45000\pi}{20000\pi} = 2.25$$

Assuming a quarter of the total surface area of an epidermal cell faces the external medium,

$$\text{Exposed surface area} = \frac{2\pi rl}{4} = \frac{2\pi 10 * 200}{4} = \frac{4000\pi}{4} = 1000\pi\,\mu m^2$$

$$\text{Surface area of a root-hair } = 2\pi rl = 2\pi * 5 * 1000 = 10000\pi\,\mu m^2$$

$$\therefore \text{the exposed surface area of a root-hair cell} = 11000\pi\,\mu m^2$$

The surface area increase $= \frac{11000\pi}{1000\pi} = 11$, i..e. 11 fold higher surface area than an epidermal cell.

Assuming the Pi-transporter density is the same, a root-hair cell can bring in approximately 11 times more Pi. This was tested by simulating the CytoPi to steady state assuming the trichoblast has 11 fold higher exposed surface area. This alteration shows elevated CytoPi level in the trichoblast and neighbouring cells, Case 2 in Figure 5.7, which is in excellent agreement with the predictions from the actual mature root-hair geometry, Case 1 in Figure 5.7. In reality, this increase in the level of Pi is diluted by being in a cell whose volume is 2.25 times larger. Therefore, for the same volume as an epidermal cell, the increase in Pi uptake would be $\frac{11}{2.25} = 4.89$. This difference has been implemented in the geometry, where the trichoblast is defined as taking 4.89 time more Pi than the other epidermal cells. This modification shows an increase in CytoPi level in the trichoblast and neighbouring cells (Figure 5.5, case 3) compared to the hair-less root (Figure 5.5, case 4).

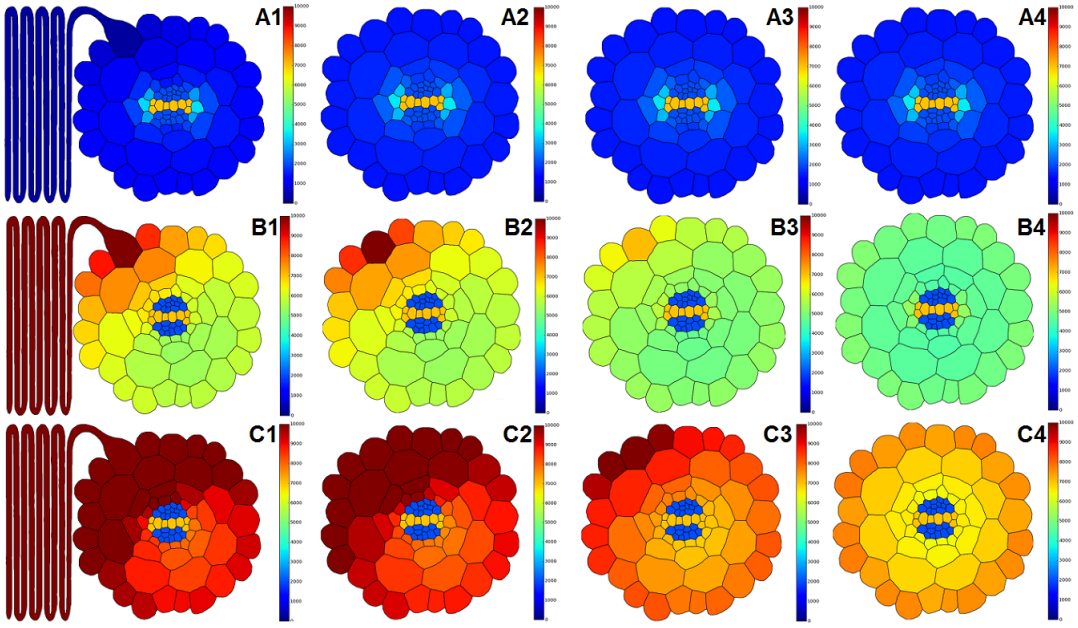

Figure 5.7: Effect of altered surface area of a trichoblast cell on CytoPi distribution under different external Pi-conditions
A, B and C represent deficient, normal and high external phosphate conditions, respectively. Cases1-4 respectively correspond to the previous mature root-hair model, a trichoblast with 11 fold higher uptake, a trichoblast with 4.89 fold higher uptake and a trichoblast with no hair. The diameter of root is100 μm.

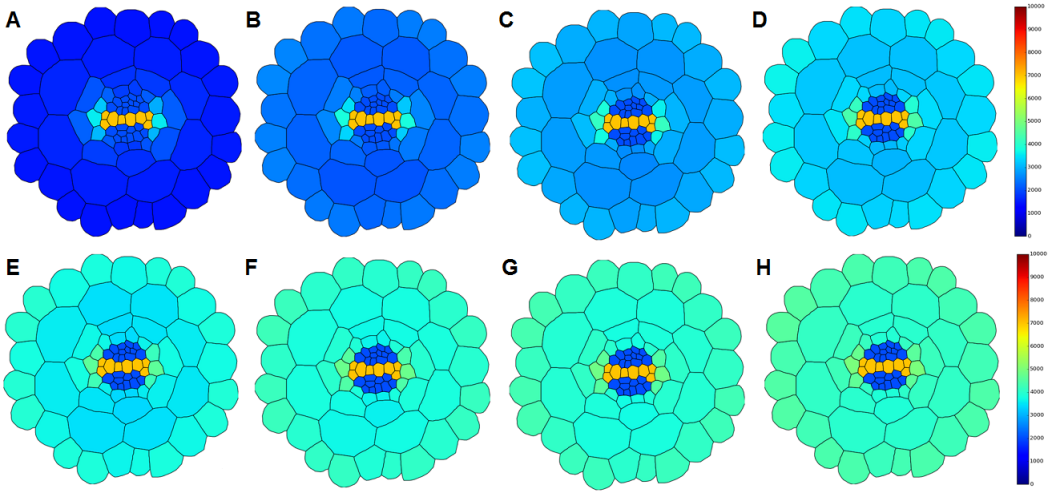

Figure 5.8: Spatio-temporal distribution of Cytosolic Pi across *Arabidopsis* root. Following phosphate stress with (A), time-course simulation of Cytosolic Pi upon phosphate re-supply (B-H).

It may also be instructive to investigate the recovery of a root from Pi stress. On initialising the hairless geometry with values from the stressed steady state but defining external Pi as normal, the CytoPi concentration evolves to steady state following Pi resupply within the time-frame of 20 units, Figure 5.8. The time course suggests that, after epidermal cells, the endodermal and pericycle cells that begin to recover before the cortex. The lower levels of the latter might be due to their larger volume.

5.3.2 Phosphate flux model for Rice

The CytoPi levels in multi-cell rice root model attained steady states under all external phosphate, Figure 5.9A1-C1. These look similar to the equivalent in *Arabidopsis*, Figure 5.5, except those in high phosphate condition, Figure 5.9C. This is probably due to both differences in geometry (i.e. cell size and number; and inter-cellular gaps) and also the model parameter values. Rice root has about four-fold more epidermal cells and hence larger surface area, capable of taking up more Pi. Also, the intercellular gaps offer an additional source of phosphate to the cortical cells.

On manually introducing cortical aerenchyma with lacunae into the root geometry, the model simulations show three effects, Figure 5.9 A2-C2. First, the root CytoPi levels are lower in total in keeping with the published data (Hu *et al.*, 2014). Second, the extent of the CytoPi decrease in the individual cortical cells appears to be related to how close the regions of aerenchyma are from each other. Thus, in Figure 5.9B2 and C2, the two and three cells wide cortical section between the aerenchyma shows lowest CytoPi level. Third, cells that are external to aerenchyma also have reduced CytoPi levels. Similar results were observed in the actual aerenchymatous root geometry, Figure 5.9A3-C3. This is probably, due to lacunae allowing phosphate to move to the vasculature much faster, because they constitute a single compartment/cell (rather than three), have far smaller volume than the equivalent cortical cell file and are not utilising the Pi themselves (see, Figure 5.10). This is consistent with earlier reported evidence (van der Weele *et al.*, 1996b). The lower CytoPi level of the external cells might cause these cells to be less metabolically active or trigger the phosphate stress response, though any significance of this is unclear. The aerenchymatous roots in Figure 5.9 B3 and C3 have remarkably lower CytoPi levels than those in Figure 5.9 B2 and C2. This again can be attributed to differences in geometry. There are sightly more epidermal cells (93 and 88 in Case 2 and 3, respectively), more aerenchymatous regions, some larger gaps below the exodermis and more layers of cortex.

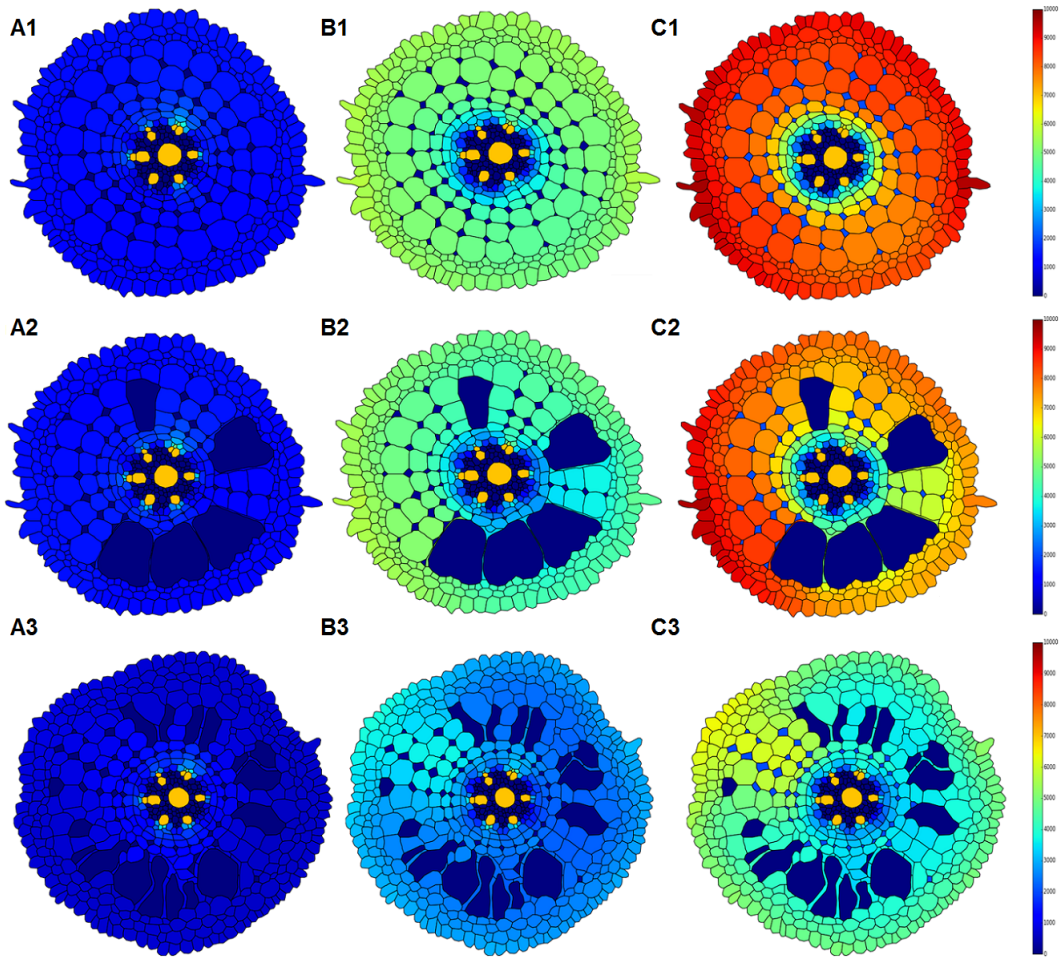

Figure 5.9: Effect of aerenchyma on CytoPi distribution under different external Pi conditions.
A, B and C, respectively corresponds to deficient, normal and high external phosphate conditions. Case 1 depicts normal rice root cross-section while Case 2 and 3 represents manually developed and realistic, aerenchymatous rice root cross-section, respectively.

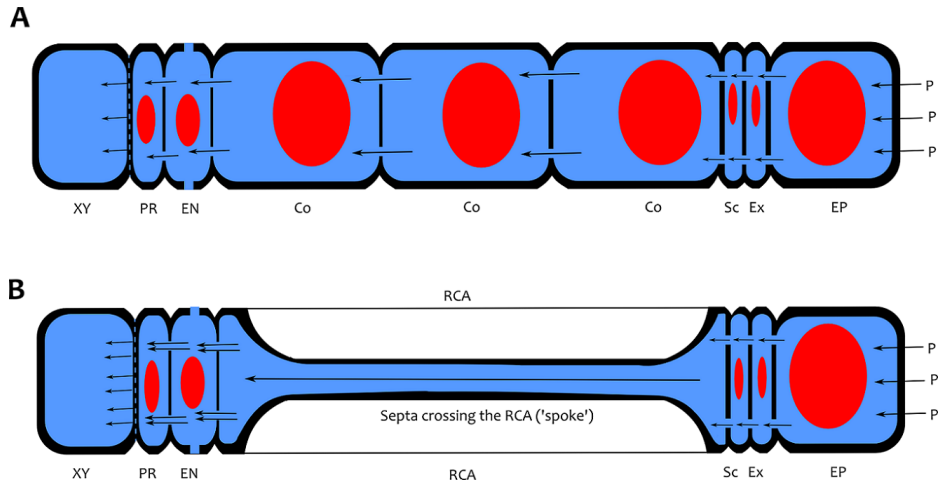

Figure 5.10: Potential explanation for decreased Pi-content in aerenchymatous root. The flow of nutrient, in this case phosphate, across the file of cells belonging to different tissue-types in normal (A) and aerenchymatous (B) root. Compared to normal roots, an aerenchymatous root with fluid-filled lacunae (spoke) offers less resistance to the flow of nutrient from outer to the inner tissue, thereby increasing nutrient acquisition. EP: epidermis, Ex: exodermis, Sc: Schelerenchyma, RCA: root cortical aerenchyma, Co: Cortex, EN: endodermis, PR: pericycle and XY: Xylem.

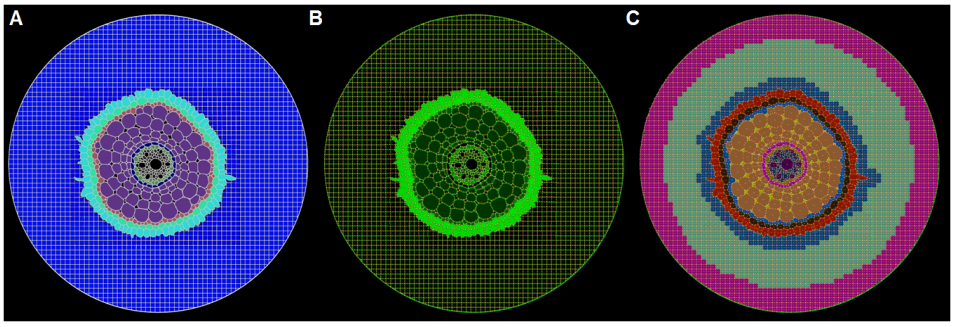

Figure 5.11: Vertex structure to model root-soil interaction.
(A) Inverted image (B) Segmented and (C) annotated geometry, representing root-coil interaction. The centre root region with cells well annotated for different tissue-types. The maroon boundary depicting epidermal cells of the root, followed by the pixelated bands in dark blue, greenish-blue and pink colour representing soil-solution, zone of less-readily and least-readily available phosphate, respectively.

5.4 Discussion and Conclusion

This study has developed credible multi-cellular models for phosphate uptake and transport in *Arabidopsis* and Rice root cross-sections comprised of real cell geometries. They all were able to attain steady state phosphate distribution under all external phosphate conditions. However, the parameter values needed to achieve steady states appear to be sensitive to the root geometry. In the *Arabidopsis* model, young trichoblasts were observed to have lower CytoPi level under both normal and high external phosphate conditions. This is due to the higher number of cortical cell adjacent to them, which increases the Pi sink. This could be a possible part of the trigger for root-hair initiation, involving signalling mediated by hormones namely auxin strigolactones and ethylene, and genetic regulators such as Altred Phosphate Starvation Response 1 (APSR1), Root Hair Defective 6 (RHD6), RHD6-Like4 (RSL4), and Root Hair-Specifics (RHSs) (Cho & Lee, 2013).

Various studies have indicated the significance of RCA toward enhancing Resource-Use-Efficiency, including phosphate, nitrogen and water (Hu *et al.*, 2014; Lynch, 2011, 2013, 2015; Postma & Lynch, 2011a,b; Saengwilai *et al.*, 2014; York *et al.*, 2015). However, most of these RCA studies have focused on its role in saving root carbon cost in favour of soil exploration, either for water or nutrients. But, it may also have a role in root hydraulics, which in turn, regulates the uptake and transport of both water and nutrients (Vadez, 2014). The observations in this work certainly favour the latter. Consistent with previous findings, the simulations predict a decrease in root phosphate content in the presence of aerenchyma and an increase in phosphate flux across the root through lacunae (Drew & Saker, 1986; van der Weele *et al.*, 1996a). These spoke-like structures form bridges between the stele and outer root layers and if lined or filled with aqueous solution allow smooth passage for the nutrients to flow though aerenchyma (Ranathunge *et al.*, 2003; Vadez, 2014). Thus, aerenchyma and fluid-filled lacunae could both be traits to improve Phosphorus Acquisition Efficiency in rice.

Although beyond the scope of this thesis, there are several potential areas for further study. Perhaps the most pressing need is for a better representation of the vasculature. Xylem phosphate will depend upon transpiration rate and availability of Pi in pericycle cells. Phosphate mobilisation is known to occur in response to phosphate stress, whereby phosphate is transported from shoot-to-root via the phloem (Jeschke *et al.*, 1997; Schachtman *et al.*, 1998). In view of this, the model could be developed to allow the phloem to be a phosphate source under defined circumstances.

The model also assumes a hydroponic environment in which external phosphate and other nutrients are constant and uniform. However, in soil phosphate is neither constantly available nor uniformly distributed. The uptake of phosphate from soil solution creates a zone of depletion and its replenishment depend on the form and amount of phosphate available in the surrounding soil. As the soil solution can radially moving to the root endodermis, a decreasing phosphate gradient could from along the path and thus, across the intercellular gaps. In addition, roots exudates affect the availability of phosphate ions in the surrounding soil environment. Altogether, soil-root interactions are complex and an important area of research. In view of this, the root vertex structure has been extended by including a mesh surrounding the root to represent the soil environment, Figure 5.11. Phosphate dynamics within the soil could then be incorporated, with am initial prescribed distribution of different phosphate pools, Figure 5.11C. Furthermore, the root geometry could be modified to represent mycorrhizae and explore its role in phosphate uptake. Ultimately, one could link these models to a growing root model to simulate aspects of root ageing.

While the modelling presented here focuses on how cell-scale phosphate transport affects phosphate distribution at a tissue scale, coupling with sub-cellular network dynamics could also be instructive. Various phosphate-stress-responsive genes are spatio-differentially expressed in different root tissues under normal conditions , Table 5.2. The phosphate regulation model from the previous chapter could be embedded into the individual compartments (cells) to test the hypothesis that differential expression is due to the difference in the concentration of Pi and miR399. Such a multi-cellular model could form a platform to explore the impact of tissue/cell-specific gene expression in regulating phosphate uptake and transport under different environmental conditions and root anatomies.

Gene	MSU id (LOC_Os)	P+			P-
		EES	Cortex	EPS	
ARP6	01g16414				→
bHLH32	03g15440				→
CAX1	11g05070				↘
CAX3**	02g21009				↗
IPK1	04g56580				↘
IPS1**	03g05334				↗
LPR1	01g03530				↘
MYB62**	01g03720				↗
PHF1	07g09000				↗
PHO1	02g56510				↗
PHO2	05g48390				↘
PHR1	03g21240				↘
PHR2	07g25710				↘
PHT1;1**	04g10800				↗
PHT1;2	03g05620				↗
PHT1;4	04g10750				↗
PHT1;6	08g45000				↗
PHT1;8	10g30790				↗
PHT2;1**	02g38020				↘
PLD1	05g29050				↘
PTF1	06g09370				→
SIZ1	05g03430				→
SPX1	06g40120				↗
SPX3	10g25310				↗
SQD1	07g01030				↗
ZAT6**	03g32230				↗

Very high | High | Medium | Low | Very low | Nil

Table 5.2: Expression of PSI genes in rice root tissues under normal conditions. EES: Epidermis, Exodermis, Sclerenchyma ; EPS: Endodermis, Pericycle, Stele **Overall expression is very low, relative differential expression in shown Note: The table is generated using the dataset available on RiceXPro database (ricexpro.dna.affrc.go.jp). This gene expression dataset represents different tissue types from root tip and elongation zone, under normal conditions. Directional arrows with black, green and red colour respectively depicts no change , upregulation and downregulation in the transcript levels following 21 days of phosphate stress (Pi-). This expression levels are relative to the phosphate sufficient condition (Pi+) at day 21 and are adopted from the published mSEQ dataset (Secco *et al.*, 2013) .

Chapter 6

Conclusions

In this thesis, the aim has been to use systems approaches to increase understanding of the regulation of phosphate uptake in plants at different spatial scales. The major aspect of this research involved the development of mathematical models concerning phosphate acquisition and transport at cellular and multi-cellular scales, though laboratory work was also carried out. Prior to this work, phosphate uptake models had been developed for supra-tissue scales and have often focused on phosphorus dynamics in soil, to identify ways of optimising its availability. No models have appeared in the literature, which connect phosphate uptake dynamics with the genotype of the plant. To improve phosphorus-use efficiency in plants, there are increasing needs to explore the interactions between genotype, phenotype and environment, i.e. low phosphate conditions.

In view of this, the mathematical models for molecular regulation of phosphate uptake in rice have been developed, see Chapter 3 and 4. These cell-scale models in combination with laboratory experiments have offered insights into the regulation of PHO2 and IPS1. To investigate the interaction between different cell-types and the effect of root anatomies on phosphate flux, multicellular models for phosphate uptake and transport have also been developed, using realistic geometries for *Arabidopsis* and Rice roots, see Chapter 5. Furthermore, whole-root ionomics time-course data have been generated, see Appendix A. In one sense, a systems approach involves cycling between "wet" and "dry" lab experiments. The discoveries concerning PHO2 regulation are an example of one and a half such cycles. Using the terminologies proposed in Appendix D, this project has identified knowledge gaps, resolved different hypotheses and offered potential regulatory models for experimental validation. In the case of IPS1, root-hairs and the fluid-filled lacunae crossing aerenchyma, model predictions have lead to hypotheses, which need experimental testing.

In brief, this study has led to eight interesting hypotheses, which can be the starting point for further research:

1. PHO2 protein mediates the degradation of it own transcriptional activator (TA) to maintain constant PHO2 levels.

Transcription factors belonging to MYB, WRKY, bHLH, bZIP, MADS-box and DOF families are predicted to be the potential candidates for TA. However, Yeast-1-hybrid screening and ChIP-PCR are needed for experimental identification and validation of TA's identity. The degradation of TA by ubiquitination can be investigated in five steps : (i) make a CRISPR PHO2-construct in which only the active site residues have been modified, which should show a different phenotype under normal and a Pi-starvation time course, (ii) ubiquitin binding-site prediction of TA candidates, (iii) once TA have been identified raise antibody against it and perform western blots of protein extracts. The presence of Ubiquitin-modification is revealed by multiple bands in western blots probed with anti-TA and anti-Ubiquitin antibodies, (iv) developing mutant with impaired ubiquitin binding site in TA and probing the PSR phenotype, (v) performing *in-vitro* ubiquitination of TA by PHO2 protein (UBC24).

2. The binding affinity of the transcriptional activator (TA) of PHO2 is impaired by a phosphate-sensitive transcriptional repressor/inhibitor (TI).

There are two possibilities for TI: (i) Post-translational modification (PTM) and (ii) Protein-Protein interaction (PPI). Potential PTM sites (for example for SUMOylation or de/phosphorylation) can be initially predicted by sequence analysis. This could be followed by generating western blots for the proteins from normal and stressed plants, and probing with TA antibody for size change and with antibodies against protein modifiers, which may include SUMO and phosphoproteins. On the other hand, PPI could be investigated by (i) performing Yeast-2-Hybrid assay (using TA as the bait) (ii) developing prey knock out lines and studying their effect on the PSR (iii) performing *in-vitro* protein binding with cross-linking in presence and absence of Pi.

3. IPS1 RNA is protected from degradation by phosphate-sensitive RNA binding proteins, of which PUMILIOs are candidates, causing elevation in its levels.

This hypothesis could be validated by two set of experiments. The first involves performing Poly-A tail PCR for IPS1 under deficient and re-supplied Pi conditions. This would offer a preliminary experimental validation for the alteration in half-life of IPS1 under Pi stress. The second experiment involves RNA-pull down assay, wherein a biotinylated synthetic IPS1 RNA with and without poly-A can be used to pull-

down the binding protein/s from Pi starved and re-supplied root cell-extracts. The extracted RNA-protein complexes could be than analysed using LC-MS/MS to identify potential Pi-sensitive IPS1-binding proteins. Confirmation of their role can be achieved by using *in-vitro* cross-linking in the presence and absence of Pi followed by Electrophoretic mobility shift assays.

4. Cortical cells are the last to recover from phosphate stress because they are larger.

Ideally, this can be investigated by using genetically-encoded high-resolution FRET nanosensors, which allow *in-vivo* spatio-temporal quantification of intracellular Pi in different root tissues under sufficient, deficient and repleted Pi condition(Jones *et al.*, 2013; Mukherjee *et al.*, 2015; Okumoto, 2014).

5. Trichoblast cells have lower cytosolic phosphate than neighbouring cells and this acts as a trigger for root-hair initiation.

Though the concentration of Pi in trichoblasts could be quantified using the above FRET (Fluorescence Resonance Energy Transfer)-nanosensor technique, linking the decrease in Pi concentration to root-hair initiation (RHI) needs further investigation. This could be done by assessing the members of RHI network, involving both genetic and hormonal regulators, for the potential Pi-sensitive PTM (eg. SUMOylation or de/phosphorylation) and responsiveness to Pi-sensitive proteins (eg. PHR2). This could experimentally tested in the similar manner described in section 2 above. Furthermore, the Pi-sensitive RHI promoter could be fused with fluorescence marker (e.g. VENUS or GFP) to study its expression dynamics in response to low Pi. Potentially, this could be complemented with Pi-nanosensor as a second fluorophore to capture the Pi dynamics in parallel.

6. The phosphate entering a root-hair cell is passed on to raise the cytosolic phosphate of neighbouring trichoblasts, deterring them from producing root-hairs where they are not needed.

To investigate this hypothesis for root-hair patterning, Pi-nanosensor fused mutant could be grown in presence of Pi analogues (eg. Phosphite). Moreover, plasmodesmata blockers (e.g. salicylic acid) (Sager & Lee, 2014; Wu & Gallagher, 2013) could be exogenously applied to the mutant grown in Pi-deficient conditions. In either experiments, if the hypothesis is true, impaired root-hair patterning would be observed.

7. Fluid-filled lacunae transversing aerenchyma increase phosphate flux radially across the root.

This hypothesis, firstly, need more detailed OpenAlea simulations for further assessment. For experimentally validation, labeled Pi or FRET- nanosensors could be used

to measure time course dynamics of Pi uptake and its loading into the xylem across the root/s with different anatomies.

8. Fluid-filled lacunae are a useful trait to enhance phosphate acquisition efficiency in low-phosphate conditions and have the potential to improve the acquisition efficiencies of other nutrients.

This trait can be tested *in-silico* using SimRoot (Lynch *et al.*, 1997; Postma & Lynch, 2011b). However, the phosphate uptake efficiency of aerenchymatous roots with dry or fluid-filled lacunae could be evaluated by growing plants under different phosphate conditions and simultaneously quantifying the total above-ground phosphorus level in plants with their aerenchymatous anatomies throughout their root systems.

Arising from this project, there are several avenues to enhance the understanding of phosphate regulation in plants. The first among these is the analysis of the data on elemental uptake and content, presented in Appendix A. This dataset offers the temporal signatures for the uptake of different elements under normal and phosphate-deficient conditions. Besides uptake rates, the dataset can lead to a temporal understanding of the interactions between different plant nutrients. In addition, this dataset can be used to develop whole-root phosphate/resource uptake models in SimRoot (Lynch *et al.*, 1997). Indeed, improving upon this pilot-scale ionomics experiment, a full-scale experiment is desirable with more plants, a range of phosphate treatments initiated at different developmental stages and parallel plant sampling and measurements including dry weight, hydroponic pH, plant phenotypes and physiology. This would offer more precise insights into nutrient uptake dynamics and their interactions under normal and different external phosphate conditions.

The cell-scale models can be improved by expanding the utilisation parameter (U) to a function that includes phosphate flux across the vacuoles, changes in metabolism, the shift to sulfo-lipids and growth rate. Phosphate uptake can be studied at different fixed external phosphate concentrations to discover the external conditions under which different parts of the regulatory network operates, while bifurcation analysis of the model could be performed to identify gene combinations giving improved uptake under low external phosphate. Furthermore, the external phosphate can be represented as a variable, which is a function of phosphate uptake, root exudation and soil properties. This could pave the way for a much better understanding of root-soil interactions.

The multicellular root models can be improved by modifying the representation of xylem (to include a term for phosphate-dependent transpiration) and phloem (by including a term for phosphate-flux from phloem to root tissues). Indeed, there is

the need for a more thorough literature search to gain precise values for the model parameters. These models can be used to evaluate the rates of phosphate uptake and flux across tissues. Furthermore, these tissue models can be expanded to include soil conditions and mycorrhizae to understand their impact on phosphate uptake.

Ultimately, the cell-scale and multicellular models must be integrated to investigate the spatio-temporal expression of genes. This combined model can be used to identify potent gene-anatomy combinations, leading to improved phosphate-acquisition efficiency. Moreover, these models can be merged with other published (see Appendix C) or novel models. For example, the model for genetic regulation of phosphate uptake can be integrated with the models concerning other resource uptake (including nitrogen and water) (Alekhina *et al.*, 2000; De Schepper & Steppe, 2010; Dunbabin *et al.*, 2002; Payvandi *et al.*, 2014), lateral-root formation (Lucas *et al.*, 2008; Péret *et al.*, 2012, 2013), and root-hair patterning and development (Benitez *et al.*, 2008; Jones *et al.*, 2009; Payne & Grierson, 2009).

To conclude this thesis, the famous quote of Sir Winston Churchill comes to mind :

'This is not the end. But it is, perhaps, the end of the beginning'.

References

Alekhina, N D, Kharitonashvili, E V, Riznichenko, G Y, Plusnina, T Y, Sidorov, S V, & Rubin, A B. 2000. A multi compartments model of nitrate metabolism regulation in plant roots. *Journal of Biological Systems*, **8**(3), 219–235.

Amasino, R M, & Michaels, S D. 2010. The timing of flowering. *Plant Physiol*, **154**(2), 516–520.

Amijee, F, Barraclouch, B P, & Tinker, P. 1991. Modeling phosphorus uptake and utilization by plants. *Pages 63–75 of: Phosphorus nutrition of grain legumes in the semi-arid tropics.* International Crops Research Institute for the Semi-Arid Tropics, Patancheru, Andhra Pradesh, India.

Aung, K, Lin, S I, Wu, C C, Huang, Y T, Su, C L, & Chiou, T J. 2006. pho2, a phosphate overaccumulator, is caused by a nonsense mutation in a microRNA399 target gene. *Plant Physiol*, **141**(3), 1000–1011.

Bai, Z, Li, H, Yang, X, Zhou, B, Shi, X, Wang, B, Li, D, Shen, J, Chen, Q, Qin, W, Oenema, O, & Zhang, F. 2013. The critical soil P levels for crop yield, soil fertility and environmental safety in different soil types. *Plant and Soil*, **372**(1-2), 27–37.

Band, L R, Úbeda-Tomás, S, Dyson, R J, Middleton, A M, Hodgman, T C, Owen, M R, Jensen, O E, Bennett, M J, & King, J R. 2012a. Growth-induced hormone dilution can explain the dynamics of plant root cell elongation. *Proc Natl Acad Sci U S A*, **109**(19), 7577–7582.

Band, L R, Wells, D M, Larrieu, A, Sun, J, Middleton, A M, French, A P, Brunoud, G, Sato, E M, Wilson, M H, Péret, B, Oliva, M, Swarup, R, Sairanen, I, Parry, G, Ljung, K, Beeckman, T, Garibaldi, J M, Estelle, M, Owen, M R, Vissenberg, K, Hodgman, T C, Pridmore, T P, King, J R, Vernoux, T, & Bennett, M J. 2012b. Root gravitropism is regulated by a transient lateral auxin gradient controlled by a tipping-point mechanism. *Proc Natl Acad Sci U S A*, **109**(12), 4668–4673.

Band, L R, Wells, D M, Fozard, J A, Ghetiu, T, French, A P, Pound, M P, Wilson, M H, Yu, L, Li, W, Hijazi, H I, Oh, J, Pearce, S P, Perez-Amador, M A, Yun, J, Kramer, E, Alonso, J M, Godin, C, Vernoux, T, Hodgman, T C, Pridmore, T, Swarup, R, King, J R, & Bennett, M J. 2014. Systems Analysis of Auxin Transport in the Arabidopsis Root Apex. *Plant Cell*, **26**(3), 862–875.

Bari, R, Datt Pant, B, Stitt, M, & Scheible, W R. 2006. PHO2, microRNA399, and PHR1 define a phosphate-signaling pathway in plants. *Plant Physiol*, **141**(3), 988–999.

Bariola, P A, Howard, C J, Taylor, C B, Verburg, M T, Jaglan, V D, & Green, P J. 1994. The Arabidopsis ribonuclease gene RNS1 is tightly controlled in response to phosphate limitation. *The Plant Journal*, **6**(5), 673–685.

Barrow, N J. 1983. A mechanistic model for describing the sorption and desorption of phosphate by soil. *Journal of Soil Science*, **34**(4), 733–750.

Baxter, I. 2009. Ionomics: studying the social network of mineral nutrients. *Curr Opin Plant Biol*, **12**(3), 381–386.

Baxter, I. 2010. Ionomics: The functional genomics of elements. *Brief Funct Genomics*, **9**(2), 149–156.

Baxter, I, & Dilkes, B P. 2012. Elemental profiles reflect plant adaptations to the environment. *Science*, **336**(6089), 1661–1663.

Baxter, I R, Vitek, O, Lahner, B, Muthukumar, B, Borghi, M, Morrissey, J, Guerinot, M L, & Salt, D E. 2008. The leaf ionome as a multivariable system to detect a plant's physiological status. *Proc Natl Acad Sci U S A*, **105**(33), 12081–12086.

Bayle, V, Arrighi, J F, Creff, A, Nespoulous, C, Vialaret, J, Rossignol, M, Gonzalez, E, Paz-Ares, J, & Nussaume, L. 2011. Arabidopsis thaliana high-affinity phosphate transporters exhibit multiple levels of posttranslational regulation. *Plant Cell*, **23**(4), 1523–1535.

Beemster, G T, & Baskin, T I. 1998. Analysis of cell division and elongation underlying the developmental acceleration of root growth in Arabidopsis thaliana. *Plant Physiol*, **116**(4), 1515–1526.

Benitez, M, Espinosa-Soto, C, Padilla-Longoria, P, & Alvarez-Buylla, E R. 2008. Interlinked nonlinear subnetworks underlie the formation of robust cellular patterns in Arabidopsis epidermis: a dynamic spatial model. *BMC Syst Biol*, **2**, 98.

Berg, A S, & Joern, B C. 2006. Sorption dynamics of organic and inorganic phosphorus compounds in soil. *J Environ Qual*, **35**(5), 1855–1862.

Bieleski, R L. 1973. Phosphate Pools, Phosphate Transport, and Phosphate Availability. *Annual Review of Plant Physiology*, **24**(1), 225–252.

Brady, Siobhan M, Zhang, Lifang, Megraw, Molly, Martinez, Natalia J, Jiang, Eric, Yi, Charles S, Liu, Weilin, Zeng, Anna, Taylor-Teeples, Mallorie, Kim, Dahae, Ahnert, Sebastian, Ohler, Uwe, Ware, Doreen, Walhout, Albertha J M, & Benfey, Philip N. 2011. A stele-enriched gene regulatory network in the Arabidopsis root. *Molecular Systems Biology*, **7**(1).

Brewer, P B, Koltai, H, & Beveridge, C A. 2013. Diverse roles of strigolactones in plant development. *Mol Plant*, **6**(1), 18–28.

Brown, L K, George, T S, Dupuy, L X, & White, P J. 2013. A conceptual model of root hair ideotypes for future agricultural environments: what combination of traits should be targeted to cope with limited P availability? *Ann Bot*, **112**(2), 317–330.

Bruex, A, Kainkaryam, R M, Wieckowski, Y, Kang, Y H, Bernhardt, C, Xia, Y, Zheng, X, Wang, J Y, Lee, M M, Benfey, P, Woolf, P J, & Schiefelbein, J. 2012. A Gene Regulatory Network for Root Epidermis Cell Differentiation in Arabidopsis. *PLoS Genetics*, **8**(01), 1–20.

Cao, Y, Yan, Y, Zhang, F, Wang, H, Gu, M, Wu, X, Sun, S, & Xu, G. 2014. Fine characterization of OsPHO2 knockout mutants reveals its key role in Pi utilization in rice. *J Plant Physiol*, **171**(3-4), 340–348.

Castro, P H, Tavares, R M, Bejarano, E R, & Azevedo, H. 2012. SUMO, a heavyweight player in plant abiotic stress responses. *Cell Mol Life Sci*, **69**(19), 3269–3283.

Chapin III, F S. 1991. Effects of Multiple Environmental Stresses on Nutrient Availability and Use. *Pages 67–88 of:* Pell, Harold A MooneyWilliam E WinnerEva J (ed), *Response of Plants to Multiple Stresses*. San Diego: Academic Press.

Chavez Montes, R A, Coello, G, Gonzalez-Aguilera, K L, Marsch-Martinez, N, de Folter, S, & Alvarez-Buylla, E R. 2014. ARACNe-based inference, using curated microarray data, of Arabidopsis thaliana root transcriptional regulatory networks. *BMC Plant Biology*, **14**(1), 1–14.

Chen, Y F, Li, L Q, Xu, Q, Kong, Y H, Wang, H, & Wu, W H. 2009. The WRKY6 transcription factor modulates PHOSPHATE1 expression in response to low Pi stress in Arabidopsis. *Plant Cell*, **21**(11), 3554–3566.

Chen, Z H, Nimmo, G A, Jenkins, G I, & Nimmo, H G. 2007. BHLH32 modulates several biochemical and morphological processes that respond to Pi starvation in Arabidopsis. *Biochem J*, **405**(1), 191–198.

Chen, Z H, Jenkins, G I, & Nimmo, H G. 2008. Identification of an F-box protein that negatively regulates P(i) starvation responses. *Plant Cell Physiol*, **49**(12), 1902–1906.

Cheng, N H, Pittman, J K, Shigaki, T, Lachmansingh, J, LeClere, S, Lahner, B, Salt, D E, & Hirschi, K D. 2005. Functional association of Arabidopsis CAX1 and CAX3 is required for normal growth and ion homeostasis. *Plant Physiol*, **138**(4), 2048–2060.

Cheng, X, Ruyter-Spira, C, & Bouwmeester, H. 2013. The interaction between strigolactones and other plant hormones in the regulation of plant development. *Front Plant Sci*, **4**, 199.

Chew, Y H, & Halliday, K J. 2011. A stress-free walk from Arabidopsis to crops. *Curr Opin Biotechnol*, **22**(2), 281–286.

Chin, J H, Gamuyao, R, Dalid, C, Bustamam, M, Prasetiyono, J, Moeljopawiro, S, Wissuwa, M, & Heuer, S. 2011. Developing rice with high yield under phosphorus deficiency: Pup1 sequence to application. *Plant Physiol*, **156**(3), 1202–1216.

Chiou, T J, & Lin, S I. 2011. Signaling network in sensing phosphate availability in plants. *Annu Rev Plant Biol*, **62**, 185–206.

Cho, H T, & Lee, R D W. 2013. Auxin, the organizer of the environmental/hormonal signals for root hair growth. *Frontiers in Plant Science*, **4**(448).

Clemente, R M, Vives, V, Zandalinas, S I, López-Climent, M F., Munoz, V, & Gómez-Cadenas, A. 2013. Biotechnological approaches to study plant responses to stress. *Biomed Res Int*, **2013**, 654120,10.

Committee, Plant Science Research Summit. 2011. *The Green Frontier: A Unified Vision for Plant Research (http://plantsummit.wordpress.com/).*

Conn, S, & Gilliham, M. 2010. Comparative physiology of elemental distributions in plants. *Ann Bot*, **105**(7), 1081–1102.

Conti, L, Price, G, O'Donnell, E, Schwessinger, B, Dominy, P, & Sadanandom, A. 2008. Small Ubiquitin-Like Modifier Proteases OVERLY TOLERANT TO SALT1 and -2 Regulate Salt Stress Responses in Arabidopsis. *The Plant Cell*, **20**(10), 2894–2908.

Cook, K B, Hughes, T R, & Morris, Q D. 2015. High-throughput characterization of protein-RNA interactions. *Brief Funct Genomics*, **14**(1), 74–89.

Cordell, D, & Neset, T S. 2013. Phosphorus vulnerability: A qualitative framework for assessing the vulnerability of national and regional food systems to the multi-dimensional stressors of phosphorus scarcity. *Global Environmental Change*, **24**, 108–122.

Cordell, D, & White, S. 2013. Sustainable phosphorus measures: strategies and technologies for achieving phosphorus security. *Agronomy*, **3**(1), 86–116.

Coudert, Y, Perin, C, Courtois, B, Khong, N G, & Gantet, P. 2010. Genetic control of root development in rice, the model cereal. *Trends Plant Sci*, **15**(4), 219–226.

Cross, A F, & Schlesinger, W H. 1995. A literature review and evaluation of the Hedley fractionation- Applications to the biogeochemical cycle of soil phosphorus in natural ecosystems. *Geoderma*, **64**(3-4), 197–214.

Czarnecki, O, Yang, J, Weston, D J, Tuskan, G A, & Chen, J G. 2013. A dual role of strigolactones in phosphate acquisition and utilization in plants. *Int J Mol Sci*, **14**(4), 7681–7701.

Dakora, F D, & Phillips, D A. 2002. Root exudates as mediators of mineral acquisition in low-nutrient environments. *Plant and Soil*, **245**(1), 35–47.

De Schepper, V, & Steppe, K. 2010. Development and verification of a water and sugar transport model using measured stem diameter variations. *J Exp Bot*, **61**(8), 2083–2099.

de Wit, C T. 1959. Potential photosynthesis of crop surfaces. *Netherlands Journal of Agricultural Science*, **7**(2), 141–149.

Devaiah, B N, & Raghothama, K G. 2007. Transcriptional Regulation of Pi Starvation Responses by WRKY75. *Plant Signal Behav*, **2**(5), 424–425.

Devaiah, B N, Nagarajan, V K, & Raghothama, K G. 2007a. Phosphate homeostasis and root development in Arabidopsis are synchronized by the zinc finger transcription factor ZAT6. *Plant Physiol*, **145**(1), 147–159.

Devaiah, B N, Karthikeyan, A S, & Raghothama, K G. 2007b. WRKY75 transcription factor is a modulator of phosphate acquisition and root development in Arabidopsis. *Plant Physiol*, **143**(4), 1789–1801.

Devaiah, B N, Madhuvanthi, R, Karthikeyan, A S, & Raghothama, K G. 2009. Phosphate starvation responses and gibberellic acid biosynthesis are regulated by the MYB62 transcription factor in Arabidopsis. *Mol Plant*, **2**(1), 43–58.

Drew, M. C., & Saker, L. R. 1986. Ion Transport to the Xylem in Aerenchymatous Roots of Zea mays L. *Journal of Experimental Botany*, **37**(1), 22–33.

Duckett, C. M., Grierson, C., Linstead, P., Schneider, K., Lawson, E., Dean, C., Poethig, S., & Roberts, K. 1994. Clonal relationships and cell patterning in the root epidermis of Arabidopsis. *Development*, **120**(9), 2465–2474.

Dunbabin, V M, Diggle, A J, Rengel, Z, & van Hugten, R. 2002. Modelling the interactions between water and nutrient uptake and root growth. *Plant and Soil*, **239**(1), 19–38.

Dupuy, L, Mackenzie, J, Rudge, T, & Haseloff, J. 2008. A system for modelling cell-cell interactions during plant morphogenesis. *Ann Bot*, **101**(8), 1255–1265.

Elser, J J. 2012. Phosphorus: a limiting nutrient for humanity? *Curr Opin Biotechnol*, **23**(6), 833–838.

Fang, Zhaoyuan, Shao, Chuan, Meng, Yijun, Wu, Ping, & Chen, Ming. 2009. Phosphate signaling in Arabidopsis and Oryza sativa. *Plant Science*, **176**(2), 170–180.

FAO. 2002. *World Agriculture: Towards 2015/2030. Summary report.* Tech. rept.

Flavell, R. 2009. Role of model plant species. *Methods Mol Biol*, **513**, 1–18.

Foley, S W, Vandivier, L E, Kuksa, P P, & Gregory, B D. 2015. Transcriptome-wide measurement of plant RNA secondary structure. *Curr Opin Plant Biol*, **27**, 36–43.

Ford, L. P., & Wilusz, J. 1999. 3'-Terminal RNA structures and poly(U) tracts inhibit initiation by a 3'->5' exonuclease in vitro. *Nucleic Acids Res*, **27**(4), 1159–1167.

Foreman, J, & Dolan, L. 2001. Root Hairs as a Model System for Studying Plant Cell Growth. *Annals of Botany*, **88**(1), 1–7.

Foyer, C, & Spencer, C. 1986. The relationship between phosphate status and photosynthesis in leaves : Effects on intracellular orthophosphate distribution, photosynthesis and assimilate partitioning. *Planta*, **167**(3), 369–375.

Fozard, J A, Lucas, M, King, J R, & Jensen, O E. 2013. Vertex-element models for anisotropic growth of elongated plant organs. *Front Plant Sci*, **4**, 233.

Franco-Zorrilla, J M, Valli, A, Todesco, M, Mateos, I, Puga, M I, Rubio-Somoza, I, Leyva, A, Weigel, D, Garcia, J A, & Paz-Ares, J. 2007. Target mimicry provides a new mechanism for regulation of microRNA activity. *Nat Genet*, **39**(8), 1033–1037.

Gallie, D. R., & Walbot, V. 1990. RNA pseudoknot domain of tobacco mosaic virus can functionally substitute for a poly(A) tail in plant and animal cells. *Genes Dev*, **4**(7), 1149–1157.

Gamuyao, R, Chin, J H, Pariasca-Tanaka, J, Pesaresi, P, Catausan, S, Dalid, C, Slamet-Loedin, I, Tecson-Mendoza, E M, Wissuwa, M, & Heuer, S. 2012. The protein kinase Pstol1 from traditional rice confers tolerance of phosphorus deficiency. *Nature*, **488**(7412), 535–539.

Gaxiola, R A, Edwards, M, & Elser, J J. 2011. A transgenic approach to enhance phosphorus use efficiency in crops as part of a comprehensive strategy for sustainable agriculture. *Chemosphere*, **84**(6), 840–845.

George, E, Marschner, H, & Jakobsen, I. 1995. Role of Arbuscular Mycorrhizal Fungi in Uptake of Phosphorus and Nitrogen From Soil. *Critical Reviews in Biotechnology*, **15**(3-4), 257–270.

Giehl, Ricardo F H, Gruber, Benjamin D, & von Wirén, Nicolaus. 2014. It's time to make changes: modulation of root system architecture by nutrient signals. *Journal of Experimental Botany*, **65**(3), 769–778.

Gilbert, N. 2009. Environment: The disappearing nutrient. *Nature*, **461**(7265), 716–718.

Glazier, & Graner. 1993. Simulation of the differential adhesion driven rearrangement of biological cells. *Phys Rev E Stat Phys Plasmas Fluids Relat Interdiscip Topics*, **47**(3), 2128–2154.

Godfray, H C, Beddington, J R, Crute, I R, Haddad, L, Lawrence, D, Muir, J F, Pretty, J, Robinson, S, Thomas, S M, & Toulmin, C. 2010. Food security: the challenge of feeding 9 billion people. *Science*, **327**(5967), 812–818.

Gonzalez, E, Solano, R, Rubio, V, Leyva, A, & Paz-Ares, J. 2005. PHOSPHATE TRANSPORTER TRAFFIC FACILITATOR1 is a plant-specific SEC12-related protein that enables the endoplasmic reticulum exit of a high-affinity phosphate transporter in Arabidopsis. *Plant Cell*, **17**(12), 3500–3512.

Graner, & Glazier. 1992. Simulation of biological cell sorting using a two-dimensional extended Potts model. *Phys Rev Lett*, **69**(13), 2013–2016.

Grant, R F, & Robertson, J A. 1997. Phosphorus uptake by root systems: mathematical modelling in ecosys. *Plant and Soil*, **188**(2), 279–297.

Green, P J. 1994. The Ribonucleases of Higher Plants. *Annual Review of Plant Physiology and Plant Molecular Biology*, **45**(1), 421–445.

Gregory, Peter J, & George, Timothy S. 2011. Feeding nine billion: the challenge to sustainable crop production. *Journal of Experimental Botany*, **62**(15), 5233–5239.

Grierson, C, Nielsen, E, Ketelaarc, T, & Schiefelbein, J. 2014. Root hairs. *Arabidopsis Book*, **12**, e0172.

Gstaiger, M, & Aebersold, R. 2009. Applying mass spectrometry-based proteomics to genetics, genomics and network biology. *Nat Rev Genet*, **10**(9), 617–627.

Guo, B., Jin, Y., Wussler, C., Blancaflor, E. B., Motes, C. M., & Versaw, W. K. 2008. Functional analysis of the Arabidopsis PHT4 family of intracellular phosphate transporters. *New Phytologist*, **177**(4), 889–898.

Gutierrez, R A, Lejay, L V, Dean, A, Chiaromonte, F, Shasha, D E, & Coruzzi, G M. 2007. Qualitative network models and genome-wide expression data define carbon/nitrogen-responsive molecular machines in Arabidopsis. *Genome Biology*, **8**(1), 1–13.

Ha, S, & Tran, L S. 2014. Understanding plant responses to phosphorus starvation for improvement of plant tolerance to phosphorus deficiency by biotechnological approaches. *Crit Rev Biotechnol*, **34**(1), 16–30.

Hamant, O, Heisler, M G, Jönsson, H, Krupinski, P, Uyttewaal, M, Bokov, P, Corson, F, Sahlin, P, Boudaoud, A, Meyerowitz, E M, Couder, Y, & Traas, J. 2008. Developmental patterning by mechanical signals in Arabidopsis. *Science*, **322**(5908), 1650–1655.

Hammond, J P, & White, P J. 2008. Sucrose transport in the phloem: integrating root responses to phosphorus starvation. *J Exp Bot*, **59**(1), 93–109.

Hammond, J P, Bennett, M J, Bowen, H C, Broadley, M R, Eastwood, D C, May, S T, Rahn, C, Swarup, R, Woolaway, K E, & White, P J. 2003. Changes in gene expression in Arabidopsis shoots during phosphate starvation and the potential for developing smart plants. *Plant Physiol*, **132**(2), 578–596.

Hammond, J P, Broadley, M R, & White, P J. 2004. Genetic Responses to Phosphorus Deficiency. *Annals of Botany*, **94**(3), 323–332.

He, C J, Morgan, P W, & Drew, M C. 1992. Enhanced Sensitivity to Ethylene in Nitrogen- or Phosphate-Starved Roots of Zea mays L. during Aerenchyma Formation. *Plant Physiol*, **98**(1), 137–142.

Hellman, L M, & Fried, M G. 2007. Electrophoretic mobility shift assay (EMSA) for detecting protein-nucleic acid interactions. *Nat Protoc*, **2**(8), 1849–1861.

Heppell, J, Talboys, P, Payvandi, S, Zygalakis, K C, Fliege, J, Withers, P J, Jones, D L, & Roose, T. 2015a. How changing root system architecture can help tackle a reduction in soil phosphate (P) levels for better plant P acquisition. *Plant Cell Environ*, **38**(1), 118–128.

Heppell, J, Payvandi, S, Talboys, P, Zygalakis, K C, Fliege, J, Langton, D, Sylvester-Bradley, R, Walker, R, Jones, D L, & Roose, T. 2015b. Modelling the optimal phosphate fertiliser and soil management strategy for crops. *Plant and Soil*, 1–15.

Hermans, C, Hammond, J P, White, P J, & Verbruggen, N. 2006. How do plants respond to nutrient shortage by biomass allocation? *Trends Plant Sci*, **11**(12), 610–617.

Hernandez, I, & Munne-Bosch, S. 2015. Linking phosphorous availability with photo-oxidative stress in plants. *Journal of Experimental Botany*, **66**(10), 2889–2900.

Hickman, R, Hill, C, Penfold, C A, Breeze, E, Bowden, L, Moore, J D, Zhang, P, Jackson, A, Cooke, E, Bewicke-Copley, F, Mead, A, Beynon, J, Wild, D L, Denby,

K J, Ott, S, & Buchanan-Wollaston, V. 2013. A local regulatory network around three NAC transcription factors in stress responses and senescence in Arabidopsis leaves. *Plant J*, **75**(1), 26–39.

Hill, K, Porco, S, Lobet, G, Zappala, S, Mooney, S, Draye, X, & Bennett, M J. 2013. Root systems biology: integrative modeling across scales, from gene regulatory networks to the rhizosphere. *Plant Physiol*, **163**(4), 1487–1503.

Hindmarsh, A C. 1983. ODEPACK, A Systematized Collection of ODE Solvers. *Pages 55–64 of:* Stepleman, R S (ed), *Scientific Computing*, vol. 1. North-Holland, Amsterdam: IMACS Transactions on Scientific Computation.

Hinsinger, P, Gobran, G R, Gregory, P J, & Wenzel, W W. 2005. Rhizosphere geometry and heterogeneity arising from root-mediated physical and chemical processes. *New Phytol*, **168**(2), 293–303.

Hinsinger, P, Bengough, A G, Vetterlein, D, & Young, I M. 2009. Rhizosphere: biophysics, biogeochemistry and ecological relevance. *Plant and Soil*, **321**(1-2), 117–152.

Hinsinger, P, Herrmann, L, Lesueur, D, Robin, A, Trap, J, Waithaisong, K, & Plassard, C. 2015. Impact of roots, microorganisms and microfauna on the fate of soil phosphorus in the rhizosphere. *Pages 375–407 of: Annual Plant Reviews Volume 48*. John Wiley & Sons, Inc.

Hodgman, T C, & Ajmera, I. 2015. The successful application of systems approaches in plant biology. *Progress in biophysics and molecular biology*, **117**(1), 59–68.

Hoops, S, Sahle, S, Gauges, R, Lee, C, Pahle, J, Simus, N, Singhal, N, Xu, L, Mendes, P, & Kummer, U. 2006. COPASI-a COmplex PAthway SImulator. *Bioinformatics*, **22**(24), 3067–3074.

Hou, X L, Wu, P, Jiao, F C, Jia, Q J, Chen, H M, Yu, J, Song, X W, & Yi, K K. 2005. Regulation of the expression of OsIPS1 and OsIPS2 in rice via systemic and local Pi signalling and hormones. *Plant, Cell & Environment*, **28**(3), 353–364.

Hu, B, Zhu, C, Li, F, Tang, J, Wang, Y, Lin, A, Liu, L, Che, R, & Chu, C. 2011. LEAF TIP NECROSIS1 plays a pivotal role in the regulation of multiple phosphate starvation responses in rice. *Plant Physiol*, **156**(3), 1101–1115.

Hu, B, Henry, A, Brown, K M, & Lynch, J P. 2014. Root cortical aerenchyma inhibits radial nutrient transport in maize (Zea mays). *Ann Bot*, **113**(1), 181–189.

Hucka, M, Finney, A, Sauro, H M, Bolouri, H, Doyle, J C, Kitano, H, Arkin, A P, Bornstein, B J, Bray, D, Cornish-Bowden, A, Cuellar, A A, Dronov, S, Gilles, E D, Ginkel, M, Gor, V, Goryanin, I I, Hedley, W J, Hodgman, T C, Hofmeyr, J H, Hunter, P J, Juty, N S, Kasberger, J L, Kremling, A, Kummer, U, Le Novère, N, Loew, L M, Lucio, D, Mendes, P, Minch, E, Mjolsness, E D, Nakayama, Y, Nelson, M R, Nielsen, P F, Sakurada, T, Schaff, J C, Shapiro, B E, Shimizu, T S, Spence, H D, Stelling, J, Takahashi, K, Tomita, M, Wagner, J, Wang, J, & Forum, SBML. 2003. The systems biology markup language (SBML): a medium for representation and exchange of biochemical network models. *Bioinformatics*, **19**(4), 524–531.

Hunter, J.D. 2007. Matplotlib: A 2D Graphics Environment. *Computing in Science & Engineering*, **9**(3), 90–95.

Hurley, B A, Tran, H T, Marty, N J, Park, J, Snedden, W A, Mullen, R T, & Plaxton, W C. 2010. The dual-targeted purple acid phosphatase isozyme AtPAP26 is essential for efficient acclimation of Arabidopsis to nutritional phosphate deprivation. *Plant Physiol*, **153**(3), 1112–1122.

Jaschke, W D, Peuke, A D, Pate, J S, & Hartung, W. 1997. Transport, synthesis and catabolism of abscisic acid (ABA) in intact plants of castor bean (Ricinus communis L.) under phosphate deficiency and moderate salinity. *Journal of Experimental Botany*, **48**(9), 1737–1747.

Javot, H, Pumplin, N, & Harrison, M J. 2007. Phosphate in the arbuscular mycorrhizal symbiosis: transport properties and regulatory roles. *Plant Cell Environ*, **30**(3), 310–322.

Jeffry, D S, & Keith, J J. 2014. CRISPR-Cas systems for editing, regulating and targeting genomes. *Nat Biotechnol*, **32**(4), 347–355.

Jeschke, W D, Kirkby, E A, Peuke, A D, Pate, J S, & Hartung, W. 1997. Effects of P deficiency on assimilation and transport of nitrate and phosphate in intact plants of castor bean (Ricinus communis L.). *Journal of Experimental Botany*, **48**(1), 75–91.

Jia, H, Ren, H, Gu, M, Zhao, J, Sun, S, Zhang, X, Chen, J, Wu, P, & Xu, G. 2011. The phosphate transporter gene OsPht1;8 is involved in phosphate homeostasis in rice. *Plant Physiol*, **156**(3), 1164–1175.

Jiang, C, Gao, X, Liao, L, Harberd, N P, & Fu, X. 2007. Phosphate starvation root architecture and anthocyanin accumulation responses are modulated by the gibberellin-DELLA signaling pathway in Arabidopsis. *Plant Physiol*, **145**(4), 1460–1470.

Jin, C, Fang, C, Yuan, H, Wang, S, Wu, Y, Liu, X, Zhang, Y, & Luo, J. 2015. Interaction between carbon metabolism and phosphate accumulation is revealed by a mutation of a cellulose synthase-like protein, CSLF6. *J Exp Bot*, **66**(9), 2557–2567.

Jobbagy, E G, & Jackson, R B. 2001. The distribution of soil nutrients with depth: Global patterns and the imprint of plants. *Biogeochemistry*, **53**(1), 51–77.

Johnston, A E, & Steen, I. 2000. *Understanding phosphorus and its use in agriculture.*

Jones, A R, Kramer, E M, Knox, K, Swarup, R, Bennett, M J, Lazarus, C M, Leyser, H M, & Grierson, C S. 2009. Auxin transport through non-hair cells sustains root-hair development. *Nat Cell Biol*, **11**(1), 78–84.

Jones, Alexander M., Grossmann, Guido, Danielson, Jonas Åh, Sosso, Davide, Chen, Li-Qing, Ho, Cheng-Hsun, & Frommer, Wolf B. 2013. In vivo biochemistry: applications for small molecule biosensors in plant biology. *Curr Opin Plant Biol*, **16**(3), 389–395.

Jones, C, Hatier, J, Cao, M, Fraser, K, & Rasmussen, S. 2015. Metabolomics of plant phosphorus-starvation response. *Pages 215–236 of: Annual Plant Reviews Volume 48.* John Wiley & Sons, Inc.

Jonsson, H, Heisler, M G, Shapiro, B E, Meyerowitz, E M, & Mjolsness, E. 2006. An auxin-driven polarized transport model for phyllotaxis. *Proceedings of the National Academy of Sciences of the United States of America*, **103**(5), 1633–1638.

Jouhet, J, Maréchal, E, Baldan, B, Bligny, R, Joyard, J, & Block, M A. 2004. Phosphate deprivation induces transfer of DGDG galactolipid from chloroplast to mitochondria. *J Cell Biol*, **167**(5), 863–874.

Karthikeyan, A S, Varadarajan, D K, Jain, A, Held, M A, Carpita, N C, & Raghothama, K G. 2007. Phosphate starvation responses are mediated by sugar signaling in Arabidopsis. *Planta*, **225**(4), 907–918.

Kennelly, M, O'Mara, J, Rivard, C, Miller, L, & Smith, D. 2012. Introduction to abiotic disorders in plants. *The Plant Health Instructor*, 10.1094/PHI–I–2012–10–29–01.

Keyes, S D, Daly, K R, Gostling, N J, Jones, D L, Talboys, P, Pinzer, B R, Boardman, R, Sinclair, I, Marchant, A, & Roose, T. 2013. High resolution synchrotron imaging of wheat root hairs growing in soil and image based modelling of phosphate uptake. *New Phytol*, **198**(4), 1023–1029.

Kirk, G J. 2002. Modelling root-induced solubilization of nutrients. *Plant and Soil*, **245**(1), 49–57.

Krouk, G, Mirowski, P, LeCun, Y, Shasha, D E, & Coruzzi, G M. 2010. Predictive network modeling of the high-resolution dynamic plant transcriptome in response to nitrate. *Genome Biology*, **11**(12), 1–19.

Kruse, J, Abraham, M, Amelung, W, Baum, C, Bol, R, Kühn, O, Lewandowski, H, Niederberger, J, Oelmann, Y, Rüger, C, Santner, J, Siebers, M, Siebers, N, Spohn, M, Vestergren, J, Vogts, A, & Leinweber, P. 2015. Innovative methods in soil phosphorus research: A review. *Journal of Plant Nutrition and Soil Science*, **178**(1), 43–88.

Kuo, Hui-Fen, & Chiou, Tzyy-Jen. 2011. The Role of MicroRNAs in Phosphorus Deficiency Signaling. *Plant Physiology*, **156**(3), 1016–1024.

Kurepa, Jasmina, Walker, Joseph M., Smalle, Jan, Gosink, Mark M., Davis, Seth J., Durham, Tessa L., Sung, Dong-Yul, & Vierstra, Richard D. 2003. The Small Ubiquitin-like Modifier (SUMO) Protein Modification System in Arabidopsis : ACCUMULATION OF SUMO1 AND -2 CONJUGATES IS INCREASED BY STRESS. *Journal of Biological Chemistry*, **278**(9), 6862–6872.

Lahner, B, Gong, J, Mahmoudian, M, Smith, E L, Abid, K B, Rogers, E E, Guerinot, M L, Harper, J F, Ward, J M, McIntyre, L, Schroeder, J I, & Salt, D E. 2003. Genomic scale profiling of nutrient and trace elements in Arabidopsis thaliana. *Nat Biotechnol*, **21**(10), 1215–1221.

Lai, F, Thacker, J, Li, Y, & Doerner, P. 2007. Cell division activity determines the magnitude of phosphate starvation responses in Arabidopsis. *Plant J*, **50**(3), 545–556.

Lambers, H, Finnegan, P M, Laliberté, E, Pearse, S J, Ryan, M H, Shane, M W, & Veneklaas, E J. 2011. Update on phosphorus nutrition in Proteaceae. Phosphorus nutrition of proteaceae in severely phosphorus-impoverished soils: are there lessons to be learned for future crops? *Plant Physiol*, **156**(3), 1058–1066.

Lan, P, Li, W, & Schmidt, W. 2015. OMICS Approaches Towards Understanding Plant Phosphorus Acquisition and Use. *Pages 65–97 of: Annual Plant Reviews Volume 48*. John Wiley & Sons, Inc.

Larsen, S. 1967. Soil Phosphorus. *Pages 151–210 of:* Norman, A G (ed), *Advances in Agronomy*, vol. Volume 19. Academic Press.

Laveille, M. 2014. *Mixed Effects Models for the Population Approach: Models, Tasks, Methods, and Tools*. Chapman and Hall/CRC Biostatistics Series. 383pp. ISBN 9781482226508.

Lavenus, J, Band, L, Middleton, A, Wilson, M, Lucas, M, Laplaze, L, & Bennett, M. 2012. Toward a Virtual Root: Interaction of Genomics and Modeling to Develop Predictive Biology Approaches. *Pages 79–92 of: Root Genomics and Soil Interactions*. Blackwell Publishing Ltd.

Lee, T, Oh, T, Yang, S, Shin, J, Hwang, S, Kim, C Y, Kim, H, Shim, H, Shim, J E, Ronald, P C, & Lee, I. 2015. RiceNet v2: an improved network prioritization server for rice genes. *Nucleic Acids Research*, **43**(W1), W122–127.

Leitner, D, Klepsch, S, Ptashnyk, M, Marchant, A, Kirk, G J D, Schnepf, A, & Roose, T. 2010. A dynamic model of nutrient uptake by root hairs. *New Phytol*, **185**(3), 792–802.

Li, L, Stoeckert, C J, & Roos, D S. 2003. OrthoMCL: identification of ortholog groups for eukaryotic genomes. *Genome Res*, **13**(9), 2178–2189.

Li, Z, Gao, Q, Liu, Y, He, C, Zhang, X, & Zhang, J. 2011. Overexpression of transcription factor ZmPTF1 improves low phosphate tolerance of maize by regulating carbon metabolism and root growth. *Planta*, **233**(6), 1129–1143.

Lin, S, Santi, C, Jobet, E, Lacut, E, El Kholti, N, Karlowski, W M., Verdeil, J, Breitler, J C, Périn, C, Ko, S, Guiderdoni, E, Chiou, TJ, & Echeverria, M. 2010. Complex Regulation of Two Target Genes Encoding SPX-MFS Proteins by Rice miR827 in Response to Phosphate Starvation. *Plant and Cell Physiology*, **51**(12), 2119–2131.

Lin, S I, & Chiou, T J. 2008. Long-distance movement and differential targeting of microRNA399s. *Plant Signal Behav*, **3**(9), 730–732.

Lin, S I, Chiang, S F, Lin, W Y, Chen, J W, Tseng, C Y, Wu, P C, & Chiou, T J. 2008. Regulatory network of microRNA399 and PHO2 by systemic signaling. *Plant Physiol*, **147**(2), 732–746.

Lin, W, Liao, Y, Yang, T J W, Pan, C, Buckhout, T J, & Schmidt, W. 2011. Coexpression-Based Clustering of Arabidopsis Root Genes Predicts Functional Modules in Early Phosphate Deficiency Signaling. *Plant Physiology*, **155**(3), 1383–1402.

Lin, W Y, Lin, S I, & Chiou, T J. 2009. Molecular regulators of phosphate homeostasis in plants. *J Exp Bot*, **60**(5), 1427–1438.

Lin, W Y, Huang, T K, Leong, S J, & Chiou, T J. 2013. Long-distance call from phosphate: systemic regulation of phosphate starvation responses. *J Exp Bot*, **65**(7), 1817–1827.

Liu, F, Wang, Z, Ren, H, Shen, C, Li, Y, Ling, H Q, Wu, C, Lian, X, & Wu, P. 2010. OsSPX1 suppresses the function of OsPHR2 in the regulation of expression of OsPT2 and phosphate homeostasis in shoots of rice. *Plant J*, **62**(3), 508–517.

Liu, T Y, Lin, W Y, Huang, T K, & Chiou, T J. 2014. MicroRNA-mediated surveillance of phosphate transporters on the move. *Trends Plant Sci*, **19**(10), 647–655.

Liu, X M, Nguyen, X C, Kim, K E, Han, H J, Yoo, J, Lee, K, Kim, M C, Yun, D J, & Chung, W S. 2013. Phosphorylation of the zinc finger transcriptional regulator ZAT6 by MPK6 regulates Arabidopsis seed germination under salt and osmotic stress. *Biochem Biophys Res Commun*, **430**(3), 1054–1059.

Lloyd, J C, & Zakhleniuk, O V. 2004. Responses of primary and secondary metabolism to sugar accumulation revealed by microarray expression analysis of the Arabidopsis mutant, pho3. *J Exp Bot*, **55**(400), 1221–1230.

Lopez-Arredondo, D L, Leyva-Gonzalez, M A, Gonzalez-Morales, S I, Lopez-Bucio, J, & Herrera-Estrella, L. 2014. Phosphate nutrition: improving low-phosphate tolerance in crops. *Annu Rev Plant Biol*, **65**, 95–123.

Lopez-Bucio, J, Hernandez-Abreu, E, Sanchez-Calderon, L, Nieto-Jacobo, M F, Simpson, J, & Herrera-Estrella, L. 2002. Phosphate availability alters architecture and causes changes in hormone sensitivity in the Arabidopsis root system. *Plant Physiol*, **129**(1), 244–256.

Lucas, M, Godin, C, Jay-Allemand, C, & Laplaze, L. 2008. Auxin fluxes in the root apex co-regulate gravitropism and lateral root initiation. *J Exp Bot*, **59**(1), 55–66.

Lucas, M, Laplaze, L, & Bennett, M J. 2011. Plant systems biology: network matters. *Plant Cell Environ*, **34**(4), 535–553.

Lv, Q, Zhong, Y, Wang, Y, Wang, Z, Zhang, L, Shi, J, Wu, Z, Liu, Y, Mao, C, Yi, K, & Wu, P. 2014. SPX4 Negatively Regulates Phosphate Signaling and Homeostasis through Its Interaction with PHR2 in Rice. *Plant Cell*, **26**(4), 1586–1597.

Lynch, J P. 2011. Root phenes for enhanced soil exploration and phosphorus acquisition: tools for future crops. *Plant Physiol*, **156**(3), 1041–1049.

Lynch, J P. 2013. Steep, cheap and deep: an ideotype to optimize water and N acquisition by maize root systems. *Annals of Botany*, **112**(2), 347–357.

Lynch, J P. 2015. Root phenes that reduce the metabolic costs of soil exploration: opportunities for 21st century agriculture. *Plant, Cell & Environment*, **38**(9), 1775–1784.

Lynch, J P, Nielsen, K, Davis, R D., & Jablokow, A. 1997. SimRoot: Modelling and visualization of root systems. **188**(1), 139–151–.

Ma, Z, Bielenberg, D G, Brown, K M, & Lynch, J P. 2001. Regulation of root hair density by phosphorus availability in Arabidopsis thaliana. *Plant, Cell & Environment*, **24**(4), 459–467.

Ma, Z, Baskin, T I, Brown, K M, & Lynch, J P. 2003. Regulation of root elongation under phosphorus stress involves changes in ethylene responsiveness. *Plant Physiol*, **131**(3), 1381–1390.

Maathuis, F J. 2009. Physiological functions of mineral macronutrients. *Curr Opin Plant Biol*, **12**(3), 250–258.

Marbach, D, Costello, J C, Küffner, R, Vega, N M, Prill, R J, Camacho, D M, Allison, K R, Kellis, M, Collins, J J, Stolovitzky, G, & Consortium, DREAM5. 2012. Wisdom of crowds for robust gene network inference. *Nat Methods*, **9**(8), 796–804.

Marschner, H. 1995. Functions of Mineral Nutrients- Macronutrients. *Pages 229–312 of:* Marschner, Horst (ed), *Mineral Nutrition of Higher Plants (Second Edition)*. London: Academic Press.

Marschner, P. 2008. The role of rhizosphere microorganisms in relation to P uptake by plants. *Pages 165–176 of:* White, P J, & Hammond, J P (eds), *The Ecophysiology of Plant-Phosphorus Interactions*. Plant Ecophysiology, vol. 7. Springer Netherlands.

Martin, A C, del Pozo, J C, Iglesias, J, Rubio, V, Solano, R, de La Pena, A, Leyva, A, & Paz-Ares, J. 2000. Influence of cytokinins on the expression of phosphate starvation responsive genes in Arabidopsis. *Plant J*, **24**(5), 559–567.

Marzec, Marek, Muszynska, Aleksandra, & Gruszka, Damian. 2013. The Role of Strigolactones in Nutrient-Stress Responses in Plants. *International Journal of Molecular Sciences*, **14**(5), 9286–9304.

Mayzlish-Gati, E, De-Cuyper, C, Goormachtig, S, Beeckman, T, Vuylsteke, M, Brewer, P B, Beveridge, C A, Yermiyahu, U, Kaplan, Y, Enzer, Y, Wininger, S, Resnick, N, Cohen, M, Kapulnik, Y, & Koltai, H. 2012. Strigolactones are involved in root response to low phosphate conditions in Arabidopsis. *Plant Physiol*, **160**(3), 1329–1341.

McNear Jr., D H. 2013. *The Rhizosphere - Roots, Soil and Everything In Between.*

Mei, H, Cheng, N H, Zhao, J, Park, S, Escareno, R A, Pittman, J K, & Hirschi, K D. 2009. Root development under metal stress in Arabidopsis thaliana requires the H+/cation antiporter CAX4. *New Phytol*, **183**(1), 95–105.

Merks, R, Guravage, M, Inzé, D, & Beemster, T S. 2011. VirtualLeaf: an open-source framework for cell-based modeling of plant tissue growth and development. *Plant Physiol*, **155**(2), 656–666.

Mimura, T. 1999. Regulation of Phosphate Transport and Homeostasis in Plant Cells. *Pages 149–200 of:* Kwang, W Jeon (ed), *International Review of Cytology*, vol. Volume 191. Academic Press.

Mimura, T. 2001. Physiological control of phosphate uptake and phosphate homeostasis in plant cells. *Functional Plant Biology*, **28**(7), 655–660.

Mimura, T, Sakano, K, & Shimmen, T. 1996. Studies on the distribution, retranslocation and homeostasis of inorganic phosphate in barley leaves. *Plant, Cell & Environment*, **19**(3), 311–320.

Mironova, V V, Omelyanchuk, N A, Savina, M S, Ponomarenko, P M, Ponomarenko, M P, Likhoshvai, V A, & Kolchanov, N A. 2013. How multiple auxin responsive

elements may interact in plant promoters: a reverse problem solution. *J Bioinform Comput Biol*, **11**(1), 1340011.

Mittler, R, & Blumwald, E. 2010. Genetic engineering for modern agriculture: challenges and perspectives. *Annu Rev Plant Biol*, **61**, 443–462.

Miura, K, & Ohta, M. 2010. SIZ1, a small ubiquitin-related modifier ligase, controls cold signaling through regulation of salicylic acid accumulation. *Journal of Plant Physiology*, **167**(7), 555 – 560.

Miura, K, Rus, A, Sharkhuu, A, Yokoi, S, Karthikeyan, A S, Raghothama, K G, Baek, D, Koo, Y D, Jin, J B, Bressan, R A, Yun, D J, & Hasegawa, P M. 2005. The Arabidopsis SUMO E3 ligase SIZ1 controls phosphate deficiency responses. *Proc Natl Acad Sci U S A*, **102**(21), 7760–7765.

Miura, K, Jin, J Bo, Lee, J, Yoo, C, Stirm, V, Miura, T, Ashworth, E N, Bressan, R A, Yun, D, & Hasegawa, P M. 2007. SIZ1-Mediated Sumoylation of ICE1 Controls CBF3/DREB1A Expression and Freezing Tolerance in Arabidopsis. *The Plant Cell*, **19**(4), 1403–1414.

Miura, K, Sato, A, Ohta, M, & Furukawa, J. 2011a. Increased tolerance to salt stress in the phosphate-accumulating Arabidopsis mutants siz1 and pho2. *Planta*, **234**(6), 1191–1199.

Miura, K, Lee, J, Gong, Q, Ma, S, Jin, J B, Yoo, C Y, Miura, T, Sato, A, Bohnert, H J, & Hasegawa, P M. 2011b. SIZ1 regulation of phosphate starvation-induced root architecture remodeling involves the control of auxin accumulation. *Plant Physiol*, **155**(2), 1000–1012.

Miura, K, Okamoto, H, Okuma, E, Shiba, H, Kamada, Hand Hasegawa, P M, & Murata, Y. 2013. SIZ1 deficiency causes reduced stomatal aperture and enhanced drought tolerance via controlling salicylic acid-induced accumulation of reactive oxygen species in Arabidopsis. *The Plant Journal*, **73**(1), 91–104.

Monaco, M K, Stein, J, Naithani, S, Wei, S, Dharmawardhana, P, Kumari, S, Amarasinghe, V, Youens-Clark, K, Thomason, J, Preece, J, Pasternak, S, Olson, A, Jiao, Y, Lu, Z, Bolser, D, Kerhornou, A, Staines, D, Walts, B, Wu, G, D'Eustachio, P, Haw, R, Croft, D, Kersey, P J, Stein, L, Jaiswal, P, & Ware, D. 2014. Gramene 2013: comparative plant genomics resources. *Nucleic Acids Res*, **42**(Database issue), D1193–9.

Morcuende, R, Bari, R, Gibon, Y, Zheng, W, Pant, B D, Bläsing, O, Usadel, B, Czechowski, T, Udvardi, M K, Stitt, M, & Scheible, W R. 2007. Genome-wide reprogramming of metabolism and regulatory networks of Arabidopsis in response to phosphorus. *Plant Cell Environ*, **30**(1), 85–112.

Mortimer, S A, Kidwell, M A, & Doudna, J A. 2014. Insights into RNA structure and function from genome-wide studies. *Nat Rev Genet*, **15**(7), 469–479.

Mukherjee, P, Banerjee, S, Wheeler, A, Ratliff, L A, Irigoyen, S, Garcia, L R, Lockless, S W, & Versaw, W K. 2015. Live Imaging of Inorganic Phosphate in Plants with Cellular and Subcellular Resolution. *Plant Physiology*, **167**(3), 628–638.

Muller, R, Morant, M, Jarmer, H, Nilsson, L, & Nielsen, T H. 2007. Genome-wide analysis of the Arabidopsis leaf transcriptome reveals interaction of phosphate and sugar metabolism. *Plant Physiol*, **143**(1), 156–171.

Muraro, D, Voβ, U, Wilson, M, Bennett, M, Byrne, H, De Smet, I, Hodgman, C, & King, J. 2013. Inference of the genetic network regulating lateral root initiation in Arabidopsis thaliana. *IEEE/ACM Trans Comput Biol Bioinform*, **10**(1), 50–60.

Muraro, D, Mellor, N, Pound, M P, Help, H, Lucas, M, Chopard, J, Byrne, H M, Godin, C, Hodgman, T C, King, J R, Pridmore, T P, Helariutta, Y, Bennett, M J, & Bishopp, A. 2014. Integration of hormonal signaling networks and mobile microRNAs is required for vascular patterning in Arabidopsis roots. *Proc Natl Acad Sci U S A*, **111**(2), 857–862.

Murtaugh, P A. 2014. In defense of P values. *Ecology*, **95**(3), 611–617.

Nagai, T, & Honda, H. 2001. A dynamic cell model for the formation of epithelial tissues. *Philosophical Magazine Part B*, **81**(7), 699–719.

Nagarajan, V K, & Smith, A P. 2012. Ethylene's role in phosphate starvation signaling: more than just a root growth regulator. *Plant Cell Physiol*, **53**(2), 277–286.

Narsai, R, Howell, K A, Millar, H A, O'Toole, N, Small, I, & Whelan, J. 2007. Genome-wide analysis of mRNA decay rates and their determinants in Arabidopsis thaliana. *Plant Cell*, **19**(11), 3418–3436.

Natr, L. 1992. Mineral nutrients-A ubiquitous stress factor for photosynthesis. *Photosynthetica*, **27**, 271–294.

Nikiforova, V J, Daub, C O, Hesse, H, Willmitzer, L, & Hoefgen, R. 2005. Integrative gene-metabolite network with implemented causality deciphers informational fluxes of sulphur stress response. *Journal of Experimental Botany*, **56**(417), 1887–1896.

Niu, Y F, Chai, R S, Jin, G L, Wang, H, Tang, C X, & Zhang, Y S. 2012. Responses of root architecture development to low phosphorus availability: a review. *Ann Bot*, **112**(2), 391–408.

Nussaume, L, Kanno, S, Javot, H, Marin, E, Pochon, N, Ayadi, A, Nakanishi, T M, & Thibaud, M C. 2011. Phosphate Import in Plants: Focus on the PHT1 Transporters. *Front Plant Sci*, **2**, 83.

Obata, T, & Fernie, A R. 2012. The use of metabolomics to dissect plant responses to abiotic stresses. *Cell Mol Life Sci*, **69**(19), 3225–3243.

Ohkama-Ohtsu, N, & Wasaki, J. 2010. Recent progress in plant nutrition research: cross-talk between nutrients, plant physiology and soil microorganisms. *Plant Cell Physiol*, **51**(8), 1255–1264.

Okumoto, S. 2014. *Plant Metabolism: Methods and Protocols*. Humana Press,Totowa, NJ. Chap. Quantitative Imaging Approaches for Small-Molecule Measurements Using FRET Sensors in Plants, pages 55–64.

Oono, Y, Kawahara, Y, Kanamori, H, Mizuno, H, Yamagata, H, Yamamoto, M, Hosokawa, S, Ikawa, H, Akahane, I, Zhu, Z, Wu, J, Itoh, T, & Matsumoto, T. 2011. mRNA-Seq Reveals a Comprehensive Transcriptome Profile of Rice under Phosphate Stress. *Rice*, **4**(2), 50–65.

Oono, Y, Kobayashi, F, Kawahara, Y, Yazawa, T, Handa, H, Itoh, T, & Matsumoto, T. 2013a. Characterisation of the wheat (Triticum aestivum L.) transcriptome by de novo assembly for the discovery of phosphate starvation-responsive genes: gene expression in Pi-stressed wheat. *BMC Genomics*, **14**, 77.

Oono, Y, Kawahara, Y, Yazawa, T, Kanamori, H, Kuramata, M, Yamagata, H, Hosokawa, S, Minami, H, Ishikawa, S, Wu, J, Antonio, B, Handa, H, Itoh, T, & Matsumoto, T. 2013b. Diversity in the complexity of phosphate starvation transcriptomes among rice cultivars based on RNA-Seq profiles. *Plant Mol Biol*, **83**(6), 523–537.

Overvoorde, P, Fukaki, H, & Beeckman, T. 2010. Auxin control of root development. *Cold Spring Harb Perspect Biol*, **2**(6), a001537.

Pan, Y, Bradley, G, Pyke, K, Ball, G, Lu, C, Fray, R, Marshall, A, Jayasuta, S, Baxter, C, van Wijk, R, Boyden, L, Cade, R, Chapman, N H, Fraser, P D, Hodgman, C, & Seymour, G B. 2013. Network inference analysis identifies an APRR2-like gene linked to pigment accumulation in tomato and pepper fruits. *Plant Physiol*, **161**(3), 1476–1485.

Panigrahy, M, Rao, D N, & Sarla, N. 2009. Molecular mechanisms in response to phosphate starvation in rice. *Biotechnol Adv*, **27**(4), 389–397.

Pant, B D, Buhtz, A, Kehr, J, & Scheible, W R. 2008. MicroRNA399 is a long-distance signal for the regulation of plant phosphate homeostasis. *Plant J*, **53**(5), 731–738.

Pant, B D, Pant, P, Erban, A, Huhman, D, Kopka, J, & Scheible, W R. 2015. Identification of primary and secondary metabolites with phosphorus status-dependent abundance in Arabidopsis, and of the transcription factor PHR1 as a major regulator of metabolic changes during phosphorus limitation. *Plant Cell Environ*, **38**(1), 172–187.

Paszkowski, Uta, & Gutjahr, Caroline. 2013. Multiple control levels of root system remodeling in arbuscular mycorrhizal symbiosis. *Frontiers in Plant Science*, **4**(204), 1–8.

Payne, R J, & Grierson, C S. 2009. A Theoretical Model for ROP Localisation by Auxin in Arabidopsis Root Hair Cells. *Plos One*, **4**(12), e8337.

Payvandi, S, Daly, K R, Jones, D L, Talboys, P, Zygalakis, K C, & Roose, T. 2014. A mathematical model of water and nutrient transport in xylem vessels of a wheat plant. *Bull Math Biol*, **76**(3), 566–596.

Péret, B, Clément, M, Nussaume, L, Desnos, T, Peret, B, Clement, M, Nussaume, L, & Desnos, T. 2011. Root developmental adaptation to phosphate starvation: better safe than sorry. *Trends Plant Sci*, **16**(8), 442–450.

Péret, B, Li, G, Zhao, J, Band, L R, Voß, U, Postaire, O, Luu, D T, Da Ines, O, Casimiro, I, Lucas, M, Wells, D M, Lazzerini, L, Nacry, P, King, J R, Jensen, O E, Schäffner, A R, Maurel, C, & Bennett, M J. 2012. Auxin regulates aquaporin function to facilitate lateral root emergence. *Nat Cell Biol*, **14**(10), 991–998.

Péret, B, Middleton, A M, French, A P, Larrieu, A, Bishopp, A, Njo, M, Wells, D M, Porco, S, Mellor, N, Band, L R, Casimiro, I, Kleine-Vehn, J, Vanneste, S, Sairanen,

I, Mallet, R, Sandberg, G, Ljung, K, Beeckman, T, Benkova, E, Friml, J, Kramer, E, King, J R, De Smet, I, Pridmore, T, Owen, M, & Bennett, M J. 2013. Sequential induction of auxin efflux and influx carriers regulates lateral root emergence. *Mol Syst Biol*, **9**, 699.

Péret, Benjamin, Larrieu, Antoine, & Bennett, Malcolm J. 2009. Lateral root emergence: a difficult birth. *J Exp Bot*, **60**(13), 3637–3643.

Perez-Torres, CA, Lopez-Bucio, J, & Herrera-Estrella, L. 2009. Low phosphate signaling induces changes in cell cycle gene expression by increasing auxin sensitivity in the Arabidopsis root system. *Plant Signal Behav*, **4**(8), 781–783.

Pierre, W H, & Parker, F W. 1927. Soil phosphorus studies II. The concentration of organics and inorganic phosphorus in the soil solution and soil extracts and the availability of organic phosphorus to plants. *Soil Science*, **24**(2), 119–128.

Pitt-Francis, J, Bernabeu, M O, Cooper, J, Garny, A, Momtahan, L, Osborne, J, Pathmanathan, P, Rodriguez, B, Whiteley, J P, & Gavaghan, D J. 2008. Chaste: using agile programming techniques to develop computational biology software. *Philos Trans A Math Phys Eng Sci*, **366**(1878), 3111–3136.

Plaxton, W C, & Shane, M W. 2015. The Role of Post-Translational Enzyme Modifications in the Metabolic Adaptations of Phosphorus-Deprived Plants. *Pages 99–123 of: Annual Plant Reviews Volume 48*. John Wiley & Sons, Inc.

Plaxton, W C, & Tran, H T. 2011. Metabolic adaptations of phosphate-starved plants. *Plant Physiol*, **156**(3), 1006–1015.

Plaxton, William C, & Carswell, M Christian. 1999. Metabolic aspects of the phosphate starvation response in plants. *Pages 349–372 of: Plant responses to environmental stresses: from phytohormones to genome reorganization*. Marcel Dekker, New York.

Poirier, Y, & Bucher, M. 2002. Phosphate transport and homeostasis in Arabidopsis. *Arabidopsis Book*, **1**, e0024.

Poirier, Y, & Jung, J. 2015. Phosphate Transporters. *Pages 125–158 of: Annual Plant Reviews Volume 48*. John Wiley & Sons, Inc.

Postma, J A, & Lynch, J P. 2011a. Root Cortical Aerenchyma Enhances the Growth of Maize on Soils with Suboptimal Availability of Nitrogen, Phosphorus, and Potassium. *Plant Physiology*, **156**(3), 1190–1201.

Postma, J A, & Lynch, J P. 2011b. Theoretical evidence for the functional benefit of root cortical aerenchyma in soils with low phosphorus availability. *Ann Bot*, **107**(5), 829–841.

Pound, M P, French, A P, Wells, D M, Bennett, M J, & Pridmore, T P. 2012. CellSeT: novel software to extract and analyze structured networks of plant cells from confocal images. *Plant Cell*, **24**(4), 1353–1361.

Pradal, C, Dufour-Kowalski, S, Boudon, F, Fournier, C, & Godin, C. 2008. OpenAlea: a visual programming and component-based software platform for plant modelling. *Functional Plant Biology*, **35**(10), 751–760.

Pratt, J, Boisson, A M, Gout, E, Bligny, R, Douce, R, & Aubert, S. 2009. Phosphate (Pi) starvation effect on the cytosolic Pi concentration and Pi exchanges across the tonoplast in plant cells: an in vivo 31P-nuclear magnetic resonance study using methylphosphonate as a Pi analog. *Plant Physiol*, **151**(3), 1646–1657.

Ptashnyk, M, Roose, T, Jones, D L, & Kirk, G J. 2011. Enhanced zinc uptake by rice through phytosiderophore secretion: a modelling study. *Plant Cell Environ*, **34**(12), 2038–2046.

Raboy, V. 2009. Approaches and challenges to engineering seed phytate and total phosphorus. *Plant Science*, **177**(4), 281–296.

Raghothama, K G. 1999. Phosphate Acquisition. *Annu Rev Plant Physiol Plant Mol Biol*, **50**, 665–693.

Raghothama, K G, & Karthikeyan, A S. 2005. Phosphate acquisition. *Pages 37–49 of:* Lambers, Hans, & Colmer, TimothyD (eds), *Root Physiology: from Gene to Function*. Plant Ecophysiology, vol. 4. Springer Netherlands.

Ramaekers, L, Remans, R, Rao, I M, Blair, M W, & Vanderleyden, J. 2010. Strategies for improving phosphorus acquisition efficiency of crop plants. *Field Crops Research*, **117**(2-3), 169–176.

Ranathunge, K, Steudle, E, & Lafitte, R. 2003. Control of water uptake by rice (Oryza sativa L.) - role of the outer part of the root. **217**(2), 193–205.

Rausch, C, & Bucher, M. 2002. Molecular mechanisms of phosphate transport in plants. *Planta*, **216**(1), 23–37.

Raven, J A. 2015. Interactions between Nitrogen and Phosphorus metabolism. *Pages 187–214 of: Annual Plant Reviews Volume 48*. John Wiley & Sons, Inc.

Ray, D K, Ramankutty, N, Mueller, N D, West, P C, & Foley, J A. 2012. Recent patterns of crop yield growth and stagnation. *Nat Commun*, **3**, 1293.

Ray, D K, Mueller, N D, West, Paul C, & Foley, J A. 2013. Yield Trends Are Insufficient to Double Global Crop Production by 2050. *PLoS ONE*, **8**(6), e66428.

Reynolds, M P, Pask, A J, & Mullan, D M. 2012. *Physiological breeding I: interdisciplinary approaches to improve crop adaptation*. Mexico, D.F., Mexico: CIMMYT, ISBN 978-970-648-181-8, 188pp.

Ribot, C, Wang, Y, & Poirier, Y. 2008. Expression analyses of three members of the AtPHO1 family reveal differential interactions between signaling pathways involved in phosphate deficiency and the responses to auxin, cytokinin, and abscisic acid. *Planta*, **227**(5), 1025–1036.

Richardson, A. 2009. Regulating the phosphorus nutrition of plants: molecular biology meeting agronomic needs. *Plant and Soil*, **322**(1), 17–24.

Richardson, A E, Lynch, J P, Ryan, P R, Delhaize, E, Smith, F Andrew, Smith, S E, Harvey, P R, Ryan, M H, Veneklaas, E J, Lambers, H, Oberson, A, Culvenor, R A, & Simpson, R J. 2011. Plant and microbial strategies to improve the phosphorus efficiency of agriculture. *Plant and Soil*, **349**(1-2), 121–156.

Robinson, W D, Park, J, Tran, H T, Del Vecchio, H A, Ying, S, Zins, J L, Patel, K, McKnight, T D, & Plaxton, W C. 2012. The secreted purple acid phosphatase isozymes AtPAP12 and AtPAP26 play a pivotal role in extracellular phosphate-scavenging by Arabidopsis thaliana. *J Exp Bot*, **63**(18), 6531–6542.

Rojas-Triana, M, Bustos, R, Espinosa-Ruiz, A, Prat, S, Paz-Ares, J, & Rubio, V. 2013. Roles of ubiquitination in the control of phosphate starvation responses in plants. *J Integr Plant Biol*, **55**(1), 40–53.

Roose, T, & Fowler, A C. 2004. A mathematical model for water and nutrient uptake by plant root systems. *J Theor Biol*, **228**(2), 173–184.

Rose, T J, Liu, L, & Wissuwa, M. 2013. Improving phosphorus efficiency in cereal crops: Is breeding for reduced grain phosphorus concentration part of the solution? *Front Plant Sci*, **4**, 444.

Rubio, V, Linhares, F, Solano, R, Martin, A C, Iglesias, J, Leyva, A, & Paz-Ares, J. 2001. A conserved MYB transcription factor involved in phosphate starvation signaling both in vascular plants and in unicellular algae. *Genes Dev*, **15**(16), 2122–2133.

Rubio, V, Bustos, R, Irigoyen, M L, Cardona-Lopez, X, Rojas-Triana, M, & Paz-Ares, J. 2009. Plant hormones and nutrient signaling. *Plant Mol Biol*, **69**(4), 361–373.

Rudge, T, & Haseloff, J. 2005. A Computational Model of Cellular Morphogenesis in Plants. *Pages 78–87 of:* CapcarrÃšre, MathieuS., Freitas, AlexA., Bentley, PeterJ., Johnson, ColinG., & Timmis, Jon (eds), *Advances in Artificial Life*. Lecture Notes in Computer Science, vol. 3630. Springer Berlin Heidelberg.

Rudge, T J, Steiner, P J, Phillips, A, & Haseloff, J. 2012. Computational modeling of synthetic microbial biofilms. *ACS Synth Biol*, **1**(8), 345–352.

Rudge, T J, Federici, F, Steiner, P J, K, Anton, & Haseloff, J. 2013. Cell polarity-driven instability generates self-organized, fractal patterning of cell layers. *ACS Synth Biol*, **2**(12), 705–714.

Rychter, A M, & Randall, D D. 1994. The effect of phosphate deficiency on carbohydrate metabolism in bean roots. *Physiologia Plantarum*, **91**(3), 383–388.

Saengwilai, P, Nord, E A, Chimungu, J G, Brown, K M, & Lynch, J P. 2014. Root Cortical Aerenchyma Enhances Nitrogen Acquisition from Low-Nitrogen Soils in Maize. *Plant Physiology*, **166**(2), 726–735.

Sager, R, & Lee, J. 2014. Plasmodesmata in integrated cell signalling: Insights from development and environmental signals and stresses. *Journal of Experimental Botany*.

Salt, D E. 2004. Update on plant ionomics. *Plant Physiol*, **136**(1), 2451–2456.

Salt, D E, Baxter, I, & Lahner, B. 2008. Ionomics and the study of the plant ionome. *Annu Rev Plant Biol*, **59**, 709–733.

Sánchez-Calderón, L, & et Al. 2011. Sensing and Signaling of PO4-3. *Pages 191–224 of:* Geisler, Markus, & Venema, Kees (eds), *Transporters and Pumps in Plant Signaling, Signaling and Communications in Plants 7*. Signaling and Communication in Plants, vol. 7. Springer Berlin Heidelberg.

Sánchez-Calderón, L, López-Bucio, J, Chacón-López, A, Cruz-Ramírez, A, Nieto-Jacobo, F, Dubrovsky, J G, & Herrera-Estrella, L. 2005. Phosphate starvation induces a determinate developmental program in the roots of Arabidopsis thaliana. *Plant Cell Physiol*, **46**(1), 174–184.

Schachtman, D P, Reid, R J, & Ayling, S M. 1998. Phosphorus Uptake by Plants: From Soil to Cell. *Plant Physiology*, **116**(2), 447–453.

Scheible, W, & Rojas-Triana, M. 2015. Sensing, signalling, and control of phosphate starvation in plants: molecular players and applications. *Pages 23–63 of: Annual Plant Reviews Volume 48*. John Wiley & Sons, Inc.

Schiefelbein, J W, & Somerville, C. 1990. Genetic Control of Root Hair Development in Arabidopsis thaliana. *Plant Cell*, **2**(3), 235–243.

Schlüter, U, Colmsee, C, Scholz, U, Bräutigam, A, Weber, A P, Zellerhoff, N, Bucher, M, Fahnenstich, H, & Sonnewald, U. 2013. Adaptation of maize source leaf metabolism to stress related disturbances in carbon, nitrogen and phosphorus balance. *BMC Genomics*, **14**, 442.

Schnepf, A, & Roose, T. 2006. Modelling the contribution of arbuscular mycorrhizal fungi to plant phosphate uptake. *New Phytol*, **171**(3), 669–682.

Schnepf, A, Roose, T, & Schweiger, P. 2008. Impact of growth and uptake patterns of arbuscular mycorrhizal fungi on plant phosphorus uptake- a modelling study. *Plant and Soil*, **312**(1-2), 85–99.

Schnepf, A, Jones, D, & Roose, T. 2011. Modelling nutrient uptake by individual hyphae of arbuscular mycorrhizal fungi: temporal and spatial scales for an experimental design. *Bull Math Biol*, **73**(9), 2175–2200.

Secco, D, Baumann, A, & Poirier, Y. 2010. Characterization of the rice PHO1 gene family reveals a key role for OsPHO1;2 in phosphate homeostasis and the evolution of a distinct clade in dicotyledons. *Plant Physiol*, **152**(3), 1693–1704.

Secco, D, Wang, C, Shou, H, & Whelan, J. 2012a. Phosphate homeostasis in the yeast Saccharomyces cerevisiae, the key role of the SPX domain-containing proteins. *FEBS Lett*, **586**(4), 289–295.

Secco, D, Jabnoune, M, Walker, H, Shou, H X, Wu, P, Poirier, Y, & Whelan, J. 2013. Spatio-Temporal Transcript Profiling of Rice Roots and Shoots in Response to Phosphate Starvation and Recovery. *Plant Cell*, **25**(11), 4285–4304.

Secco, David, Wang, Chuang, Arpat, Bulak A, Wang, Zhiye, Poirier, Yves, Tyerman, Stephen D, Wu, Ping, Shou, Huixia, & Whelan, James. 2012b. The emerging importance of the SPX domain-containing proteins in phosphate homeostasis. *New Phytol*, **193**(4), 842–851.

Selim, H M. 2015. Influence of Phosphates on Retention and Mobility of Zinc, Cadmium, and Vanadium in Soils. *Pages 97–122 of: Phosphate in Soils*. Advances in Trace Elements in the Environment. CRC Press.

Shen, J, Yuan, L, Zhang, J, Li, H, Bai, Z, Chen, X, Zhang, W, & Zhang, F. 2011. Phosphorus dynamics: from soil to plant. *Plant Physiol*, **156**(3), 997–1005.

Shin, Heungsop Hwa-Soo S, Shin, Heungsop Hwa-Soo S, Chen, Rujin, & Harrison, Maria J. 2006. Loss of At4 function impacts phosphate distribution between the roots and the shoots during phosphate starvation. *Plant J*, **45**(5), 712–726.

Shin, R, Berg, R H, & Schachtman, D P. 2005. Reactive oxygen species and root hairs in Arabidopsis root response to nitrogen, phosphorus and potassium deficiency. *Plant Cell Physiol*, **46**(8), 1350–1357.

Silberbush, M, & Barber, S A. 1983. Sensitivity of simulated phosphorus uptake to parameters used by a mechanistic-mathematical model. *Plant and Soil*, **74**(1), 93–100.

Smith, F W. 2002. The phosphate uptake mechanism. *Plant and Soil*, **245**(1), 105–114.

Smith, F W, Mudge, S R, Rae, A L, & Glassop, D. 2003. Phosphate transport in plants. *Plant and Soil*, **248**(1), 71–83.

Smith, S E, Jakobsen, I, Grønlund, M, & Smith, F A. 2011. Roles of arbuscular mycorrhizas in plant phosphorus nutrition: interactions between pathways of phosphorus uptake in arbuscular mycorrhizal roots have important implications for understanding and manipulating plant phosphorus acquisition. *Plant Physiol*, **156**(3), 1050–1057.

Solfanelli, C, Poggi, A, Loreti, E, Alpi, A, & Perata, P. 2006. Sucrose-specific induction of the anthocyanin biosynthetic pathway in Arabidopsis. *Plant Physiol*, **140**(2), 637–646.

Spassov, Danislav S, & Jurecic, Roland. 2003. The PUF family of RNA-binding proteins: does evolutionarily conserved structure equal conserved function? *IUBMB Life*, **55**(7), 359–366.

Stevenson-Paulik, Jill, Bastidas, Robert J., Chiou, Shean-Tai, Frye, Roy A., & York, John D. 2005. Generation of phytate-free seeds in Arabidopsis through disruption of inositol polyphosphate kinases. *Proceedings of the National Academy of Sciences of the United States of America*, **102**(35), 12612–12617.

Stoma, S, Lucas, M, Chopard, J, Schaedel, M, Traas, J, & Godin, C. 2008. Flux-based transport enhancement as a plausible unifying mechanism for auxin transport in meristem development. *PLoS Comput Biol*, **4**(10), e1000207.

Svistoonoff, S, Creff, A, Reymond, M, Sigoillot-Claude, C, Ricaud, L, Blanchet, A, Nussaume, L, & Desnos, T. 2007. Root tip contact with low-phosphate media reprograms plant root architecture. *Nat Genet*, **39**(6), 792–796.

Syers, J K, Johnston, E, & Curtin, D. 2008. Efficiency of soil and fertilizer phosphorus use: Reconciling changing concepts of soil phosphorus behaviour with agronomic information. FAO fertilizer and plant nutrition bulletin, vol. 18. FAO, Rome, Italy.

Tan, X, Calderon-Villalobos, L A, Sharon, M, Zheng, C, Robinson, C V, Estelle, M, & Zheng, N. 2007. Mechanism of auxin perception by the TIR1 ubiquitin ligase. *Nature*, **446**(7136), 640–645.

Tardieu, F. 2010. Why work and discuss the basic principles of plant modelling 50 years after the first plant models? *Journal of Experimental Botany*, **61**(8), 2039–2041.

Taylor-Teeples, M, Lin, L, de Lucas, M, Turco, G, Toal, T W, Gaudinier, A, Young, N F, Trabucco, G M, Veling, M T, Lamothe, R, Handakumbura, P P, Xiong, G, Wang, C, Corwin, J, Tsoukalas, A, Zhang, L, Ware, D, Pauly, M, Kliebenstein, D J, Dehesh, K, Tagkopoulos, I, Breton, G, Pruneda-Paz, J L, Ahnert, S E, Kay, S A, Hazen, S P, & Brady, S M. 2015. An Arabidopsis Gene Regulatory Network for Secondary Cell Wall Synthesis. *Nature*, **517**(7536), 571–575.

Thornley, J H. 1976. *Mathematical Models in Plant Physiology: A Quantitative Approach to Problems in Plant and Crop Physiology.* Academic Press, ISBN: 9780126905502.

Tian, J, Wang, X, Tong, Y, Chen, X, & Liao, H. 2012. Bioengineering and management for efficient phosphorus utilization in crops and pastures. *Current Opinion in Biotechnology*, **3**(6), 866–871.

Ticconi, C A, & Abel, S. 2004. Short on phosphate: plant surveillance and countermeasures. *Trends Plant Sci*, **9**(11), 548–555.

Ticconi, C A, Lucero, R D, Sakhonwasee, S, Adamson, A W, Creff, A, Nussaume, L, Desnos, T, & Abel, S. 2009. ER-resident proteins PDR2 and LPR1 mediate the developmental response of root meristems to phosphate availability. *Proc Natl Acad Sci U S A*, **106**(33), 14174–14179.

Tinker, P B, & Nye, P. 2000. *Solute Movement in the Rhizosphere*. Oxford University Press. 370pp. ISBN 0-19-512492-8.

Tomscha, J L, Trull, M C, Deikman, J, Lynch, J P, & Guiltinan, M J. 2004. Phosphatase under-producer mutants have altered phosphorus relations. *Plant Physiol*, **135**(1), 334–345.

Tonelli, C, & Inze, D. 2009. *Crop Productivity for Food - from models to crops*. Tech. rept. European Plant Science Organisation, Brussels - Belgium http://www.epsoweb.org/workshop-plant-productivity-food-1.

Tran, H T, Qian, W, Hurley, B A, She, Y M, Wang, D, & Plaxton, W C. 2010. Biochemical and molecular characterization of AtPAP12 and AtPAP26: the predominant purple acid phosphatase isozymes secreted by phosphate-starved Arabidopsis thaliana. *Plant Cell Environ*, **33**(11), 1789–1803.

Trull, M C, Guiltinan, M J, Lynch, J P, & Deikman, J. 1997. The responses of wild-type and ABA mutant Arabidopsis thaliana plants to phosphorus starvation. *Plant, Cell & Environment*, **20**(1), 85–92.

Tyburski, J, Dunajska, K, & Tretyn, A. 2009. Reactive oxygen species localization in roots of Arabidopsis thaliana seedlings grown under phosphate deficiency. *Plant Growth Regulation*, **59**(1), 27–36.

Umehara, M, Hanada, A, Magome, H, Takeda-Kamiya, N, & Yamaguchi, S. 2010. Contribution of strigolactones to the inhibition of tiller bud outgrowth under phosphate deficiency in rice. *Plant Cell Physiol*, **51**(7), 1118–1126.

Vadez, V. 2014. Root hydraulics: The forgotten side of roots in drought adaptation. *Field Crops Research*, **165**(Aug.), 15–24.

van Belkum, A, Abrahams, J P, Pleij, C W, & Bosch, L. 1985. Five pseudoknots are present at the 204 nucleotides long 3' noncoding region of tobacco mosaic virus RNA. *Nucleic Acids Res*, **13**(21), 7673–7686.

van der Weele, C M, Canny, M J, & McCully, M E. 1996a. Water in aerenchyma spaces in roots. A fast diffusion path for solutes. *Plant and Soil*, **184**(1), 131–141.

van der Weele, C.M., Canny, M.J., & McCully, M.E. 1996b. Water in aerenchyma spaces in roots. A fast diffusion path for solutes. **184**(1), 131–141.

Vance, C P. 2010. Quantitative trait loci, epigenetics, sugars, and microRNAs: quaternaries in phosphate acquisition and use. *Plant Physiol*, **154**(2), 582–588.

Varkonyi-Gasic, E, Rongmei, W, Marion, W, Walton, E F, & Hellens, R P. 2007. Protocol: a highly sensitive RT-PCR method for detection and quantification of microRNAs. *Plant Methods*, **3**, 12.

Veljanovski, V, Vanderbeld, B, Knowles, V L, Snedden, W A, & Plaxton, W C. 2006. Biochemical and molecular characterization of AtPAP26, a vacuolar purple acid phosphatase up-regulated in phosphate-deprived Arabidopsis suspension cells and seedlings. *Plant Physiol*, **142**(3), 1282–1293.

Veneklaas, E J, Lambers, H, Bragg, J, Finnegan, P M, Lovelock, C E, Plaxton, W C, Price, C A, Scheible, W R, Shane, M W, White, P J, & Raven, J A. 2012. Opportunities for improving phosphorus-use efficiency in crop plants. *New Phytol*, **195**(2), 306–320.

Versaw, W K, & Harrison, M J. 2002. A chloroplast phosphate transporter, PHT2;1, influences allocation of phosphate within the plant and phosphate-starvation responses. *Plant Cell*, **14**(8), 1751–1766.

Wan, Y, Kertesz, M, Spitale, R C, Segal, E, & Chang, H Y. 2011. Understanding the transcriptome through RNA structure. *Nat Rev Genet*, **12**(9), 641–655.

Wang, C, Ying, S, Huang, H, Li, K, Wu, P, & Shou, H. 2009a. Involvement of OsSPX1 in phosphate homeostasis in rice. *Plant J*, **57**(5), 895–904.

Wang, Z, Hu, H, Huang, H, Duan, K, Wu, Z, & Wu, P. 2009b. Regulation of OsSPX1 and OsSPX3 on expression of OsSPX domain genes and Pi-starvation signaling in rice. *J Integr Plant Biol*, **51**(7), 663–674.

Weliky, M., & Oster, G. 1990. The mechanical basis of cell rearrangement. I. Epithelial morphogenesis during Fundulus epiboly. *Development*, **109**(2), 373–386.

White, P J. 2012. Chapter 3 - Long-distance Transport in the Xylem and Phloem. *Pages 49 – 70 of:* Marschner, Petra (ed), *Marschner's Mineral Nutrition of Higher Plants (Third Edition)*, third edition edn. San Diego: Academic Press.

Williamson, L C, Ribrioux, S P, Fitter, A H, & Leyser, H M. 2001. Phosphate availability regulates root system architecture in Arabidopsis. *Plant Physiol*, **126**(2), 875–882.

Wissuwa, M. 2003. How do plants achieve tolerance to phosphorus deficiency? Small causes with big effects. *Plant Physiol*, **133**(4), 1947–1958.

Wissuwa, M, Wegner, J, Ae, N, & Yano, M. 2002. Substitution mapping of Pup1: a major QTL increasing phosphorus uptake of rice from a phosphorus-deficient soil. *Theor Appl Genet*, **105**(6-7), 890–897.

Withers, P J, van Dijk, K C, Neset, T S, Nesme, T, Oenema, O, Rubæk, G H, Schoumans, O F, Smit, B, & Pellerin, S. 2015. Stewardship to tackle global phosphorus inefficiency: The case of Europe. *Ambio*, **44**(2), 193–206.

Wolf, Ann M, & Baker, D E. 1985. Comparisons of soil test phosphorus by Olsen, Bray P1, Mehlich I and Mehlich III methods. *Communications in Soil Science and Plant Analysis*, **16**(5), 467–484.

Wu, S, & Gallagher, K L. 2013. Intact microtubules are required for the intercellular movement of the SHORT-ROOT transcription factor. *Plant J*, **74**(1), 148–159.

Yi, K, Wu, Z, Zhou, J, Du, L, Guo, L, Wu, Y, & Wu, P. 2005. OsPTF1, a novel transcription factor involved in tolerance to phosphate starvation in rice. *Plant Physiol*, **138**(4), 2087–2096.

York, L M, Galindo-Castañeda, T, Schussler, J R, & Lynch, J P. 2015. Evolution of US maize (Zea mays L.) root architectural and anatomical phenes over the past 100 years corresponds to increased tolerance of nitrogen stress. *Journal of Experimental Botany*, **66**(8), 2347–2358.

Yoshida, S, Forno, D, Cock, J, & Gomez, K. 1976. *Laboratory Manual for Physiological Studies of Rice*. 3rd edn. The International Rice Research Institute (IRRI), Manila, The Philippines.

Yuan, H, & Liu, D. 2008. Signaling components involved in plant responses to phosphate starvation. *J Integr Plant Biol*, **50**(7), 849–859.

Zamore, P D, Williamson, J R, & Lehmann, R. 1997. The Pumilio protein binds RNA through a conserved domain that defines a new class of RNA-binding proteins. *RNA*, **3**(12), 1421–1433.

Zhang, Q, Wang, C, Tian, J, Li, K, & Shou, H. 2011. Identification of rice purple acid phosphatases related to phosphate starvation signalling. *Plant Biol (Stuttg)*, **13**(1), 7–15.

Zhang, Z, Liao, H, & Lucas, W J. 2014. Molecular mechanisms underlying phosphate sensing, signaling and adaptation in plants. *J Integr Plant Biol*, **56**(3), 192–220.

Zhou, J, Jiao, F, Wu, Z, Li, Y, Wang, X, He, X, Zhong, W, & Wu, P. 2008. OsPHR2 is involved in phosphate-starvation signaling and excessive phosphate accumulation in shoots of plants. *Plant Physiol*, **146**(4), 1673–1686.

Zhu, W, Miao, Q, Sun, D, Yang, G, Wu, C, Huang, J, & Zheng, C. 2012. The mitochondrial phosphate transporters modulate plant responses to salt stress via affecting ATP and gibberellin metabolism in Arabidopsis thaliana. *PLoS ONE*, **7**(8), e43530.

Zi, Z, Zheng, Y, Rundell, A E, & Klipp, E. 2008. SBML-SAT: a systems biology markup language (SBML) based sensitivity analysis tool. *BMC Bioinformatics*, **9**, 342.

Ziadi, N, Whalen, J K, Messiga, A J, & Morel, C. 2013. Assessment and modeling of soil available phosphorus in sustainable cropping systems. *Adv. Agron*, **122**, 85–126.

Zinovyev, A, Morozova, N, Gorban, A N, & Harel-Belan, A. 2013. Mathematical modeling of microRNA-mediated mechanisms of translation repression. *Adv Exp Med Biol*, **774**, 189–224.

Zygalakis, K C, & Roose, T. 2012. A mathematical model for investigating the effect of cluster roots on plant nutrient uptake. *The European Physical Journal Special Topics*, **204**(1), 103–118.

Zygalakis, K C, Kirk, G J, Jones, D L, Wissuwa, M, & Roose, T. 2011. A dual porosity model of nutrient uptake by root hairs. *New Phytol*, **192**(3), 676–688.

Appendix A

Uptake of different elements by normal and phosphate starved plants

Introduction

The objective of this pilot study is to quantify the uptake rates of different elements and their levels in the plant tissues at different times under normal and deficient Pi conditions. This novel approach allows non-destructive quantification, which is an advantage over destructive methods that require more plants and suffer large variability. Such an approach has not previously been reported in the literature (David Salt, personal communication). In conjunction with themes of this thesis, this time-series dataset can be used to develop mathematical models of nutrient uptake in growing plants. Thus, this experimental work could form the basis of another modelling study in future. Indeed, this pilot work act as a proof-of-concept for the approach an from the basis of a full-scale experiment.

Materials and Methods

Plant materials and growth conditions

Rice (*Oryza sativa* cv Nipponbare) was used in this study. Prior to germination, rice seeds were washed and surface sterilised by washing them in 70% ethanol, followed by rinsing with distilled water then soaking for 30 minutes in 2% hypochlorite solution and finally, rinsing thrice with distilled water. These seeds were germinated on moist

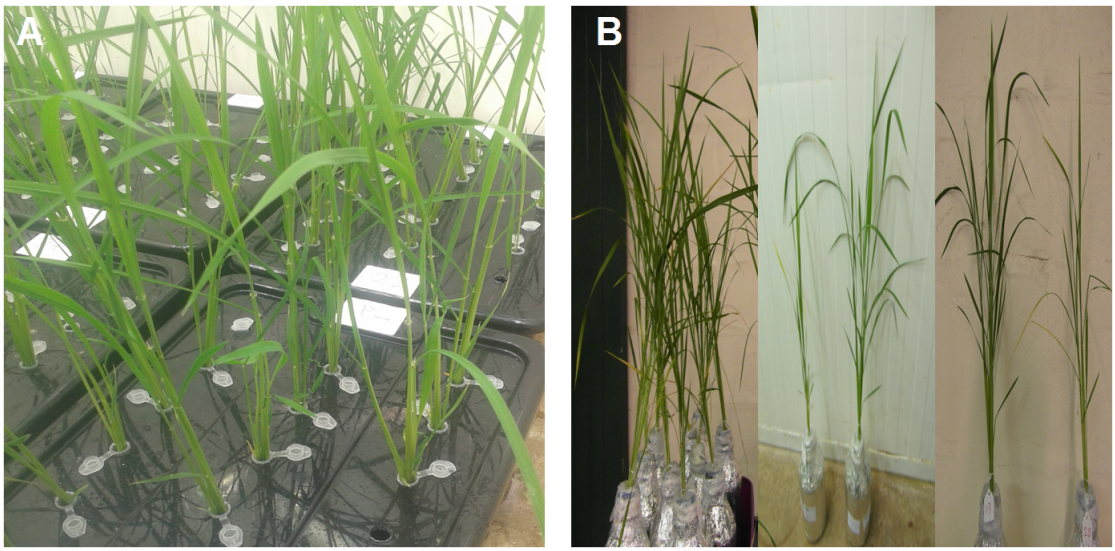

Figure A.1: Images of rice plant grown in boxes and bottles

Whatman filter paper on petri dishes for 5 days, intially for three days without light and temperature $30°C$ followed by two days in light conditions ($12\,h$ photoperiod) at $20°C$. On the sixth day, the seedlings were transferred into boxes containing the hydroponic solution and grown under controlled conditions (day/night temperature of $24°C$ and a $12\,h$ photoperiod, 200 $\mu moles$ photons $m^{-2}s^{-1}$), allowing 0.5 liters of hydroponic solution per plant (i.e 17 seedling per 9L box).

The hydroponic solution consisted of a modified solution as described by Yoshida et al. (1976), containing $1.425\,mM\ NH_4NO_3$, $0.513\,mM\ K_2SO_4$, $0.998\,mM\ CaCl_2$, $1.643\,mM MgSO_4$, $0.075\,\mu M\ (NH_4)_6Mo_7O_{24}$, $0.25\,mM\ NaSiO_3$, $0.009\,mM\ MnCl_2$, $0.019\,\mu M\ H_3BO_3$, $0.155\,\mu M\ CuSO_4$, $0.152\,\mu M\ ZnSO_4$, and $0.125\,mM\ Na-EDTA-Fe$, with $320\,\mu M$ either NaH_2PO_4 or $NaCl$, resulting in the +Pi and −Pi conditions. The pH of the solution was adjusted to 5.5 (with HCl) and the solution was renewed every 3 days throughout the experiment irrespective of the treatments.

Initially, plants were grown for two week in the boxes under the normal conditions. On day15 (referred to as day 0 of treatment), nine of these plants were transferred to the solution box lacking Pi for 21 days, while the equal number of plants continuously remained in the box with Pi-sufficient solution (control), FigureA.1 A. Besides these, ten plants were transferred to the individual hydroponic bottles, allowing ~1-1.2 liter of solution per plant, again for 21 days, FigureA.1 B. One half of these bottles contained Pi-deficient solution (treatment) while remaining half served as a control with Pi-sufficient media. To avoid any evaporation , the opening of the bottles holding the plants were securely sealed using paraffin tapes.

Figure A.2: Effect of P stress on rice roots and leaves

Hydroponic and plant sampling

On day 0 of treatment, an aliquot (~ 50ml) of the fresh hydroponic solution (form the storage tanks) was stored and also the weight of each bottle (excluding the plant) with freshly-prepared hydroponic solution were recorded. After three days, the bottles without their plants were weighed again and further ~50ml aliquot of the respective hydroponic solution were taken. Fresh solution was added to each bottle and their weights were recorded. This weighing and sampling procedure was repeated at intervals of 3 day for the 21 days. The differences in weight , primarily, reflect the amount of solution taken up by the plants over the three day period.

Tissue (i.e. roots and leaves) samples were taken on days 0 and 21 of treatment. The sampling was performed as follows: whole plants were taken out from the hydroponic system, briefly dried using blotting paper, roots and leaves were separated and freezed in liquid nitrogen. These leaf and root samples were stored at -80°C until used for the analyses. For the plants grown together in hydroponic boxes, the tissue samples were pooled together, thereby increasing the mass but reducing the overall number of samples. In this work, individual tissue samples from nine plants at a given time were evenly pooled together leading to three biological replicates. Though, for the plants grown in the bottles, the collected tissue samples (at day 21) were not pooled and the samples from each plant/ bottle were treated separately. This becomes particularly important to calculate the uptake of an element with its concentration in the tissues.

Physiological measurements

Photosynthesis

Photosynthesis measurements were taken using *Li-Cor LI-6400XT* system, which measures photosynthesis (A_{max}), transpiration rate, chlorophyll fluorescence and stomatal conductance. The measurements were conducted for both treatments with 4 replicates each. Measurements were taken before the treatment started and at the end of the treatment. To take the measurements, the flow of CO_2 was set at a constant $400\,\mu mol\,s^{-1}$ and the temperature set to $24°C$. The middle part of one leaf from the plant was placed in the system's gas exchange chamber and the program was run. The program lights a source with a $1,000\,\mu moles$ per $m^{-2}s^{-1}$intensity for 4 minutes and then turns it completely off. During this period, the system measured the CO_2 absorbed by the leaf to determine the photosynthetic activity as well as the chlorophyll fluorescence and stomatal activity. Each plant was measured twice, on different leaves. The Photosystem II (PSII) and water use efficiencies were calculated using the LiCor measurements and the formula described as follows:

$$PSII\,Efficiency = \frac{Fv'}{Fm'}$$

$$Water\,Use\,Efficiency = \frac{A_{max}}{10,000 * Transpriation\,rate}$$

SPAD

SPAD stands for "Special Products Analysis Division" for chorlophyll. The SPAD meter (*SPAD 502 Plus Chlorophyll Meter*, Spectrum Technologies) is clamped on a leaf and utilizes the 650 and 940 nm wavelengths to determine a relative chlorophyll index/ content of the plant. The instrument was clamped on a leaf and held until the meter beeped. The reading (i.e. relative chlorophyll index) appeared on the display and was recorded. The measurements were made at 3 times per plant on different areas of the leaves.

Sample preparation for elemental analyses

The different elements/ions in the samples were quantified using three analytical instrument: Inductively coupled plasma mass spectrometer (ICP-MS), anion analyser and Total Organic Carbon (TOC)/Total Nitrogen (TN) analyser. These instruments

work on the principle of mass spectrometry, anion chromatography and combustion catalytic oxidation, respectively. The first method quantifies the concentration of the 21 elements in the sample, excluding nitrogen, carbon and chlorine, while second, quantifies the concentrations of nitrate, phosphate and sulphate ions in the samples. The third method is specifically used for the quantification of total carbon and nitrogen, both organic and inorganic in the samples. The collected hydroponics and tissues samples were processed in different ways for each instrument i.e for ICP-MS and for anions and carbon/nitrogen analyser.

Hydroponic solution

For the ICP-MS, 9.6 mL of the hydroponic solution sample was mixed with 0.4 mL of 50% (v/v) Nitric Acid (HNO_3), for anion chromatography 1.5 ml of hydroponic samples were directly used, while for TOC/TN analyser the hydroponic samples were diluted (1:10) with final volume of 10 ml were used.

Tissue samples

Acid Digestion for ICP-MS Half of all the tissue samples stored in liquid nitrogen were initially oven dried at 60°C for 3 days. 200 mg of the dried samples were acidified in microwave tubes by adding following : 1 ml of Milli-Q water, 2 ml of nitric acid (68%) and 1 mL of hydrogen peroxide. These acidified samples were left overnight along with two tubes of certified reference materials (Tomato leaves SRM 1573a) and two blanks (i.e. with 2ml HNO_3, 1ml Milli-Q H_2O and 1ml H_2O_2) and then irradiated in microwave (Anton Paar multiware Pro 3000, rotor : MF50) for 90 minutes to complete the digestion. 6 mL of MilliQ water were added to each sample tube, making final volumes of 10 mL. These were further diluted by mixing 0.8 ml of nitric acid (68%) with 9.2 ml of the digestant. These final diluted solutions were run on the ICP-MS instrument.

Water extraction for Anion , TOC and TON analysis

The other half of all the frozen tissue samples were ground (with mortar and pestle) and freeze dried at -70°C in a vacuum environment for 48 hours. 20mg of the freeze dried samples were mixed with 1.5 mL of deionized water containing 20 mg of insoluble polyvinyl polypyrrolidone (PVPP). The mixture was incubated at 4°C for 60 minutes on a shaker. The sample tubes were then incubated in the water bath at 90°C for 15 minutes. The sample tubes were than centrifuged at 14000 rpm at 4°C for 15 minutes

and 0.5 mL of supernatant, the water extractant, were collected into fresh tubes for the analysis.

Data analyses

The initial dataset from ICP-MS, AC and TOC/TN analyzer, were made available as the relative concentrations of element and ions in the sample. For hydroponic samples, these concentrations were adjusted for the amount of total water loss to account for differences in the concentration of the elements and ions. For the tissue samples, the elemental and ion concentrations were adjusted with the mass of the tissue used in the respective sample preparation.

Results

Plant fresh weight and length

The length and fresh weight measurements for day 0 and day 21, distinctly showed the impact of phosphate stress on the plants (Figure A.3). There is a distinct difference in the fresh weight and length of the plant at the start and end of the treatment. The same is observed for the shoots, though not for roots, Figure A.3A and D. The Pi starved plants have significantly lower shoot:root weight and shoot:root length ratio, compared to those under normal conditions, reflecting the promotion of root elongation in response to Pi deficiency, Figure A.3B and E.

The linear density (LD) (i.e. mass per unit length) of both shoot and root in significantly reduced under stress, though the LD of starved root is higher than that of its shoot, FigureA.3 C. The relative growth rate (RGR) or the.change in fresh weight (W) over the interval t_1 and $t_2$was calculated as follows:

$$RGR = \frac{(W_2 - W_1)}{(t_2 - t_1)}$$

Figure A.3F, shows that the Pi starved root and shoot have significantly lower RGR than those under normal conditions. The RGR of the whole plant under stress is ~3.6 times lower than in Pi sufficient conditions.

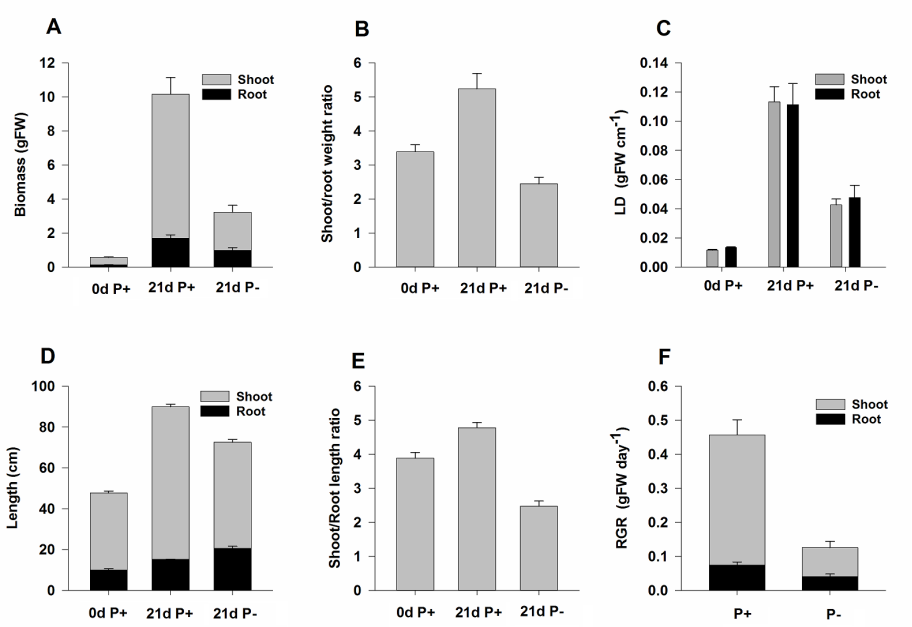

Figure A.3: Fresh weight and length of normal and Pi starved plants

Photosynthesis

The physiological measurements taken with the Li-Cor system and SPAD are shown in FigureA.4. PSII efficiency and Water Use Efficiency (WUE) were calculated from those values, to show how efficiently the plants use their resources. The former is used to describe the efficiency of PSII (main part of the chlorophyll pigment-protein compound) at performing photochemistry and the latter is the ratio of carbon uptake vs. water transpired.

Photosynthesis activity per unit leaf area (A) is significantly greater under normal conditions, Figure A.4A. As the opening of stomata and the exchange of water are tightly proportional to each other, the stomatal conductance (g) and transpiration rate (E) responses were very similar and both were significantly lowered in phosphate starved plants, Figure A.4B and C. PSII and water use efficiency were higher under normal conditions, Figure A.4F. The chlorophyll content varies very slightly throughout plant development under normal condition, but, were distinctly lower under no Pi treatment. Altogether, both phenotypic and physiological measurements, distinctly indicates the effect of P stress on the plants.

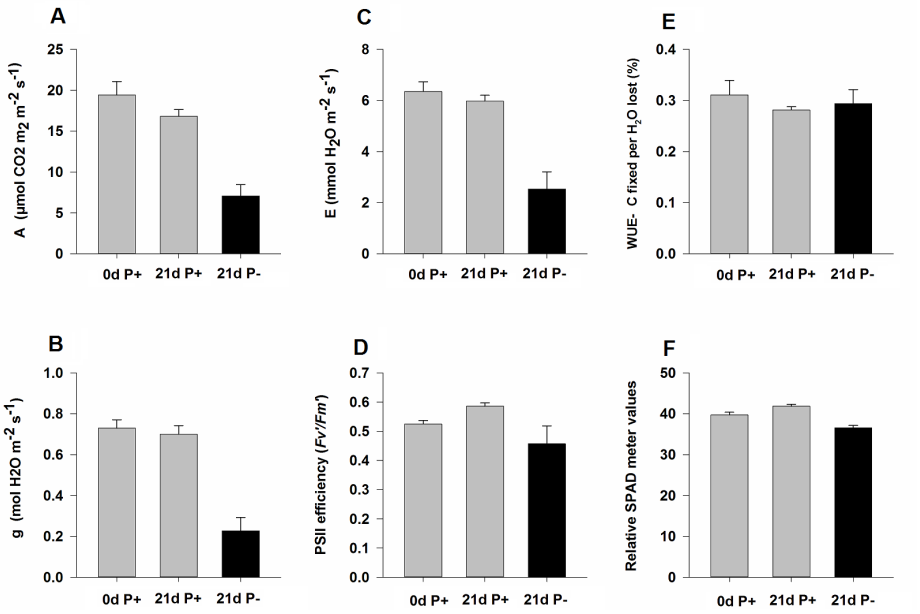

Figure A.4: Physiological measurements of normal and Pi starved plants

Rate of water uptake

The loss of water was measured by weighing the sealed bottles before (Figure A.5A) and after (Figure A.5B) renewing the solutions every third day. As the bottles were thoroughly sealed with paraffin strips there are least chances for any loss of water via evaporation. The rate of water loss or uptake by the plant was calculated by taking the difference in mass of water over the time interval (i.e. 72 hours). Figure A.5C, shows that after day 12 between the two treatments, uptake increases with time under normal conditions while remains at a steady low rate in Pi starved plants. Perhaps, the decrease in stomatal conductance is responsible for the decrease in water uptake under low phosphate conditions.

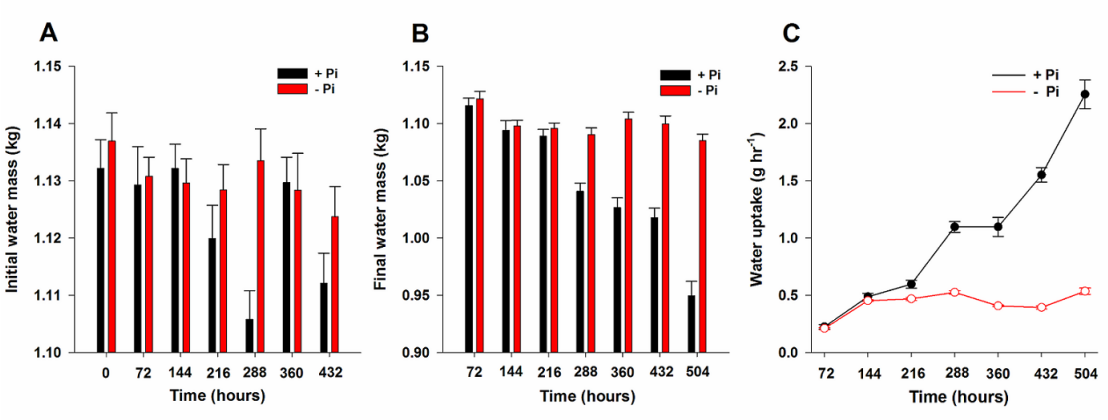

Figure A.5: Water uptake dynamics under normal and deficient Pi conditions (A): initial mass of water supplied, (B) : Final mass of water after 72 hours and (C): Rate of water uptake by normal and Pi starved rice plants.

Elemental uptake under normal and Pi deficient conditions

Uptake of macro and micro nutrient in elemental form

The uptake of N, P and K consistently increases under normal Pi condition, reflecting water uptake, Figure A.6A-C. S, Ca and Mg shows more complex oscillating profiles on day 3, 9 and possibly day 15 under normal conditions, Figure A.6D-F. The negative mass values probably correspond to no uptake rather than exudation, because the elements become more concentrated as the volume of the hydroponic solution goes down. Consistent with previous ionomic studies, Ca and Mg profiles are very similar. Potentially, the oscillation could be due to delays in the feedback signaling between the uptake and increased ion requirement. However, this needs further investigation. Under P deficient conditions, the uptake of N and K decline. For Ca and Mg, the oscillations are less extreme and out of phase up to day 12, following which it becomes almost flat. Up to day 12, the profile of S is very similar to Ca and Mg but later the uptake resembles the profile for normal P condition.

Among micro-nutrients, the uptake profile of Fe qualitative resembles Ca and Mg under both normal and stress conditions, Figure A.7A and A.6E-F. However, the profiles of Cu and Mn seems to be unaffected by the stress, indicating that their concentrations increase in the Pi stressed plants, Figure A.7B and E. The uptake of B and Mo in both treatments show a drop between day 3 and 6, but otherwise their uptake slightly increases over time, with the exception of B in Pi stressed plants at day 21, Figure A.7D and F. Zn uptake increase steadily under normal condition but

varies around this uptake under P stress, Figure A.7C.

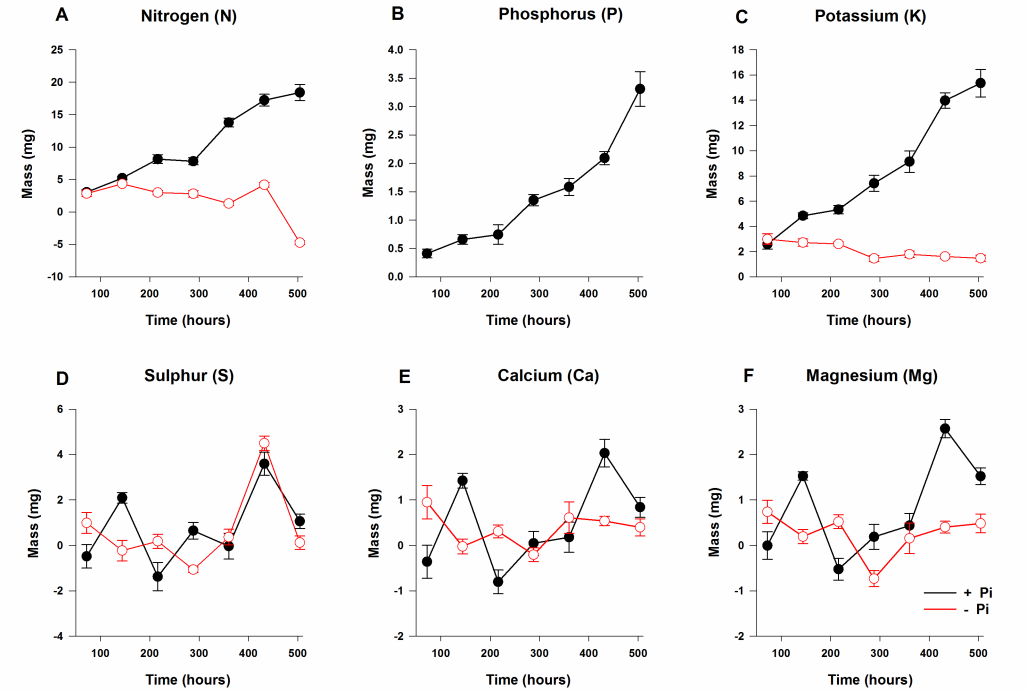

Figure A.6: Uptake of macro-elements under normal and deficient Pi conditions

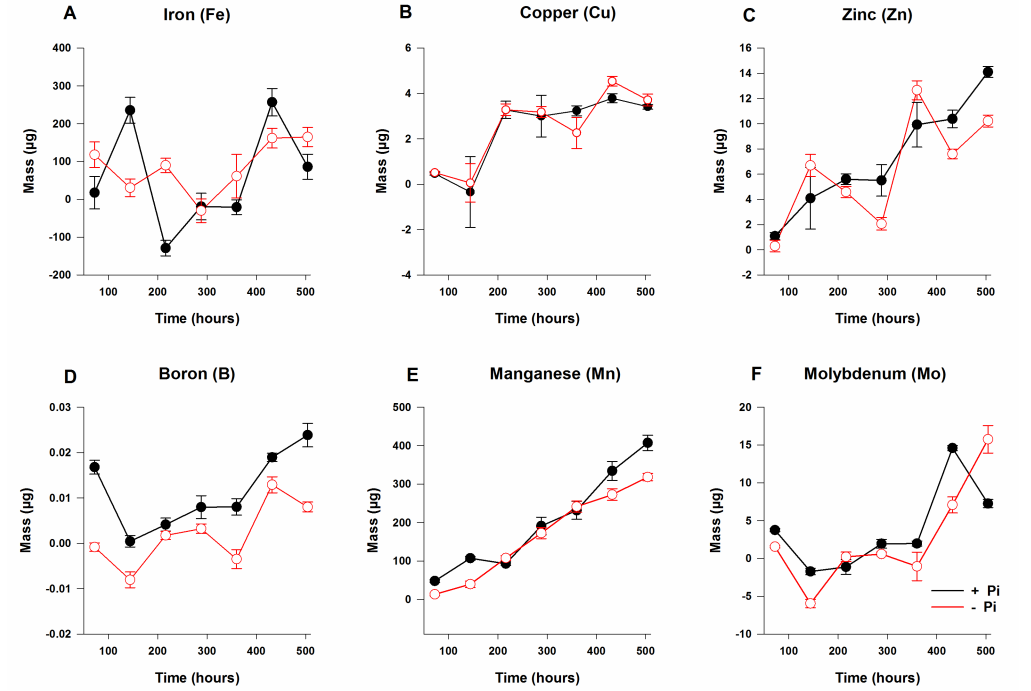

Figure A.7: Uptake of micro-elements under normal and deficient Pi conditions

Uptake of Anions and carbon

Figure A.8 show uptake of Nitrate, Phosphate and Sulphate anions under normal and stressed conditions. Consistent with the total nitrogen profile, the uptake of nitrate ions increases in normal condition but decline under P stress and again, corresponds to water uptake. The phosphate uptake increases slowly until day 18, but steeply doubles in the following 72 hours under normal conditions. Notably, the uptake profile of sulphate ions do not show any oscillation and is thus quite different from that of sulphur in both normal and stress conditions. The uptake of sulphate ion increases slowly until day 12, following which the uptake drops under normal condition but steadily increase under P stress.

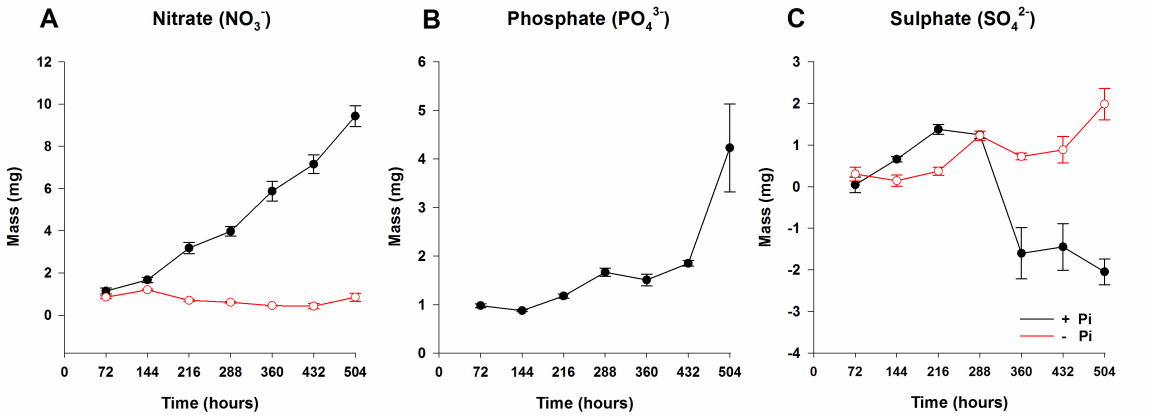

Figure A.8: Anion uptake under normal and Pi deficient condition

The uptake profiles of organic, inorganic and total carbon are qualitatively very similar to each other under both normal and stress conditions, Figure A.9, whereby the uptake of carbon drops after day 6.

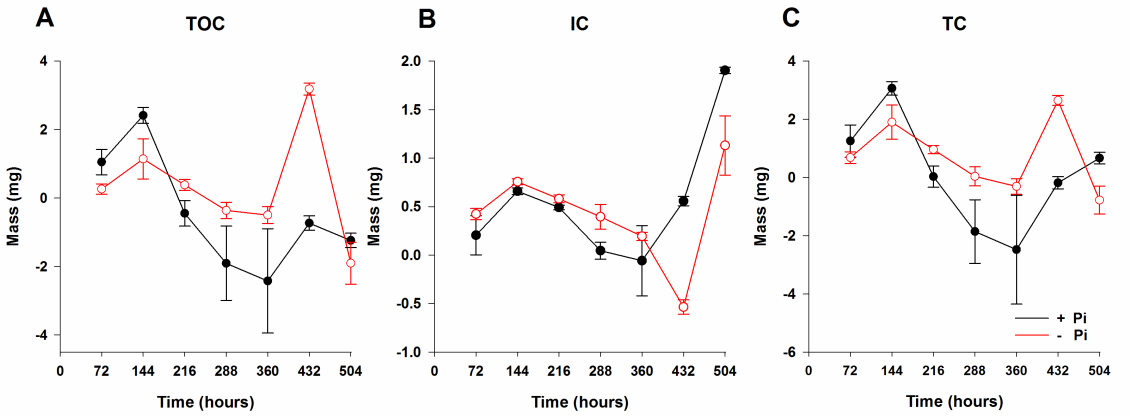

Figure A.9: Organic, inorganic and total carbon uptake under normal and deficient Pi condition

Concentration of element in the tissue samples

Relative to the control tissue samples, the concentration of N, P and K were lower and that of Fe, Cu and Zn were higher in Pi starved tissue samples. In all the plots presented below, $21_N d$ and $21_B d$ respectively corresponds to the pooled 21-day samples from the plants grown together in the boxes and bottles. All the error bars displayed are from $\pm$ standard error.

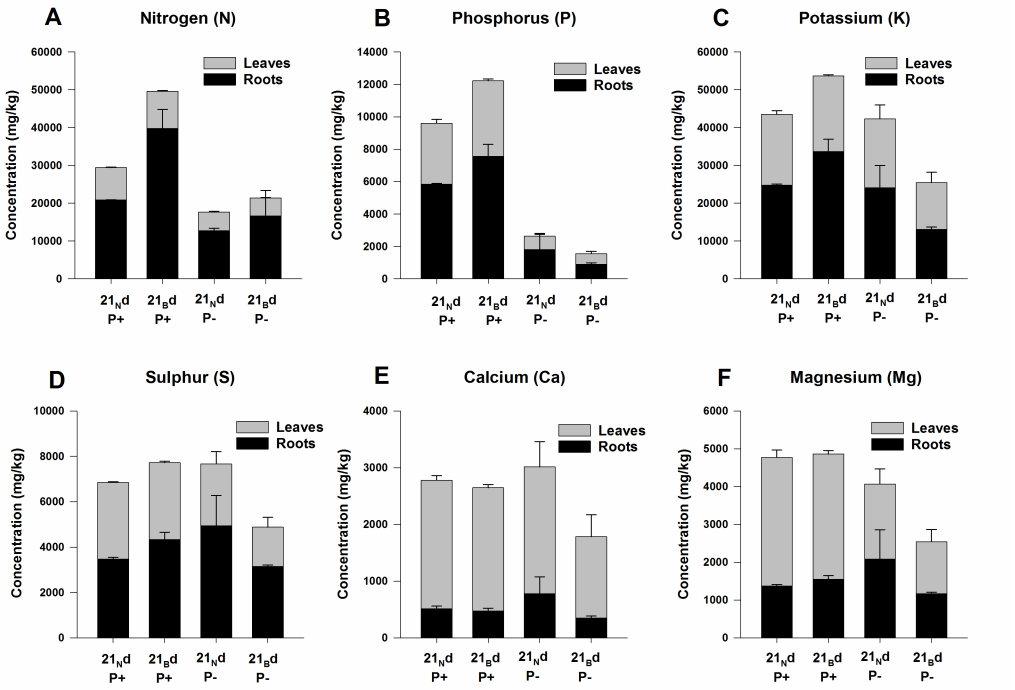

Figure A.10: Concentration of macro-elements in leaves and roots samples from normal and Pi starved plants.

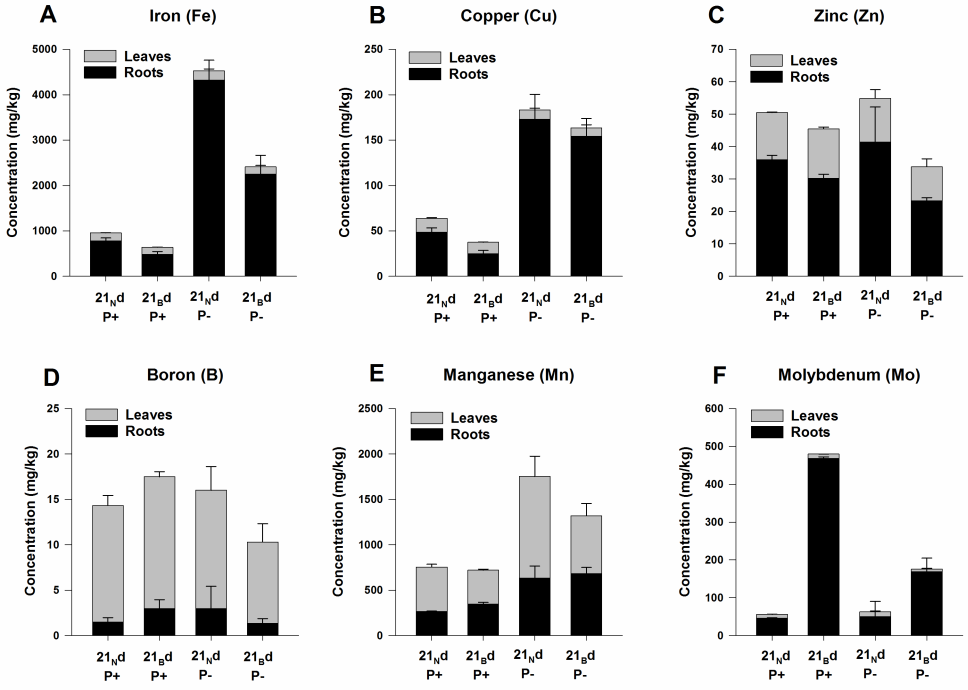

Figure A.11: Concentration of micro-elements in leaves and roots samples from normal and P starved plants.

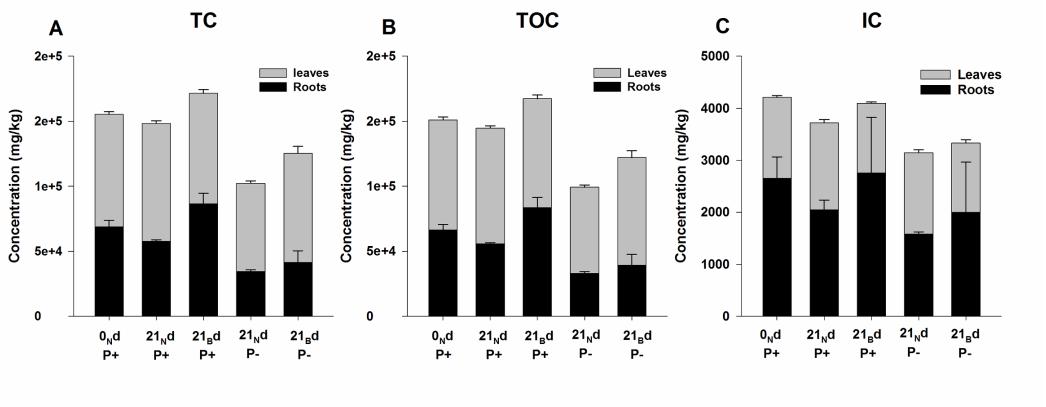

Figure A.13: Concentration of carbon leaves and roots samples from normal and Pi starved plants.

A, B and C represents total , organic and inorganic carbon, respectively.

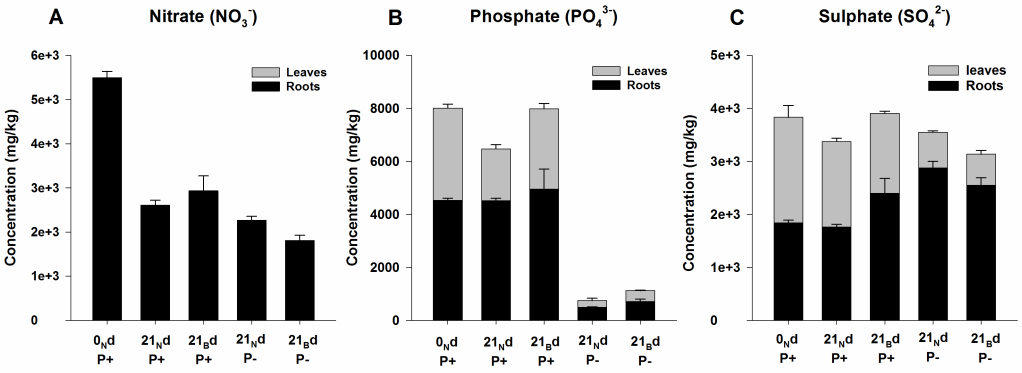

Figure A.12: Concentration of anions in leaves and roots samples from normal and Pi starved plants.

Rate of phosphate (PO_4^{3-}) uptake and its content in plants

The rate of P loss or uptake was calculated by taking the difference in mass of Pi over each time interval. Figure A.14A, show that the rate of P and PO_4 uptake increases with time under normal P supply. However, the uptake profile of PO_4 is distinctly lower than that of total phosphorus. Figure A.14B, shows the mass of phosphate ion in the plants grown together in the boxes at day 0 and 21 under normal and deficient P conditions. These masses are the product of phosphate concentration and the weight of the plant at the respective time. The mass of phosphate ions in the plants under P deficient condition was extremely low compared to that under normal conditions at both day 0 and 21.

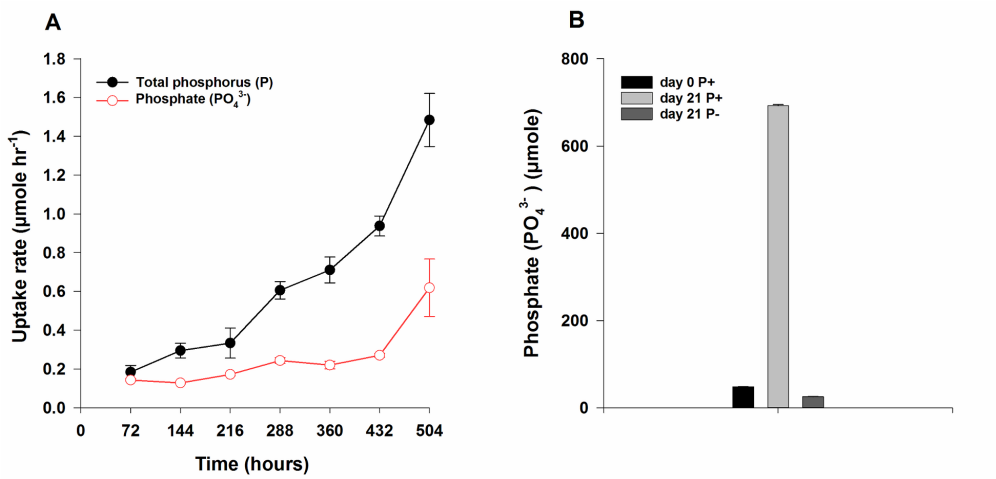

Figure A.14: Uptake rate and tissue content of phosphate.
(A) Rate of phosphorus and phosphate uptake under normal Pi-conditions (B) Mass of phosphate in normal and Pi-starved plants at day 0 and 21 of the treatment.

Next steps

The ionomic dataset generated in this study offers the temporal signatures for the uptake of different elements by the rice plant under both normal and phosphate-deficient conditions. Preliminary analysis of this dataset, presented in this section, distinctly indicates the impact of phosphate stress on the uptake of other elements. Due to time constraint, a thorough analysis of this dataset has not been possible within the scope of thesis. This analyses needed include tests to identify the statistical significance in the observations, correlation analysis to dissect the relationship between different elements both in plant tissues and across the time-course, and principal component analysis to visualize the differences among the mineral elements in tissues under two treatments. Furthermore, uptake rates of different elements can be calculated, as done for phosphate in Figure A.14A and could be used to develop whole root phosphate/resource uptake models in SimRoot (**?**).

Though this pilot-scale experiment was successful in generating insightful ionomic dataset, there is still scope for improvement. This includes using more plants, a range of phosphate treatments initiated at different developmental stages and parallel plant sampling and measurements including dry weight, pH of the hydroponic solution, plant phenotypes and physiology.

Appendix B

Current strategies at global, national and field scale

Of the total phosphorus used for global food production annually, only 20% actually becomes part of the food consumed, while the majority is lost permanently or temporarily at various stages from mine to fork (Schröder et al., 2010; Cordell & White, 2013). Such considerable losses offer substantial opportunities for improving efficiency of phosphorus management systems, recycling and reuse and enhancing uptake and use efficiency by plant. These opportunities operate at different scales; global, national, local, field and plant scales. The existing strategies and practices utilising these opportunities are discussed as follows.

Global scale

Due to the inequitable geographical distribution of phosphorus reserves, countries dependent on imports are concern over geo-political dynamics of phosphorus. Despite phosphorus being essential to food production, there are no adequate international actions to ensure its access for long-term food security. Phosphate prices hiked in 2008 by 800% putting the issue of global phosphate scarcity into the mainstream international agenda (Cordell et al., 2009). Whereby, there has been increasing support, awareness and advocacy for sustainable management of phosphate. Apart from isolated examples in a few countries, at the international level there are a lack of strategic frameworks and policies to stimulate and support the development and efficient use of renewable phosphorus fertilisers and their efficient use and equitable access by all the world's farmers. Besides these, there is a lack of consensus on the various subjects, including the life expectancy of global phosphate rock reserves. There is an ambigu-

ity of roles and absence of responsibilities among those organisations who could take the lead on phosphorus security. These include the UN's FAO and UNEP, the fertiliser industry and national governments. Currently by default, the market governs the global phosphate resources, but it alone could hardly solve the rising problem in a sustainable, equitable, and timely manner. Taking the initiative, researchers are forming new global and national platforms, such as the Global Phosphorus Research Initiative (GPRI), European Sustainable Phosphorus Platform (ESPP) and the Dutch Nutrient Platform to address this global issue. Perhaps, it is high time to form an Intergovernmental Panel on Phosphorus Security (SPS committee 2012).

National and Field scale

This scale encompasses different sectors of the food system, from mining to food consumption and wastewater. Broadly, the strategies across these sectors either aim to reduce the demand, or secure supply.

Demand reduction

Proper management of storage and application methods, rate, time and place of fertilisers, would minimise P losses and the consequent environmental risks. Different phosphorus management strategies are required for different soil, environment and crop types across the world. One common management criterion is to maintain critical phosphorus levels by replenishing the soil at same rate that it is being removed (Cordell and White, 2013).

To limit the application and immobilisation of phosphate in soil, there are increasing incentives for replacing the 'fixed insurance' method by a 'precision farming' application. Such targeted applications (e.g. near to the roots or intensely rooted part of a soil, as a seed dressing, or foliage feed) are more economic and offer less risk to the environment (Withers et al., 2014; Withers et al., 2015). Other P fertiliser placement methods include reduced application for better utilisation of legacy soil P, sub-surface banding near to the seed row, and shallow incorporation on a vertical plane with appropriate spreading pattern horizontally (Simpson et al., 2011). Further, to improve the efficiency of phosphorus fertiliser, a number of commercial formulations are available that reduce P immobilisation and enhance the mobilisation of native fixed P. These include polymer-coated organo-mineral and liquid product for soil applications and bioinoculants (McLaughlin et al., 2011). The use of slow-release fertilisers and/or

targeted sub-surface application can reduce incidental P loss and environmental risk.

The loss of soil phosphorus from farms results from erosion by water, wind, tillage and harvesting. The infiltration capacity or structural quality of the soils can be improved by various combinations of techniques including, mulching, ridge tillage, sub-soiling, contour ploughing, buffer stripping, cover crop establishment, conversion of arable land into grass land and agroforestry (Cordell & White, 2013). However, the optimal combinations have to be determined for each field individually.

A good level of biodiversity also influences the availability and P uptake by plants. Given this fact, various farm soils are inoculated with microbes to improve P availability (Sharma et al., 2013). For example, Plant Growth Promoting Rhizobacteria (PGPR) directly increases plant available P by solubilisation and mineralisation of fixed P (Ahemad and Kibret, 2014). Another rhizobacteria (e.g. Azospirillum), indirectly enhances plant P acquisition by production of phytohormones that stimulate root growth. The commercial inoculants of PGPR have been developed but their widespread application has remained limited due to the inconsistent performance in different environment and poor understanding of associated mechanisms (Richardson et al., 2011) . On similar lines, there are commercial chemical formulations for application to soil, which activate plant gene/s that enhance soil P availability, its uptake and ultimate crop productivity. However, this strategy has remained expensive for the farmers.

The awareness of these strategies is increasing slowly among the farmer communities of the developing world. In some countries, mechanisms have been devised for encouraging farmers to manage phosphate more effectively in area at risk from phosphorus pollution. For example, the UK have several initiatives including Catchment Sensitive Farming (CSF), Tried and tested nutrient management and SWARM knowledge hub, to aid farmers in reducing P pollution in agriculture. Between 2006 and 2014, the CSF scheme reduced agricultural P losses on average by ~9% (total phosphorus) and ~7% (reactive phosphorus) (Wentworth, 2014)

As livestock utilise only a small fraction of organic phosphate present in plant components, inorganic phosphate supplements are added to their feed, which account for 5% of the global phosphate supply. A high proportion of total phosphorus ends up in manure. In countries, like Denmark and the Netherlands, an artificial enzyme, 'phytase', is added to the pig feed to breakdown phosphate compounds to a form that is easily absorbed (SCU, 2013). In Canada, genetically-engineered pig 'Enviropig' has been developed that can directly digest the phosphate, thereby reducing the need for phosphate supplements and its level in manure (Forsberg et al., 2003).

Human dietary shift toward phosphorus intensive products has a large contribution in amplifying global P cycle. Compared to vegetarian diet, production of meat and dairy food requires more land and fertilisers, ~ 3 times more phosphate. Meat consumption accounts for 72% of the global average P footprint (Geneviève, 2012) thereby challenging sustainable management of P. Certainly, societal initiative to promote less phosphorus intensive food products i.e. vegetal base, could play an important role, particularly in high P footprint countries, in reducing phosphorus demand along with other human health and environment issues.

Approximately, 55% of phosphorus in food for human consumption is lost as waste during processing, transportation and storage (Cordell et al., 2009). In 2013, it was estimated that total annual food waste rose to ~12 million tonne within the UK (valued over £19bn and 20mt greenhouse gas emission). Three quarter of this could have been avoided. Decreasing waste in food production and consumption chain would obviously reduce P demand (Cordell and White, 2013).

Food additives comprise 5-10% of the P in domestic waste water in the UK. As only a few alternatives to P-based additives have been licensed for food production, the Environment Agency has initiated the work to find potential alternatives. P compounds also form a core component of detergents, accounting for ~ 10% of the globally mined P. As one of the regulatory measure, the EU has imposed limits on the use of P in the domestic cleaning products. However, such regulation does not apply to industrial products (Wentworth, 2014).

Securing supply by enhancing P recycling, recovery and re-use

Though livestock manure is still extensively used around the world as fertilisers, it is unevenly distributed and remains concentrated in certain regions. The livestock production regions have excess of P while crop-growing districts run short for it. For sustainability, recycling of manure to maintain the balance across these regions is important but this demands technology, transportation and logistics. Technologies and facilities for manure dissemination exist but are used to only a limited extent, perhaps due to associated cost and inefficiencies.

P-rich bioresources such as composts, anaerobic digestates, municipal biosolids and biochars, are also used as the fertilisers. In addition, P is extracted from waste streams from swine and dairy farms, abattoirs, vegetable processing plants and other industrial by-products. The negative constraints on widespread use of such bioresources mainly include biogeochemical risks, energy efficiency, production cost and transportability. Interestingly, human excreta make up about ~14% of the globally lost phosphorus.

If optimally recovered, it could satisfy up to 22% of the current global demand for P (Cordell and White, 2013). With population growth and the dietary shift, P concentrations in this bioresource could be even greater in future. However, the primary focus of the current sanitation systems is to remove waste while nutrient recycling for agriculture is secondary and challenging because of their diluted levels in centralised water-based systems and associated energy cost for the recovery.

There are numerous solutions for recovering phosphorus from waste sources, ranging in scale from small, such as direct urine use and composting faeces and solid bio-waste, to large, such as recovery of struvite from Wastewater Treatment Plants (WWTPs) (SCU, 2013). Different local scale initiatives for P recovery and reuse have been implemented in various countries including Sweden, Denmark, India, Niger and South Africa. Struvite recovered from WWTPs produces high quality of P fertilisers which is being used in treatment plants of some major cities in North America and UK. Besides these, P is also recovered from sewage sludge ash for industrial use in the Netherlands (Cordell et al., 2011). In some European countries, the governments are encouraging P recovery from waste water streams and recycling it to land. For example, ICL fertiliser in Amsterdam has made legal agreement with Dutch government to use 15% recycled P in manufacturing of fertilisers by 2015 and aim to use 100% by 2025 (Wentworth, 2014).

There is great potential for recovery of phosphorus from mining remnants and thereby extending the life expectancy of reserves. It is estimated that around 15-30% of P is lost, during mining, processing and handling (Cordell and White, 2013). Furthermore, there is an additional environmental risk from the presence of heavy or radioactive metals, like cadmium, radium and thorium, in the mining-waste products. However, technologies are being developed to address these issues. Globally, there is a trend towards improving recovery rates in the mining of lower grade P rock, whose use is limited by the higher impurity content (Wentworth, 2014) . Also, there are increasing interests and investments in exploring new phosphate rock deposits, most notably in Saudi Arabia, Australia and seabed sediments off the coast of Namibia (SCU, 2013).

In summary, the cost of recycled fertiliser is considerably higher today than the cost of imported mineral phosphorus fertiliser. It is essential to develop and implement technologies for safe and efficient extraction of P, along with identifying the trade-offs in using alternative bioresources. In the future, continued technological development and higher prices of mineral phosphorus are likely to result in the replacement of imported fertiliser with P.

Appendix B References

Ahemad M, Kibret M. 2014. Mechanisms and applications of plant growth promoting rhizobacteria: Current perspective. Journal of King Saud University - Science 26(1): 1-20. **Cordell D, Drangert J-O, White S. 2009.** The story of phosphorus: Global food security and food for thought. Global Environmental Change 19(2): 292-305.

Cordell D, Rosemarin A, Schröder JJ, Smit AL.2011. Towards global phosphorus security: A systems framework for phosphorus recovery and reuse options. Chemosphere 84(6): 747-758.

Cordell D, White S. 2013. Sustainable phosphorus measures: strategies and technologies for achieving phosphorus security. Agronomy 3(1): 86-116.

Forsberg CW, Phillips JP, Golovan SP, Fan MZ, Meidinger RG, Ajakaiye A, Hilborn D, Hacker RR. 2003. The Enviropig physiology, performance, and contribution to nutrient management advances in a regulated environment: The leading edge of change in the pork industry. Journal of Animal Science 81(14): E68-E77.

Geneviève SM, Bennett EM, Elser JJ. 2012. The role of diet in phosphorus demand. Environmental Research Letters 7(4): 044043.

McLaughlin M, McBeath T, Smernik R, Stacey S, Ajiboye B, Guppy C. 2011. The chemical nature of P accumulation in agricultural soils—implications for fertiliser management and design: an Australian perspective. Plant and Soil 349(1-2): 69-87.

Richardson A, Lynch J, Ryan P, Delhaize E, Smith FA, Smith S, Harvey P, Ryan M, Veneklaas E, Lambers H, Oberson A, Culvenor R, Simpson R. 2011. Plant and microbial strategies to improve the phosphorus efficiency of agriculture. Plant and Soil 349(1-2): 121-156.

Schröder JJ, Cordell D, Smit AL, Rosemarin A 2010. Sustainable Use of Phosphorus, prepared for European Union tender project ENV.B.1/ETU/2009/0025. Report 357. Wageningen: Plant Research International, Wageningen University and Research Centre. 122.

SCU (Science Communication Unit) 2013. Science for Environment Policy In depth Report: Sustainable Phosphorus Use. Prepared for the European Commission DG Environment. Bristol, UK: University of the West of England.

SPS Committee 2012. Blueprint for Global Phosphorus Security. 3rd Sustainable Phosphorus Summit. Sydney, Australia : University of Technology

Sharma SB, Sayyed RZ, Trivedi MH, Gobi TA. 2013. Phosphate solubilizing microbes: sustainable approach for managing phosphorus deficiency in agricultural soils. Springer plus 2: 587.

Simpson R, Oberson A, Culvenor R, Ryan M, Veneklaas E, Lambers H, Lynch J, Ryan P, Delhaize E, Smith FA, Smith S, Harvey P, Richardson A. 2011. Strategies and agronomic interventions to improve the phosphorus-use efficiency of farming systems. Plant and Soil 349(1-2): 89-120.

Wentworth J 2014. Phosphate Resources. POSTnote (477) The Parliamentary Office of Science and Technology. London. UK.

Withers PJ, Sylvester-Bradley R, Jones DL, Healey JR, Talboys PJ. 2014. Feed the crop not the soil: rethinking phosphorus management in the food chain. Environmental Science and Technology 48(12): 6523-6530.

Withers PJ, van Dijk KC, Neset TS, Nesme T, Oenema O, Rubæk GH, Schoumans OF, Smit B, Pellerin S. 2015. Stewardship to tackle global phosphorus inefficiency: The case of Europe. Ambio 44(2): 193-206.

Appendix C

Catalogue of Plant systems models

Various plants systems models available across the literature are listed in the table below. The model are systematically categorised based on biological phenomenon it represents, along with their corresponding spatial scales, applied modelling technique and advantages they have brought.
Acronyms used in the catalogue are listed as following:
Physical scales
S: Subcellular, C: Cellular, T: Tissue, O: Organ, W: Whole plant, M: Multicellular, MS: Multi-scale, F: Field
Modelling methods
Od: Ordinary differential equations, Pd: Partial differential equations, St: Stochastic approach, Co: Computational methods, FE: Finite element Analysis, Bo: Boolean modelling, Al: Algebraic equations, Em: Empirical model, Con: Continuum model, V: Vertex based approach, PN: Petri-net approach, FSPM: Functional structural plant model.
Model gains
K: Fill knowledge gap, D: Distinction between hypotheses, P: Prediction, S: Smarter experiments.

The 14 models highlighted in green are available for reuse in the BioModels repository (http://www.ebi.ac.uk/biomodels-main/) (**) are the models developed as the part of Mathematics in the Plant Sciences Study Group, organised by Centre for Plant Integrative Biology, University of Nottingham. The models in the form of reports can be found at (http://www.cpib.ac.uk/outreach/mpssg/). Note: Crop models have not been included here as there is extensive literature on its name and have already been well documented in the form of various books (Thornley & Johnson, 1990; Thornley & France, 2007).

Biological phenomenon	Area of study	Scale	Method	Gain	Reference
Biomechanics	Cell wall expansion	S	Pd	PK	(Dyson *et al.*, 2012)
	Anther opening	T	Pd	PD	(Nelson *et al.*, 2012)
	Seed wrinkling in germination	O	Pd	PS	(Pearce *et al.*, 2011)
	Deformation of epidermis	T	FE	P	(Qian *et al.*, 2010)
	Cell wall growth	C	FE	PK	(Huang *et al.*, 2012)
	Cell growth	C	Pd	PK	(Dyson & Jensen, 2010)
	Root elongation and bending	T	Pd	P	(Dyson *et al.*, 2014)
Genetic regulation	Flowering	S	PN	PD	(Kaufmann *et al.*, 2010)
		S	Bo	PDK	(Espinosa-Soto *et al.*, 2004)
		S	Od	PK	(van Mourik *et al.*, 2010)
		P	Process-based phenology	P	(Wilczek *et al.*, 2010)
		S	Automata-theoretical	P	(Skryabin *et al.*, 2004)
	Shoot apical meristem	M	Od	P	**(Jonsson *et al.*, 2005)**
		S	Od	PKS	(Vernoux *et al.*, 2011)
	Auxin signalling	S	Od	PK	(Middleton *et al.*, 2010)
	GA signalling	S	Od	PK	**(Middleton *et al.*, 2012)**
	Root Gravitropism	S	Od	PKS	**(Band *et al.*, 2012a)**
	Cytokinin–Auxin in root cell fate	S	Od	PDS	**(Muraro *et al.*, 2011)**
	Cytokinin–Auxin Sig. in RA	M	Od	PS	(Muraro *et al.*, 2013)
	Ethylene signalling	S	Od	P	(Díaz & Alvarez-Buylla, 2006)
	Cytokinin-WUS in SAM	S	Od	PK	(Gordon *et al.*, 2009)
	Hormone crosstalk	S	Od	PKS	(Liu *et al.*, 2010)
	GA dilution	MS	Od/Pd	PKS	(Band *et al.*, 2012b)

	Vesicle trafficking in Pollen tube		S	Od	PK	(Kato *et al.*, 2010)
	ABA signalling in guard cell		S	Bo	PK	(Li *et al.*, 2006)
	ABA-Ethylene in guard cell		S	Od	PK	(Beguerisse-Dıaz *et al.*, 2012)
	Circadian clock		S	Od	PKD	**(Pokhilko *et al.*, 2012)**
			S	Od	P	(Locke *et al.*, 2005a)
			S	Od	PS	(Locke *et al.*, 2005b)
			S	Od	PK	(Locke *et al.*, 2006)
			S	Od	P	**(Pokhilko *et al.*, 2010)**
			S	Od	P	**(Pokhilko *et al.*, 2013)**
			S	Od	P	**(Troein *et al.*, 2011)**
	Root hair patterning		M	Bo	P	(Benítez *et al.*, 2008)
	Leaf hair patterning		M	Bo	PK	(Savage *et al.*, 2008)
			M	Od	PS	(Digiuni *et al.*, 2008)
	Vascular Patterning		M	Od	PK	(Muraro *et al.*, 2014)
Hormone flux and dynamics	Auxin	SAM	M	Od	P	(Stoma *et al.*, 2008)
			T	Co	PS	(O'Connor *et al.*, 2014)
		polar diffusion	M	Od	PD	(Goldsmith *et al.*, 1981)
		Efflux	C	Od	PD	(Fozard *et al.*, 2013)
		Root elongation	M	Od	PK	(Band & King, 2012)
		Transport in root	S	Od	P	(Hosek *et al.*, 2012)
			M	Od/Pd	PK	(Grieneisen *et al.*, 2007)
			M	Od	P	(Novoselova *et al.*, 2013)
			M	V/Od	PK	(Band *et al.*, 2014)
		Epidermal cell	M	Od	PK	(Jones *et al.*, 2009)
		Bud activation	M	L-system	PK	(Prusinkiewicz *et al.*, 2009)
		Root Gravitropism	M	Od	PD	(Swarup *et al.*, 2005)
		Tissue polarisation / canalization	M	Od	PKS	(Wabnik *et al.*, 2010)
		Lateral root formation	S	Bo	P	(Lucas *et al.*, 2008)

			M	Co	P	(Laskowski *et al.*, 2008)
			T	Od	P	(Péret *et al.*, 2012)
			T	Od	PKS	(Péret *et al.*, 2013)
		Vein formation	M	Od	Pd	(Feugier *et al.*, 2005)
			M	Od	P	(Feugier & Iwasa, 2006)
			M	Od	P	(Fujita & Mochizuki, 2006)
		Phyllotaxis	M	Od	PK	(Jonsson *et al.*, 2006)
			M	Od	PDK	(Bayer *et al.*, 2009)
			M	Od	PK	(Smith *et al.*, 2006)
			M	Od	PK	(Merks *et al.*, 2007)
		Floral organ development	MS?	Od	PK	(van Mourik *et al.*, 2012)
			S	Od	PS	(Middleton et al., 2009)**
		ROP Localisation in root hair	C	Od	PK	(Payne & Grierson, 2009)
		Distribution in roots	M	Od	PK?	(Mironova *et al.*, 2010)
		RAM	M	Od	PK	(Mironova *et al.*, 2012)
		Wood grain pattern formation	T	Pd	P	(Kramer & Borkowski, 2004)
	ABA		S	St	PK	(Dupeux *et al.*, 2011)
	Jasmonate		S	Od, St	P	(Banerjee & Bose, 2011)
	Brassinosteroids		S	Od	P	(van Esse *et al.*, 2012)
			S	Bo	PK	(Sankar *et al.*, 2011)
Tissue/organ patterning, growth and development	Leaf growth		T	Co	P	(Wang *et al.*, 2004)
	Leaf margin development		MS	Od	PK	(Bilsborough *et al.*, 2011)
	Leaf venation		O	Co	P	(Runions *et al.*, 2005)
	Stromal guard cells		S	Co	P	(Chen *et al.*, 2012)
			O	Od	PD	(Eamus & Shanahan, 2002)
			M	Al	P	(Buckley *et al.*, 2003)
	Seed germination		S	Od	PDS	(Penfield *et al.,* 2007)**
			M	Pd	PS	(Middleton *et al.,* 2008)**

	Shoot apical meristem development	M	Od	PK	(Nikolaev *et al.*, 2007)
		M	Od	PDK	(de Reuille *et al.*, 2006)
	Pollen tube development, guidance and growth	C	FE	P	(Fayant *et al.*, 2010)
		S	St	PD	(Stewman *et al.*, 2010)
		C	Od	PS	(Hill *et al.*, 2012)
	Cuticular patterning in flower petals	T	Pd	PKS	(Antoniou Kourounioti *et al.*, 2013)
	Fruit development	O	Co	P	(Bertin *et al.*, 2003)
	Malic acid accumulation	S	Al	P	(Lobit *et al.*, 2006)
	Fruit quality	S/O	Od	P	(Lescourret & Génard, 2005)
	Fruit ripening	MS	Cn	PK	(Ho *et al.*, 2010)
	Fruit growth	O	Al	P	(Bertin *et al.*, 2007)
		O	Od	P	(Fishman & Génard, 1998)
		O	Al	P	(Fanwoua *et al.*, 2013)
	Fruit development	O	Od	P	(Hall *et al.*, 2013)
	Effect of water stress on fruit growth	O	Em	P	(Génard & Huguet, 1996)
	Root architecture	O	Em	P	(Page & Gerwitz, 1974)
		O	Nu	P	(Lungley, 1973)
		O	Nu	P	(Diggle, 1988)
		O	Co	P	(Lynch *et al.*, 1997)
		MS	Od/Co	P	(Wu *et al.*, 2007)
		O	Nu/Co	P	(Dupuy *et al.*, 2005)
		MS	Nu/Co	P	(Drouet & Pagès, 2007)
		O	FE	P	(Dunbabin *et al.*, 2006)
		O	Con	P	(Bastian *et al.*, 2008)
		O	Pd	P	(Heinen *et al.*, 2003)
		T	Pd	P	(Dupuy *et al.*, 2010)
	Shoot architecture	W	L-system	P	(Prusinkiewicz *et al.*)
		W	Co	P	(Prusinkiewicz *et al.*, 2007)
	Organ abscission	M	Od	P	(McCue *et al.*, 2009)**
		S	Od	P	(Deng *et al.*, 2007)
	Root growth hydraulics	O	Pd	P	(Wiegers *et al.*, 2009)

	Plant morphogenesis	M	Od	P	(Dupuy *et al.*, 2008)
	Plant stem cell regulation	M	Od	PK	(Geier *et al.*, 2008)
		M	Pd	P	(Hohm *et al.*, 2010)
	Plant development	W	Em	PS	(Mundermann *et al.*, 2005)
	Sepal patterning	T	Co	P	(Roeder *et al.*, 2010)
	Flowering time control	W	OOP/Od	P	(Welch *et al.*, 2005)
		S	Od	PK	(Dong *et al.*, 2012)
		MS	Nu	P	(Brown *et al.*, 2013)
		F	Em	P	(Chew *et al.*, 2012)
Supply-uptake	Root growth and uptake	O	L-system	P	(Leitner, D *et al.*, 2010a)
		O	Al	P	(King *et al.*, 2003)
	Water and nutrient uptake	O	Co	P	(Dunbabin *et al.*, 2002)
		T	Pd	P	(Payvandi *et al.*, 2014)
	Uptake by Root hair	O	Pd	PS	(Leitner, D *et al.*, 2010b)
		O	Pd	P	(Zygalakis *et al.*, 2011)
		O	FE	PD	(Keyes *et al.*, 2013)
	Soil-root hydraulics	O	FSM	P	(Draye *et al.*, 2010)
	AMF	O	Pd	PS	(Schnepf *et al.*, 2011)
		O	Pd	PK	(Schnepf *et al.*, 2008)
		O	Pd	P	(Schnepf & Roose, 2006)
	Effect of root clustering	O	Pd	P	(Zygalakis & Roose, 2012)
	Solute transport to root	O	Pd	P	(Roose & Kirk, 2009)
	Water and sugar transport	W	Od	PD	(De Schepper & Steppe, 2010)
	Nitrogen uptake	O	Al	P	(Pedersen *et al.*, 2010)
		S	Od	P	(Alekhina *et al.*, 2000)
	Phosphorus uptake	W	Co	P	(Grant & Robertson, 1997)
	Phosphate uptake under deficiency	W	Od	P	(Wissuwa, 2003)
	Potassium uptake	O	Od	P	(Roshani *et al.*, 2009)
	Zinc uptake	M	Od	PK	(Claus & Chavarría-Krauser, 2013)
		O	Pd	P	(Ptashnyk *et al.*, 2011)

Physiology and metabolism Books: (Thornley, 1976; Thornley & Johnson, 1990; Thornley & France, 2007)	Photosynthesis	S	Od/Pd	P	(Farquhar & Caemmerer, 1982)
		S	Od	PS	(Laisk *et al.*, 2006)
		S	Od	P	(Hahn, 1987)
	Membrane transport	S	Al	PK	(Shabala *et al.*, 2006)
	Plant- soil interaction	MS	Pd	P	(Roose & Schnepf, 2008)
		O	FSM	P	(Diggle & Dunbabin, 2013)
	Flavonoid pathway	S	Od	PS	(Olsen *et al.*, 2009)
	Photosystem ii	S	Od	P	(Lazár & Jablonský, 2009)
		S	Od	P	**(Rovers & Giersch, 1995)**
		S	Od	P	(Guo & Tan, 2011)
	Sucrose metabolism	S	Od	P	(Uys *et al.*, 2007)
	RuBisCO	S	Od	PD	(McNevin *et al.*, 2006)
		S	Od	P	(Arnold & Nikoloski, 2011)
	Plastoquinone kinetics	S	Od	P	(Guo & Tan, 2009)
	Isoprene emission	S	Em	PD	(Morfopoulos *et al.*, 2013)
	Calvin cycle	S	Od	P	**(Poolman *et al.*, 2004)**
	MAPK activation	S	Od	P	**(Pathak *et al.*, 2013)**
	PPR7	S	Od	P	**(Zeilinger *et al.*, 2006)**
	Aspartate metabolism	S	Od	P	**(Curien *et al.*, 2009)**
	Chloroplastic Starch Degradation	S	Od	P	**(Nag *et al.*, 2011)**

Appendix C References

Alekhina N, Kharitonashvili E, Riznichenko G, Plusnina T, Sidorov S, Rubin A. 2000. A multi compartments model of nitrate metabolism regulation in plant roots. Journal of Biological Systems 8(3): 219-235.

Antoniou Kourounioti RL, Band LR, Fozard JA, Hampstead A, Lovrics A, Moyroud E, Vignolini S, King JR, Jensen OE, Glover BJ. 2013. Buckling as an origin of ordered cuticular patterns in flower petals. J R Soc Interface 10(80): 20120847.

Arnold A, Nikoloski Z. 2011. A quantitative comparison of Calvin-Benson cycle models. Trends Plant Sci 16(12): 676-683.

Band LR, King JR. 2012. Multiscale modelling of auxin transport in the plant-root elongation zone. J Math Biol 65(4): 743-785.

Band LR, Wells DM, Fozard JA, Ghetiu T, French AP, Pound MP, Wilson MH, Yu L, Li W, Hijazi HI, Oh J, Pearce SP, Perez-Amador MA, Yun J, Kramer E, Alonso JM, Godin C, Vernoux T, Hodgman TC, Pridmore TP, Swarup R, King JR, Bennett MJ. 2014. Systems Analysis of Auxin Transport in the Arabidopsis Root Apex. Plant Cell.26(3):862-75.

Band LR, Wells DM, Larrieu A, Sun J, Middleton AM, French AP, Brunoud G, Sato EM, Wilson MH, Péret B, Oliva M, Swarup R, Sairanen I, Parry G, Ljung K, Beeckman T, Garibaldi JM, Estelle M, Owen MR, Vissenberg K, Hodgman TC, Pridmore TP, King JR, Vernoux T, Bennett MJ. 2012a. Root gravitropism is regulated by a transient lateral auxin gradient controlled by a tipping-point mechanism. Proc Natl Acad Sci U S A 109(12): 4668-4673.

Band LR, Úbeda-Tomás S, Dyson RJ, Middleton AM, Hodgman TC, Owen MR, Jensen OE, Bennett MJ, King JR. 2012b. Growth-induced hormone dilution can explain the dynamics of plant root cell elongation. Proc Natl Acad Sci U S A 109(19): 7577-7582.

Banerjee S, Bose I. 2011. Transient pulse formation in jasmonate signaling pathway. Journal of Theoretical Biology 273(1): 188-196.

Bastian P, Chavarría-Krauser A, Engwer C, Jäger W, Marnach S, Ptashnyk M. 2008. Modelling in vitro growth of dense root networks. J Theor Biol 254(1): 99-109.

Bayer EM, Smith RS, Mandel T, Nakayama N, Sauer M, Prusinkiewicz P, Kuhlemeier C. 2009. Integration of transport-based models for phyllotaxis and midvein formation. Genes Dev 23(3): 373-384.

Beguerisse-Dıaz M, Hernández-Gómez MC, Lizzul AM, Barahona M, Desikan R. 2012. Compound stress response in stomatal closure: a mathematical model of ABA and ethylene interaction in guard cells. BMC Syst Biol 6: 146.

Benítez M, Espinosa-Soto C, Padilla-Longoria P, Alvarez-Buylla ER. 2008. Interlinked nonlinear subnetworks underlie the formation of robust cellular patterns in Arabidopsis epidermis: a dynamic spatial model. BMC Syst Biol 2: 98.

Bertin N, Genard M, Fishman S. 2003. A model for an early stage of tomato fruit development: cell multiplication and cessation of the cell proliferative activity. Ann Bot 92(1): 65-72.

Bertin N, Lecomte A, Brunel B, Fishman S, Génard M. 2007. A model describing cell polyploidization in tissues of growing fruit as related to cessation of cell proliferation. J Exp Bot 58(7): 1903-1913.

Bilsborough GD, Runions A, Barkoulas M, Jenkins HW, Hasson A, Galinha C, Laufs P, Hay A, Prusinkiewicz P, Tsiantis M. 2011. Model for the regulation of Arabidopsis thaliana leaf margin development. Proc Natl Acad Sci U S A 108(8): 3424-3429.

Brown HE, Jamieson PD, Brooking IR, Moot DJ, Huth NI. 2013. Integration of molecular and physiological models to explain time of anthesis in wheat. Ann Bot 112(9): 1683-1703.

Buckley TN, Mott KA, Farquhar GD. 2003. A hydromechanical and biochemical model of stomatal conductance. Plant, Cell & Environment 26(10): 1767-1785.

Chen ZH, Hills A, Bätz U, Amtmann A, Lew VL, Blatt MR. 2012. Systems dynamic modeling of the stomatal guard cell predicts emergent behaviors in transport, signaling, and volume control. Plant Physiol 159(3): 1235-1251.

Chew YH, Wilczek AM, Williams M, Welch SM, Schmitt J, Halliday KJ. 2012. An augmented Arabidopsis phenology model reveals seasonal temperature control of flowering time. New Phytol 194(3): 654-665.

Claus J, Chavarría-Krauser A. 2013. Implications of a zinc uptake and transport model. Plant Signal Behav 8(5): e24167.

Curien G, Bastien O, Robert-Genthon M, Cornish-Bowden A, Cárdenas ML, Dumas R. 2009. Understanding the regulation of aspartate metabolism using a model based on measured kinetic parameters. Mol Syst Biol 5: 271. de Reuille PB, Bohn-Courseau I, Ljung K, Morin H, Carraro N, Godin C, Traas J. 2006.
Computer simulations reveal properties of the cell-cell signaling network at the shoot apex in Arabidopsis. Proc Natl Acad Sci U S A 103(5): 1627-1632.

De Schepper V, Steppe K. 2010. Development and verification of a water and sugar transport model using measured stem diameter variations. J Exp Bot 61(8): 2083-2099.

Deng Y, Wu Y, Li Y, Zhang P, Yang M, Shi C, Zheng C, Yu S. 2007. A mathematical model for predicting grape berry drop during storage. Journal of Food Engineering 78(2): 500-511.

Diggle AJ. 1988. ROOTMAP—a model in three-dimensional coordinates of the growth and structure of fibrous root systems. Plant and Soil 105(2): 169-178.

Diggle AJ, Dunbabin VM 2013. Using Simulation Modeling of Root Growth and Function as an Aid in Breeding for Increased Water- and Nutrient-Use Efficiency. Improving Water and Nutrient-Use Efficiency in Food Production Systems: John Wiley & Sons, Inc, 177-186.

Digiuni S, Schellmann S, Geier F, Greese B, Pesch M, Wester K, Dartan B, Mach V, Srinivas BP, Timmer J, Fleck C, Hulskamp M. 2008. A competitive complex formation mechanism underlies trichome patterning on Arabidopsis leaves. Mol Syst Biol 4: 217.

Dong Z, Danilevskaya O, Abadie T, Messina C, Coles N, Cooper M. 2012. A gene regulatory network model for floral transition of the shoot apex in maize and its dynamic modeling. PLoS One 7(8): e43450.

Draye X, Kim Y, Lobet G, Javaux M. 2010. Model-assisted integration of physiological and environmental constraints affecting the dynamic and spatial patterns of root water uptake from soils. J Exp Bot 61(8): 2145-2155.

Drouet J-L, Pagès L. 2007. GRAAL-CN: A model of GRowth, Architecture and ALlocation for Carbon and Nitrogen dynamics within whole plants formalised at the organ level. Ecological Modelling 206(3–4): 231-249.

Dunbabin V, McDermott S, Bengough AG. 2006. Upscaling from Rhizosphere to Whole Root System: Modelling the Effects of Phospholipid Surfactants on Water and Nutrient Uptake. Plant and Soil 283(1-2): 57-72.

Dunbabin VM, Diggle AJ, Rengel Z, van Hugten R. 2002. Modelling the interactions between water and nutrient uptake and root growth. Plant and Soil 239(1): 19-38.

Dupeux F, Santiago J, Betz K, Twycross J, Park S, Rodriguez L, Gonzalez-Guzman M, Jensen M, Krasnogor N, Blackledge M, Holdsworth M, Cutler S, Rodriguez P, Marquez J. 2011. A thermodynamic switch modulates abscisic acid receptor sensitivity. Embo Journal 30(20): 4171-4184.

Dupuy L, Fourcaud T, Stokes A, Danjon F. 2005. A density-based approach for the modelling of root architecture: application to Maritime pine (Pinus pinaster Ait.) root systems. J Theor Biol 236(3): 323-334.

Dupuy L, Mackenzie J, Rudge T, Haseloff J. 2008. A system for modelling cell-cell interactions during plant morphogenesis. Ann Bot 101(8): 1255-1265.

Dupuy L, Vignes M, McKenzie BM, White PJ. 2010. The dynamics of root meristem distribution in the soil. Plant Cell Environ 33(3): 358-369.

Dyson R, Band L, Jensen O. 2012. A model of crosslink kinetics in the expanding plant cell wall: Yield stress and enzyme action. Journal of Theoretical Biology 307: 125-136.

Dyson R, Jensen O. 2010. A fibre-reinforced fluid model of anisotropic plant cell growth. Journal of Fluid Mechanics 655: 472-503.

Dyson RJ, Vizcay-Barrena G, Band LR, Fernandes AN, French AP, Fozard JA, Hodgman TC, Kenobi K, Pridmore TP, Stout M, Wells DM, Wilson MH, Bennett MJ, Jensen OE. 2014. Mechanical modelling quantifies the functional importance of outer tissue layers during root elongation and bending. New Phytol. 202(4):1212-22

Díaz J, Alvarez-Buylla ER. 2006. A model of the ethylene signaling pathway and its gene response in Arabidopsis thaliana: pathway cross-talk and noise-filtering properties. Chaos 16(2): 023112.

Eamus D, Shanahan ST. 2002. A rate equation model of stomatal responses to vapour pressure deficit and drought. BMC Ecol 2: 8.

Espinosa-Soto C, Padilla-Longoria P, Alvarez-Buylla ER. 2004. A gene regulatory network model for cell-fate determination during Arabidopsis thaliana flower development that is robust and recovers experimental gene expression profiles. Plant Cell 16(11): 2923-2939.

Fanwoua J, de Visser P, Heuvelink E, Yin X, Struik P, Marcelis L. 2013. A dynamic model of tomato fruit growth integrating cell division, cell growth and endoreduplication. Functional Plant Biology 40(11): 1098-1114.

Farquhar GD, Caemmerer S 1982. Modelling of Photosynthetic Response to Environmental Conditions. In: Lange OL, Nobel PS, Osmond CB, Ziegler H eds. Physiological Plant Ecology II: Springer Berlin Heidelberg, 549-587.

Fayant P, Girlanda O, Chebli Y, Aubin CE, Villemure I, Geitmann A. 2010. Finite element model of polar growth in pollen tubes. Plant Cell 22(8): 2579-2593.

Feugier FG, Iwasa Y. 2006. How canalization can make loops: a new model of reticulated leaf vascular pattern formation. J Theor Biol 243(2): 235-244.

Feugier FG, Mochizuki A, Iwasa Y. 2005. Self-organization of the vascular system in plant leaves: inter-dependent dynamics of auxin flux and carrier proteins. J Theor Biol 236(4): 366-375.

Fishman S, Génard M. 1998. A biophysical model of fruit growth: simulation of seasonal and diurnal dynamics of mass. Plant, Cell & Environment 21(8): 739-752.
Fozard JA, King JR, Bennett MJ. 2013. Modelling auxin efflux carrier phosphorylation and localization. J Theor Biol 319: 34-49. Fujita H, Mochizuki A. 2006.
Geier F, Lohmann JU, Gerstung M, Maier AT, Timmer J, Fleck C. 2008. A quantitative and dynamic model for plant stem cell regulation. PLoS One 3(10): e3553.
Goldsmith MH, Goldsmith TH, Martin MH. 1981. Mathematical analysis of the chemosmotic polar diffusion of auxin through plant tissues. Proc Natl Acad Sci U S A 78(2): 976-980.
Gordon SP, Chickarmane VS, Ohno C, Meyerowitz EM. 2009. Multiple feedback loops through cytokinin signaling control stem cell number within the Arabidopsis shoot meristem. Proc Natl Acad Sci U S A 106(38): 16529-16534.
Grant RF, Robertson JA. 1997. Phosphorus uptake by root systems: mathematical modelling in ecosys. Plant and Soil 188(2): 279-297.
Grieneisen VA, Xu J, Marée AF, Hogeweg P, Scheres B. 2007. Auxin transport is sufficient to generate a maximum and gradient guiding root growth. Nature 449(7165): 1008-1013.
Guo Y, Tan J. 2009. A kinetic model structure for delayed fluorescence from plants. Biosystems 95(2): 98-103.
Guo Y, Tan J. 2011. Modeling and simulation of the initial phases of chlorophyll fluorescence from Photosystem II. Biosystems 103(2): 152-157.
Génard M, Huguet JG. 1996. Modeling the response of peach fruit growth to water stress. Tree Physiol 16(4): 407-415.
Hahn BD. 1987. A Mathematical Model of Photorespiration and Photosynthesis. Annals of Botany 60(2): 157-169.
Hall AJ, Minchin PE, Clearwater MJ, Génard M. 2013. A biophysical model of kiwifruit (Actinidia deliciosa) berry development. J Exp Bot 64(18): 5473-5483.

Heinen M, Mollier A, De Willigen P. 2003. Growth of a root system described as diffusion. II. Numerical model and application. Plant and Soil 252(2): 251-265.

Hill AE, Shachar-Hill B, Skepper JN, Powell J, Shachar-Hill Y. 2012. An osmotic model of the growing pollen tube. PLoS One 7(5): e36585.

Ho QT, Verboven P, Verlinden BE, Nicolaï BM. 2010. A model for gas transport in pear fruit at multiple scales. J Exp Bot 61(8): 2071-2081.

Hohm T, Zitzler E, Simon R. 2010. A Dynamic Model for Stem Cell Homeostasis and Patterning in Arabidopsis Meristems. Plos One 5(2).

Hosek P, Kubes M, Lanková M, Dobrev PI, Klíma P, Kohoutová M, Petrásek J, Hoyerová K, Jirina M, Zazímalová E. 2012. Auxin transport at cellular level: new insights supported by mathematical modelling. J Exp Bot 63(10): 3815-3827.

Huang R, Becker AA, Jones IA. 2012. Modelling cell wall growth using a fibre-reinforced hyperelastic–viscoplastic constitutive law. Journal of the Mechanics and Physics of Solids 60(4): 750-783.

Jones AR, Kramer EM, Knox K, Swarup R, Bennett MJ, Lazarus CM, Leyser HM, Grierson CS. 2009. Auxin transport through non-hair cells sustains root-hair development. Nat Cell Biol 11(1): 78-84.

Jonsson H, Heisler M, Reddy G, Agrawal V, Gor V, Shapiro B, Mjolsness E, Meyerowitz E. 2005. Modeling the organization of the WUSCHEL expression domain in the shoot apical meristem. Bioinformatics 21: I232-I240.

Jonsson H, Heisler M, Shapiro B, Meyerowitz E, Mjolsness E. 2006. An auxin-driven polarized transport model for phyllotaxis. Proc Natl Acad Sci U S A 103(5): 1633-1638.

Kato N, He H, Steger AP. 2010. A systems model of vesicle trafficking in Arabidopsis pollen tubes. Plant Physiol 152(2): 590-601.

Kaufmann K, Nagasaki M, Jáuregui R. 2010. Modelling the molecular interactions in the flower developmental network of Arabidopsis thaliana. In Silico Biol 10(1): 125-143.

Keyes SD, Daly KR, Gostling NJ, Jones DL, Talboys P, Pinzer BR, Boardman R, Sinclair I, Marchant A, Roose T. 2013. High resolution synchrotron imaging of wheat root

hairs growing in soil and image based modelling of phosphate uptake. New Phytol 198(4): 1023-1029.

King J, Gay A, Sylvester-Bradley R, Bingham I, Foulkes J, Gregory P, Robinson D. 2003. Modelling cereal root systems for water and nitrogen capture: towards an economic optimum. Ann Bot 91(3): 383-390.

Kramer E, Borkowski M. 2004. Wood grain patterns at branch junctions: modeling and implications. Trees 18(5): 493-500.

Laisk A, Eichelmann H, Oja V. 2006. C3 photosynthesis in silico. Photosynth Res 90(1): 45-66. **Laskowski M, Grieneisen VA, Hofhuis H, Hove CA, Hogeweg P, Marée AF, Scheres B. 2008.** Root system architecture from coupling cell shape to auxin transport. PLoS Biol 6(12): e307.

Lazár D, Jablonský J. 2009. On the approaches applied in formulation of a kinetic model of photosystem II: Different approaches lead to different simulations of the chlorophyll alpha fluorescence transients. J Theor Biol 257(2): 260-269.

Leitner D, Klepsch S, Bodner G, Schnepf A. 2010a. A dynamic root system growth model based on L-Systems. Plant and Soil 332(1-2): 177-192.

Leitner D, Klepsch S, Ptashnyk M, Marchant A, Kirk G, Schnepf A, Roose T. 2010b. A dynamic model of nutrient uptake by root hairs. New Phytologist 185(3): 792-802.

Lescourret F, Génard M. 2005. A virtual peach fruit model simulating changes in fruit quality during the final stage of fruit growth. Tree Physiol 25(10): 1303-1315.

Li S, Assmann SM, Albert R. 2006. Predicting essential components of signal transduction networks: a dynamic model of guard cell abscisic acid signaling. PLoS Biol 4(10): e312.

Liu J, Mehdi S, Topping J, Tarkowski P, Lindsey K. 2010. Modelling and experimental analysis of hormonal crosstalk in Arabidopsis. Mol Syst Biol 6: 373.

Lobit P, Genard M, Soing P, Habib R. 2006. Modelling malic acid accumulation in fruits: relationships with organic acids, potassium, and temperature. J Exp Bot 57(6): 1471-1483.

Locke JC, Kozma-Bognár L, Gould PD, Fehér B, Kevei E, Nagy F, Turner MS, Hall A, Millar AJ. 2006. Experimental validation of a predicted feedback loop in the multi-oscillator clock of Arabidopsis thaliana. Mol Syst Biol 2: 59.

Locke JC, Millar AJ, Turner MS. 2005a. Modelling genetic networks with noisy and varied experimental data: the circadian clock in Arabidopsis thaliana. J Theor Biol 234(3): 383-393.

Locke JC, Southern MM, Kozma-Bognár L, Hibberd V, Brown PE, Turner MS, Millar AJ. 2005b. Extension of a genetic network model by iterative experimentation and mathematical analysis. Mol Syst Biol 1: 2005.0013.

Lucas M, Godin C, Jay-Allemand C, Laplaze L. 2008. Auxin fluxes in the root apex co-regulate gravitropism and lateral root initiation. J Exp Bot 59(1): 55-66.

Lungley DR. 1973. The growth of root systems — A numerical computer simulation model. Plant and Soil 38(1): 145-159.

Lynch J, Nielsen K, Davis R, Jablokow A. 1997. SimRoot: Modelling and visualization of root systems. Plant and Soil 188(1): 139-151.

McCue SW, Bartsch T, Dyson R, Beguerisse-Diaz M, Jensen O 2009. Modelling cell separation during plant organ abscission. Proceedings of the Mathematics in the Plant Sciences Study Group. The Centre for Plant Integrative Biology, University of Nottingham.

Middleton AM, Dyson RJ, Band LR, Grandison S, Wells DM, Holman TJ, J Twycross, Jensen O. 2008. The Mechanics of Arabidopsis Seed Germination. Proceedings of the Mathematics in the Plant Sciences Study Group. The Centre for Plant Integrative Biology, University of Nottingham.

Middleton AM, JP Ward JP, King JR. 2009. A model for floral organ development in Arabidopsis Proceedings of the Mathematics in the Plant Sciences Study Group. The Centre for Plant Integrative Biology, University of Nottingham.

McNevin D, von Caemmerer S, Farquhar G. 2006. Determining RuBisCO activation kinetics and other rate and equilibrium constants by simultaneous multiple non-linear

regression of a kinetic model. J Exp Bot 57(14): 3883-3900.
Merks RM, Van de Peer Y, Inzé D, Beemster GT. 2007. Canalization without flux sensors: a traveling-wave hypothesis. Trends Plant Sci 12(9): 384-390.
Middleton AM, King JR, Bennett MJ, Owen MR. 2010. Mathematical modelling of the Aux/IAA negative feedback loop. Bull Math Biol 72(6): 1383-1407.
Middleton AM, Úbeda-Tomás S, Griffiths J, Holman T, Hedden P, Thomas SG, Phillips AL, Holdsworth MJ, Bennett MJ, King JR, Owen MR. 2012. Mathematical modeling elucidates the role of transcriptional feedback in gibberellin signaling. Proc Natl Acad Sci U S A 109(19): 7571-7576.
Mironova V, Omelyanchuk N, Novoselova E, Doroshkov A, Kazantsev F, Kochetov A, Kolchanov N, Mjolsness E, Likhoshvai V. 2012. Combined in silico/in vivo analysis of mechanisms providing for root apical meristem self-organization and maintenance. Annals of Botany 110(2): 349-360.
Mironova V, Omelyanchuk N, Yosiphon G, Fadeev S, Kolchanov N, Mjolsness E, Likhoshvai V. 2010. A plausible mechanism for auxin patterning along the developing root. Bmc Systems Biology 4.
Morfopoulos C, Prentice IC, Keenan TF, Friedlingstein P, Medlyn BE, Peñuelas J, Possell M. 2013. A unifying conceptual model for the environmental responses of isoprene emissions from plants. Ann Bot 112(7): 1223-1238.
Mundermann L, Erasmus Y, Lane B, Coen E, Prusinkiewicz P. 2005. Quantitative modeling of Arabidopsis development. Plant Physiology 139(2): 960-968.
Muraro D, Byrne H, King J, Bennett M. 2013. The role of auxin and cytokinin signalling in specifying the root architecture of Arabidopsis thaliana. J Theor Biol 317: 71-86.
Muraro D, Byrne H, King J, Voss U, Kieber J, Bennett M. 2011. The influence of cytokinin-auxin cross-regulation on cell-fate determination in Arabidopsis thaliana root development. J Theor Biol 283(1): 152-167.
Muraro D, Mellor N, Pound MP, Help H, Lucas M, Chopard J, Byrne HM, Godin C,

Hodgman TC, King JR, Pridmore TP, Helariutta Y, Bennett MJ, Bishopp A. 2014. Integration of hormonal signaling networks and mobile microRNAs is required for vascular patterning in Arabidopsis roots. Proc Natl Acad Sci U S A 111(2): 857-862.

Nag A, Lunacek M, Graf PA, Chang CH. 2011. Kinetic modeling and exploratory numerical simulation of chloroplastic starch degradation. BMC Syst Biol 5: 94.

Nelson MR, Band LR, Dyson RJ, Lessinnes T, Wells DM, Yang C, Everitt NM, Jensen OE, Wilson ZA. 2012. A biomechanical model of anther opening reveals the roles of dehydration and secondary thickening. New Phytol 196(4): 1030-1037.

Nikolaev SV, Penenko AV, Lavrekha VV, Melsness ED, Kolchanov NA. 2007. A model study of the role of proteins CLV1, CLV2, CLV3, and WUS in regulation of the structure of the shoot apical meristem. Ontogenez 38(6): 457-462.

Novoselova E, Mironova V, Omelyanchuk N, Kazantsev F, Likhoshvai V. 2013. Mathematical modeling of Auxin transport in protoxylem and protophloem of Arabidopsis thaliana root tips. Journal of Bioinformatics and Computational Biology 11(1).

O'Connor DL, Runions A, Sluis A, Bragg J, Vogel JP, Prusinkiewicz P, Hake S. 2014. A division in PIN-mediated auxin patterning during organ initiation in grasses. PLoS Comput Biol 10(1): e1003447.

Olsen KM, Slimestad R, Lea US, Brede C, Løvdal T, Ruoff P, Verheul M, Lillo C. 2009. Temperature and nitrogen effects on regulators and products of the flavonoid pathway: experimental and kinetic model studies. Plant Cell Environ 32(3): 286-299.

Page ER, Gerwitz A. 1974. Mathematical models, based on diffusion equations, to describe root systems of isolated plants, row crops, and swards. Plant and Soil 41(2): 243-254. **Pathak RK, Taj G, Pandey D, Arora S, Kumar A. 2013.** Modeling of the MAPK machinery activation in response to various abiotic and biotic stresses in plants by a system biology approach. Bioinformation 9(9): 443-449.

Payne R, Grierson C. 2009. A Theoretical Model for ROP Localisation by Auxin in Arabidopsis Root Hair Cells. Plos One 4(12).

Payvandi S, Daly KR, Jones DL, Talboys P, Zygalakis KC, Roose T. 2014. A mathematical model of water and nutrient transport in xylem vessels of a wheat plant. Bull Math Biol 76(3): 566-596.

Pearce S, King J, Holdsworth M. 2011. Axisymmetric indentation of curved elastic membranes by a convex rigid indenter. International Journal of Non-Linear Mechanics 46(9): 1128-1138.

Pedersen A, Zhang K, Thorup-Kristensen K, Jensen L. 2010. Modelling diverse root density dynamics and deep nitrogen uptake - A simple approach. Plant and Soil 326(1): 493-510.

Pokhilko A, Fernández AP, Edwards KD, Southern MM, Halliday KJ, Millar AJ. 2012. The clock gene circuit in Arabidopsis includes a repressilator with additional feedback loops. Mol Syst Biol 8: 574.

Pokhilko A, Hodge SK, Stratford K, Knox K, Edwards KD, Thomson AW, Mizuno T, Millar AJ. 2010. Data assimilation constrains new connections and components in a complex, eukaryotic circadian clock model. Mol Syst Biol 6: 416.

Pokhilko A, Mas P, Millar AJ. 2013. Modelling the widespread effects of TOC1 signalling on the plant circadian clock and its outputs. BMC Syst Biol 7: 23.

Poolman MG, Assmus HE, Fell DA. 2004. Applications of metabolic modelling to plant metabolism. J Exp Bot 55(400): 1177-1186.

Prusinkiewicz P, Crawford S, Smith RS, Ljung K, Bennett T, Ongaro V, Leyser O. 2009. Control of bud activation by an auxin transport switch. Proc Natl Acad Sci U S A 106(41): 17431-17436.

Prusinkiewicz P, Erasmus Y, Lane B, Harder LD, Coen E. 2007. Evolution and development of inflorescence architectures. Science 316(5830): 1452-1456.

Ptashnyk M, Roose T, Jones DL, Kirk GJ. 2011. Enhanced zinc uptake by rice through phytosiderophore secretion: a modelling study. Plant Cell Environ 34(12): 2038-2046.

Penfield S, Fozard J. 2008. Network properties underlying seed germination control . Proceedings of the Mathematics in the Plant Sciences Study Group. The Centre for Plant Integrative Biology, University of Nottingham.

Péret B, Li G, Zhao J, Band LR, Voß U, Postaire O, Luu DT, Da Ines O, Casimiro I, Lucas M, Wells DM, Lazzerini L, Nacry P, King JR, Jensen OE, Schäffner AR, Maurel C, Bennett MJ. 2012. Auxin regulates aquaporin function to facilitate lateral root emergence. Nat Cell Biol 14(10): 991-998.

Péret B, Middleton AM, French AP, Larrieu A, Bishopp A, Njo M, Wells DM, Porco S, Mellor N, Band LR, Casimiro I, Kleine-Vehn J, Vanneste S, Sairanen I, Mallet R, Sandberg G, Ljung K, Beeckman T, Benkova E, Friml J, Kramer E, King JR, De Smet I, Pridmore T, Owen M, Bennett MJ. 2013. Sequential induction of auxin efflux and influx carriers regulates lateral root emergence. Mol Syst Biol 9: 699.

Qian M, Wells D, Jones A, Becker A. 2010. Finite element modelling of cell wall properties for onion epidermis using a fibre-reinforced hyperelastic model. Journal of Structural Biology 172(3): 300-304.

Roeder AH, Chickarmane V, Cunha A, Obara B, Manjunath BS, Meyerowitz EM. 2010. Variability in the control of cell division underlies sepal epidermal patterning in Arabidopsis thaliana. PLoS Biol 8(5): e1000367.

Roose T, Kirk GJD. 2009. The solution of convection–diffusion equations for solute transport to plant roots. Plant and Soil 316(1-2): 257-264.

Roose T, Schnepf A. 2008. Mathematical models of plant-soil interaction. Philos Trans A Math Phys Eng Sci 366(1885): 4597-4611.

Roshani G, Narayanasamy G, Datta S. 2009. Modelling potassium uptake by wheat. International Journal of Plant Production 3(2): 55-68.

Rovers W, Giersch C. 1995. Photosynthetic oscillations and the interdependence of photophosphorylation and electron transport as studied by a mathematical model. Biosystems 35(1): 63-73.

Runions A, Fuhrer M, Lane B, Federl P, Anne-Ga, Rolland-Lagan l, Prusinkiewicz P. 2005. Modeling and visualization of leaf venation patterns. ACM Trans. Graph. 24(3): 702-711.

Sankar M, Osmont KS, Rolcik J, Gujas B, Tarkowska D, Strnad M, Xenarios I, Hardtke CS. 2011. A qualitative continuous model of cellular auxin and brassinosteroid signaling and their crosstalk. Bioinformatics 27(10): 1404-1412.

Savage NS, Walker T, Wieckowski Y, Schiefelbein J, Dolan L, Monk NA. 2008. A mutual support mechanism through intercellular movement of CAPRICE and GLABRA3 can pattern the Arabidopsis root epidermis. PLoS Biol 6(9): e235.

Schnepf A, Jones D, Roose T. 2011. Modelling nutrient uptake by individual hyphae of arbuscular mycorrhizal fungi: temporal and spatial scales for an experimental design. Bull Math Biol 73(9): 2175-2200.

Schnepf A, Roose T. 2006. Modelling the contribution of arbuscular mycorrhizal fungi to plant phosphate uptake. New Phytol 171(3): 669-682.

Schnepf A, Roose T, Schweiger P. 2008. Impact of growth and uptake patterns of arbuscular mycorrhizal fungi on plant phosphorus uptake - a modelling study. Plant and Soil 312(1-2): 85-99.

Shabala S, Shabala L, Gradmann D, Chen Z, Newman I, Mancuso S. 2006. Oscillations in plant membrane transport: model predictions, experimental validation, and physiological implications. J Exp Bot 57(1): 171-184.

Skryabin K, Alekseev D, Ezhova T, Kozlov V, Kudryavtsev V, Nosov M, Penin A, Choob V, Shestakov S, Shul'ga O. 2004. A mathematical model of genetic control of determination of floral organ identity in Arabidopsis thaliana. Biology Bulletin 31(4): 346-353.

Smith RS, Guyomarc'h S, Mandel T, Reinhardt D, Kuhlemeier C, Prusinkiewicz P. 2006. A plausible model of phyllotaxis. Proc Natl Acad Sci U S A 103(5): 1301-1306.

Stewman SF, Jones-Rhoades M, Bhimalapuram P, Tchernookov M, Preuss D, Dinner AR. 2010. Mechanistic insights from a quantitative analysis of pollen tube guidance. BMC Plant Biol 10: 32.

Stoma S, Lucas M, Chopard J, Schaedel M, Traas J, Godin C. 2008. Flux-based transport enhancement as a plausible unifying mechanism for auxin transport in meristem development. PLoS Comput Biol 4(10): e1000207.

Swarup R, Kramer EM, Perry P, Knox K, Leyser HM, Haseloff J, Beemster GT, Bhalerao R, Bennett MJ. 2005. Root gravitropism requires lateral root cap and epidermal cells for transport and response to a mobile auxin signal. Nat Cell Biol 7(11): 1057-1065.

Thornley JHM. 1976. Mathematical Models in Plant Physiology: A Quantitative Approach to Problems in Plant and Crop Physiology: Academic Press. Thornley JHM, France J. 2007. Mathematical Models in Agriculture: Quantitative Methods for the Plant, Animal and Ecological Sciences: CABI Pub.

Welch SM, Roe JL, Das S, Dong Z, He R, Kirkham MB. 2005. Merging genomic control networks and soil-plant-atmosphere-continuum models. Agricultural Systems 86(3): 243-274.

Wiegers BS, Cheer AY, Silk WK. 2009. Modeling the hydraulics of root growth in three dimensions with phloem water sources. Plant Physiol 150(4): 2092-2103.

Wilczek A, Burghardt L, Cobb A, Cooper M, Welch S, Schmitt J. 2010. Genetic and physiological bases for phenological responses to current and predicted climates. Philosophical Transactions of the Royal Society B-Biological Sciences 365(1555): 3129-3147.

Wissuwa M. 2003. How do plants achieve tolerance to phosphorus deficiency? Small causes with big effects. Plant Physiol 133(4): 1947-1958.

Wu L, McGechan MB, McRoberts N, Baddeley JA, Watson CA. 2007. SPACSYS: Integration of a 3D root architecture component to carbon, nitrogen and water cycling-Model description. Ecological Modelling 200(3-4): 343-359.

Zeilinger MN, Farré EM, Taylor SR, Kay SA, Doyle FJ. 2006. A novel computational model of the circadian clock in Arabidopsis that incorporates PRR7 and PRR9. Mol Syst Biol 2: 58.

Zygalakis KC, Kirk GJ, Jones DL, Wissuwa M, Roose T. 2011. A dual porosity model of nutrient uptake by root hairs. New Phytol 192(3): 676-688.

Zygalakis KC, Roose T. 2012. A mathematical model for investigating the effect of cluster roots on plant nutrient uptake. The European Physical Journal Special Topics 204(1): 103-118.

Appendix D

Supplementary Information - Chapter 3

>

NOTE 1: Calculations for the parameter values

Calculation for the production rate of PHO2 (m_5)

Equation for PHO2:

$$\frac{d\,[PHO2]}{dt} = m_5 - k_6\,[miR399][PHO2] - d_4[PHO2]$$

Assuming PHO2 at quasi steady state:

$$m_5 - k_6\,[miR399][PHO2] - d_4[PHO2] = 0$$

Under normal conditions,

$$[miR399] = 0 \text{ and } [PHO2] = 1$$

Rearranging LHS:

$$m5 - d_4 = 0 \quad \text{i.e.} \quad m5 = d_4 = 0.3741$$

Calculation for the V_{max} for phosphate uptake by LPHT (k_{13}) and Rate constant for internal utilisation of CytoPi, (U)

Equation for CytoPi:

$$\frac{d\,[CytoPi]}{dt} = \frac{k_{11}[PHT][E]}{k_{12}+[E]} - \frac{k_{13}[E]}{k_{14}+[E]} - \frac{k_{15}[PHO1][CytoPi]}{k_{16}+[CytoPi]} - U[CytoPi]$$

Under normal conditions, the value of high affinity transporter$[PHT] = 0$ and Pi efflux transporter $[PHO1] = 0$. Assuming CytoPi at a quasi steady state:

$$\frac{k_{13}[E]}{k_{14}+[E]} - U[CytoPi] = 0$$

The term for Pi uptake corresponds to the total Pi brought into the cell under normal conditions and U corresponds to the amount of Pi used or stored in vacuoles. Assuming that 80% of Pi is stored in the vacuoles, then the cytosolic Pi (CytoPi) reflects remaining 20% of the Pi brought in the cell. Thus, for the given $[CytoPi] = 5000\,\mu M$, then the cytoplasmic Pi is $25000\,\mu M$, corresponding to the total Pi taken up by low affinity transporters.

$\therefore$ $$\frac{k_{13}[E]}{k_{14}+[E]} = 25000 \text{ and } U[CytoPi] = 25000$$

The values for k_{14} and E are 177 and 200, respectively.

$\therefore$ $$k_{13} = \frac{25000}{0.5305} = 47125.353 \text{ and } U = 5$$

NOTE 2: PiOM Model in MLXTRAN format

```
INPUT:
parameter = {m1,m2,m3,m4,m6,m7,m8,k2,k3,k4,k5,k9,k10,k11,k15,k16,Y1,Y2,beta}
EQUATION:
d1= 0.028875
d2=0.028875
d3=0.05775
d4=0.37419
d5=0.086625
d6=0.086625
d7=0.138
k1=1
k6=0.009
k7=k6/(1+Y1)
k8=k7*Y2
k12=23
k13=47125.3
k14=177
U=5
n=2
r=4
E=0.0001
t0 = 0
SIZ1_0 = 0
PHR2_0 = 0
PHR2S_0 = 0
miR399_0 = 0
PHO2_0 = 1
PHO1_0 = 0
PHT_0 = 0
CytoPi_0 = 5000
IPS1_0 = 0
IMC_0 = 0
ddt_SIZ1 = m1/(1 + (CytoPi/k1)^n) - d1*SIZ1
ddt_PHR2 = m2 - k2*PHR2*CytoPi - m3*PHR2*SIZ1/(k3 + PHR2) + k4*PHR2S -
d2*PHR2
ddt_PHR2S = m3*PHR2*SIZ1/(k3 + PHR2) - k4*PHR2S
ddt_miR399 = beta/(1+CytoPi) + (m4*PHR2S^n)/(k5^n + PHR2S^n)- k6*miR399*PHO2
- k7*miR399*IPS1+ k8*IMC - d3*miR399
ddt_PHO2 = m5 - k6*miR399*PHO2 - d4*PHO2
ddt_PHO1 = m6/((1+ PHO2)*(1+CytoPi))- d5*PHO1
ddt_PHT = m7*(PHR2S^n)/((k9^n + PHR2S^n)*(1+PHO2)) - d6*PHT
ddt_IPS1 = m8*(PHR2S^r)/(k10^r + PHR2S^)- k7*miR399*IPS1 + k8*IMC - d7*IPS1
ddt_IMC = k7*miR399*IPS1 - k8*IMC - d7*IMC
ddt_CytoPi = k11*PHT*E/(k12+E) + k13*E/(k14+E)- k15*CytoPi*PHO1/(k16+CytoPi)
- U*CytoPi
OUTPUT:
output = {miR399,PHO2,IPS1}
```

Parameters	P1	E1	P2	E2	P3	E3	P4	E4	P5	E5	P6	E6	P7	E7
m1	1	0.87	0.87651	0.61043	0.61043	0.60586	0.61043	0.4088	0.4088	0.34654	0.34654	0.4017	0.4017	0.42208
m2	1	0.14	0.14548	0.11147	0.11147	0.09069	**0.2**	0.1765	**0.2**	0.2	0.2	0.2	0.2	0.2
m3	1	1.49	1.4995	1.60112	1.60112	3.0102	1.60112	2.2067	2.2067	3.2233	3.2233	3.61274	3.61274	3.5318
m4	1	13.19	13.19108	17.71357	17.71357	11.32366	6.3	6.91307	6.91307	6.70225	6.70225	6.64339	6.64339	6.63974
m6	1	0.02	0.0243	0.00714	0.00714	0.00442	0.00714	0.00635	0.00635	0.0037	0.0037	0.00313	0.00313	0.00279
m7	1	1.45	1.45629	1.46229	1.46229	1.49643	1.46229	0.54305	0.54305	2.66623	2.66623	2.41378	2.41378	2.59092
m8	1	90.95	90.95821	105.03934	**1000**	796.99511	**1000**	680.19628	**1000**	191.1368	**1000**	737.53837	**1000**	693.32734
k2	1	0.77	0.77592	1.29827	1.29827	0.30815	1.29827	0.0712	0.0712	0.00383	0.00383	0.00247	0.00247	0.00199
k3	1	2.03	2.03011	2.54835	2.54835	1.91167	2.54835	1.85615	1.85615	1.20187	1.20187	1.10527	1.10527	1.14666
k4	1	0.32	0.32085	0.14541	0.14541	0.09613	0.14541	0.01564	0.01564	0.00871	0.00871	0.00794	0.00794	0.00814
k5	1	16.94	16.94403	18.4973	18.4973	20.18231	24	26.11693	26.11693	28.50022	28.50022	28.83186	28.83186	28.88717
k9	1	3.72595	3.72595	3.79115	3.79115	3.59343	3.79115	10.36129	10.36129	0.90479	0.90479	0.7801	0.7801	0.76934
k10	1	0.26849	0.26849	0.60301	**70**	37.56531	**70**	69.09793	69.09793	38.11847	**70**	74.07617	**70**	64.689
k11	1	0.65239	0.65239	0.15625	0.15625	0.14065	0.15625	0.12843	0.12843	0.13212	0.13212	0.12018	0.12018	0.12505
k15	1	0.05931	0.05931	0.02052	0.02052	0.05858	0.02052	0.06131	0.06131	0.05392	0.05392	0.05744	0.05744	0.05457
k16	1	0.5887	0.5887	0.29005	0.29005	0.4711	0.29005	0.17303	0.17303	0.12138	0.12138	0.11616	0.11616	0.11738
beta	1	9.25841	9.25841	8.35878	0.1	0.16656	0.16656	0.16786	0.16786	0.16823	0.16823	0.16823	0.16823	0.16823
Y1	1	30.16	30.16	37.18	**1000**	521.1	**10000**	34204.64	34204.64	32300.92	32300.92	33178.9	32300.92	33178.9
Y2	1	2.24	2.24	1.355	1	1.34	1	1.37	1.37	0.44	0.44	0.413	0.413	0.4769

Table D.1: List of the initial and estimated parameters from each round of model fitting
This table summaries all the used initial values and the corresponding parameter estimates from each round of model fitting. Initial values (P) and parameter estimates (E) for model fitting round (estimation run) 1 to 8. Values in bold are manually modified initial value to achieve appropriate fits.

PCR protocol

Actin was used for the control house-keeping gene for the qPCR analysis. The primers for both Actin and PHO2 used in this work were designed and tested in a previously published study by (Hu *et al.* , 2011) and are presented in Table D.4. The amplification of both Actin and PHO2 was done with the master-mix recipe given in Table D.5.The program used for the PCR is as follows: (1) Initial denaturation step at 95 °C for 5 minutes; (2) 35 cycles of denaturation at 95 °C for 30 seconds, Annealing at 58°C for 30 seconds, and extension at 72 °C for 30 seconds; (3) Final extension for 10 minutes at 72 °C . The samples were then run on a 1% agarose gel to assess their amplification quality, see Figure D.1. The gel was run at 60 Volts for 30 minutes and stained with SYBR Safe DNA gel stain.

qPCR protocol

For the qPCR reaction, the reaction mix was prepared following the recipe given in Table D.6 to achieve a total reaction volume of 20µl for each well. The 96-well plate with respective reaction mixes and cDNA templates in each well was carefully sealed with a LightCycler 480 Multiwell Sealing Foil and placed on the Roche LightCycler's loading frame to start the run. The run was programmed with the parameters shown in Table D.7. From the resulting Ct values, the fold change in gene expression was calculated using the caomparative CT Method ($\Delta\Delta CT$ Method) .

Primer name	Sequence (5'-3')
PHO2-F	CGAGAATTTTGTCAAGGAGCA
PHO2-R	TCACGAGCATGTCCAACAA
Actin-F	CAACACCCCTGCTATGTACG
Actin-R	CCAACACAATACCTGTGGTACG

Table D.4: List of primers for qRT-PCR

Primers were adopted from following article:

Hu, B., C. Zhu, F. Li, J. Tang, Y. Wang, A. Lin, L. Liu, R. Che, and C. Chu (2011). LEAF TIP NECROSIS1 plays a pivotal role in the regulation of multiple phosphate starvation responses in rice. Plant Physiol 156(3), 1101–1115.

Parameters	SD_P1	SD_E1	SD_P2	SD_E2	SD_P3	SD_E3	SD_P4	SD_E4	SD_P5	SD_E5	SD_P6	SD_E6	SD_P7	SD_E7
m1	1	0.00056	1	0.00355	1	0.02989	1	0.00241	1	0.0147	0.1	0.01573	0.1	0.00359
m2	1	0.00032	1	0.00023	1	0.00063	1	0.00003	0.01	0.00105	0.1	0.00104	0.1	0.00099
m3	1	0.0024	1	0.00718	1	0.00363	1	0.01514	1	0.01542	0.1	0.02669	0.1	0.00515
m4	1	0.00048	1	0.07343	1	0.00067	1	0.00007	1	0.00008	0.1	0.01573	0.1	0.02066
m6	1	0.00451	1	0.01263	1	0.012	1	0.01548	1	0.01296	0.1	0.00104	0.1	0.00036
m7	1	0.05171	1	0.06558	1	0.09959	1	0.00163	1	0.01023	0.1	0.02669	0.1	0.0171
m8	1	0.00046	1	0.00071	1	0.00176	1	0.00055	1	0.00573	0.1	0.00319	0.1	0.00317
k2	1	0.02569	1	0.01943	1	0.01248	1	0.00163	1	0.00599	0.1	0.04842	0.1	0.01269
k3	1	0.01397	1	0.02008	1	0.03735	1	0.0018	1	0.01276	0.1	0.00378	0.1	0.00316
k4	1	0.00245	1	0.00314	1	0.01309	1	0.01728	1	0.0894	0.1	0.019	0.1	0.06508
k5	1	0.00279	1	0.00122	1	0.00005	1	0.00013	1	0.00043	0.1	0.00026	0.1	0.00055
k9	1	0.00833	1	0.03601	1	0.25413	1	0.37539	1	0.03612	0.1	0.12679	0.1	0.01784
k10	1	0.016	1	0.00764	1	0.00113	1	0.00151	1	0.00105	0.1	0.00278	0.1	0.00735
k11	1	0.01036	1	0.11416	1	0.06004	1	0.03705	1	0.06518	0.1	0.04051	0.1	0.02384
k15	1	0.00847	1	0.00932	1	0.09262	1	0.03275	1	0.10101	0.1	0.00195	0.1	0.02492
k16	1	0.01384	1	0.03604	1	0.14632	1	0.01671	1	0.01725	0.1	0.00728	0.1	0.02365
beta	1	0.00041	1	0.00065	1	0.00537	0.1	0.00156	0.01	0.00041	0.1	0.0126	0.1	0.05
Y1	1	0.002	1	0.00288	1	0.21388	1	3.5249	1	2.7737	1	0.0126	1	0.04975
Y2	1	0.049	1	0.003	1	0.011	1	0.11533	1	0.09	1	0.00711	1	0.013

Table D.2: List of the initial and estimated standard deviation (SD) for parameters from each round of model fitting.

Parameters	PiOM	PdTA	PdRP	PsMD	PsTR	PsRA	PiOM_sd	PdTA_sd	PdRP_sd	PsMD_sd	PsTR_sd	PsRA_sd
m1	0.422	0.42	0.42684	0.423	0.42624	0.419	0.004	0.00276	0.00027	0.00217	0.00529	0.00244
m2	0.2	0.198	0.19735	0.198	0.19641	0.198	0.001	0.00038	0.00035	0.00157	0.00065	0.000363
m3	3.532	3.54	3.51576	3.53	3.52692	3.58	0.005	0.00107	0.00098	0.000685	0.00192	0.0097
m4	6.639	6.56	6.52457	6.65	6.52561	6.74	0.021	0.00154	0.00057	0.000773	0.00163	0.00116
m6	0.003	0.00278	0.00274	0.00283	0.0028	0.00284	0.0004	0.00042	0.00612	0.00366	0.00089	0.00112
m7	2.6083	2.58	2.59539	2.65	2.59284	2.59	0.0171	0.00162	0.00236	0.00831	0.0031	0.00106
m8	693.33	698	693.41146	693	695.86281	695	0.0032	0.000783	0.00226	0.00155	0.00255	0.000693
k2	0.002	0.00201	0.00201	0.002	0.002	0.00202	0.013	0.00193	0.00118	0.002	0.00047	0.00343
k3	1.147	1.16	1.1542	1.14	1.16149	1.15	0.003	0.00274	0.00257	0.00112	0.00183	0.000648
k4	0.008	0.00803	0.00808	0.0081	0.00804	0.00811	0.065	0.00798	0.00571	0.000375	0.00027	0.00171
k5	28.89	29.3	27.44477	29	27.49014	28.9	0.0006	0.000228	0.00059	0.00121	0.0003	0.000835
k9	0.769	0.764	0.75781	0.762	0.75835	0.761	0.017	0.00204	0.00174	0.00417	0.00181	0.00206
k10	64.69	65	64.7655	64.9	64.58041	65.2	0.0074	0.000558	0.00045	0.00133	0.00007	0.00108
k11	0.1251	0.125	0.12371	0.125	0.1265	0.126	0.024	0.00117	0.00289	0.00264	0.00251	0.00253
k15	0.0546	0.0548	0.05552	0.0538	0.05376	0.0549	0.025	0.000137	0.00287	0.00452	0.00274	0.00699
k16	0.1174	0.118	0.11541	0.117	0.11697	0.116	0.024	0.00255	0.00397	0.000964	0.00075	0.0011
beta	0.1682	0.169	0.16651	0.168	0.16638	0.166	0.02	0.000796	0.00659	0.00165	0.00684	0.0119
k6	0.009	0.00252	0.00785	0.00519	0.00711	0.00768	nan	0.603	0.01633	0.61	0.01813	0.59
d4	0.374	7.95	2.03	0.50	0.86	0.79	nan	2.05	1.07687	0.00232	0.59541	0.00399
d8	nan	0.0178	0.04163	1.83	1.38067	nan	nan	0.0588	0.01062	0.00501	0.00764	nan
k17	nan	nan	2.14	nan	nan	nan	nan	nan	0.00454	nan	nan	nan
k18	nan	nan	nan	992.1	544.1	nan	nan	nan	nan	2.75	0.56	nan
k19	nan	nan	nan	nan	1.86	nan	nan	nan	nan	nan	0.11	nan
k20	nan	nan	nan	nan	nan	0.233	nan	nan	nan	nan	nan	0.0105
m9	nan	7.12E-7	1.7E-06	0.554	0.72	nan	nan	2.3e-07	4.5e-7	2e-7	3.06e-7	nan
Y1	33178.9	10100	9945.07	10000	10071.43	10000	0.04975	0.002	0.0011	0.00347	0.00336	0.0005
Y2	0.4769	0.2	0.145	0.11	0.5533	0.1	0.013	0.00305	0.00685	0.00123	0.00141	0.0018

Table D.3: Parameter estimates for each hypothesis model.

Reagent	Volume
25 mM MgCl2	1 µl
10mM dNTPs	0.4 µl
Taq Polymerase (Invitrogen)	0.4 µl
cDNA template	2 µl
10x MasterMix	2 µl
Forward primer	0.4 µl
Reverse primer	0.4 µl
Nuclease free water	13.4 µl

Table D.5: Master mix recipe for PCR

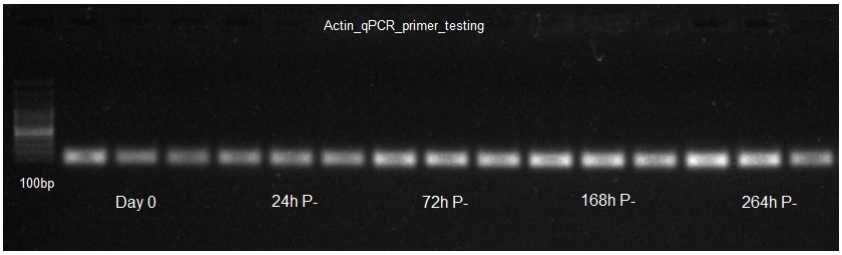

<

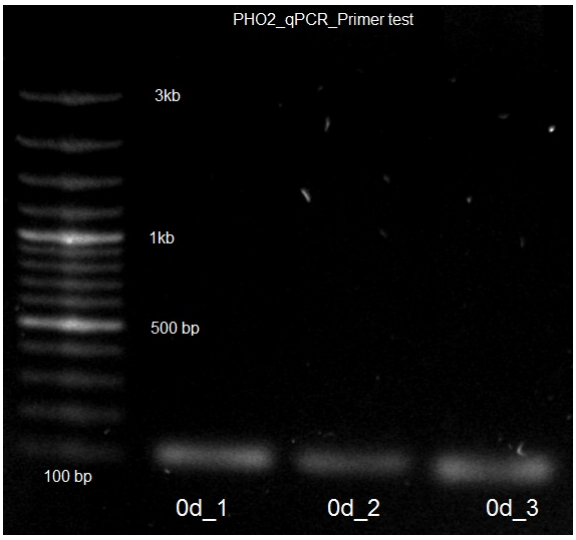

Figure D.1: qRT-PCR primer testing

Reagent	volume
PCR grade water	$3\,\mu l$
PCR Primer10x	$2\,\mu l$
Master Mix 2x	$10\,\mu l$
cDNA template	$5\,\mu l$

Table D.6: Master mix recipe for qPCR

Program	Cycles	Temperatures	Time (min)
Pre-Incubation	1	95°C	10:00
Amplification	45		
Denature	1	95°C	0:10
Annealing	1	58°C	0:20
Extension	1	72°C	0:30
Melting Curve	1		
	1	95°C	0:05
	1	65°C	1:00
	1	97°C	Continuous
Cooling	1	40°C	0:10

Table D.7: Roche LightCycler 480 program parameters

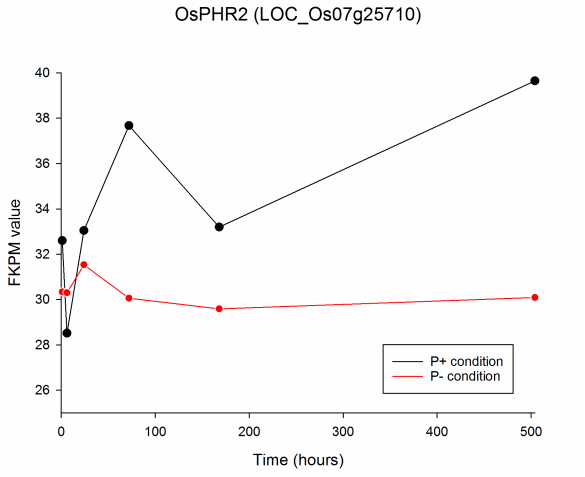

Figure D.2: PHR2 mRNA profile under phosphate sufficient and deficient conditions from RNA-SEQ dataset

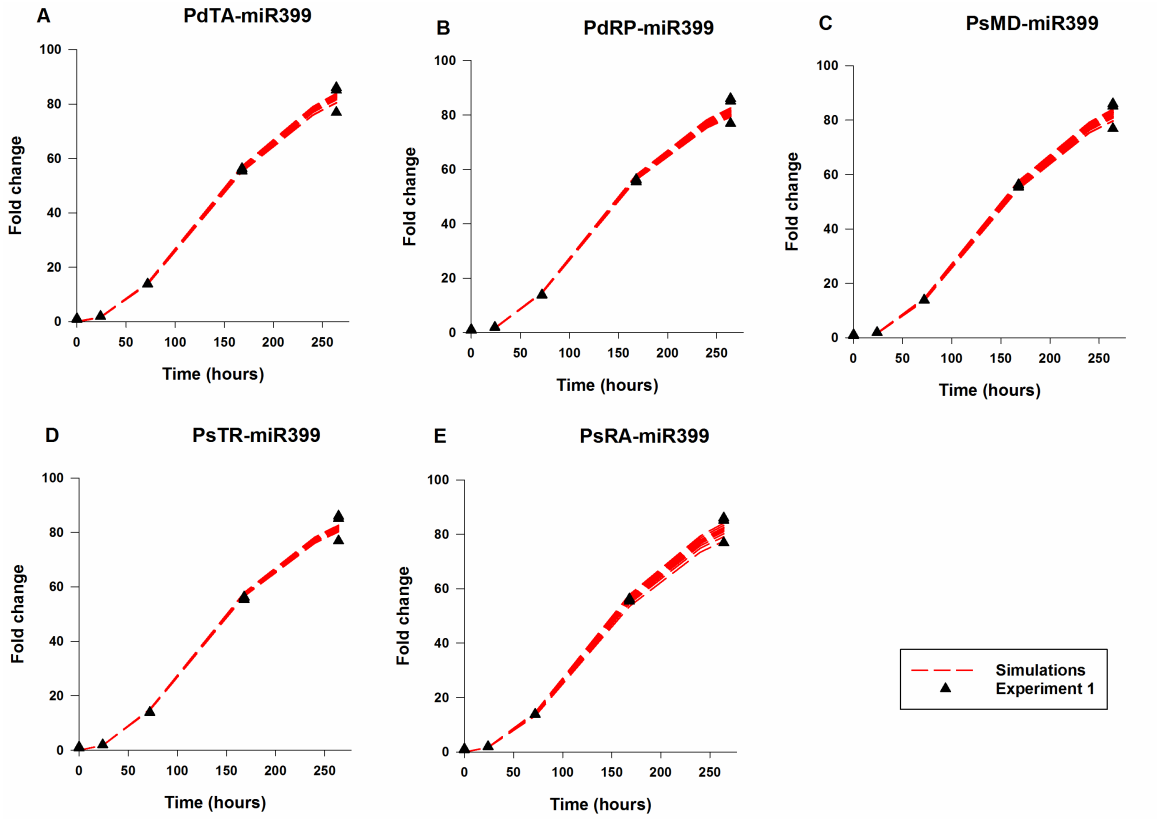

Figure D.3: All five models show a good fit to miR399 dataset

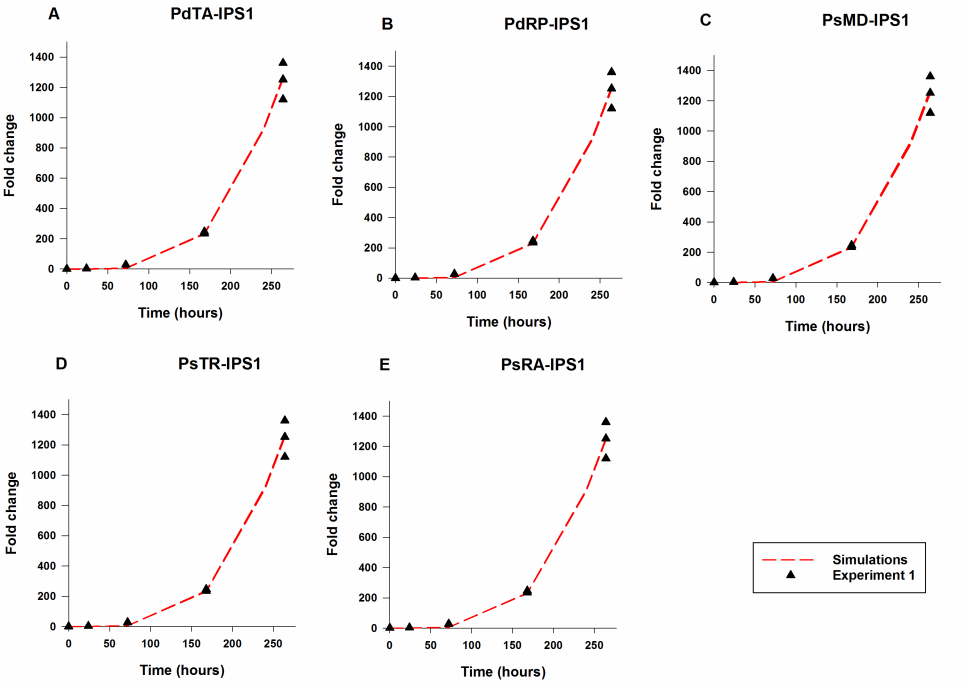

Figure D.4: All five models show a good fit to IPS1 dataset

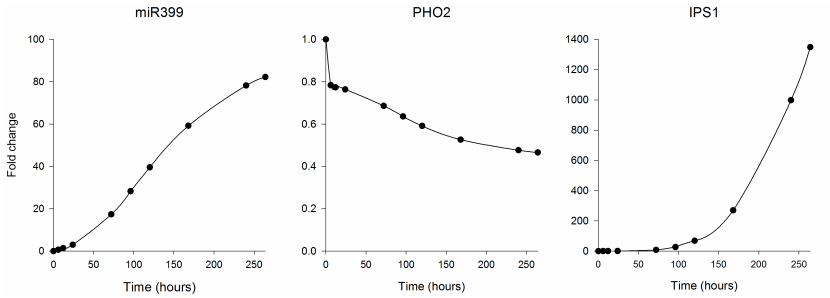

Figure D.5: miR399, PHO2 and IPS1 profiles under Pi deficient condition following alteration in parameter values

500 bp sequence upstream of PHO2 gene (Loc_Os05g48390)

–3'—CTATAGTATTACATAGACCACTTGTTTTGTACTATTAATGAAGATTAT
TTTTAAAATTTTTAAATTTTTATATAATTAAATAGACAATTTGTGATAGTAA
TGTGCTCAATAAATCAAACAGGTCTATAGAAAAAGAAAAAAAGCCATGC
AAAATAGAATTCCAGTACAACCATACCGTCTAAACAAAAGGAGAAACTC
GACTTAAAAAACTTAAAAAACAAGAATATTATAGAAGAACCTAATATCAA
ATAAATAGAACGAGTGAGACTTCCAATCTGGATCGGCTAGCCATCATATC
TACCTCTACTCTCAAGGGAAGGAAAATAACGCCACAATGGTGCAGCATCT
TTAGTTCCATTAACTTGACCACTAATTCACTGTCTTAAATTACTGCTGCAG
TTAGGCACACATCGTTTCACTTCACACAAGTGGCAGGAGCAAACAGTGAG
AGCATGGGAAGAAAACGAGTAAAAAAAATTCGATTACGTTTTCCAATCCGC—
5'–

Tool	Family	Position	Strand	Hit Sequence	Tool	Family	Position	Strand	Hit Sequence	Tool	Family	Position	Strand	Hit Sequence
PlantPAN	bHLH	17	+	accACTTGt	Jaspar	BHLH112	17	+	accacttgt	PROMO	MYB2	167	+	AACC
PlantPAN	Homeodomain;TALE	364	+	TGACC	Jaspar	SPL8	23	+	tgttttgtactattaa	PROMO	MYB2	193	+	AACT
PlantPAN	Myb/SANT	239	+	ctaATATCaa	Jaspar	EDT1	32	+	ctattaatga	PROMO	MYB2	207	+	AACT
PlantPAN	Myb/SANT;G2-like	221	+	agAATATtat	Jaspar	ATHB-6	106	+	tcaataaat	PROMO	MYB2	235	+	AACC
PlantPAN	Myb/SANT	239	+	ctaATATCa	Jaspar	CDF2	137	+	aaaaaagcca	PROMO	MYB2	256	+	AACG
PlantPAN	Myb/SANT	292	+	tcATATCta	Jaspar	DOF5.6	137	+	aaaaaagc	PROMO	MYB2	325	+	AACG
PlantPAN	Myb/SANT	341	+	cagcATCTTt	Jaspar	DOF5.7	137	+	aaaaaagc	PROMO	MYB2	350	+	AGTT
PlantPAN	Homeodomain;HD-ZIP	32	+	ctaTTAATga	Jaspar	CDF3	138	+	aaaaagcca	PROMO	MYB2	359	+	AACT
PlantPAN	MADS box;MIKC;M-type	178	+	tctaaacaaaaggAGAAActc	Jaspar	Dof2	140	+	aaagcc	PROMO	MYB2	397	+	AGTT
PlantPAN	MADS box;MIKC;M-type	121	+	ggtctatagaaaaAGAAAaaa	Jaspar	Dof3	140	+	aaagcc	PROMO	MYB2	411	+	CGTT
PlantPAN	MADS box;MIKC	181	+	aaaCAAAAggagaaa	Jaspar	MNB1A	140	+	aaagc	PROMO	MYB2	462	+	AACG
PlantPAN	bHLH	425	-	aCAAGTggc	Jaspar	PBF	140	+	aaagc	PROMO	MYB2	485	+	CGTT
PlantPAN	WRKY	362	-	cTTGACca	Jaspar	ARR1	291	+	atcatatcta					
PlantPAN	WRKY	361	-	acTTGACcac	Jaspar	MYB24	397	+	cagttaggc					
PlantPAN	MADF	466	-	gaGTAAAaaa	Jaspar	MYB46	399	+	gttaggca					
PlantPAN	WRKY	362	-	cTTGACca	Jaspar	MYB59	399	+	gttaggca					
PlantPAN	WRKY	361	-	acTTGACcac	Jaspar	ATHB-6	71	-	ttaattata					
PlantPAN	MADF	466	-	gaGTAAAaaa	Jaspar	KAN1	222	-	taatattc					
PlantPAN	Myb/SANT;G2-like	221	-	agaATATTat	Jaspar	MYB59	236	-	attaggtt					
PlantPAN	WRKY	362	-	cTTGACca	Jaspar	MYB24	237	-	atattaggt					
PlantPAN	WRKY	360	-	aacTTGACcac	Jaspar	WRKY18	361	-	gtggtcaagt					
PlantPAN	WRKY	362	-	cTTGACca	Jaspar	WRKY8	361	-	tggtcaagt					
PlantPAN	Homeodomain;HD-ZIP	31	-	actATTAAtga	Jaspar	WRKY2	362	-	tggtcaag					
PlantPAN	Homeodomain;HD-ZIP	355	-	ccATTAActt	Jaspar	WRKY25	362	-	tggtcaag					
PlantPAN	WRKY	362	-	cTTGACca	Jaspar	WRKY40	362	-	tggtcaag					
PlantPAN	WRKY	358	-	ttaacTTGACcac	Jaspar	WRKY63	362	-	tggtcaag					
PlantPAN	Myb/SANT	240	-	taATATCaa	Jaspar	BHLH112	425	-	gccacttgt					
PlantPAN	WRKY	363	-	TTGACcactaa	Jaspar	NAC043	482	-	aaaacgtaat					

Table D.8: Transcription Factor Binding Site prediction for PHO2 upstream region
The upstream 500 bp sequence of OsPHO2 gene (given above) was scan for transcription factor binding site using online tools including PlantPAN (plantpan2.itps.ncku.edu.tw), Jaspar (jaspar.genereg.net) and PROMO (alggen.lsi.upc.es). Top hits with score (>0.8) is presented in the table.

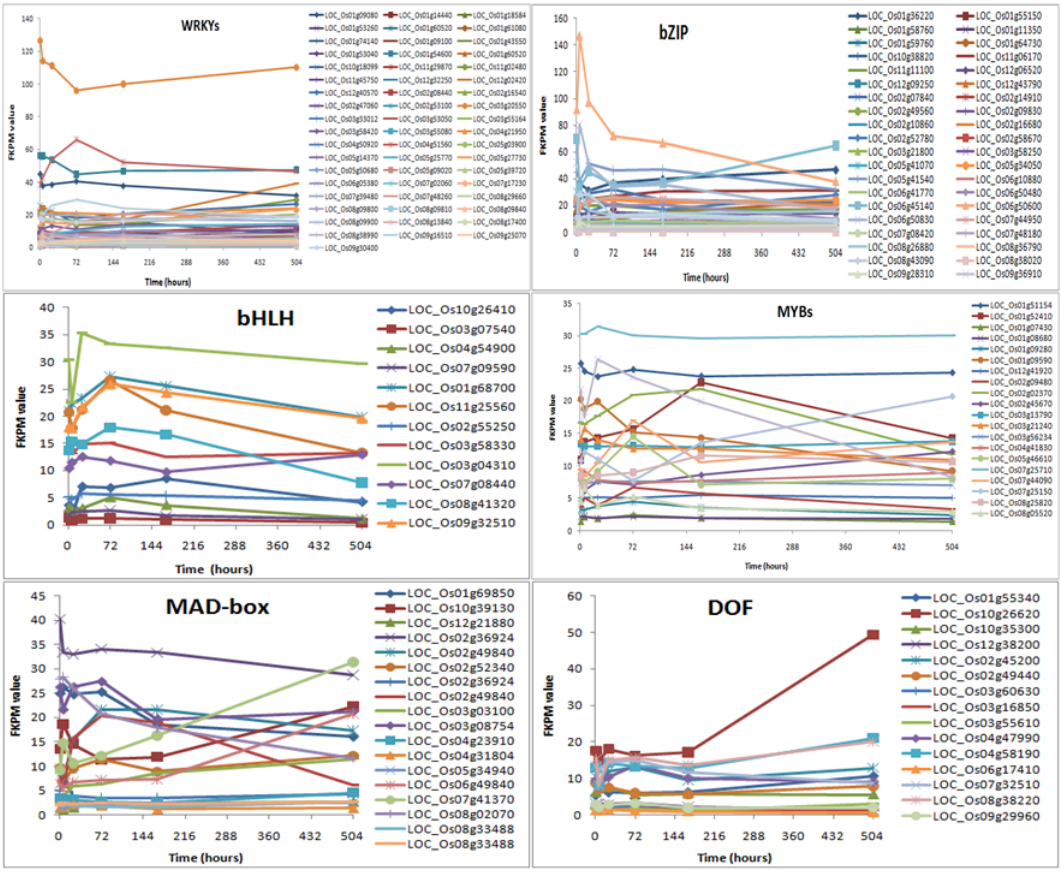

Figure D.6: Expression profile of the candidate for TA under Pi stress

Appendix E

Supplementary Information - Chapter 4

Score	RBP Name	Start	End	Matching sequence	Score	RBP Name	Start	End	Matching sequence
11.070935	A2BP1	315	320	UGCAUG	7.2294196	Pum2	598	601	UGUA
9.8958058	HNRNPA1	412	417	UAGGGA	6.6279899	MBNL1	234	237	UGCU
8.9484945	NONO	413	417	AGGGA	6.6279899	MBNL1	96	99	UGCU
8.6696024	RBMY1A1	12	16	CUCAA	6.4668404	EIF4B	305	308	GGAA
8.6471013	A2BP1	316	320	GCAUG	6.33985	KHSRP	214	217	GUCC
8.6272192	RBMY1A1	12	16	CUCAA	6.33985	KHSRP	516	519	GUCC
8.6272192	RBMY1A1	19	23	CUCAA	4.652088863	KHDRBS3	527	532	AAUAAU
7.3693752	FUS	387	390	GGUG	4.62028767	SFRS1	304	307	AGGA
7.3693752	FUS	407	410	GGUG	4.62028767	SFRS1	473	476	AGGA
7.2294196	Pum2	452	455	UGUA	4.40359056	ELAVL1	510	513	GUUU
7.2294196	Pum2	579	582	UGUA	4.40359056	ELAVL1	439	442	GUUU
7.2294196	Pum2	496	499	UGUA	4.40359056	ELAVL1	504	507	GUUU
7.2294196	Pum2	366	369	UGUA	4.40359056	ELAVL1	547	550	GUUU
7.2294196	Pum2	142	145	UGUA	4.40359056	ELAVL1	552	555	GUUU

Table E.1: List of predicted proteins and corresponding binding sites in IPS1 sequence

Parameters	PiOM	PsTR	PiOM_sd	PsTR_sd
m1	0.45467	0.39981	0.03105	0.09896
m2	0.18314	0.18035	0.00153	0.00307
m3	3.41894	3.75762	0.03735	0.02465
m4	7.51522	7.37237	0.00119	0.00269
m6	0.0031	0.00186	0.0403	0.02154
m7	2.48841	2.6484	0.05588	0.01812
m8	11.54216	10.44999	0.0049	0.00737
m9	nan	0.55473	nan	0.04173
k2	0.00211	0.00203	0.05489	0.13268
k3	1.0059	1.16091	0.01639	0.00984
k4	0.00823	0.00669	0.02189	0.04078
k5	30.91275	30.40525	0.01234	0.00785
k6	0.009	0.00962	nan	0.01085
k7	6.13E-06	0.000174069	1.2E-08	1.7E-05
k8	5.57E-07	0.001434235	1.2E-09	0.00105
k9	0.85494	0.76694	0.03064	0.04294
k10	33.62706	30.0196	0.00438	0.0067
k11	0.12875	0.11749	0.02579	0.06357
k15	0.05582	0.06955	0.02476	0.20403
k16	0.11191	0.11367	0.01394	0.04096
k18	nan	468.87226	nan	0.04532
k19	nan	2.31958	nan	0.04383
d4	0.375	0.27944	nan	0.00691
d8	nan	1.7301	nan	0.10474
r	2.38675	2.47921	0.00771	0.00449

Table E.2: Parameter estimates and corresponding standard deviations for PiOM-RP and PsTR-RP models. nan: parameter not part of the model or fixed during estimation